

**From Activation to Inhibition:
p53 and PNKP as Targets for Cancer Therapy**

by

Sara Ibrahim Omar

A thesis submitted in partial fulfillment of the requirements for the degree of

Doctor of Philosophy

in

Cancer Sciences

Department of Oncology

University of Alberta

© Sara Ibrahim Omar, 2019

Abstract

Cancer remains a challenging disease to tackle. The heterogeneity and evolution of the disease necessitates the development of diverse approaches to treat cancer. In this thesis, two different approaches have been undertaken to address this issue. The first aim was to activate the master tumor suppressor protein, p53. The second aim was to inhibit polynucleotide kinase phosphatase, a DNA repair enzyme.

The first target, p53, has been coined the 'guardian of the genome'. It is a transcription factor that orchestrates protective actions in response to cellular stress. p53 pathways are always inactivated in cancer cells. This is not surprising given the highly significant role of the protein in cells. p53 is inactivated due to mutations in the TP53 gene in about 50% of cancers. This makes p53 the most mutated protein in all cancer types. Mutant p53 accumulates in cells. Reactivation of mutant p53 can, therefore, induce a massive response leading to cancer cell death. This effect can theoretically be very selective to abnormal cells carrying the mutant. Only a few small molecules that restore the wild-type activity to mutant p53 have been identified. One of these molecules, called APR-246, is currently in clinical trials. The exact effect of APR-246 on the structure of mutant p53 is not fully understood. Four aims are discussed in this thesis: (1) understanding the interaction of known mutant p53 activators with the protein, (2) understanding the effect of three high frequency single-point mutations on the structure and DNA binding ability of the protein (3) understanding how the active form of APR-246 alters the DNA binding of mutant p53 and (4) virtually screening for novel mutant p53 activators.

Atomistic models of three p53 mutants carrying the R175H, G245S or R273H mutation were created. The models revealed that the flexibility of loops L1, L2 and L3 in the DNA binding domain of p53 was correlated. Binding energy calculations also revealed that the mutations change the binding profile of the mutant proteins with DNA. Another striking similarity was that all three mutants exhibited distortions in their alignment with DNA compared to the wild-type protein. These distortions might further contribute to alterations in the transcriptional activity of p53 mutants.

A previous study indicated that alkylating mutant p53 activators react with C124. We docked both alkylating and non-alkylating mutant p53 activators at this site. Docking results suggested that alkylating activators do not directly interact with C124 but their reactive moieties were directed towards the thiol of C124. However, non-alkylating activators were predicted to directly interact with C124. Poses of the non-alkylating ligands are logical given that they were predicted to interact with the proposed reactivation site. On the other hand, poses of the alkylating modifiers could be considered transitional state before reaction occurs. The covalently modified R175H and R273H p53 mutants were also simulated. It was observed that the wild-type and drugged mutants 'sat' on the DNA *via* a 'base'. However, there was a loss of interactions between regions of this base, in the mutant variants, and DNA. These results suggest that the alkylation of mutants' C124 anchors the L1 loop of p53 to DNA. Therefore, the modified proteins were aligned with DNA in a manner similar to wild-type p53, unlike the mutants.

The second target, polynucleotide kinase phosphatase, is involved in repairing cellular DNA. Inhibition of this novel target promises to have synergistic effects in combination with current cancer treatment modalities that act by damaging DNA. In addition, this DNA repair enzyme

has been found to be synthetically lethal to cells with phosphatase and tensin homolog (PTEN) or Src Homology region 2 domain-containing Phosphatase-1 (SHP-1) deficiency, which are common in some types of cancer. Virtual screening of a 3.7 million compounds was performed in a multiple-technique approach. The first step of screening was based on pharmacophore modelling followed by pharmacophore-assisted docking. Six of the top hits were purchased for experimental validation. The measured dissociation constants from tryptophan fluorescence quenching assays ranged from 55 to 450 nM. Further, one of the compounds had an IC_{50} of $\sim 13 \mu M$. Iterations of structural optimization of these molecules could yield a potent polynucleotide kinase phosphatase inhibitor that could be used in combination cancer therapy.

Dedication

To

My dearest Grandmother, Nahed

and

My two uncles, Mahmoud (El-Sayed) and Omar

who passed away during my writing of this thesis.

I am forever sorry I was away...

Acknowledgments

“Humankind. Be both”. My supervisor, Dr. Jack A. Tuszynski, is both.

I am sincerely thankful to Jack for being a wonderful mentor and friend. Jack has a unique sense of leadership. He gives his students the freedom to grow, trust, encouragement and a lot of support, which I really admire and am truly very grateful for.

I would also like to thank my supervisory committee members, Drs. Manijeh Pasdar and Mark Glover for their guidance and advice. Special thanks to Mark for his discussions and for being a constant critic of my work – it always pushed me to think more carefully. I am also very grateful to Manijeh for our long discussions and chats. I would also like to thank her for allowing me to join her journal club – it taught me a lot.

I would also like to thank all the students, faculty and staff members of the Department of Oncology. My special thanks go to Drs. Roseline Godbout, Mary Hitt and Alan Underhill. I am truly grateful to Dr. Underhill who really stands up for students, which I have experienced personally.

Also, I would like to thank our collaborators on the PNKP project at the Weinfeld, Glover and Hall labs (University of Alberta).

Many many thanks to my amazing friends and colleagues at the Tuszynski lab. We’ve shared so much joy, fun, laughter and even sorrows and stress together. My first thanks goes to Philip Winter, the first lab member I was introduced to. Philip is very kind, supportive, reliable and my last-minute resort that always works. To Sahar Arbabimoghdam (ArbabiNo), Mahshad Moshari (Salty), Niloofar Nayebi (Niloo), Francesco Gentile (ElSignor), Jordane Preto (JP), Aarat Kalra (Grandpa), Marco Lepre (the Rising Star) and Douglas Friesen (Ted): thank you all very much. Another special thanks goes to Holly Freedman. She’s been a very supportive friend, especially during the time of my candidacy exam. I will never forget that. ArbabiNo, thank you for always being by my side during both the worst and the best of times.

Beyond Thank You. To my parents, Eman Shamma and Ibrahim Omar, I am indebted to you both for absolutely everything. I owe you what I accomplished, what I am and what I will ever be. I am beyond thankful and grateful for all your love, support, encouragement and faith. Your words and advice always echo in my mind and have taught me to always keep trying. May God always bless you and help me make you happy.

Beyond Thank You. To Ali Ibrahim Omar and Salma Ibrahim Omar, I am extremely grateful to have a brother and sister like you two. Thank you for listening, for your support and for your advice. Your presence in this world makes it a better place.

TABLE OF CONTENTS

ABSTRACT	II
DEDICATION	V
ACKNOWLEDGMENTS	VI
LIST OF TABLES	XIV
LIST OF FIGURES	XV
LIST OF ABBREVIATIONS	XX
CHAPTER 1	1
1.1 BACKGROUND	2
1.2 P53: MASTER TUMOR SUPPRESSOR	3
1.2.1 FUNCTIONS OF P53	3
1.2.2 STRUCTURE OF P53	4
1.2.3 P53 RE	6
1.2.4 P53 IN CANCER AND THERAPEUTIC STRATEGIES	6
➤ Inhibition of wt-p53 by endogenous p53 inhibitors	7
➤ Inhibition of wt-p53 activity by mutation	8
1.2.5 AIMS FOR P53	9
1.3 PNKP: DNA REPAIR ENZYME	10
1.3.1 FUNCTION OF PNKP	10
➤ BER	11
➤ SSBR	11
➤ DSBR	12

1.3.2	STRUCTURE OF PNKP	13
1.3.3	INHIBITION OF PNKP FOR COMBINATION CANCER THERAPY	14
1.3.4	SYNTHETIC LETHALITY OF PNKP INHIBITION	16
1.3.5	AIM FOR PNKP	17
1.4	REFERENCES	19
CHAPTER 2		31
2.1	INTRODUCTION	33
2.2	RESULTS	36
2.2.1	EQUILIBRATION AND REPRESENTATIVE STRUCTURE EXTRACTION OF R273H-MP53	36
2.2.2	DOCKING SMALL LIGAND ACTIVATORS TO R273H-MP53	37
2.2.3	ADMET PROPERTIES OF THE LIGANDS	45
2.3	DISCUSSION	49
2.3.1	CREATING REPRESENTATIVE STRUCTURE FOR C124 BINDING POCKET	49
2.3.2	DOCKING P53 ACTIVATORS TO R273H-MP53	50
2.3.3	PREDICTING ADMET PROPERTIES OF P53 ACTIVATOR COMPOUNDS	53
2.4	CONCLUSIONS	53
2.5	METHODS	54
2.5.1	PREPARATION OF THE P53-R273H STRUCTURE	54
2.5.2	MD SIMULATIONS	55
2.5.3	RMSD-BASED STRUCTURE CLUSTERING	55
2.5.4	DOCKING	56
2.5.5	ADMET PREDICTION	57
2.6	REFERENCES	59

CHAPTER 3	65
3.1 INTRODUCTION	67
3.2 RESULTS	70
3.2.1 CONFORMATIONAL ANALYSIS: APO P53 PROTEINS	70
3.2.2 CONFORMATIONAL ANALYSIS: P53 DIMERS IN COMPLEX WITH THE DNA	74
3.2.3 EBE ANALYSIS	78
3.3 DISCUSSION	81
3.4 MATERIALS AND METHODS	88
3.4.1 3D STRUCTURE PREPARATION	88
3.4.2 MOLECULAR DYNAMICS SIMULATION	89
3.4.3 CONFORMATIONAL CHANGE ANALYSIS: RMSD AND RMSF	90
3.4.4 CONFORMATIONAL ANALYSIS: FMA	90
3.4.5 CLUSTERING	91
3.4.6 BINDING ENERGY CALCULATION	91
3.5 REFERENCES	93
CHAPTER 4	99
4.1 INTRODUCTION	101
4.2 RESULTS AND DISCUSSION	104
4.2.1 G245S-MP53 PROTEIN MODELS	104
4.2.2 COVALENT DOCKING OF THE FILTERED ZINC LIBRARY	106
4.2.3 ADMET PROPERTY PREDICTIONS	110
4.2.4 COMPOUND 2: THE BEST POTENTIAL HIT	112
4.3 CONCLUSIONS	114

4.4	METHODS AND MODELS	114
4.4.1	LIGAND LIBRARY PREPARATION	114
4.4.2	G245S-MP53 PREPARATION	115
4.4.3	RMSD-BASED CLUSTERING	115
4.4.4	COVALENT DOCKING USING DOCKTITE	116
4.4.5	ADMET PREDICTOR™	117
4.5	REFERENCES	118
CHAPTER 5		122
5.1	INTRODUCTION	124
5.2	RESULTS	127
5.2.1	P53-DNA COMPLEX STRUCTURES	127
5.2.2	BINDING ENERGY OF P53 TO DNA	129
5.2.3	PLACEMENT OF THE DNA	140
5.2.4	RMSF OF P53 RESIDUES	142
5.2.5	CONTROL R175H-CMQB-P53 AND R273H-CMQB-P53 SIMULATIONS	146
5.3	DISCUSSION	149
5.3.1	BINDING AND ALIGNMENT OF P53 TO DNA	149
5.4	ADDITIONAL COMMENTARY	157
5.5	CONCLUSIONS	159
5.6	METHODS AND MODELS	161
5.6.1	CREATING THE P53-DNA COMPLEX MODELS	161
5.6.2	MD SIMULATIONS OF P53	162
5.6.3	COVALENT DOCKING	163
5.6.4	ROOT-MEAN-SQUARE DEVIATION AND RESIDUE FLUCTUATIONS	163

5.6.5	BINDING ENERGY CALCULATIONS	163
5.7	REFERENCES	165
CHAPTER 6		170
6.1	INTRODUCTION	172
6.2	RESULTS	172
6.2.1	HPNKP HOMOLOGY MODEL	172
6.2.2	STAGE I: PHARMACOPHORE SCREENING	173
6.2.3	STAGE II: PHARMACOPHORE-ASSISTED DOCKING	176
6.2.4	STAGE III: COMPOUND ASSESSMENT	179
6.3	DISCUSSION	185
6.3.1	HPNKP PROTEIN MODEL	185
6.3.2	VIRTUAL SCREENING OF THE CoCoCo DATABASE	186
6.4	CONCLUSIONS	190
6.5	METHODS AND MODELS	191
6.5.1	CREATING THE HPNKP MODELS	191
6.5.2	DNA BINDING ENERGY CALCULATIONS	191
6.5.3	VIRTUAL SCREENING USING PHARMACOPHORE MODELING AND DOCKING	192
6.6	REFERENCES	194
CHAPTER 7		196
7.1	MUTANT P53	197
7.1.1	SUMMARY	197
7.1.2	FUTURE DIRECTIONS	202
7.2	POLYNUCLEOTIDE KINASE PHOSPHATASE (PNKP)	204

7.2.1	SUMMARY	204
7.2.2	FUTURE DIRECTIONS	205
7.3	REFERENCES	207
	BIBLIOGRAPHY	209
	APPENDICES	236
	APPENDIX I.	237
	APPENDIX II.	238
	APPENDIX III.	242

LIST OF TABLES

Table 2.1. A list of distances between S116 H and C124 S for MQ, NB, STIMA-1 and MIRA-1 as well as the distance between Ser121 O and C124 S.	41
Table 2.2. A list of Autodock binding energies (kcal/mol) and ligand efficiencies in the order of decreasing binding energies.	45
Table 2.3. ADMET Predictor™ estimations for the docked ligands.	47
Table 3.1. A table of the EBE between the p53 dimer and the DNA, the BE between the p53 monomer A and B, the BE between monomer A and the DNA and the BE between monomer B and the DNA.	79
Table 4.1: The top ten hits from our covalent docking virtual screening.	107
Table 4.2: The predicted ADMET properties of MQ and the top 10 potential hits from our covalent docking screen.	110
Table 5.1. Covalent docking results of MQ to C124 of the representative structures of the two p53 mutants.	128
Table 6.1. Results of the six compounds that were purchased for experimental validation.	181
Appendix Table i. The predicted top twenty potential PNKP phosphatase inhibitors from our in silico screen.	238

LIST OF FIGURES

Figure 1.1. p53 responds to a variety of cellular stresses and activates protective mechanisms to maintain the integrity of cells.....	3
Figure 1.2. p53 is composed of four main domains and is mostly mutated in the DBD (adapted from [39])......	5
Figure 1.3. PNKP dephosphorylates the 3' end and phosphorylates the 5' end of damaged DNA.....	11
Figure 1.4. A schematic of the PNKP domains: fork-head associated domain and DNA phosphatase and kinase domains.....	13
Figure 1.5. DNA repair enzymes can play a role in cancer cell resistance.	16
Figure 2.1. Plot of the RMSD of backbone atoms of residues 99 to 286 of p53-R273H model with reference to the structure at 0 ns.....	36
Figure 2.2. a) Plot of DBI and b) SSR/SST values for cluster counts from 2 to 100.	37
Figure 2.3. The top predicted pose of PHIKAN083 in Y220C-mp53.....	38
Figure 2.4. Docked poses showing MQ (green), NB (orange), MIRA-1 (blue) and STIMA-1 (pink) all binding at the same position and showing common interactions with residues S116 and G117.....	39
Figure 2.5. Ligand-interaction schemes of the alkylating ligands (a) MQ (b) NB (c) MIRA-1 (d) STIMA-1 (e) CP-31398 and (f) Stictic acid with R273H-mp53.....	40
Figure 2.6. Docked pose for PRIMA-1 (orange) and APR-246 (green) in R273H-mp53.	42
Figure 2.7. Ligand-interactions scheme showing the interacting residues between R273H-mp53 and a) ellipticine, b) 9-OH ellipticine and c) WR-1065.....	43

Figure 2.8. Plots of the distances between a) S116 (H) and C124 (S) and b) Ser121 (O) and C124 (S) during the last 50 ns of the simulation. 44

Figure 3.1. The RMSD plot of the backbone heavy atoms of both wt-p53 (blue) and G245S-mp53 (red) apo monomers over 1 μ s of MD simulations..... 71

Figure 3.2. The RMSF plot of the backbone heavy atoms of the apo monomers of wt-p53 (blue) and G245S-mp53 (red). The loops L1, L2 and L3 are indicated 72

Figure 3.3. R248 in monomer B of wt-p53 makes direct or water mediated contacts with DNA backbone thus retaining its water crystal structures is important 73

Figure 3.4. A plot of the RMSF of apo wt-p53 backbone calculated over all the MD trajectory filtered on the ewMCM. The loops L1, L2, L3 are labeled 74

Figure 3.5. A plot of the RMSD of monomers B of the p53-dimer in complex with DNA; wt-p53 (blue), G245S-mp53 (red)..... 75

Figure 3.6. The centroids of the two most populated clusters, (a) wt-1 and (b) wt-2 of the wt-p53 dimer and (c) mt-1 and (d) mt-2 of the G245S-mp53 dimer. The rotation of monomer B in the mutant is evident in mt-2 in monomer B (blue) relative to monomer A (green)..... 75

Figure 3.7. The RMSF plot for the backbone atoms of monomer B in the p53 dimer. Residues E224, V225 and G226 have higher fluctuations in G245S-mp53 compared to wt-p53..... 76

Figure 3.8. The minimized structure of the wt-p53 dimer in ribbon representation. Monomer A is in green, monomer B in blue and the DNA is grey. The magenta spheres are residues E224, V225 and G226, which are at the interface between the

two p53 monomers. The loop L1 and helix-2 in monomer B interact with the major groove of DNA, while in monomer A they interact with the DNA terminus. 77

Figure 3.9. Plots of the DBI, pSF and SSR/SST clustering metrics for the equilibrated (A) apo and (B) DNA-bound G245S-mp53. The pSF values were normalized to fit on the graph. 78

Figure 3.10. A histogram of the per-residue EBE decomposition for (A) monomers A and (B) monomers B, each in complex with DNA for both the wt-p53 (blue) and G245S-mp53 (red). Only the residues with EBE higher or lower than 1 kcal/mol are reported. The x-axis represents the residue numbers, the y-axis represents the EBE and the bars represent SD. A more pronounced redistribution of EBE is observed for monomer B. 81

Figure 4.1: Plots of the DBI, pSF and SSR/SST clustering metrics for the equilibrated (A) apo and (B) DNA-bound G245S-mp53. 105

Figure 4.2: Compound 2 covalently bound to G245S-mp53. 113

Figure 5.1. RMSD of the p53 variants non-hydrogen atoms over 750 ns. 129

Figure 5.2. A bar graph of the EBEs of the p53 variants to DNA. 131

Figure 5.3. A bar graph of the decomposition of the EBE per-residue of p53 to the DNA. 134

Figure 5.4. The difference in the EBE contribution of the mutant protein residues vs. wt-p53. 135

Figure 5.5. The difference in the EBE contribution of R175H-CmQA-p53 and R175H-CmQB-p53 vs. wt-p53. 137

Figure 5.6. The difference in the EBE contribution of R273H-CmQA-p53 and R273H-CmQB-p53 vs. wt-p53.....	139
Figure 5.7. Superimposition of the p53 variants shows the displacement of the DNA in the mutants' complexes.....	140
Figure 5.8. DNA RMSD in the p53 variant complexes compared to the wt-p53 DNA from 300 to 750 ns.....	141
Figure 5.9. RMSF of the p53 variants DBD from 300 to 750 ns of the MD simulation.	144
Figure 5.10. RMSF of the p53 drugged mutants' DBD from 300 to 750 ns of the MD simulation.....	145
Figure 5.11. A bar graph of the EBE per-residue decomposition of p53 to DNA in the control simulations.....	147
Figure 5.12. Superimposition of the p53 variants shows the displacement of the DNA in the mutants' complexes and R273H-CmQB-p53 from the control simulations. ...	148
Figure 5.13. The wt-p53-DNA complex structure.	151
Figure 5.14. Structure of the capped CmQ residue.....	162
Figure 6.1. The RMSD of PNKP during 250 ns of MD simulations.	173
Figure 6.2. A schematic of the screening workflow to find potential PNKP phosphatase inhibitors.	175
Figure 6.3. An example of a pharmacophore model for the PNKP complex structure.	177
Figure 6.4. The MMGBSA calculated binding energy (kcal/mol) of the DNA to PNKP from 20 to 250 ns.....	178
Figure 6.5. The interaction scheme of the docked DNA with PNKP in its lowest binding energy conformation.....	179

Figure 6.6. The ligand interactions between the six tested compounds (A-F) and hPNKP homology model.	183
Figure 6.7. The EMSA results for compounds A-F obtained from Cameron Murray (Glover lab) who performed the experiments and interpreted the results.	184
Appendix Figure i. Cross-validation of the maximally correlated motion by FMA employing as functional quantity the RMSD of loop L3 throughout the whole MD simulation.	237

LIST OF ABBREVIATIONS

2-AP	2-aminopurine
μM	Micromolar
ADMET	Absorption, distribution, metabolism, excretion and toxicity
ADMET_Risk	ADMET risk score
ADP	Adenosine diphosphate
ADP	adenosine diphosphate
ALT	Alanine transaminase
AP	Abasic (Apurinic/Apyrimidinic)
APE1	AP endonuclease I
ASPP2	Apoptosis-stimulating of p53 protein 2
AST	Aspartate transaminase
ATP	Adenosine triphosphate
BBB_Filter	Blood-brain barrier permeability
BER	Base excision repair
CHA	Common Hits Approach
CmQ	Methylene quinuclidinone bound cysteine
CoCoCo	Commercial Compounds Collection
DB	Double-bond
DBD	DNA binding domain
DBI	Davies-Bouldin
DLT	Dose limiting toxicity

DN	Dominant negative
DNA-PK	DNA-dependent protein kinase
DSB	Double-strand breaks
DSBR	Double-strand break repair
EBE	Estimated binding energy
EM	Electron microscopy
EMSA	Electrophoretic mobility shift assay
ewMCM	Ensemble-weighted maximal correlated motion
FEN1	Flap endonuclease 1
FHA	Fork-head associated
FMA	Functional mode analysis
G245S-mp53	G245S mutant p53
GB	Generalized Born
GOF	Gain-of-function
HSQC NMR	Heteronuclear Single Quantum Correlation Nuclear Magnetic Resonance
hPNKP	human PNKP
IC₅₀	Half maximal inhibition concentrations
IR	Ionizing radiation
K_d	Dissociation constant
LE	Ligand efficiency
LOF	Loss-of-function
logP	Partition coefficient

LOH	Loss of heterozygosity
MD	Molecular Dynamics
MDM2	Mouse double minute 2 homolog
MIRA-1	Mutant p53-dependent Induction of Rapid Apoptosis-1
MMGBSA	Molecular Mechanics Generalized Born Surface Area
MOE	Molecular Operating Environment
mp53	Mutant p53
mPNKP	Mouse PNKP
MQ	Methylene quinuclidinone
NB	3-Methylene-2-norbornanone
NHEJ	Non-homologous end-joining
nM	Nanomolar
NMA	Normal mode analysis
NMR	Nuclear Magnetic Resonance
NVT	Constant-temperature, constant-volume ensemble
PARP	Poly adenosine diphosphate polymerase
PCA	Principal component analysis
PD	Pharmacodynamic
PDB	Protein Data Bank
Pgp_Inh	Efflux by glycoproteins
Pgp_Substr	Inhibition of glycoproteins
PK	Pharmacokinetic
PNKP	Polynucleotide kinase phosphatase

Polβ	DNA polymerase beta
PRIMA-1	p53-reactivation and induction of massive apoptosis
PRIMA-1	p53 reactivation and induction of massive apoptosis
pSF	pseudo F-statistic
PTEN	Phosphatase and tensin homolog
R175H-CmQA-p53	R175H mutant p53 covalently bound to epimer A of MQ at C124
R175H-CmQB-p53	R175H mutant p53 covalently bound to epimer B of MQ at C124
R175H-mp53	R175H mutant p53
R273H-CmQA-p53	R273H mutant p53 covalently bound to epimer A of MQ at C124
R273H-CmQB-p53	R273H mutant p53 covalently bound to epimer B of MQ at C124
R273H-mp53	R273H mutant p53
RE	Response elements
RESP	Restrained electrostatic potential
RMSD	Root-mean-square deviation
RMSF	Root-mean-square fluctuation
ROS	Reactive oxygen species
S+P_{eff}	Intestinal membrane
S+Sw	Native solubility
SASA	Solvent accessible area
SD	Standard deviation
SHP-1	Src homology region 2 domain-containing phosphatase-1
siRNA	Small interfering RNA
SOF	Separation-of-function

SSB	Single-strand breaks
SSBR	Single-strand break repair
SSR/SST	Ratio of the sum of squares regression to the total sum of squares
STIMA-1	SH group Targeting and Induction of Massive Apoptosis-1
TAD	Transactivation domain
TOX_hERG_Filter	Inhibition of the human Ether-à-go-go-Related Gene potassium channel
TOX_SGOT	Serum glutamic-oxaloacetic transaminase
TOX_SGPT	Serum glutamate pyruvate transaminase
U-MB	Universal Molecular Beacon
vdW	van der Waals
wt	Wild-type
wt-p53	wild-type p53
XRCC1	X-ray cross complementing group 1
XRCC4	X-ray cross complementing group 4
Y220C-mp53	Y220C mutant p53

Chapter 1

Introduction

1.1 Background

Cancer is a complex disease of many types [1]. An estimate of 80,800 people died of cancer in 2017 in Canada [2]. Due to the lethality and heterogeneity of the disease, there is a dire need to develop therapies based on diverse and strategic targets in cancer cells. Conventional cancer therapy has largely been based on genotoxic agents and ionizing radiation (IR) [3]. These treatment modalities depend on the strategy of inducing DNA damage, which consequently leads to cell death [3]. One problem of targeting cellular DNA is that cells have inherent mechanisms for repairing the damage and hence could be resistant to treatment [4-6]. Another issue with conventional therapy is the fact that it is non-specific as it can affect the DNA of both normal and cancer cells. In this thesis, two proteins were targeted for the development of anti-cancer therapy to overcome each of these two issues.

To address the issue of non-specificity, we targeted a transcription factor called p53. This protein is very often mutated in cancer cells. Reactivation of mutant p53 (mp53) promises to be an effective cancer treatment that is specific to abnormal cells. **Our aim was to understand the effect of mutations and the effect of current mp53 activators on p53 structures. Another aim was to find potential mp53 activators using covalent docking.**

To address the issue of cancer cell resistance to conventional therapy, we targeted a DNA repair enzyme called, polynucleotide kinase phosphatase (PNKP). **Our aim was to use virtual screening to find small molecule PNKP inhibitors.** This class of molecules is intended to complement current treatment modalities to overcome resistance. More specifically, PNKP inhibitors can be used to sensitize cells to chemotherapy and IR.

1.2 p53: Master tumor suppressor

1.2.1 Functions of p53

p53 is a sequence-specific transcription factor [7]. It has been dubbed as the ‘Guardian of the genome’ due to the central role it plays in cells (Figure 1.1) [7]. It has both transcriptional and non-transcriptional dependent activities, including cytoplasmic functions [7-14]. p53 regulates the cell-cycle, DNA repair, senescence, metabolism and apoptosis in normal cells [7-10, 15, 16]. In fact, the network that p53 regulates is massive, as reviewed in [17, 18]. It is, therefore, considered the ultimate tumor suppressor protein [7, 19]. In cells, p53 is regulated and subjected to a very wide-variety of post-translational modifications, reviewed in [20-24].

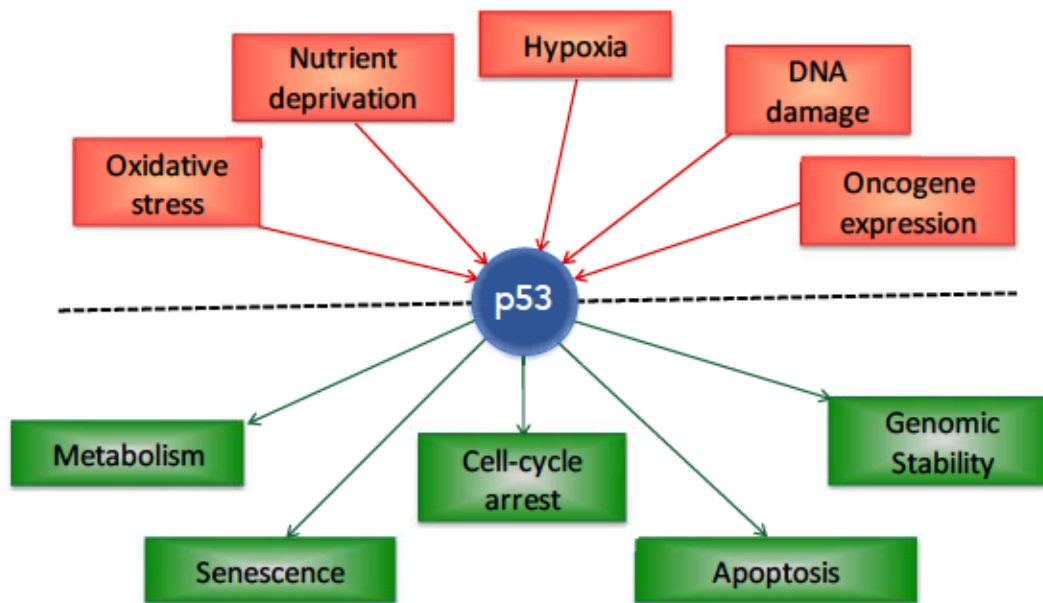


Figure 1.1. p53 responds to a variety of cellular stresses and activates protective mechanisms to maintain the integrity of cells.

There is an enormous body of literature on p53. There are also two dedicated websites for *TP53* (<http://p53.fr/>) and (<http://p53.iarc.fr/>). Below is the background on the aspects of p53 relevant to the aims of this thesis.

1.2.2 Structure of p53

p53 is a 393 amino acid multi-domain protein [25]. A schematic of the p53 domains is shown in Figure 1.2. Briefly described, the first of these domains is a transactivation domain, which is composed of two transcriptional activation subdomains, TAD1 (residues 1-42) and 2 (residues 43-83) [26]. TAD1 and 2 bind cofactors to activate transcription [26-28]. The second domain composed of residues 64 to 92 is a proline-rich domain. It is primarily involved in protein-protein interactions between p53 and its partners [29, 30]. The biggest domain in p53 is the DNA binding domain (DBD) formed by residues 95 to 300 [31]. The DBD binds and recognises short DNA sequences in the promoter regions of target genes called the p53 response elements (RE) (briefly explained in 1.2.3). p53 binds to DNA as a tetramer; this oligomerization occurs through the interaction of the tetramerization domains of p53 (residues 324 to 355) [32, 33]. The DBD is joined to the tetramerization domain through a flexible linker (residues 301-323) [30]. The C-terminus of p53, residues 360 to 393, form the regulatory domain of the protein [30]. From its name, this versatile domain is involved in regulating the function of p53 [34]. It plays a role in the initial p53 binding to DNA, p53 stability as well as recruitment of cofactors [34-38].

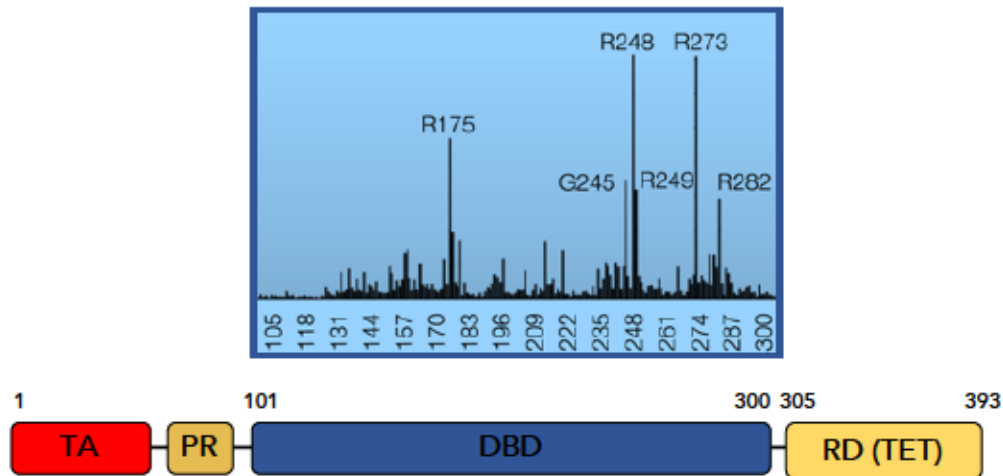


Figure 1.2. p53 is composed of four main domains and is mostly mutated in the DBD (adapted from [39]).

The protein is composed of four main domains: transactivation, proline-rich, DBD and tetramerization domains. The plot shows the relative frequencies of the DBD residue mutations. Six mutations are the most frequent and are termed ‘hot-spot’ mutations. Mutations in R248 and R273 are categorized as contact mutations, whereas the rest are classed as structural mutations since they affect the DNA binding ability of p53 although they do not interact directly with it.

In the apo form of p53, all domains of the protein are intrinsically disordered except for the DBD and tetramerization domain [34]. It is due to this reason that there are no experimentally-determined structures of the full-length p53 using Nuclear Magnetic Resonance spectroscopy (NMR) nor X-ray crystallography. However, there have been attempts to reconstruct the full-length protein structure using lower resolution techniques such as coupled chemical cross-linking and mass spectroscopy [40], small-angle X-ray scattering, NMR and electron microscopy (EM) in a multi-technique approach [41] or EM alone [42]. More interestingly, *in silico* modeling was used to create the full-length protein to understand its dynamics and interactions with different RE using molecular dynamics (MD) simulations [43].

1.2.3 p53 RE

Canonical p53 RE are composed of two repeats of a 'RRRCWWGYYY' motif separated by 0 to 18 base-pair spacers; R = Adenine or Guanine, C = Cytosine, W = Adenine or Thymine, G = Guanine and Y = Cytosine or Thymine [43-45]. As mentioned before, p53 binds to its RE as tetramers. Generally, shorter spacers allow for the increased interactions between the p53 monomers [46]. However, p53 has different affinities to different RE [43]. The protein tetramer can also bind to non-canonical RE [45], which adds more diversity and complexity to the functions of p53. Some of the canonical and non-canonical p53 RE are reviewed in [45-49].

1.2.4 p53 in cancer and therapeutic strategies

As mentioned before, p53 is central in maintaining the integrity of cells. It is, therefore, not surprising that the p53 pathway is inoperative in almost all types of cancer: a strategic advantage that allows uncontrolled cell growth and metastasis [50, 51]. In line with the important protective role of p53 in cells, individuals with inherited germline mutations in *TP53* often develop Li Fraumeni syndrome, which is characterized by the development of multiple primary tumors as well as childhood and early adulthood cancers [52, 53]. On the other hand, large animals that live long would be expected to have a high prevalence of cancer since their large number of cells is more likely to develop and accumulate mutations. However, elephants, as an example, defy this theory in what is called Peto's Paradox [54]. In fact, it was found that cancer prevalence in elephants was less than expected [54, 55]. This has been attributed to the presence of twenty copies of *TP53* in elephants, compared to one

copy in humans [54, 55]. These observations reflect the unequivocal role of p53 in cellular integrity protection and tumor suppression.

In 50% of human cancers, p53 functions are impaired due to mutations or deletions in the *TP53* gene [56]. While the remaining 50% of cancer cells harbor wild-type p53 (wt-p53), the protein's pathways are still deregulated [57]. Several strategies have been employed to restore the protective functions of p53 in cells. This thesis is focused on the restoration of the wt activity to mp53. However, an overview of wt-p53 inhibition is also given below.

➤ Inhibition of wt-p53 by endogenous p53 inhibitors

p53 protein levels in cells are tightly controlled since the protein is involved in numerous signalling networks [58, 59]. Under normal conditions, p53 protein levels in cells are low [60-62]. However, under stress conditions, when the actions of p53 are required, the protein is stabilized through post-translational modifications and regulation of its inhibitors, reviewed in [60-63]. Two proteins that play a major role in negatively regulating p53 are mouse double minute 2 homolog (MDM2) and MDMX [60, 61, 64-69]. Briefly described, MDM2 is a p53-specific E3 ubiquitin-protein ligase [70, 71]. MDM2 binds directly to p53 [68, 72] causing the nuclear exportation of p53, promotion of its proteosomal degradation and inhibition of its transcriptional activity [71]. MDMX, a homologue of MDM2, also binds to p53 and inhibits its transcriptional activity [73, 74]. These two proteins are overexpressed in some types of cancer and hence become oncogenic [74]; they inhibit and promote the degradation of the cell's guardian.

One strategy to overcome the effects of MDM2 and MDMX overexpression was to find small molecules or peptides to inhibit the binding of these oncogenic proteins to p53. Several inhibitors have been found [57, 71, 75-82]. Indeed, several of these molecules have made it

to clinical trials including AMG 232 [83, 84] RG7112, RO5503781, MI-773 and DS-3032b [75].

➤ Inhibition of wt-p53 activity by mutation

As mentioned above, p53 is mutated in about 50% of all cancers [50, 51, 85]. More than 45,000 mutations in *TP53* have been reported in the TP53 database [86]. 95% of these mutations occur in the region coding for the DBD of p53 [39]. p53 is not expressed in 10% of these cases as they result in nonsense mutations or deletions [85]. Therapeutic strategies in these cases are largely based on gene therapy to re-introduce wt-p53 back in cells using viral vectors [19, 87]. Alternative ways of introducing wt-p53 to cells included the direct injection of DNA or the use of cationic liposomes containing the transgene [19, 87].

Almost all remaining mutations in *TP53* result in missense mutations [85]. As demonstrated in Figure 1.2, almost all residues in the p53 DBD are susceptible to mutation [39]. However, there are six high frequency missense mutations (Figure 1.2) that constitute 40% of the cases of DBD mutations [39, 85, 88]. These ‘hot-spot’ mutations are in codons 175, 248, 245, 249, 273 and 282 [39, 85, 88]. Mutations in codons 157 and 220 are also highly frequent [85]. Structurally, p53 mutants are categorized into contact and structural/conformational mutants [39, 89, 90]. When one of the DBD residues that directly interact with the DNA is mutated, such as mutations in R273 or R248, the mp53 protein is categorized as a contact mutant [51, 90]. In the case of structural p53-mutants, the mutated residue (such as R175, 245, 249 and 282) does not interact directly with DNA but causes conformational alterations or unfolding of the protein [51, 90].

p53 mutants can also be functionally categorized. While all six hot-spot mutations compromise the wt activity of the protein, different mutations can have different

consequences in cells [17]. A single mutation in one allele can alter the transcriptional ability of p53 despite the presence of the wt protein [17]. This phenomenon is called the dominant negative (DN) effect [91, 92]. While the exact DN mechanism is not fully understood, it has been attributed to the lower binding affinity of the mt-wt tetramers binding to the DNA or the sequestration of transcriptional cofactors by mp53 [93]. In other cases, when only the missense mutant is expressed in cells, a loss-of-function (LOF) mutant phenotype is produced whereby p53 loses its transactivation ability [17, 93, 94]. Another category of p53 mutants are the separation-of-function (SOF) mutants in which the mutants only lose some of their wt activity [17, 94]. The most aggressive p53 functional phenotype are the gain-of-function (GOF) mutants, reviewed in [17, 91, 95]. GOF mutants not only lose their wt-p53 functions but also acquire new oncogenic functions [17, 91, 95, 96]. These mutants fully manifest themselves after the loss of the wt-p53 allele, which is termed ‘loss of heterozygosity’ [97]. Several studies have demonstrated tumor regression upon restoration of wt-p53 activity [19, 98-100]. Reviews on mp53 activators can be found in [51, 87, 99, 101-103]. Molecules that have been identified to activate R273H and R175H are APR-246 and its derivatives PRIMA-1 [104], MIRA-1 [105], STIMA-1 [106] and 3-methylene-2-norbornanone [107]. APR-246 is the only activator that has, so far, proven to be clinically successful; it is currently in phase-II clinical trials [108, 109]. A more detailed description of these activators is given in the introduction of Chapter 5.

1.2.5 Aims for p53

Restoration of the wt activity to mp53 promises to be an effective approach to treat cancer. APR-246 is a first-in-class drug that reactivates mp53 and is currently in clinical trials [108, 109]. In this thesis, *in silico* modeling was used to achieve four main goals:

- Understand the interaction pattern of mp53 activators from the literature with R273H-mp53 using non-covalent docking.
- Understand the effect of mutation on the G245S hotspot structural mutant in its DNA-bound and apo forms.
- Understand and compare the effect of mutation on the hotspot structural and contact mutants, R175H-mp53 and R273H-mp53, with respect to their DNA binding. Also, the effect of drugging these mutants with APR-246's active metabolite was also studied.
- Find potential G245S-mp53 activators using covalent docking.

1.3 PNKP: DNA repair enzyme

1.3.1 Function of PNKP

PNKP is a bifunctional DNA repair enzyme; it dephosphorylates 3' ends and phosphorylates 5' ends of damaged nuclear and mitochondrial DNA through its phosphatase and kinase functions, respectively (Figure 1.3) [110, 111]. The catalytic actions of PNKP provide the correct substrate for downstream enzymes in the DNA repair pathways to complete the repair process. It is worth mentioning that the phosphatase activity of PNKP is stronger than its kinase activity [112].



Figure 1.3. PNKP dephosphorylates the 3' end and phosphorylates the 5' end of damaged DNA.

PNKP is involved in three DNA repair pathways: base excision repair (BER), single strand break repair (SSBR) and double strand break repair (DSBR) pathways. Although these pathways are complex and their exact mechanisms are not fully understood, there are general agreed upon models outlined below:

➤ BER

This pathway is activated to repair damage caused by IR, reactive oxygen species (ROS) and alkylating agents that lead to small non-distorting base modifications or abasic (AP) sites [4, 113]. Monofunctional DNA glycosylases first remove the damaged bases then AP endonuclease I (APE1) cleaves the DNA backbone at the AP site. Alternatively, bifunctional DNA glycosylases, which possess both glycosylase and AP endonuclease activities catalyze both reactions [113]. The DNA products of the latter type of glycosylases possess 3' phosphate termini. The rest of the repair process then goes through the short or long patch SSBR pathways described below.

➤ SSBR

Single-strand breaks (SSB), especially those induced by IR or as by-products of the BER pathway, are associated with loss of nucleotides [113-116]. Poly(ADP-ribose) polymerase (PARP) recognises this SSB and initiates the repair process. X-ray cross complementing group 1 (XRCC1), PNKP, DNA ligase and DNA polymerase β (Pol β) are all recruited to the

break site. PNKP dephosphorylates 3' phosphate termini at the breaks so the DNA can be repaired by downstream proteins in the short or long patch repair pathways [113-116].

In the short patch repair, Pol β , which possesses both deoxyribose phosphate lyase and DNA polymerase activities, first removes the deoxyribose phosphate residue then fills the one nucleotide gap [114]. The DNA backbone is then sealed by DNA ligase. Alternatively, if the 5' deoxyribose phosphate residue is modified, Pol β would not be able to cleave the substrate and hence the long patch repair is activated instead. Initially, nucleotides are added to the 3' hydroxyl terminus by Pol β then continued beyond the damaged site by DNA polymerase δ and ϵ [113-116]. This creates a DNA flap, which is then cleaved by flap endonuclease 1 (FEN1), followed by DNA ligase sealing of the DNA backbone [113-116].

➤ DSBR

Double-strand breaks (DSB) in DNA can be caused by IR or ROS [117]. One of the DSBR pathways in which PNKP is involved is called the non-homologous end-joining (NHEJ) [4]. A heterodimer composed of two proteins called Ku70 and Ku80 recognise the double strand break and recruits DNA-dependent protein kinase (DNA-PK), which in turn tethers the two DNA strands together [118]. X-ray cross complementing group 4 (XRCC4) scaffolding protein then recruits PNKP to process the hydroxyl and phosphate DNA termini. DNA ligase then binds the DNA backbones together [118].

Some excellent reviews on the DNA repair pathways described above can be found in [113, 115, 117-120].

1.3.2 Structure of PNKP

PNKP is a 521 amino-acid protein composed of a fork-head associated (FHA) domain joined by a flexible linker to a fused catalytic domain (Figure 1.4) [4, 111]. The FHA domain interacts with phosphorylated XRCC1 and XRCC4 proteins involved in the SSBR and DSBR pathways. It has been suggested that this interaction increases the affinity of PNKP to DNA [121]. Other studies indicated that XRCC1 and XRCC4 increase the turnover of PNKP [4, 122, 123]. The DNA phosphatase and kinase activities of PNKP are carried out by the catalytic domain of the protein (residues 146-516).

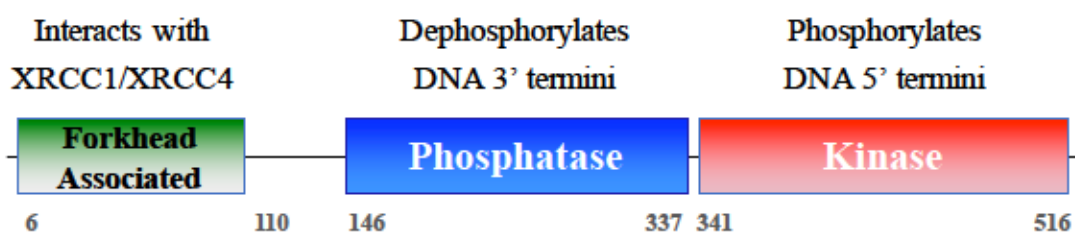


Figure 1.4. A schematic of the PNKP domains: fork-head associated domain and DNA phosphatase and kinase domains.

X-ray resolved structures of PNKP revealed that both the phosphatase and kinase active-sites of PNKP have a magnesium ion, which is essential for both catalysis as well as maintaining the stability of the high negative charges at the active-sites [124, 125].

The phosphatase subdomain of PNKP is composed of residues 146 to 337. It has been proposed that the 3' phosphate of the damaged DNA is stabilized by Mg^{2+} , T217 and K260 [126]. The 3' phosphate group transiently binds to the carboxyl side-chain of D171, in an in-line nucleophilic attack by the latter, forming a covalent phospho-aspartate intermediate that is stabilized by the phosphatase active-site Mg^{2+} [124, 126]. D173 then protonates the DNA

and a 3' hydroxyl DNA is released from the active-site. D173 then deprotonates a water molecule, which attacks the D171 covalently bound phosphate. This leads to breaking of the phospho-aspartate bond and the release of a free phosphate [124, 126].

The kinase subdomain of PNKP is composed of residues 341 to 516. At the kinase active-site, Mg^{2+} stabilizes the donating adenosine triphosphate (ATP) molecule [124-126]. It has been proposed that the anionic oxygen of D397 side-chain carboxyl group activates the 5' hydroxyl of the damaged DNA, which in turn attacks the γ -phosphate of ATP and becomes phosphorylated [126]. The products of this reaction are adenosine diphosphate (ADP) and 5' phosphate DNA.

1.3.3 Inhibition of PNKP for combination cancer therapy

As mentioned above, IR and DNA-damaging chemotherapeutics are still two essential pillars of treatment regimens for many types of cancer. IR is primarily utilized to damage cancer cells [127]. The IR-induced damage can directly affect macromolecules in cells including their DNA by causing SSB and DSB [127]. These strand breaks sometimes have damaged 3' phosphate and 5' hydroxyl ends [128]. On the other hand, indirect damage in cells by IR is induced by the generation of ROS, which can also cause oxidative damage to DNA [127]. Similarly, there are many classes of chemotherapeutics that act by damaging the DNA. Such drugs include inhibitors of topoisomerase I, an enzyme that transiently breaks phosphodiester bonds in DNA to relieve DNA supercoils during replication and transcription [129]. Examples of such inhibitors are camptothecin and irinotecan, which act by stabilizing the topoisomerase I-DNA complex forming a dead-end ternary complex associated with strand breaks [129, 130].

Ideally, these cancer regimens would lead to cell-cycle arrest and apoptosis [131]. However, a significant number of patients are resistant to these treatments because their tumors possess robust DNA repair capacity, or their tumors develop this repair capacity over time through upregulation of DNA repair enzymes (Figure 1.5) [5, 131]. For example, camptothecin stabilized complexes can be hydrolysed by tyrosyl-DNA phosphodiesterase 1, leaving behind DNA with 3' phosphate and 5' hydroxyl termini, which can be repaired by PNKP. Similarly, PNKP is also essential for the repair of SSB and DSB induced by IR.

While efforts have been made to find more potent genotoxic chemotherapies, such as higher affinity camptothecin derivatives, those compounds did not show significant improvement in clinical trials [132]. Alternatively, there have been searches to find for novel DNA damage repair targets to potentiate IR and DNA-damaging chemotherapy [133-135]. Indeed, it has been demonstrated that the down-regulation of PNKP in the human lung carcinoma A549 cell-line using small interfering RNA (siRNA) caused cells to be more susceptible to damage via IR and topoisomerase I inhibitors [136]. In a different study, HCT116 and of HeLa PNKP deficient cells were also sensitized to DNA damaging neocarzinostatin and radiation[137]. It is theoretically possible to inhibit the kinase activity or the binding of PNKP via its FHA domain to PNKP interaction partners. However, inhibiting the phosphatase activity of the enzyme has a high potential as a strategy for adjunct cancer therapy. This hypothesis is supported by the fact that the phosphatase activity of PNKP is higher than its kinase activity [112]. Also, PNKP is the major DNA phosphatase enzyme in cells [4, 111]. While APE1 possesses the same ability, its activity is much weaker than PNKP [138]. Additionally, IR, ROS and camptothecin derivatives used for cancer treatment often induce strand breaks that require processing of the 3' termini of DNA by PNKP [4].

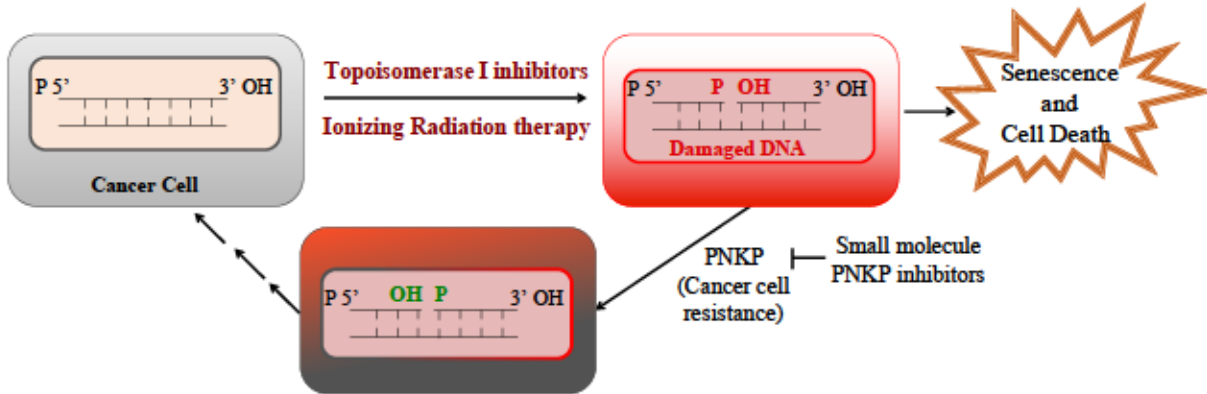


Figure 1.5. DNA repair enzymes can play a role in cancer cell resistance. Inhibition of key DNA repair enzymes such as PNKP can sensitize cells to chemotherapy and radiation leading to cell death and senescence.

Excitingly, A12B4C3, a PNKP inhibitor, has been identified using a fluorescence-based screen [139]. A12B4C3, while non-toxic to cells, sensitized A549 cells expressing PNKP to camptothecin treatment but did not have additional observed effects on treated *versus* non-treated PNKP-deficient cells [140]. In another study, A12B4C3 sensitized radioresistant PC-3 prostate cancer cells to radiation [141]. Enzyme kinetic experiments have demonstrated that this inhibitor is non-competitive [140]. However, the exact binding site of A12B4C3 is still unknown, which is a big challenge from a rational drug design and development perspective.

1.3.4 Synthetic lethality of PNKP inhibition

Synthetic lethality is a phenomenon wherein the resultant co-disruption of two proteins, but not only one of them, leads to cell death [142]. Two different synthetic lethal partners of PNKP have been discovered by genetic screening using a library of siRNA on PNKP depleted cells [143, 144]. One of the identified synthetically lethal partners of PNKP is a tumor suppressor protein called phosphatase and tensin homolog (PTEN) [143]. Although the exact

mechanism of this partnership is not fully understood, it has been found that PTEN depletion was associated with increased DNA DSB with 3' phosphate ends [143]. This was also associated with increased cell death [143].

Src homology region 2 domain-containing phosphatase-1 (SHP-1), a tyrosine phosphatase enzyme, was also found to be a synthetically lethal partner of PNKP [144]. It has been hypothesized that SHP-1 depletion leads to an increase in ROS, which damaged the DNA. Again, it is possible that the lack of PNKP to fix this damage led to cell death [144].

The synthetic lethality of PNKP and PTEN or SHP-1 provides another venue for the clinical use of PNKP inhibitors in cancer cells. Both tumor suppressor proteins, PTEN and SHP-1, are mutated in many types of cancer cells [143, 144]. Thus treatment of cancer cells with PNKP inhibitors can lead to cancer cell death with minimal impact on normal cells that carry the functional tumor suppressor proteins [143, 144].

1.3.5 Aim for PNKP

Previous research confirms that PNKP is a suitable and novel therapeutic target for cancer treatment [137, 145]. Inhibitors of PNKP can counteract radioresistance and chemoresistance in cancer cells making treatment more effective. Using PNKP inhibitors for combination cancer therapy using targeted delivery to specifically target cancer cells, to avoid damage to normal cells, could potentially reduce IR and camptothecin treatment dosage and hence could decrease adverse effects caused by these treatments. Additionally, the synthetic lethality between PNKP and its partners can also be exploited to selectively increase the efficacy of chemotherapy and radiation, especially in cancer cells with mutations in *PTEN* and *SHP-1* [143, 144]. The aim for this protein target was to:

- Find potential PNKP phosphatase inhibitors using a combination of pharmacophore and docking techniques

1.4 References

1. Hanahan D, Weinberg RA. Hallmarks of Cancer: The Next Generation. *Cell*. 2011; 144: 646-674.
2. Cancer statistics at a glance - Canadian Cancer Society; 2018.
3. Madhusudan S, Middleton MR. The emerging role of DNA repair proteins as predictive, prognostic and therapeutic targets in cancer. *Cancer Treatment Reviews*. 2005; 31: 603-617.
4. Weinfeld M, Mani RS, Abdou I, Aceytuno RD, Glover JNM. Tidying up loose ends: the role of polynucleotide kinase/phosphatase in DNA strand break repair. *Trends in biochemical sciences*. 2011; 36: 262-271.
5. Gatti L, Zunino F. Overview of tumor cell chemoresistance mechanisms. *Chemosensitivity Vol 2: in Vivo Models, Imaging, and Molecular Regulators*. 2005; 111: 127-148.
6. Kachalaki S, Ebrahimi M, Mohamed Khosroshahi L, Mohammadinejad S, Baradaran B. Cancer chemoresistance; biochemical and molecular aspects: a brief overview. *European Journal of Pharmaceutical Sciences*. 2016; 89: 20-30.
7. Levine AJ, Oren M. The first 30 years of p53: growing ever more complex. *Nature Reviews Cancer*. 2009; 9: 749-758.
8. Goldstein I, Marcel V, Olivier M, Oren M, Rotter V, Hainaut P. Understanding wild-type and mutant p53 activities in human cancer: new landmarks on the way to targeted therapies. *Cancer gene therapy*. 2011; 18: 2-11.
9. Maddocks ODK, Vousden KH. Metabolic regulation by p53. *Journal of Molecular Medicine (Berlin, Germany)*. 2011; 89: 237-245.
10. Vousden KH, Lu X. Live or let die: the cell's response to p53. *Nature Reviews.Cancer*. 2002; 2: 594-604.
11. Comel A, Sorrentino G, Capaci V, Del Sal G. The cytoplasmic side of p53's oncosuppressive activities. *FEBS Letters*. 2014; 588: 2600-2609.
12. Green DR, Kroemer G. Cytoplasmic functions of the tumour suppressor p53. *Nature*. 2009; 458: 1127-1130.

13. Follis AV, Llambi F, Ou L, Baran K, Green DR, Kriwacki RW. The DNA-binding domain mediates both nuclear and cytosolic functions of p53. *Nature Structural & Molecular Biology*. 2014; 21: 535-543.
14. Kroemer G, Pedro JMB, Galluzzi L. Novel function of cytoplasmic p53 at the interface between mitochondria and the endoplasmic reticulum. 2015; 2018.
15. Bieging KT, Attardi LD. Deconstructing p53 transcriptional networks in tumor suppression. *Trends in Cell Biology*. 2012; 22: 97-106.
16. Meek DW. Regulation of the p53 response and its relationship to cancer. *The Biochemical Journal*. 2015; 469: 325-346.
17. Kasthuber ER, Lowe SW. Putting p53 in Context. *Cell*. 2017; 170: 1062-1078.
18. Marcel V, Nguyen Van Long F, Diaz J. 40 Years of Research Put p53 in Translation. *Cancers*. 2018; 10: 152.
19. Seemann S, Maurici D, Olivier M, Fromental dCC, Hainaut P. The Tumor Suppressor Gene TP53: Implications for Cancer Management and Therapy. *Critical Reviews in Clinical Laboratory Sciences*. 2004; 41: 551-583.
20. Boehme KA, Blattner C. Regulation of p53--insights into a complex process. *Critical reviews in biochemistry and molecular biology*. 2009; 44: 367-392.
21. Brooks C, Gu W. The impact of acetylation and deacetylation on the p53 pathway. *Protein & Cell*. 2011; 2: 456-462.
22. Gu B, Zhu W. Surf the Post-translational Modification Network of p53 Regulation. *International Journal of Biological Sciences*. 2012; 8: 672.
23. Kruse J, Gu W. SnapShot: p53 Posttranslational Modifications. *Cell*. 2008; 133: 930.e1.
24. Meek DW, Anderson CW. Posttranslational modification of p53: cooperative integrators of function. *Cold Spring Harbor perspectives in biology*. 2009; 1: a000950.
25. Joerger AC, Fersht AR. The Tumor Suppressor p53: From Structures to Drug Discovery. *Cold Spring Harbor Perspectives in Biology*. 2010; 2.
26. Raj N, Attardi LD. The Transactivation Domains of the p53 Protein. *Cold Spring Harbor Perspectives in Medicine*. 2017; 7.
27. Lee CW, Arai M, Martinez-Yamout MA, Dyson HJ, Wright PE. Mapping the Interactions of the p53 Transactivation Domain with the KIX Domain of CBP. *Biochemistry*. 2009; 48: 2115-2124.

28. Lee CW, Martinez-Yamout MA, Dyson HJ, Wright PE. Structure of the p53 transactivation domain in complex with the nuclear receptor coactivator binding domain of CREB binding protein. *Biochemistry*. 2010; 49: 9964.
29. Walker KK, Levine AJ. Identification of a novel p53 functional domain that is necessary for efficient growth suppression. *Proceedings of the National Academy of Sciences*. 1996; 93: 15335-15340.
30. Beckerman R, Prives C. Transcriptional regulation by p53. *Cold Spring Harbor Perspectives in Biology*. 2010; 2: a000935.
31. Cho Y, Gorina S, Jeffrey PD, Pavletich NP. Crystal structure of a p53 tumor suppressor-DNA complex: understanding tumorigenic mutations. *Science*. 1994; 265: 346-355.
32. Chène P. The role of tetramerization in p53 function. *Oncogene*. 2001; 20: 2611.
33. Gaglia G, Guan Y, Shah JV, Lahav G. Activation and control of p53 tetramerization in individual living cells. *Proceedings of the National Academy of Sciences*. 2013; 110: 15497-15501.
34. Laptenko O, Tong DR, Manfredi J, Prives C. The Tail That Wags the Dog: How the Disordered C-Terminal Domain Controls the Transcriptional Activities of the p53 Tumor-Suppressor Protein. *Trends in Biochemical Sciences*. 2016; 41: 1022-1034.
35. Laptenko O, Shiff I, Freed-Pastor W, Zupnick A, Mattia M, Freulich E, Shamir I, Kadouri N, Kahan T, Manfredi J, Simon I, Prives C. The p53 C Terminus Controls Site-Specific DNA Binding and Promotes Structural Changes within the Central DNA Binding Domain. *Molecular Cell*. 2015; 57: 1034-1046.
36. Retzlaff M, Rohrberg J, Küpper NJ, Lagleder S, Bepperling A, Manzenrieder F, Peschek J, Kessler H, Buchner J. The regulatory domain stabilizes the p53 tetramer by intersubunit contacts with the DNA binding domain. *Journal of Molecular Biology*. 2013; 425: 144-155.
37. Wolkowicz R, Rotter V. The DNA binding regulatory domain of p53: See the C. *Pathologie Biologie*. 1997; 45: 785-796.
38. McKinney K, Mattia M, Gottifredi V, Prives C. p53 linear diffusion along DNA requires its C terminus. *Molecular Cell*. 2004; 16: 413-424.
39. Bullock AN, Fersht AR. Rescuing the function of mutant p53. *Nature Revisions Cancer*. 2001; 1: 68-76.
40. Arlt C, Ihling CH, Sinz A. Structure of full-length p53 tumor suppressor probed by chemical cross-linking and mass spectrometry. *PROTEOMICS*; 15: 2746-2755.

41. Tidow H, Melero R, Mylonas E, Freund SMV, Grossmann JG, Carazo JM, Svergun DI, Valle M, Fersht AR. Quaternary structures of tumor suppressor p53 and a specific p53–DNA complex. *Proceedings of the National Academy of Sciences*. 2007; 104: 12324-12329.
42. Pham N, Lucumi A, Cheung N, Viadiu H. The Tetramer of p53 in the Absence of DNA Forms a Relaxed Quaternary State. *Biochemistry (Washington)*. 2012; 51: 8055.
43. Demir Ö, Jeong PU, Amaro RE. Full-length p53 tetramer bound to DNA and its quaternary dynamics. *Oncogene*. 2016; 36: 1451.
44. Emamzadah S, Tropia L, Halazonetis TD. Crystal Structure of a Multidomain Human p53 Tetramer Bound to the Natural CDKN1A (p21) p53-Response Element. *Molecular Cancer Research*. 2011; 9: 1493-1499.
45. Jordan JJ, Menendez D, Inga A, Nourredine M, Bell D, Resnick MA. Noncanonical DNA Motifs as Transactivation Targets by Wild Type and Mutant p53. *PLoS Genetics*. 2008; 4.
46. Vyas P, Beno I, Xi Z, Stein Y, Golovenko D, Kessler N, Rotter V, Shakked Z, Haran TE. Diverse p53/DNA binding modes expand the repertoire of p53 response elements. *Proceedings of the National Academy of Sciences*. 2017; 114: 10624-10629.
47. Menendez D, Inga A, Resnick MA. The expanding universe of p53 targets. *Nature reviews.Cancer*. 2009; 9: 724-737.
48. Wang B, Xiao Z, Ren EC. Redefining the p53 response element. *Proceedings of the National Academy of Sciences*. 2009; 106: 14373-14378.
49. Wang B, Xiao Z, Ko HL, Ren E. The p53 response element and transcriptional repression. *Cell Cycle*. 2010; 9: 870-879.
50. Brown CJ, Lain S, Verma CS, Fersht AR, Lane DP. Awakening guardian angels: drugging the p53 pathway. *Nature Reviews Cancer*. 2009; 9: 862-873.
51. Freed-Pastor W, Prives C. Mutant p53: one name, many proteins. *Genes & development*. 2012; 26: 1268-1286.
52. Malkin D. Li-fraumeni syndrome. *Genes & Cancer*. 2011; 2: 475-484.
53. Schneider K, Zelle K, Nichols KE, Garber J. Li-Fraumeni Syndrome In: Adam MP, Ardinger HH, Pagon RA, Wallace SE, Bean LJ, Stephens K, Amemiya A (eds). *GeneReviews®*. University of Washington, Seattle. Seattle (WA). 1993.
54. Tollis M, Boddy AM, Maley CC. Peto's Paradox: how has evolution solved the problem of cancer prevention?. *BMC biology*. 2017; 15: 60.

55. Abegglen LM, Caulin AF, Chan A, Lee K, Robinson R, Campbell MS, Kiso WK, Schmitt DL, Waddell PJ, Bhaskara S, Jensen ST, Maley CC, Schiffman JD. Potential Mechanisms for Cancer Resistance in Elephants and Comparative Cellular Response to DNA Damage in Humans. *JAMA*. 2015; 314: 1850-1860.
56. Olivier M, Hollstein M, Hainaut P. TP53 Mutations in Human Cancers: Origins, Consequences, and Clinical Use In: *Cold Spring Harbor Perspectives in Biology* Collection. United States. 2010: 123-139.
57. Wade M, Li Y, Wahl GM. MDM2, MDMX and p53 in oncogenesis and cancer therapy. *Nature Reviews Cancer*. 2013; 13: 83-96.
58. Sionov RV, Hayon IL, Haupt Y. The Regulation of p53 Growth Suppression. *Landes Bioscience*. 2013.
59. Oren M. Regulation of the p53 tumor suppressor protein. *The Journal of biological chemistry*. 1999; 274: 36031-36034.
60. Chen J. Intra molecular interactions in the regulation of p53 pathway. *Translational Cancer Research*. 2016; 5: 639-649.
61. Kubbutat MHG, Jones SN, Vousden KH. Regulation of p53 stability by Mdm2. *Nature*. 1997; 387: 299-303.
62. Ozaki T, Nakagawara A. Role of p53 in Cell Death and Human Cancers. *Cancers*. 2011; 3: 994-1013.
63. Kruse J, Gu W. Modes of p53 Regulation. *Cell*. 2009; 137: 609-622.
64. Marine J, Jochemsen AG. Mdmx and Mdm2: brothers in arms?. *Cell Cycle (Georgetown, Tex.)*. 2004; 3: 900-904.
65. Wade M, Wang YV, Wahl GM. The p53 orchestra: Mdm2 and Mdmx set the tone. *Trends in Cell Biology*. 2010; 20: 299-309.
66. Berger M, Sionov RV, Levine AJ, Haupt Y. A Role for the Polyproline Domain of p53 in Its Regulation by Mdm2. *Journal of Biological Chemistry*. 2001; 276: 3785-3790.
67. Kussie PH, Gorina S, Marechal V, Elenbaas B, Moreau J, Levine AJ, Pavletich NP. Structure of the MDM2 oncoprotein bound to the p53 tumor suppressor transactivation domain. *Science (New York, N.Y.)*. 1996; 274: 948-953.
68. Ma J, Martin JD, Zhang H, Auger KR, Ho TF, Kirkpatrick RB, Grooms MH, Johanson KO, Tummino PJ, Copeland RA, Lai Z. A second p53 binding site in the central domain of Mdm2 is essential for p53 ubiquitination. *Biochemistry*. 2006; 45: 9238-9245.

69. Shan B, Li D, Brüscheiler-Li L, Brüscheiler R. Competitive Binding between Dynamic p53 Transactivation Subdomains to Human MDM2 Protein IMPLICATIONS FOR REGULATING THE p53-MDM2/MDMX INTERACTION. *Journal of Biological Chemistry*. 2012; 287: 30376-30384.
70. Moll UM, Petrenko O. The MDM2-p53 Interaction. *Molecular Cancer Research*. 2003; 1: 1001-1008.
71. Shangary S, Wang S. Small-Molecule Inhibitors of the MDM2-p53 Protein-Protein Interaction to Reactivate p53 Function: A Novel Approach for Cancer Therapy. *Annual review of pharmacology and toxicology*. 2009; 49: 223-241.
72. Chi S, Lee S, Kim D, Ahn M, Kim J, Woo J, Torizawa T, Kainosho M, Han K. Structural details on mdm2-p53 interaction. *The Journal of Biological Chemistry*. 2005; 280: 38795-38802.
73. Shvarts A, Steegenga WT, Riteco N, van Laar T, Dekker P, Bazuine M, van Ham RC, van der Houven, van Oordt, Hateboer G, van der Eb, A J, Jochemsen AG. MDMX: a novel p53-binding protein with some functional properties of MDM2. *The EMBO journal*. 1996; 15: 5349-5357.
74. Shadfian M, Lopez-Pajares V, Yuan Z. MDM2 and MDMX: Alone and together in regulation of p53. *Translational cancer research*. 2012; 1: 88-89.
75. Khoo KH, Hoe KK, Verma CS, Lane DP. Drugging the p53 pathway: understanding the route to clinical efficacy. *Nature Reviews. Drug Discovery*. 2014; 13: 217-236.
76. Riedinger C, McDonnell JM. Inhibitors of MDM2 and MDMX: a structural perspective. *Future Medicinal Chemistry*. 2009; 1: 1075-1094.
77. Zhang B, Golding BT, Hardcastle IR. Small-molecule MDM2-p53 inhibitors: recent advances. *Future Medicinal Chemistry*. 2015; 7: 631-645.
78. Liu M, Li C, Pazgier M, Li C, Mao Y, Lv Y, Gu B, Wei G, Yuan W, Zhan C, Lu W, Lu W. D-peptide inhibitors of the p53-MDM2 interaction for targeted molecular therapy of malignant neoplasms. *Proceedings of the National Academy of Sciences*. 2010; 107: 14321-14326.
79. Chang YS, Graves B, Guerlavais V, Tovar C, Packman K, To K, Olson KA, Kesavan K, Gangurde P, Mukherjee A, Baker T, Darlak K, Elkin C, et al. Stapled α -helical peptide drug development: A potent dual inhibitor of MDM2 and MDMX for p53-dependent cancer therapy. *Proceedings of the National Academy of Sciences of the United States of America*. 2013; 110: E3454.

80. Phan J, Li Z, Kasprzak A, Li B, Sebti S, Guida W, Schönbrunn E, Chen J. Structure-based Design of High Affinity Peptides Inhibiting the Interaction of p53 with MDM2 and MDMX. *Journal of Biological Chemistry*. 2010; 285: 2174-2183.
81. Barakat K, Mane J, Friesen D, Tuszynski J. Ensemble-based virtual screening reveals dual-inhibitors for the p53-MDM2/MDMX interactions. *Journal of Molecular Graphics & Modelling*. 2010; 28: 555-568.
82. Warner WA, Sanchez R, Dawoodian A, Li E, Momand J. Identification of FDA-approved drugs that computationally bind to MDM2. *Chemical Biology & Drug Design*. 2012; 80: 631-637.
83. Sun D, Li Z, Rew Y, Gribble M, Bartberger MD, Beck HP, Canon J, Chen A, Chen X, Chow D, Deignan J, Duquette J, Eksterowicz J, et al. Discovery of AMG 232, a Potent, Selective, and Orally Bioavailable MDM2-p53 Inhibitor in Clinical Development. *Journal of Medicinal Chemistry*. 2014; 57: 1454-1472.
84. Moschos SJ, Sandhu SK, Lewis KD, Sullivan RJ, Johnson DB, Zhang Y, Rasmussen E, Henary HA, Long GV. Phase 1 study of the p53-MDM2 inhibitor AMG 232 combined with trametinib plus dabrafenib or trametinib in patients (Pts) with TP53 wild type (TP53WT) metastatic cutaneous melanoma (MCM). *Journal of Clinical Oncology*. 2017; 35: 2575-2575.
85. Baugh EH, Ke H, Levine AJ, Bonneau RA, Chan CS. Why are there hotspot mutations in the *TP53* gene in human cancers?. *Cell Death and Differentiation*. 2018; 25: 154-160.
86. Leroy B, Anderson M, Soussi T. TP53 mutations in human cancer: database reassessment and prospects for the next decade. *Human Mutation*. 2014; 35: 672-688.
87. Merkel O, Taylor N, Prutsch N, Staber PB, Moriggl R, Turner SD, Kenner L. When the guardian sleeps: Reactivation of the p53 pathway in cancer. *Mutation Research/Reviews in Mutation Research*. 2017; 773: 1-13.
88. Soussi T, Wiman KG. TP53: an oncogene in disguise. *Cell Death and Differentiation*. 2015; 22: 1239-1249.
89. Olotu FA, Soliman MES. From mutational inactivation to aberrant gain-of-function: Unraveling the structural basis of mutant p53 oncogenic transition. *Journal of Cellular Biochemistry*; 119: 2646-2652.
90. Sabapathy K, Lane DP. Therapeutic targeting of p53: all mutants are equal, but some mutants are more equal than others. *Nature Reviews Clinical Oncology*. 2018; 15: 13.
91. Blagosklonny MV. p53 from complexity to simplicity: mutant p53 stabilization, gain-of-function, and dominant-negative effect. *The FASEB Journal*. 2000; 14: 1901-1907.

92. Monti P, Perfumo C, Bisio A, Ciribilli Y, Menichini P, Russo D, Umbach DM, Resnick MA, Inga A, Fronza G. Dominant-negative features of mutant p53 in germline carriers have limited impact on cancer outcomes. *Molecular cancer research : MCR*. 2011; 9: 271-279.
93. Willis A, Jung EJ, Wakefield T, Chen X. Mutant p53 exerts a dominant negative effect by preventing wild-type p53 from binding to the promoter of its target genes. *Oncogene*. 2004; 23: 2330-2338.
94. Miller M, Shirole N, Tian R, Pal D, Sordella R. The Evolution of TP53 Mutations: From Loss-of-Function to Separation-of-Function Mutants. *Journal of cancer biology & research*. 2016; 4.
95. Sigal A, Rotter V. Oncogenic Mutations of the p53 Tumor Suppressor: The Demons of the Guardian of the Genome. *Cancer Research*. 2000; 60: 6788-6793.
96. Soussi T. p53 alterations in human cancer: more questions than answers. *Oncogene*. 2007; 26: 2145-2156.
97. Alexandrova EM, Mirza SA, Xu S, Schulz-Heddergott R, Marchenko ND, Moll UM. p53 loss-of-heterozygosity is a necessary prerequisite for mutant p53 stabilization and gain-of-function in vivo. *Cell Death & Disease*. 2017; 8: e2661.
98. Mandinova A, Lee SW. The p53 pathway as a target in cancer therapeutics: obstacles and promise. *Science translational medicine*. 2011; 3.
99. Nguyen D, Liao W, Zeng SX, Lu H. Reviving the guardian of the genome: Small molecule activators of p53. *Pharmacology & Therapeutics*. 2017; 178: 92-108.
100. Bykov VJN, Eriksson SE, Bianchi J, Wiman KG. Targeting mutant p53 for efficient cancer therapy. *Nature Reviews Cancer*. 2018; 18: 89-102.
101. Mantovani F, Walerych D, Sal GD. Targeting mutant p53 in cancer: a long road to precision therapy. *The FEBS journal*. 2017; 284: 837-850.
102. Blandino G, Di Agostino S. New therapeutic strategies to treat human cancers expressing mutant p53 proteins. *Journal of experimental & clinical cancer research: CR*. 2018; 37: 30.
103. Muller PJ, Vousden K. Mutant p53 in Cancer: New Functions and Therapeutic Opportunities. *Cancer Cell*. 2014; 25: 304-317.
104. Bykov VJN, Issaeva N, Shilov A, Hultcrantz M, Pugacheva E, Chumakov P, Bergman J, Wiman KG, Selivanova G. Restoration of the tumor suppressor function to mutant p53 by a low-molecular-weight compound. *Nature medicine*. 2002; 8: 282-288.

105. Bykov VJN, Issaeva N, Zache N, Shilov A, Hulcrantz M, Bergman J, Selivanova G, Wiman KG. Reactivation of mutant p53 and induction of apoptosis in human tumor cells by maleimide analogs. *The Journal of Biological Chemistry*. 2005; 280: 30384-30391.
106. Zache N, Lambert JMR, Rokaeus N, Shen J, Hainaut P, Bergman J, Wiman KG, Bykov VN. Mutant p53 targeting by the low molecular weight compound STIMA-1. *Molecular Oncology*. 2008; 2: 70-80.
107. Reddy NL, Hill J, Ye L, Fernandes PB, Stout DM. Identification and structure-activity relationship studies of 3-methylene-2-norbornanone as potent anti-proliferative agents presumably working through p53 mediated apoptosis. *Bioorganic & medicinal chemistry letters*. 2004; 14: 5645-5649.
108. Lehmann S, Bykov VJN, Ali D, Andren O, Cherif H, Tidefelt U, Uggla B, Yachnin J, Juliusson G, Moshfegh A, Paul C, Wiman KG, Andersson P. Targeting p53 in Vivo: A First-in-Human Study With p53-Targeting Compound APR-246 in Refractory Hematologic Malignancies and Prostate Cancer. *Journal of Clinical Oncology*. 2012; 30: 3633-3639.
109. APR-246 Clinical Trials.
110. Tahbaz N, Subedi S, Weinfeld M. Role of polynucleotide kinase/phosphatase in mitochondrial DNA repair. *Nucleic Acids Research*. 2012; 40: 3484-3495.
111. Jilani A, Ramotar D, Slack C, Ong C, Yang XM, Scherer SW, Lasko DD. Molecular cloning of the human gene, PNKP, encoding a polynucleotide kinase 3'-phosphatase and evidence for its role in repair of DNA strand breaks caused by oxidative damage. *The Journal of biological chemistry*. 1999; 274: 24176-24186.
112. Dobson CJ, Allinson SL. The phosphatase activity of mammalian polynucleotide kinase takes precedence over its kinase activity in repair of single strand breaks. *Nucleic acids research*. 2006; 34: 2230-2237.
113. Moor NA, Lavrik OI. Protein-Protein Interactions in DNA Base Excision Repair. *Biochemistry (Moscow)*. 2018; 83: 411-422.
114. Krokan HE, Bjørås M. Base Excision Repair In: DNA repair, Mutagenesis, and Other Responses to DNA Damage. Cold Spring Harbor Lab. Cold Spring Harbor Perspectives in Biology. 2013: 45-66.
115. Abbotts R, Wilson DM. Coordination of DNA single strand break repair. *Free Radical Biology and Medicine*. 2017; 107: 228-244.
116. Caldecott KW. DNA single-strand break repair. *Experimental Cell Research*. 2014; 329: 2-8.

117. Davis AJ, Chen DJ. DNA double strand break repair via non-homologous end-joining. *Translational Cancer Research*. 2013; 2: 130-143.
118. Ranjha L, Howard SM, Cejka P. Main steps in DNA double-strand break repair: an introduction to homologous recombination and related processes. *Chromosoma*. 2018; 127: 187-214.
119. Povirk LF. Processing of damaged DNA ends for double-strand break repair in mammalian cells. *ISRN molecular biology*. 2012; 2012.
120. Ceccaldi R, Rondinelli B, D'Andrea AD. Repair Pathway Choices and Consequences at the Double-Strand Break. *Trends in Cell Biology*. 2016; 26: 52-64.
121. Mani RS, Karimi-Busheri F, Fanta M, Cass CE, Weinfeld M. Spectroscopic Studies of DNA and ATP Binding to Human Polynucleotide Kinase: Evidence for a Ternary Complex. *Biochemistry*. 2003; 42: 12077-12084.
122. Lu M, Mani RS, Karimi-Busheri F, Fanta M, Wang H, Litchfeld DW, Weinfeld M. Independent mechanisms of stimulation of polynucleotide kinase/phosphatase by phosphorylated and non-phosphorylated XRCC1. *Nucleic Acids Research*. 2010; 38: 510-521.
123. Aceytuno RD, Pieltz CG, Havali-Shahriari Z, Edwards RA, Rey M, Ye R, Javed F, Fang S, Mani R, Weinfeld M, Hammel M, Tainer JA, Schriemer DC, et al. Structural and functional characterization of the PNKP-XRCC4-LigIV DNA repair complex. *Nucleic Acids Research*. 2017; 45: 6238-6251.
124. Coquelle N, Havali-Shahriari Z, Bernstein N, Green R, Glover JNM. Structural basis for the phosphatase activity of polynucleotide kinase/phosphatase on single- and double-stranded DNA substrates. *Proceedings of the National Academy of Sciences of the United States of America*. 2011; 108: 21022-21027.
125. Garces F, Pearl LH, Oliver AW. The Structural Basis for Substrate Recognition by Mammalian Polynucleotide Kinase 3' Phosphatase. *Molecular cell*. 2011; 44: 385-396.
126. Bernstein NK, Karimi-Busheri F, Rasouli-Nia A, Mani R, Dianov G, Glover JNM, Weinfeld M. Polynucleotide kinase as a potential target for enhancing cytotoxicity by ionizing radiation and topoisomerase I inhibitors. *Anti-Cancer Agents in Medicinal Chemistry*. 2008; 8: 358-367.
127. Panganiban RM, Snow AL, Day RM. Mechanisms of Radiation Toxicity in Transformed and Non-Transformed Cells. *International Journal of Molecular Sciences*. 2013; 14: 15931-15958.

128. Henner WD, Grunberg SM, Haseltine WA. Enzyme Action at 3'-Termini of Ionizing Radiation-Induced Dna Strand Breaks. *Journal of Biological Chemistry*. 1983; 258: 5198-5205.
129. Pommier Y, Leo E, Zhang H, Marchand C. DNA Topoisomerases and Their Poisoning by Anticancer and Antibacterial Drugs. *Chemistry & biology*. 2010; 17: 421-433.
130. Connolly ID, Hixson JD, Nagpal S. An overview of DNA topoisomerase I inhibitors under development. *Drugs of the Future*. 2016; 41: 731.
131. Hosoya N, Miyagawa K. Targeting DNA damage response in cancer therapy. *Cancer Science*. 2014; 105: 370-388.
132. Li F, Jiang T, Li Q, Ling X. Camptothecin (CPT) and its derivatives are known to target topoisomerase I (Top1) as their mechanism of action: did we miss something in CPT analogue molecular targets for treating human disease such as cancer?. *American Journal of Cancer Research*. 2017; 7: 2350-2394.
133. Pearl LH, Schierz AC, Ward SE, Al-Lazikani B, Pearl FMG. Therapeutic opportunities within the DNA damage response. *Nature Reviews. Cancer*. 2015; 15: 166-180.
134. Vens C, Begg AC. Targeting base excision repair as a sensitization strategy in radiotherapy. *Seminars in Radiation Oncology*. 2010; 20: 241-249.
135. Gavande NS, VanderVere-Carozza PS, Hinshaw HD, Jalal SI, Sears CR, Pawelczak KS, Turchi JJ. DNA repair targeted therapy: The past or future of cancer treatment?. *Pharmacology & Therapeutics*. 2016; 160: 65-83.
136. Rasouli-Nia A, Karimi-Busheri F, Weinfeld M. Stable down-regulation of human polynucleotide kinase enhances spontaneous mutation frequency and sensitizes cells to genotoxic agents. *Proceedings of the National Academy of Sciences of the United States of America*. 2004; 101: 6905-6910.
137. Chalasani SL, Kawale AS, Akopiants K, Yu Y, Fanta M, Weinfeld M, Povirk LF. Persistent 3'-phosphate termini and increased cytotoxicity of radiomimetic DNA double-strand breaks in cells lacking polynucleotide kinase/phosphatase despite presence of an alternative 3'-phosphatase. *Dna Repair*. 2018; 68: 12-24.
138. Wiederhold L, Leppard JB, Kedar P, Karimi-Busheri F, Rasouli-Nia A, Weinfeld M, Tomkinson AE, Izumi T, Prasad R, Wilson SH. AP endonuclease-independent DNA base excision repair in human cells. *Molecular cell*. 2004; 15: 209-220.
139. Freschauf GK, Karimi-Busheri F, Ulaczyk-Lesanko A, Mereniuk TR, Ahrens A, Koshy JM, Rasouli-Nia A, Pasarj P, Holmes CFB, Rininsland F, Hall DG, Weinfeld M. Identification of a Small Molecule Inhibitor of the Human DNA Repair Enzyme Polynucleotide Kinase/Phosphatase. *Cancer research*. 2009; 69: 7739-7746.

140. Freschauf GK, Mani RS, Mereniuk TR, Fanta M, Virgen CA, Dianov GL, Grassot J, Hall DG, Weinfeld M. Mechanism of Action of an Imidopiperidine Inhibitor of Human Polynucleotide Kinase/Phosphatase. *Journal of Biological Chemistry*. 2010; 285: 2351-2360.
141. Srivastava P, Sarma A, Chaturvedi CM. Targeting DNA repair with PNKP inhibition sensitizes radioresistant prostate cancer cells to high LET radiation. *PLOS ONE*. 2018; 13: e0190516.
142. Nijman SMB. Synthetic lethality: General principles, utility and detection using genetic screens in human cells. *Febs Letters*. 2011; 585: 1-6.
143. Mereniuk TR, El Gendy MA, Mendes-Pereira AM, Lord CJ, Ghosh S, Foley E, Ashworth A, Weinfeld M. Synthetic lethal targeting of PTEN-deficient cancer cells using selective disruption of polynucleotide kinase/phosphatase. *Molecular cancer therapeutics*. 2013; 12: 2135-2144.
144. Mereniuk TR, Maranchuk RA, Schindler A, Penner-Chea J, Freschauf GK, Hegazy S, Lai R, Foley E, Weinfeld M. Genetic Screening for Synthetic Lethal Partners of Polynucleotide Kinase/Phosphatase: Potential for Targeting SHP-1-Depleted Cancers. *Cancer Research*. 2012; 72: 5934-5944.
145. Allinson SL. DNA end-processing enzyme polynucleotide kinase as a potential target in the treatment of cancer. *Future Oncology (London, England)*. 2010; 6: 1031-1042.

Chapter 2

Ranking the binding energies of p53 mutant activators and their ADMET properties

Preface

This chapter is the accepted version of the article:

Omar SI, Tuszynski J. Ranking the Binding Energies of p53 Mutant Activators and Their ADMET Properties. Chemical Biology & Drug Design 2014; 86.

which has been published in final form at [\[https://doi.org/10.1111/cbdd.12480\]](https://doi.org/10.1111/cbdd.12480). This article may be used for non-commercial purposes in accordance with the Wiley SelfArchiving Policy: [\[https://authorservices.wiley.com/author-resources/JournalAuthors/licensing-open-access/open-access/self-archiving.html\]](https://authorservices.wiley.com/author-resources/JournalAuthors/licensing-open-access/open-access/self-archiving.html).

Note: This chapter has been modified for consistency with the rest of the thesis; the methods section has been moved to the end of the chapter, some abbreviations and referencing style have been changed and supplementary material in the original publication has been moved to the body of the chapter. Additional information has been added to the discussion section for clarification.

2.1 Introduction

In normal cells, p53 functions as a transcription factor that plays major roles in the regulation of the cell cycle, DNA repair, senescence and apoptosis [1-4]. The p53-signalling pathway is inoperative in almost all types of human cancer cells [5]. Among the vast number of mechanisms exploited by cancer cells to sustain cell division, the inactivation of p53 is one of the most frequent and effective strategies [2]. This is done through different mechanisms including genetic deletion [6], defective post-translational modifications and interactions with MDM2 [7] and MDM4 [8], which are endogenous inhibitors to p53. To overcome these mechanisms, such as MDM2/4 inhibition, some strategies involved the disruption of p53-MDM protein interactions [9-11] using small ligands [12-15]. Another effective strategy to impair p53-signalling by cancer cells is through the genetic mutation of p53 [2]; it is the most mutated protein found in human cancers [16,17]. In fact, p53 is mutated in more than 50% of all cancer cells [5,16] leading to loss of its tumor suppressor function. More than 75% of p53 mutations are missense mutations and over 97% of these are located in the DNA binding domain (DBD) of p53 [18,19]. There are six 'hot-spots' that make 40% of the DBD mutations; they are single amino-acid substitutions in the DBD domain in the following residues: R175, G245, R248, R249, R273 and R282 [20]. Sarcomas and lymphomas have been shown to be less invasive on restoration of the wild-type (wt) activity of mutant p53 (mp53) in mice [18,21].

Several screening studies have helped identify small molecules that could restore mp53. The most successful of these molecules are PRIMA-1 and its methylated derivative, APR-246

[22]. In fact, the latter is the only drug candidate currently in clinical trials [23]. In cells, both PRIMA-1 and APR-246 decompose to give an active metabolite called methylene quinuclidione (MQ), characterized by a reactive double bond (DB) [24]. Evidence suggests that MQ can restore the wt activity to mp53 by reacting with the protein and was, therefore classified as an alkylating ligand [24]. In another screening study by the same group, MIRA-1 was also identified as an activator of mp53 [25]. Interestingly, this latter compound was originally characterized as being structurally different from PRIMA-1 [25]. At the time, it was not yet known that MQ is the active metabolite of PRIMA-1 [24]. Both MIRA-1 and MQ share the same characteristic feature: a reactive DB.

Other activators of mutated p53 are currently actively being identified and tested. Foster *et al.* [26] identified CP-31398 through a screening study. There are conflicting reports regarding the mechanism of action of CP-31398. While it has been suggested that CP-31398 does not bind to p53 [27], most studies indicate that the molecule interacts with mp53, restores its wt conformation [26,28] and induces cell-cycle arrest and apoptosis [29]. It has also been suggested that it can be classified as an alkylating ligand [24]. 3-Methylene-2-norbornanone (NB) is another ligand that was designed based on structure-activity relationship studies that included CP-31398 and PRIMA-1 [30]. STIMA-1, also an alkylating ligand, was designed based on CP-31398 [31].

The active metabolite of WR-2721, called WR-1065, has also been shown to restore the wt function and conformation of mp53 [32,33]. The alkaloid ellipticine and its derivatives including 9-hydroxyellipticine are the only naturally occurring ligands, which were found to activate mp53 [34]. Studies have shown that this class of compounds exerts an antitumor

effect through multiple mechanisms including: inhibition of phosphorylation [35], topoisomerase enzyme inhibition [34] and by restoring DNA binding of mp53 [36,37].

Although the exact mechanism of restoration of wt function to the different p53 mutant has not yet been fully characterized, there is evidence that several of these molecules, specifically alkylating ligands, bind covalently to thiol groups in p53 [24]. In a more recent study, a transiently open pocket between loop1 and sheet S3 in p53 mutants R175H (R175H-mp53), G245S (G245S-mp53) and R273H (R273H-mp53) has been identified [38]. This study has demonstrated that C124 is essential for the activity of PRIMA-1 on R175H-mp53 using site-directed mutagenesis. Docking of MQ, NB, MIRA-1 and STIMA-1 was performed and their potential interacting residues were identified. In addition, stictic acid was identified from the first virtual screening study performed on the pocket.

In our study, we performed docking experiments on PRIMA-1, APR-246, MQ, NB, MIRA-1, STIMA-1, stictic acid, ellipticine, 9-hydroxy-ellipticine, CP-31398, WR-1065 and WR-2721 to test and rank the binding of these compounds at the L1/S3 pocket of p53-R273H (one of the hot-spot mutations). We also calculated the ADMET properties of these compounds as they provide important implications regarding the potential of the respective compound for their future clinical use.

2.2 Results

2.2.1 Equilibration and representative structure extraction of R273H-mp53

To model the binding of the ligands to R273H-mp53, residue 273 of wt-p53 was virtually mutated to histidine using Swiss-PdbViewer [39] and simulated for 80 ns. The root-mean-square-deviation (RMSD) of the backbone atoms of p53 (excluding the last 3 residues at each terminus) was calculated over 80 ns with reference to their positions at the start of the simulation (Figure 2.1). It can be readily seen that the RMSD plateaus after 20 ns and fluctuates within a very narrow range till 80 ns.

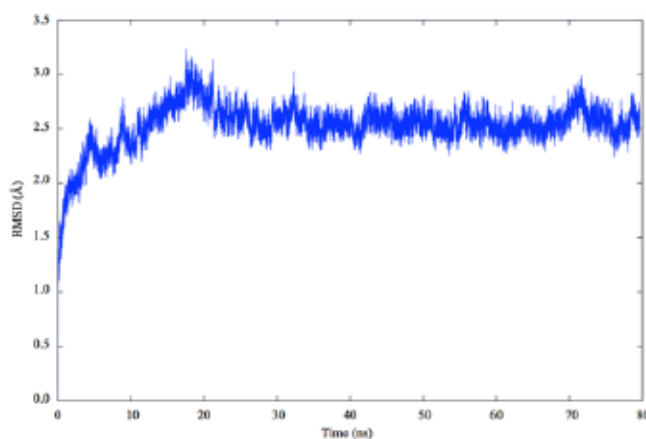


Figure 2.1. Plot of the RMSD of backbone atoms of residues 99 to 286 of p53-R273H model with reference to the structure at 0 ns.

The last 20 ns of the molecular dynamics (MD) simulation of the equilibrated mutant, represented by 2001 structures, were clustered using the average-linkage algorithm. Clustering was based on the mass-weighted RMSD of all the atoms of residues 114 to 117, 121 to 126, 133 and 140 to 144 of mp53. The plots for the DBI and SSR/SST (ratio of the

sum of squares regression to the total sum of squares) values for cluster counts of 2 to 100 are shown in Figure 2.2. The cluster count of 42 was chosen as the optimum cluster count. The representative structures of clusters that had $\geq 2\%$ of the total number of snapshots were used for docking. A total of eight clusters, which represent $\sim 87\%$ of the clustered snapshots, fulfilled this criterion. These were cluster numbers: 1 (1270 points), 4 (53 points), 8 (66 points), 9 (118 points), 10 (59 points), 14 (60 points), 20 (70 points) and 27 (42 points).

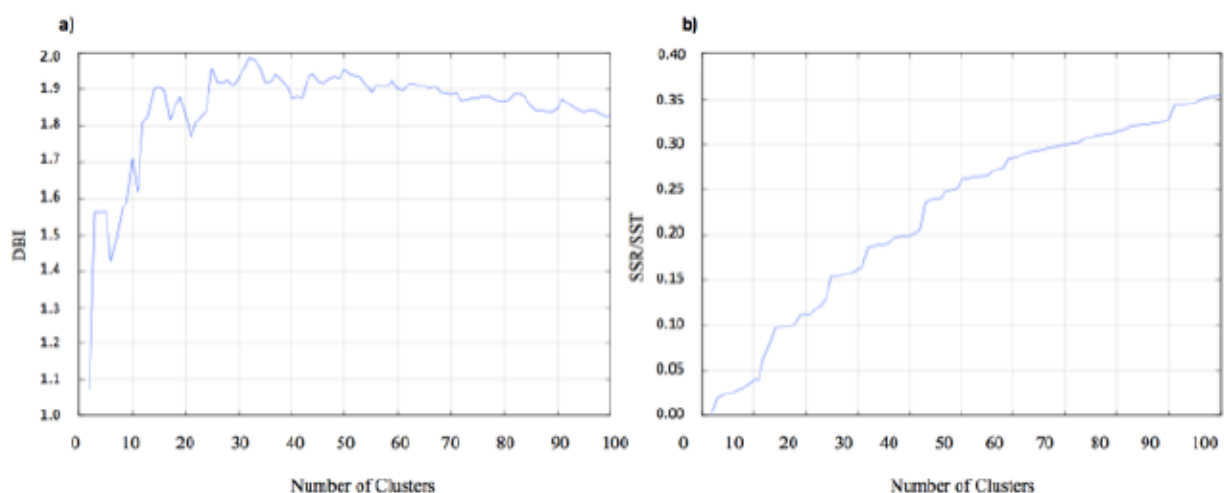


Figure 2.2. a) Plot of DBI and b) SSR/SST values for cluster counts from 2 to 100. The optimum number of clusters occurs at a local minimum DBI value and when SSR/SST values have reached a plateau. Cluster count of 42 was chosen to represent R273H-mp53.

2.2.2 Docking small ligand activators to R273H-mp53

PHIKAN083 was docked to mutant p53-Y220C (Y220C-mp53) to validate the parameters used for docking. Autodock 4.2 [40] was able to predict the correct binding pose with an 80% success rate. The RMSD of the binding pose with the least energy was 0.97 Å compared to that of the crystal structure (Figure 2.3).

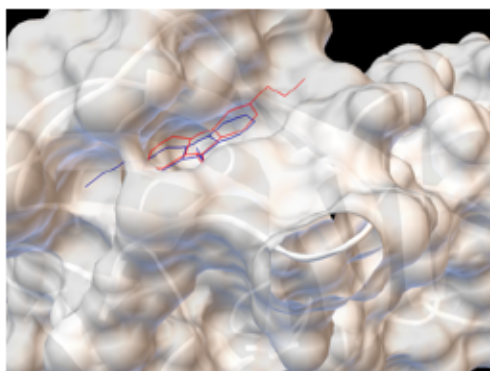


Figure 2.3. The top predicted pose of PHIKAN083 in Y220C-mp53. White= molecular surface of Y220C-mp53, red= predicted pose from docking, blue = experimentally-determined pose of PHIKAN083.

The ligands PRIMA-1, APR-246, MQ, NB, STIMA-1, MIRA-1, stictic acid, CP-31398, ellipticine, 9-hydroxy-ellipticine, WR-1065 and WR-2721 were all docked in the eight p53-R273H mutant representative structures using Autodock 4.2. The pose with the lowest energy (highest affinity) in the most populated docking cluster was chosen to represent the binding position of the respective ligand to the pocket near C124.

Docking results show that MQ, NB, STIMA-1 and MIRA-1 are all positioned within the same region of the binding pocket (Figure 2.4). Figure 2.5 shows that all four ligands interact with the backbone atoms of S116 and G117. MQ and NB have additional interactions with R282. On the other hand, MIRA-1 and STIMA-1 interact with the side-chain of S116 and the latter has an additional interaction with L114. While our simulations did not reveal a direct interaction of the ligands with C124, their reactive DB was positioned towards the thiol group of C124. The distances between the backbone hydrogen of S116 and the side-chain sulphur of C124 are shown in Table 2.1.

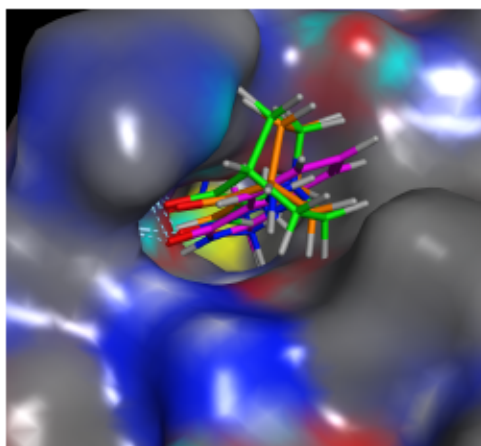


Figure 2.4. Docked poses showing MQ (green), NB (orange), MIRA-1 (blue) and STIMA-1 (pink) all binding at the same position and showing common interactions with residues S116 and G117.

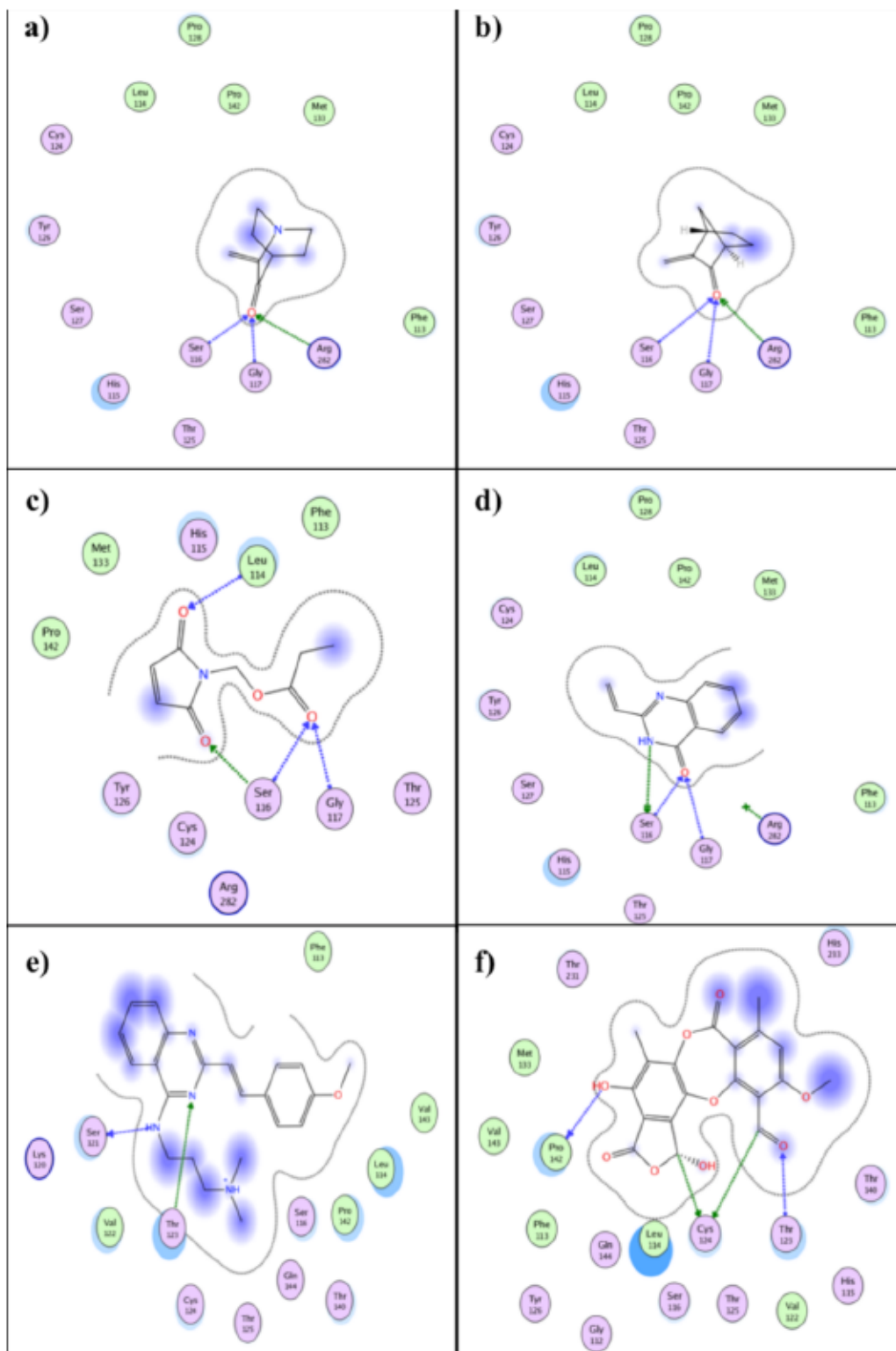


Figure 2.5. Ligand-interaction schemes of the alkylating ligands (a) MQ (b) NB (c) MIRA-1 (d) STIMA-1 (e) CP-31398 and (f) Stictic acid with R273H-mp53. DB of the first five ligands is positioned towards the thiol of C124.

Table 2.1. A list of distances between S116 H and C124 S for MQ, NB, STIMA-1 and MIRA-1 as well as the distance between Ser121 O and C124 S.

The table also shows a list of distances between the respective ligands DB and C124 S distance.

Ligand	SerO/H - C124 Distance (Å)	Ligand DB - C124 Distance (Å)
MQ	7.98	6.98
STIMA-1	7.82	3.58
MIRA-1	7.82	3.2
NB	8.22	6.83
CP	9.05	4.16

CP-31398 is also considered as an alkylating ligand, although it is less reactive [31]. The ligand interaction scheme in Figure 2.5 shows that CP-31398 likely interacts with Ser121 backbone atoms through its amine group. It also interacts with T123 through the nitrogen in its quinazoline ring. Although its reactive DB does not interact with C124, it is still positioned towards the thiol group of C124. The distance between the reactive DB of CP-31398 and the thiol group of C124 is also shown in Table 2.1. Docking results for stictic acid, which has also been proposed to act as an alkylating ligand [38], show that it interacts with the backbone of T123 and P142. In addition, it interacts with the side-chain thiol of C124.

Since MQ is considered as the active metabolite of PRIMA-1 and APR-246, the two parent compounds were also docked into the same pocket. These compounds are both generally considered inactive, as they do not have the reactive DB present in other alkylating ligands. The best docked pose for each ligand showed that they both interacted in an almost identical manner (Figure 2.6) with residues T123 and C124.

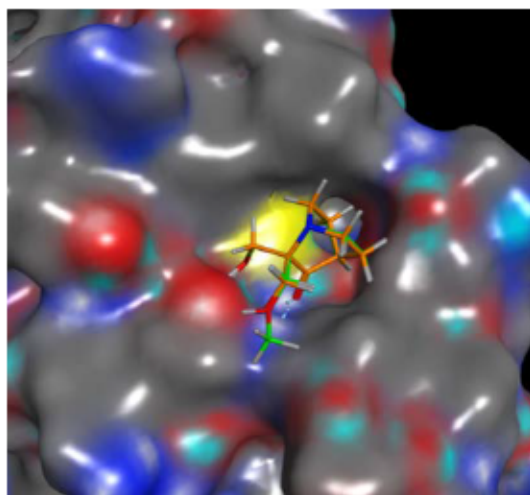


Figure 2.6. Docked pose for PRIMA-1 (orange) and APR-246 (green) in R273H-mp53.

In the best binding pose for both ellipticine and 9-hydroxy-ellipticine, the two ligands both interacted with the backbone of C124 (Figure 2.7). The more active 9-hydroxy-ellipticine [34] had an additional arene-H interaction with the side-chain of C124. On the other hand, the best docked poses for the prodrug WR-2721 and its active metabolite WR-1065 had significant differences. Although they both bind at the same location of the pocket, the ligands' orientations were 'flipped' when compared to each other; the sulphhydryl group of WR-1065 was buried in the binding pocket while in WR-2721 the phosphate head was towards the open part of the pocket. However, both ligands interacted with residues L114, S116, T123 and C124 but WR-1065 had an additional interaction with P142 while WR-2721 had an additional interaction with V122 (Figure 2.7).

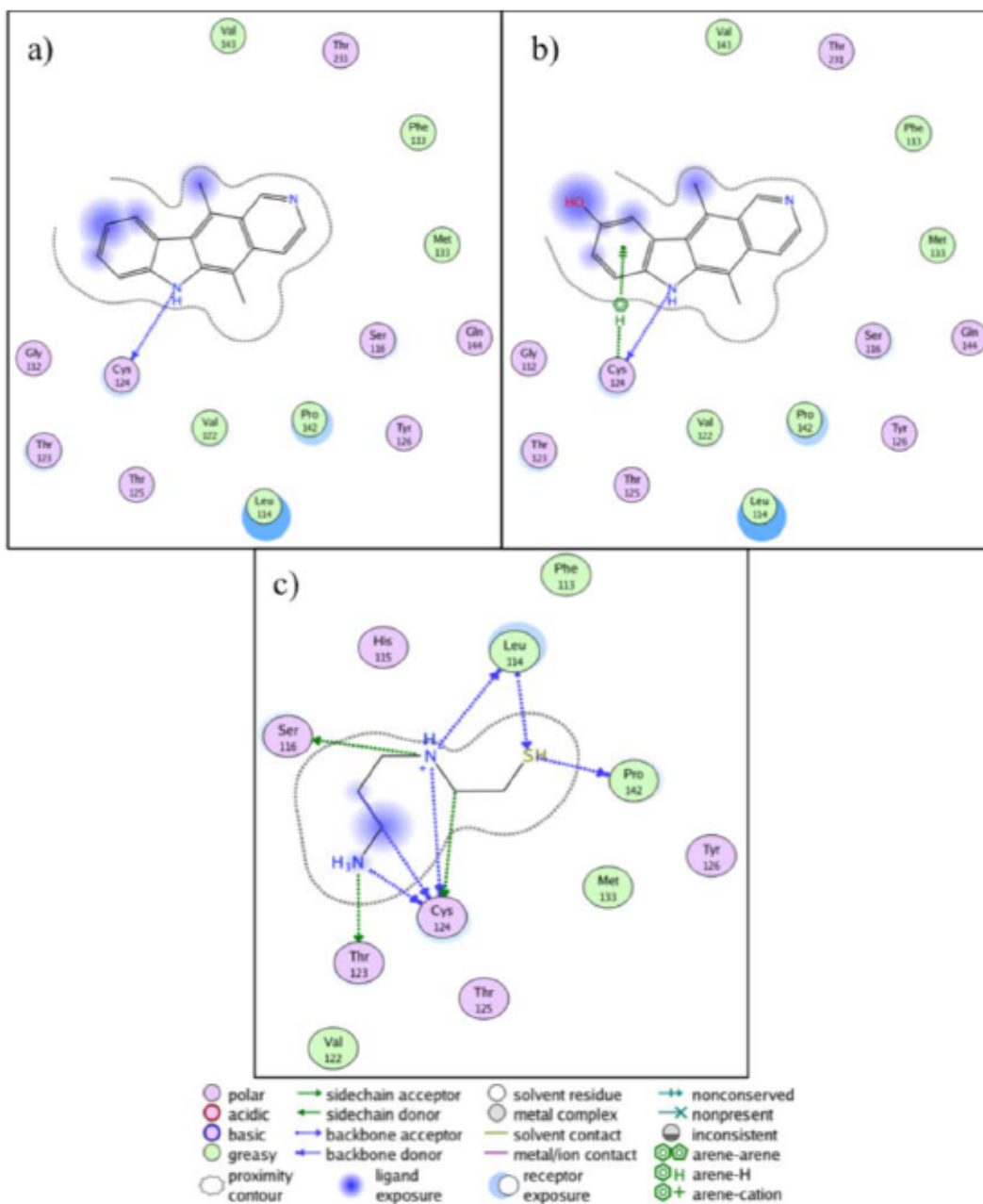


Figure 2.7. Ligand-interactions scheme showing the interacting residues between R273H-mp53 and a) ellipticine, b) 9-OH ellipticine and c) WR-1065

As mentioned above, MQ, NB, MIRA-1 and STIMA-1 interact with the backbone hydrogen of S116 and have been proposed to undergo a Michael addition reaction to the sulphur of C124 through their DB. The distances between the backbone hydrogen of S116 and sulphur of C124 were, therefore, measured over the course of the 80 ns simulation using ptraj utility

[41]. Figure 2.8 shows that the distance between these two atoms fluctuates from ~ 4.5 Å to ~ 10.9 Å. Similarly the distance between C124 sulphur atoms and the backbone oxygen of S121 (with which CP-31398 interacts) were also calculated. Fluctuations in the measured distances ranged from ~ 7.2 Å to ~ 11.7 Å, as shown in Figure 2.8b.

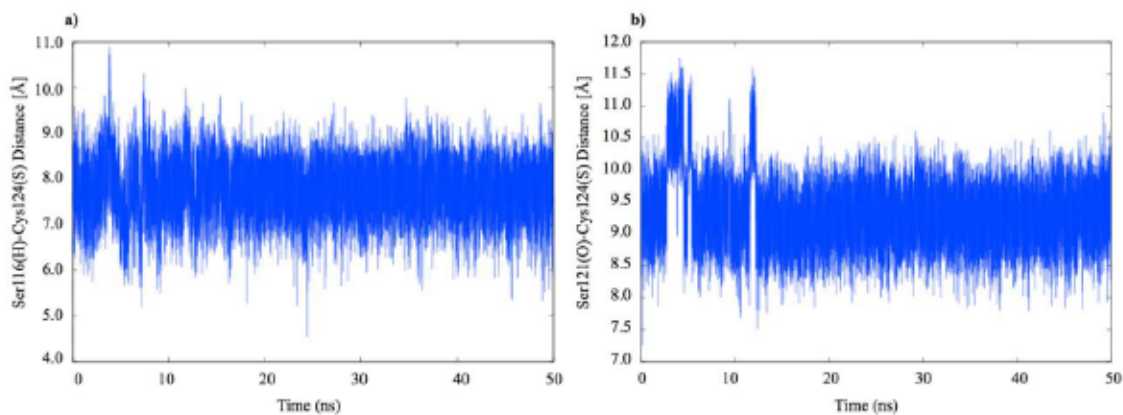


Figure 2.8. Plots of the distances between a) S116 (H) and C124 (S) and b) Ser121 (O) and C124 (S) during the last 50 ns of the simulation.

Autodock 4.2 binding energies and ligand efficiencies of the best binding poses for each ligand are listed in Table 2.2 and compared to their experimental IC_{50} .

Table 2.2. A list of Autodock binding energies (kcal·mol⁻¹) and ligand efficiencies in the order of decreasing binding energies.

The corresponding experimental IC₅₀ for each ligand is also shown. NA= not available and the dash indicates that the ligand is in the inactive form.

COMPOUND	Autodock 4.2 Binding Energy (kcal·mol ⁻¹)	Autodock 4.2 Ligand efficiency	Experimental IC ₅₀ (μM)
Stictic acid	-8.74	-0.31	NA
CP-31398	-8.01	-0.3	NA
STIMA-1	-7.63	-0.58	4.9
Ellipticine	-7.47	-0.39	NA
9-OH Ellipticine	-7.11	-0.36	NA
MIRA-1	-6.33	-0.49	10
NB	-5.92	-0.66	NA
MQ	-5.21	-0.52	14.8 ± 3.9
PRIMA-1	-4.88	-0.31	-
APR-246	-4.88	-0.38	-
WR-1065	-3.78	-0.47	NA
WR-2721	-3.69	-0.31	-

2.2.3 ADMET properties of the ligands

ADMET Predictor™ software calculates the various physico-chemical properties of chemical compounds of importance to the prediction of their pharmacokinetic profiles including absorption, distribution, metabolism, excretion and toxicity (ADMET). All compounds tested by us using this software package comply with Lipinski's Rule-of-five [42] which indicates

that they are drug-like. Table 2.3 shows that the compounds have a wide range of ADMET scores ranging from 1 (APR-246) to about 7 (CP-31398). A low score indicates low risk of toxicity while a high score virtually assures the existence of toxic risks. In addition, all compounds have a high blood-brain-barrier partition coefficient with the exception of stictic acid and the prodrug WR-2721. CP-31398 is predicted to inhibit hERG potassium channel raising concerns of cardiotoxicity. Although ellipticine also inhibits these channels, its 9-hydroxyl derivative is predicted to lack this effect. While PRIMA-1 is predicted to cause an elevation in alanine transaminase (ALT) and aspartate transaminase (AST) enzymes, its derivative APR-246, which is currently in clinical trials, is predicted not to have this effect on the levels of ALT and AST enzymes (confidence of 67% and 57% respectively). However, the active metabolite of both compounds, MQ, causes an elevation in both liver enzymes. All the other alkylating ligands, along with CP-31398, cause an increase in both AST and ALT liver enzymes, with the exception of stictic acid, which is predicted to cause an elevation of ALT enzyme only.

Table 2.3. ADMET Predictor™ estimations for the docked ligands.

An explanation of each property can be found in the methods section. Percentages between brackets are percentages of confidence. Toxicity terms are explained in 2.5.5.

Compounds	S + Peff [cm/s*10 ⁴]	S + Sw [mg/mL]	BBB_Filter	Pgp_Substr	Pgp_Inh	TOX_hERG_Filter	TOX_SGOT	TOX_SGPT	ADMET_Risk
APR-246	3.16	48.000	High	No (97%)	No (94%)	No (95%)	Normal (67%)	Normal (57%)	1
WR-1065	0.44	62.700	High	No	No (94%)	No (95%)	Normal	Normal (99%)	2.1
Stictic acid	2.3	0.013	Low	Yes (71%)	No (60%)	No (95%)	Normal (73%)	Elevated (55%)	2.46
MIRA-1	3.93	9.150	High	No (97%)	No (94%)	No (95%)	Elevated (94%)	Elevated (93%)	2.73
STIMA-1	4.82	0.221	High	No (97%)	No (94%)	No (95%)	Elevated	Elevated (98%)	2.91
WR-2721	0.26	5.010	Low	No (97%)	No (94%)	No (95%)	Normal (62%)	Normal (99%)	2.97

NB	8.01	4.980	High	No (97%)	No (94%)	No (95%)	Elevated (94%)	Elevated (79%)	3
PRIMA-1	2.16	83.900	High	No (97%)	No (94%)	No (95%)	Elevated (71%)	Elevated (84%)	3
MQ	4.94	24.500	High	No (97%)	No (94%)	No (95%)	Elevated (94%)	Elevated (79%)	3.01
90H-Ellipticine	4.28	0.008	High	Yes (67%)	No (94%)	No (76%)	Normal (73%)	Elevated	4.86
Ellipticine	6.16	0.002	High	No (97%)	No (94%)	Yes (63%)	Normal (67%)	Elevated	5.6
CP-31398	2.06	0.250	High	Yes (95%)	Yes (97%)	Yes (99%)	Elevated (94%)	Elevated (84%)	6.92

2.3 Discussion

The transcription factor protein, p53, plays a pivotal role in cells as a tumor suppressor as it responds to different types of cellular stress and performs an important function to repair DNA damage, cause cell-cycle arrest and induce cell senescence or apoptosis [1-4] in cases of severe cell damage. Several ligands were found to act as p53 activators: they restore the wild type activity to mp53. Hence, these compounds hold significant promise of improving clinical outcomes by being used in the future in a combination therapy regimen for cancer patients undergoing chemotherapy. A recent study has used computational methods to identify a transiently open L1/S3 pocket near residue C124 of wt, R175H, G245S and R273H mt-p53 at which MQ, NB, STIMA-1 and MIRA-1 bind [38]. Based on the structures of docked compounds, it is clear that they can be classified as alkylating (MQ, NB, MIRA-1, STIMA-1, stictic acid and CP-31398) and non-alkylating (ellipticine, 9-hydroxy derivative and WR-1065), respectively.

2.3.1 Creating representative structure for C124 binding pocket

In this study, we modeled the 3D structure of one of the most common p53 mutants, namely R273H-mp53 and simulated it for 80 ns. A plateau in the RMSD plot (Figure 2.1) after ~30 ns indicates that the protein structure has equilibrated. Although it would be best to dock the ligands to all structures obtained from the MD simulation, this is impractical at present by being very computationally expensive. While there is no definitive method to choose the optimum number of clusters, DBI and SSR/SST metrics were used to guide the choice of the optimal cluster number. Although SSR/SST value does not completely plateau (Figure 2.2), it

becomes more stable after the cluster count of 42. This coincides with a local minimum in the DBI value at the same point. To make the computer simulations more efficient, eight representative structures were extracted, which represent ~87% of the conformations of the pocket around C124 for the last 20 ns of the simulation.

2.3.2 Docking p53 activators to R273H-mp53

MQ, NB, STIMA-1 and MIRA-1 have been all previously docked into the C124 pocket [38]. However, this is the first study to dock the other ligand activators as discussed earlier. It must be noted that the calculations in this study were all based on molecular mechanics, thus it is impossible to predict the alkylated form of the protein using these calculations. All alkylating ligands interacted with S116 and G117, with the exception of stictic acid and CP-31398, which are much bulkier when compared to the other compounds and therefore less likely to fit into that part of the pocket. It is interesting that both parent compounds of MQ had direct interactions with C124 but compounds with the reactive DB did not. The only exception to this observation was stictic acid, which came from virtual screening studies that were based on the initial assumption that alkylating ligands interact with C124 backbone. It should be noted that stictic acid did not maintain its direct interaction with C124 after a 60 ns simulation [38]. This suggests that binding positions at this pocket are only initial interactions after which the ligand undergoes a reaction with the thiol group [24] of C124. This could explain why our simulation showed that PRIMA- and APR-246 interact with mt-p53. However, they would not be expected to react since they are missing the reactive DB. This is also evident from the interactions between stictic acid and R175H-mp53 after a 60 ns simulation; stictic acid had direct interactions with Q144 only and indirect interactions with G112, S116 and C124 through bridging water molecules [38]. In all cases, however, the DB of the alkylating

ligands was always positioned towards C124. An aliphatic C-S covalent bond length has reported to be about 1.82 Å [43] while their non-bonded interactions range between 3.8-4.2 Å in length [44]. MOE ligand interactions [45] did not predict an interaction between the DB of the alkylating ligands and S of C124. While Table 2.1 shows that STIMA-1, MIRA-1 and CP-31398 are at a distance that lies within the non-bonded interactions range of 3.8-4.2 Å, it is probable that the geometry between the DB and S of C124 does not favor the formation of an interaction. Since docking was performed using the rigid protein structure, the effect of ligands' binding on the complex structure cannot be observed in the ligand-binding pose. Note that the distance between MQ and NB is too large to form an interaction: 6.98 Å and 6.83 Å, respectively. For this reason, the distances between S116 backbone H/S121 backbone O and C124 side-chain S were measured over the last 50 ns of the simulation. S116 backbone H-C124 S distance in the predicted MQ and NB complexes were 7.98 Å and 8.22 Å, respectively. Figure 2.8 shows that these distances fluctuate significantly reaching a minimum of 4.5 Å, which suggests that the two ligands could actually get close enough to interact with C124.

Our docking studies have shown that PRIMA-1 and APR-246 interact with T123 and C124. Experimental studies have shown that PRIMA derivatives, such as PRIMA-D, that are incapable of breaking down to form MQ were inactive [24]. This observation suggests that these compounds do not bind in their native form and are metabolized to MQ before binding. It has not been confirmed that ellipticine and 9-hydroxy-ellipticine interact directly with mutant R273H-mp53 although they can restore the wt conformation to the mutant. Ellipticine and its 9-hydroxy derivative bind at the same location but the latter, which is more active [34], forms an additional arene-H interaction. Note that these two compounds interact directly

with C124, unlike alkylating agents. Ellipticine has not been found to thermally stabilize p53 when compared to CP-31398 [37]. It was, therefore, suggested that ellipticine activated mp53 through a different mechanism, which has not yet been exactly identified [46]. Our docking results showing the different interaction properties can explain these observations. It is conceivable that CP-31398 can thermally stabilize mp53 because it binds covalently to the protein. Since ellipticine non-covalently interacts with the protein, it could lose the interaction with mp53 at higher temperatures and hence cannot thermally stabilize the protein. On the other hand, the orientation of WR-1065 in the binding pocket was flipped when compared to its prodrug WR-2721. It is worth mentioning that WR-1065 and WR-2721 both showed very poor clustering when the docked poses were clustered at 1 Å; each cluster had $\leq 10\%$ of the docked poses. This could be explained by their flexibility and is consistent with a study by North *et al.* [33], which found that WR-1065 only resulted in partial restoration of the mutant p53-V272M conformation. However, poor clustering properties could also suggest that WR-1065 does not bind at that pocket since there was no prominent docked pose.

It is also interesting that the predicted Autodock binding energies qualitatively correlate with the experimental IC_{50} values for MQ [24] (PRIMA-1), STIMA-1 [31] and MIRA-1 [25]. Table 2.2 shows that STIMA-1, which has the least binding energy has the lowest IC_{50} for Saos R273H-mp53 cells while MQ, which has the most binding energy has the highest IC_{50} value.

It is worth mentioning that more rigorous but computationally much more expensive methods, such as thermodynamic integration, are likely to give more accurate binding energies.

2.3.3 Predicting ADMET properties of p53 activator compounds

As these compounds are potential chemotherapeutics, it is expected that they would have adverse effects as reflected by their ADMET_Risk score; however, their benefits should outweigh their adverse effects for a practical clinical use. The main task is to find a suitable therapeutic window in a pre-clinical and clinical efficacy and toxicity studies focusing on dose escalation and on finding a maximum tolerated dose. CP-31398 has shown an exceptionally high score of 6.92 while only 10% of the set of drugs from the World Drug Index used by ADMET Predictor™ have a score greater than 6.5. MQ, the active metabolite of APR-246 (only drug in clinical trials [23]) and PRIMA-1, has a score of 3.01. When compared to other compounds with a lower score, it has the same qualitative toxicities but better S+P_{eff} or S+Sw. The only exceptions are WR-1065 and WR-2721, which have a very low S+P_{eff} compared to MQ, as well as stictic acid. In fact, stictic acid was predicted to have low BBB permeability, and likely to have no effect on AST levels. This could be especially important since APR-246 (and hence its active metabolite MQ) had dose-limiting toxicities (DLT) in clinical trials related to elevated AST and ALT levels, confusion, fatigue and impaired talking [23]. Although stictic acid is predicted to be superior to MQ with regards to these DLT, it has a very low S+Sw and could thus have low bioavailability.

2.4 Conclusions

Designing drugs that can restore the wt function to mp53 promises to have a huge impact in the fight against cancer. A highly optimized drug could potentially target cancer cells with minimal impact on normal cells since the target, mp53, is highly specific to abnormal cells. Our results show that the alkylating ligands: MQ, MIRA-1, STIMA-1, NB and CP-31398 all

interact with backbone residues of S116 or S121 in R273H-mp53, while their double bonds are directed towards C124 thiol group. Other ligands that are not known to alkylate the protein interact directly with C124. The predicted toxicities by ADMET Predictor™ indicate that stictic acid has qualitatively less toxic adverse effects when compared to the APR-246 metabolite. Designing derivatives of stictic acid with better pharmacokinetic properties could potentially lead to a better drug with less adverse effects compared to the dose-limiting toxicities of APR-246.

2.5 Methods

2.5.1 Preparation of the p53-R273H structure

The 3D structure of the target molecule, R273H-mp53, was generated *in silico* in a manner similar to that outlined by Barakat *et al.* [15,47] using Amber99SB force-field [48]. The 1TSR-B [49] wt-p53-DNA complex crystal structure coordinates were obtained from the Protein Data Bank [50]. Swiss-PdbViewer [39] application was used to virtually mutate residue 273 of p53 from arginine to histidine. The protonation states of mp53 were calculated using the PDB2PQR [51] at pH 7 and the four Zn²⁺ coordinating residues were deprotonated. The p53-DNA complex was solvated in a TIP3P water box (containing 34,221 water molecules), thus providing a water buffer of at least 18 Å around the complex along each dimension. This system was neutralized using Na⁺ ions, which replaced water molecules with the highest electrostatic energies on their oxygen atoms. The ionic concentration was adjusted to 0.150 M by the random addition of NaCl ions to simulate physiological conditions.

2.5.2 MD Simulations

The solvated system was first minimized and then heated from 0 to 310 K (body temperature) using NAMD software [52]. Heavy restraints were placed on the backbone atoms during heating. These restraints were gradually decreased in an MD simulation before production was initiated. The fully solvated system was then simulated with no restraints at 310 K for 80 ns. To ensure that the system was fully equilibrated, the mass-weighted RMSD of the backbone residues was calculated relative to the structure at the start of the MD production. The three residues from each terminus were excluded as they are expected to be too flexible and are far from the region of interest.

2.5.3 RMSD-based structure clustering

To account for the protein flexibility using a manageable number of representative protein models, the last 20 ns of the equilibrated protein were clustered using the average-linkage algorithm [53] in PTRAJ utility of AmberTools12 [41]. Before clustering, the protein was RMSD-fitted to the minimized structure to remove differences between structures that were due to rotations or translations. 2001 protein structures representing the last 20 ns at an interval of 10 ps, were clustered into 2 to 100, based on the mass-weighted RMSD of the amino acids of residues 114 to 117, 121 to 126, 133 and 140 to 144. Two clustering metrics, Davies-Bouldin index (DBI) [54] and the percentage of variance (SSR/SST) [53], were calculated for all the clusters. The choice of the optimum number of clusters is typically made to respond to a local minimum for the DBI value and when SSR/SST plateaus [53] because increasing the number of clusters beyond the start of the plateau does not significantly improve the clustering results. Following the choice of the optimum number of clusters, the

centroid structure (representative structure) of every cluster containing more than 2% of the total clustered structures was used for docking.

2.5.4 Docking

The crystal structure of Y220C-mp53 bound to PHIKAN083 [55] (PDB ID: 2VUK [56]) was used as a control to validate our docking protocol. The ligand was removed from Y220C-mp53 and the protein structure was protonated at pH 7 using the PDB2PQR server [51]. AutodockTools [57] was used to compute the partial atomic charges of both the ligand and the protein using the Gasteiger-Marsili method [58]. The non-polar hydrogens of both the ligand and the protein were merged and the identities of all atoms were assigned according to their Autodock 4.2 atom types. AUTOTORS utility in AutodockTools was used to assign the rotatable bonds in PHIKAN083. The grid box was centered at the binding pocket near C124 of the ligand. Docking calculations were performed using the Lamarckian Genetic Algorithm [59] in Autodock 4.2 [40]. The default settings for the docking calculations were used for all parameters with the exception of the maximum number of generations and the maximum number of energy evaluations, which were set to 28,000 and 50,000,000 respectively. The docked poses were clustered based on an RMSD tolerance of 1 and 2 Å with reference to the pose with the lowest energy.

The selected activators to mp53, namely: PRIMA-1, APR-246, MIRA-1, STIMA-1, MQ, NB, stictic acid, CP-31398, ellipticine, 9-hydroxy-ellipticine, WR-1065 and WR-2721 were all docked into the representative structures of the chosen clusters. The ligands and the different protein structures were prepared as described above. The grid box was also centered at C124 pocket. The predicted poses were clustered based on their RMSD values, with tolerance values of 1 and 2 Å. The energies of the docked poses were also calculated using the

Autodock 4.2 scoring function [59]. The lowest energy structure in the biggest cluster (RMSD= 1 Å, except for WR-1065 and WR-2721) was chosen as the best binding pose for the respective protein representative structure.

2.5.5 ADMET Prediction

ADMET Predictor™ [60] is commercially available software that calculates the various descriptors of pharmacokinetic properties of tested compounds in order to predict absorption, distribution, metabolism, excretion and toxicity. It is based on artificial intelligence algorithms that account for chemical similarity and a knowledge base of a large number of compounds built into its training set. The 3D molecular structures of the ligands were input into ADMET Predictor™ [60]. Our first objective was to determine if all compounds followed Lipinski's rule-of-five. The software package was also used to predict the physico-chemical properties of the molecules such as their native solubility (S+S_w) in pure water. In addition, we were interested in quantifying the effective permeability of the different ligands across the intestinal membrane (S+P_{eff}). Other predicted properties included a qualitative measure of the blood-brain barrier permeability (BBB_Filter), its likelihood of inhibiting glycoproteins (Pgp_Substr) or being effluxed by these proteins (Pgp_Inh). Cardiotoxicity was predicted by the estimation of the likelihood of inhibiting the human Ether-à-go-go-Related Gene (TOX_hERG_Filter) potassium channel. A qualitative measure of the liver toxicity was also predicted based on the likelihood of elevation of several liver enzymes, including AST also called serum glutamic-oxaloacetic transaminase (TOX_SGOT) and ALT, also called Serum glutamate pyruvate transaminase (TOX_SGPT). In addition, a global ADMET risk score (ADMET_Risk) is calculated for each compound; this is a Simulations Plus computational filter developed using a subset of the World Drug Index. All of the above

calculations provided an overview of both the potential clinical suitability of the compounds tested and also their associated risks and side-effects.

2.6 References

1. Teodoro JG, Evans SK, Green MR. Inhibition of tumor angiogenesis by p53: A new role for the guardian of the genome. *Journal of Molecular Medicine* 2007;85(11):1175-1186.
2. Levine AJ, Oren M. The first 30 years of p53: Growing ever more complex. *Nature Reviews Cancer* 2009;9(10):749-758.
3. Muller PAJ, Vousden KH. P53 mutations in cancer. *Nature cell biology* 2013;15(1):2-8.
4. Goldstein I, Marcel V, Olivier M, Oren M, Rotter V, Hainaut P. Understanding wild-type and mutant p53 activities in human cancer: New landmarks on the way to targeted therapies. *Cancer gene therapy* 2011;18(1):2-11.
5. Vogelstein B, Lane D, Levine AJ. Surfing the p53 network. *Nature* 2000 Nov 16;408(6810):307-310.
6. Feki A, Irminger-Finger I. Mutational spectrum of p53 mutations in primary breast and ovarian tumors. *Critical reviews in oncology/hematology* 2004;52(2):103-116.
7. Momand J, Jung D, Wilczynski S, Niland J. The MDM2 gene amplification database. *Nucleic acids research* 1998;26(15):3453-3459.
8. Shvarts A, Steegenga WT, Riteco N, van Laar T, Dekker P, Bazuine M, van Ham RC, van der Houven, van Oordt, Hateboer G, van der Eb, A J, Jochemsen AG. MDMX: A novel p53-binding protein with some functional properties of MDM2. *The EMBO journal* 1996;15(19):5349-5357.
9. Nag S, Zhang X, Srivenugopal KS, Wang M-, Wang W, Zhang R. Targeting MDM2-p53 interaction for cancer therapy: Are we there yet? *Current medicinal chemistry* 2014;21(5):553-574.
10. Patel S, Player MR. Small-molecule inhibitors of the p53-HDM2 interaction for the treatment of cancer. *Expert opinion on investigational drugs* 2008;17(12):1865-1882.
11. Buolamwini JK, Addo J, Kamath S, Patil S, Mason D, Ores M. Small molecule antagonists of the MDM2 oncoprotein as anticancer agents. *Current Cancer Drug Targets* 2005;5(1):57-68.
12. Zou P, Zheng N, Yu Y, Yu S, Sun W, McEachern D, Yang Y, Yu LX, Wang S, Sun D. Preclinical pharmacokinetics of MI-219, a novel human double minute 2 (HDM2) inhibitor

and prediction of human pharmacokinetics. *Journal of Pharmacy and Pharmaceutical Sciences* 2012;15(2):265-280.

13. Zhang Z, Chu X, Liu J, Ding Q, Zhang J, Bartkovitz D, Jiang N, Karnachi P, So S, Tovar C, Filipovic ZM, Higgins B, Glenn K, Packman K, Vassilev L, Graves B. Discovery of potent and orally active p53-MDM2 inhibitors RO5353 and RO2468 for potential clinical development. *Acs Medicinal Chemistry Letters* 2014;5(2):124-127.

14. Koblisch HK, Zhao SY, Franks CF, Donatelli RR, Tominovich RM, LaFrance LV, Leonard KA, Gushue JM, Parks DJ, Calvo RR, Milkiewicz KL, Marugan JJ, Raboisson P, Cummings MD, Grasberger BL, Johnson DL, Lu TB, Molloy CJ, Maroney AC. Benzodiazepinedione inhibitors of the Hdm2 : p53 complex suppress human tumor cell proliferation in vitro and sensitize tumors to doxorubicin in vivo. *Molecular Cancer Therapeutics* 2006;5(1):160-169.

15. Barakat K, Mane J, Friesen D, Tuszynski J. Ensemble-based virtual screening reveals dual-inhibitors for the p53-MDM2/MDMX interactions. *Journal of Molecular Graphics & Modelling* 2010;28(6):555-568.

16. Freed-Pastor W, Prives C. Mutant p53: One name, many proteins. *Genes & development* 2012;26(12):1268-1286.

17. Sjöblom T, Jones S, Wood LD, Parsons DW, Lin J, Barber TD, Mandelker D, Leary RJ, Ptak J, Silliman N, Szabo S, Buckhaults P, Farrell C, Meeh P, Markowitz SD, Willis J, Dawson D, Willson JKV, Gazdar AF, Hartigan J, Wu L, Liu C, Parmigiani G, Park BH, Bachman KE, Papadopoulos N, Vogelstein B, Kinzler KW, Velculescu VE. The consensus coding sequences of human breast and colorectal cancers. *Science (New York, N.Y.)* 2006;314(5797):268-274.

18. Olivier M, Eeles R, Hollstein M, Khan MA, Harris CC, Hainaut P. The IARC TP53 database: New online mutation analysis and recommendations to users. *Human mutation* 2002;19(6):607-614.

19. Petitjean A, Achatz MIW, Borresen-Dale AL, Hainaut P, Olivier M. TP53 mutations in human cancers: Functional selection and impact on cancer prognosis and outcomes. *Oncogene* 2007 APR 2;26(15):2157-2165.

20. Hainaut P, Hernandez T, Robinson A, Rodriguez-Tome P, Flores T, Hollstein M, Harris CC, Montesano R. IARC database of p53 gene mutations in human tumors and cell lines: Updated compilation, revised formats and new visualisation tools. *Nucleic acids research* 1998;26(1):205-213.

21. Ventura A, Kirsch DG, McLaughlin ME, Tuveson DA, Grimm J, Lintault L, Newman J, Reczek EE, Weissleder R, Jacks T. Restoration of p53 function leads to tumour regression in vivo. *Nature* 2007;445(7128):661-665.

22. Bykov VJN, Issaeva N, Shilov A, Hultcrantz M, Pugacheva E, Chumakov P, Bergman J, Wiman KG, Selivanova G. Restoration of the tumor suppressor function to mutant p53 by a low-molecular-weight compound. *Nature medicine* 2002;8(3):282-288.
23. Lehmann S, Bykov VJN, Ali D, Andren O, Cherif H, Tidefelt U, Ugglä B, Yachnin J, Juliusson G, Moshfegh A, Paul C, Wiman KG, Andersson P. Targeting p53 in vivo: A first-in-human study with p53-targeting compound APR-246 in refractory hematologic malignancies and prostate cancer. *Journal of Clinical Oncology* 2012;30(29):3633-3639.
24. Lambert JMR, Gorzov P, Veprintsev DB, Soderqvist M, Segerback D, Bergman J, Fersht AR, Hainaut P, Wiman KG, Bykov VJN. PRIMA-1 reactivates mutant p53 by covalent binding to the core domain. *Cancer Cell* 2009;15(5):376-388.
25. Bykov VJN, Issaeva N, Zache N, Shilov A, Hultcrantz M, Bergman J, Selivanova G, Wiman KG. Reactivation of mutant p53 and induction of apoptosis in human tumor cells by maleimide analogs. *The Journal of Biological Chemistry* 2005;280(34):30384-30391.
26. Foster BA, Coffey HA, Morin MJ, Rastinejad F. Pharmacological rescue of mutant p53 conformation and function. *Science (New York, N.Y.)* 1999;286(5449):2507-2510.
27. Rippin TM, Bykov VJN, Freund SMV, Selivanova G, Wiman KG, Fersht AR. Characterization of the p53-rescue drug CP-31398 in vitro and in living cells. *Oncogene* 2002;21(14):2119-2129.
28. Demma MJ, Wong S, Maxwell E, Dasmahapatra B. CP-31398 restores DNA-binding activity to mutant p53 in vitro but does not affect p53 homologs p63 and p73. *The Journal of Biological Chemistry* 2004;279(44):45887-45896.
29. Roh J, Kang SK, Minn I, Califano JA, Sidransky D, Koch WM. p53-reactivating small molecules induce apoptosis and enhance chemotherapeutic cytotoxicity in head and neck squamous cell carcinoma. *Oral oncology* 2011;47(1):8-15.
30. Reddy NL, Hill J, Ye L, Fernandes PB, Stout DM. Identification and structure-activity relationship studies of 3-methylene-2-norbornanone as potent anti-proliferative agents presumably working through p53 mediated apoptosis. *Bioorganic & medicinal chemistry letters* 2004;14(22):5645-5649.
31. Zache N, Lambert JMR, Rokaeus N, Shen J, Hainaut P, Bergman J, Wiman KG, Bykov VN. Mutant p53 targeting by the low molecular weight compound STIMA-1. *Molecular Oncology* 2008;2(1):70-80.
32. North S, El-Ghissassi F, Pluquet O, Verhaegh G, Hainaut P. The cytoprotective aminothioliol WR1065 activates p21(waf-1) and down regulates cell cycle progression through a p53-dependent pathway. *Oncogene* 2000;19(9):1206-1214.

33. North S, Pluquet O, Maurici D, El-Ghissassi F, Hainaut P. Restoration of wild-type conformation and activity of a temperature-sensitive mutant of p53 (p53(V272M)) by the cytoprotective aminothiols WR1065 in the esophageal cancer cell line TE-1. *Molecular carcinogenesis* 2002;33(3):181-188.
34. Ohashi M, Oki T. Ellipticine and related anticancer agents. *Expert Opinion on Therapeutic Patents* 1996;6(12):1285-1294.
35. Ohashi M, Sugikawa E, Nakanishi N. Inhibition of P53 protein-phosphorylation by 9-hydroxyellipticine - a possible anticancer mechanism. *Japanese Journal of Cancer Research* 1995;86(9):819-827.
36. Sugikawa E, Hosoi T, Yazaki N, Gamanuma M, Nakanishi N, Ohashi M. Mutant p53 mediated induction of cell cycle arrest and apoptosis at G1 phase by 9-hydroxyellipticine. *Anticancer Research* 1999;19(4):3099-3108.
37. Peng YH, Li CG, Chen LH, Sebt S, Chen JD. Rescue of mutant p53 transcription function by ellipticine. *Oncogene* 2003;22(29):4478-4487.
38. Wassman CD, Baronio R, Demir O, Wallentine BD, Chen C, Hall LV, Salehi F, Lin D, Chung BP, Hatfield GW, Chamberlin AR, Luecke H, Lathrop RH, Kaiser P, Amaro RE. Computational identification of a transiently open L1/S3 pocket for reactivation of mutant p53. *Nature Communications* 2013;4:1407.
39. Guex N, Peitsch MC. SWISS-MODEL and the swiss-PdbViewer: An environment for comparative protein modeling. *Electrophoresis* 1997;18(15):2714-2723.
40. Morris GM, Goodsell DS, Pique ME, Lindstrom W, Huey R, Forli S, Hart WE, Halliday S, Belew R, Olson AJ. AutoDock version 4.2: Automated docking of flexible ligands to flexible receptors. The Scripps Research Institute: California 2010.
41. Case DA, Darden TA, Cheatham I.T.E., Simmerling CL, Wang J, Duke RE, Luo R, Walker RC, Zhang W, Merz KM, Roberts B, Hayik S, Roitberg A, Seabra G, Swails J, Goetz AW, Kolossváry I, Wong KF, Paesani F, Vanicek J, Wolf RM, Liu J, Wu X, Brozell SR, Steinbrecher T, Gohlke H, Cai Q, Ye X, Wang J, Hsieh M-, Cui G, Roe DR, Mathews DH, Seetin MG, Salomon-Ferrer R, Sagui C, Babin V, Luchko T, Gusarov S, Kovalenko A, Kollman PA. Amber 12. 2012.
42. Lipinski CA, Lombardo F, Dominy BW, Feeney PJ. Experimental and computational approaches to estimate solubility and permeability in drug discovery and development settings. *Advanced Drug Delivery Reviews* 1997;23(1-3):3-25.
43. Sutton LE, editor. Tables of interatomic distances and configuration in molecules & ions. Special Publication No.18 ed. Burlington House, London: The Chemical Society; 1965.

44. Bissantz C, Kuhn B, Stahl M. A medicinal chemist's guide to molecular interactions. *Journal of medicinal chemistry* 2010;53(14):5061-5084.
45. Molecular operating environment (MOE), 2012.10; chemical computing group inc., 1010 sherbrooke st. west, suite #910, montreal, QC, canada, H3A 2R7, 2016.
46. Bassett EA, Wang W, Rastinejad F, El-Deiry WS. Structural and functional basis for therapeutic modulation of p53 signaling. *Clinical Cancer Research: An Official Journal of the American Association for Cancer Research* 2008 Oct 15;14(20):6376-6386.
47. Barakat K, Issack BB, Stepanova M, Tuszynski J. Effects of temperature on the p53-DNA binding interactions and their dynamical behavior: Comparing the wild type to the R248Q mutant. *PloS One* 2011;6(11).
48. Hornak V, Abel R, Okur A, Strockbine B, Roitberg A, Simmerling C. Comparison of multiple amber force fields and development of improved protein backbone parameters. *Proteins* 2006;65(3):712-725.
49. Cho Y, Gorina S, Jeffrey PD, Pavletich NP. Crystal structure of a p53 tumor suppressor-DNA complex: Understanding tumorigenic mutations. *Science* 1994 July 15;265(5170):346-355.
50. 10.2210/pdb1tsr/pdb.
51. Dolinsky TJ, Czodrowski P, Li H, Nielsen JE, Jensen JH, Klebe G, Baker NA. PDB2PQR: Expanding and upgrading automated preparation of biomolecular structures for molecular simulations. *Nucleic acids research* 2007;35:522.
52. Phillips JC, Braun R, Wang W, Gumbart J, Tajkhorshid E, Villa E, Chipot C, Skeel RD, Kale L, Schulten K. Scalable molecular dynamics with NAMD. *Journal of Computational Chemistry* 2005;26:1781-1802.
53. Shao J, Tanner SW, Thompson N, Cheatham TE,III. Clustering molecular dynamics trajectories: 1. characterizing the performance of different clustering algorithms. *Journal of Chemical Theory and Computation* 2007;3(6).
54. Davies DL, Bouldin DW. Cluster separation measure. *IEEE Transactions on Pattern Analysis and Machine Intelligence* 1979;1(2):224-227.
55. Boeckler FM, Joerger AC, Jaggi G, Rutherford TJ, Veprintsev DB, Fersht AR. Targeted rescue of a destabilized mutant of p53 by an in silico screened drug. *Proceedings of the National Academy of Sciences of the United States of America* 2008;105(30):10360-10365.
56. 10.2210/pdb2vuk/pdb.

57. Morris GM, Huey R, Lindstrom W, Sanner MF, Belew RK, Goodsell DS, Olson AJ. AutoDock4 and AutoDockTools4: Automated docking with selective receptor flexibility. *Journal of Computational Chemistry* 2009;30(16).
58. Gasteiger J, Marsili M. Iterative partial equalization of orbital electronegativity- a rapid access to atomic charges. *Tetrahedron* 1980;36(22):3219-3228.
59. Morris GM, Goodsell DS, Halliday RS, Huey R, Hart WE, Belew RK, Olson AJ. Automated docking using a lamarckian genetic algorithm and an empirical binding free energy function. *Journal of Computational Chemistry* 1998;19(14).
60. ADMET predictor(TM) is distributed by simulations plus, inc., lancaster CA 93534 (<http://Simulations-plus.com>).

Chapter 3

Insights into the Effect of the G245S Single Point Mutation on the Structure of p53 and the Binding of the Protein to DNA

Preface

This chapter has been published as:

Lepre MG, Omar SI, Grasso G, Morbiducci U, Deriu MA, Tuszynski JA. Insights into the effect of the G245S single point mutation on the structure of p53 and the binding of the protein to DNA. Molecules) 2017; 22(8).

The MDPI journal, *Molecules*, is an open access scientific journal that states: ‘For all articles published in MDPI journals, copyright is retained by the authors. Articles are licensed under an open access Creative Commons CC BY 4.0 license’.

Contributions: *In silico* modeling in this chapter has been performed by Marco Lepre, a Masters student intern who I supervised during his internship. SIO: conceived and designed the experiments, guided the student to do all *in silico* work except functional mode analysis, analysed the data and wrote the paper. MGL: performed all the experiments, analyzed the data and wrote the paper. GG: took part in the functional mode analysis experiments. MAD: took part in the functional mode analysis experiments and contributed to editing the manuscript. UM: contributed to editing the manuscript.

Note: This chapter has been modified for consistency with the rest of the thesis; some abbreviations and referencing style have been changed and supplementary material in the original publication has been moved to the body of the chapter. Additional information has been added to the discussion for clarification.

3.1 Introduction

The transcription factor p53 is a tumor suppressor protein that responds to cellular stress such as genotoxic damage, hypoxia, and other chemical or physical stresses, leading to cell cycle arrest, DNA repair and apoptosis [1,2]. In tumors, usually an abnormal cell cycle progression is observed due to activation of oncogenes or absence/defects in tumor suppressor proteins [3]. Indeed, *TP53* is mutated in more than 50% of human tumors. These mutations alter the function of the protein, which subsequently aids cancer progression and adversely affect patient survival. It is for this reason that many efforts have been made to find novel chemotherapeutics that target p53. Such examples include gene therapy, modulating the activity of p53 regulators and restoring the wild-type activity to mutant p53 (mp53) [3-5].

Some 97% of p53 mutations occur in the core domain of the protein [6]. One of the most frequent p53 mutants is a mutation in codon 245 of p53 from glycine to serine; G245S-mp53. This mutant is classified as a structural mutant. In other words, the mutation results in a conformational change that influences the binding of p53 to DNA and thus affects the protein's transcriptional activity. The transcription factor, p53, binds as a tetramer to a double-stranded DNA consensus sequence containing two or more copies of the 10 bp half-site 50-PuPuPuC(A/T)(T/A)GPyPyPy-30 [7,8]. The mutation in G245S-mp53 is located in loop L3, which is involved in important interactions with the minor groove of DNA [8-10]. A zinc ion in the DNA binding domain (DBD) provides structural stability for the loops L2 and L3 and also has an impact on DNA-binding specificity [11].

It is difficult to pinpoint the exact effect of the G245S mutation on the process of malignant transformation and cancer progression. However, a study by Hanel and colleagues has demonstrated that while mouse embryonic fibroblasts carrying R248Q and G245S mutations

were both transcriptionally inactive for p53 target genes such as p21, mice carrying humanized G245S-mp53, similar to p53-null mice, had slower tumor onset and death compared to mice with the R248Q mutation [12]. Also, the same study by Halen [12] and another by Xu *et al.* [13] have showed that Li-Fraumeni Syndrome patients with p53 G245 germline mutations had a later onset of cancer especially when compared to patients with p53 mutations in R248, which is also located in the loop L3 of the protein. However, in a different population-based study, G245 hot spot mutations were found to be correlated with poor prognosis and survival in colon cancer patients [14]. Understanding the consequences of mutations on the p53 protein structure may serve as the starting point for studies aimed at developing novel p53 targeted cancer therapies. Currently, APR-246 is the only p53 activator that is in clinical trials [4,15]; it can restore the transcriptional activity of p53 mutants, including G245S-mp53, to p53 target genes such as PUMA and p21. Stictic acid was also shown to restore the activity of G245S-mp53 to express PUMA [16]. In addition, it increased the thermal stability of the mutant protein *in vitro* [16].

Several studies which characterize the effects of hotspot mutations on the structure of p53 and its DNA binding properties have been reported. Previous studies based on X-ray crystallography and NMR spectroscopy have given an important insight into the biological structure of the wild-type p53 (wt-p53) (either complexed with DNA or free in solution, referred to as the apo form in this chapter) [8,9,17,18]. Experimental studies have shown that the wt-p53 core domain already has a relatively low thermodynamic stability (melting temperature of 42–44°C) while G245S-mp53 has an even lower melting temperature of 39°C suggesting a moderate destabilization of the structure [19]. The moderate destabilization of this structural mutant has been further confirmed by heteronuclear single quantum correlation

nuclear magnetic resonance (HSQC NMR) spectroscopy where chemical shift changes between wt-p53 and the mutant were observed for residues in loop L2, L3 as well as terminal residues of the β -strands 4, 9 and 10, while the overall DBD structure folded as the wt-p53 [20]. As well, the crystal structure (apo protein) of the superstable mutant M133L-V203A-N239Y-G245S-N268D, a stabilized variant of the p53 core domain, suggests small conformational changes with respect to the wt in the immediate environment of the mutation site and in other key residues in the subunit interface of the core domain dimer bound to a DNA half-site [21]. However, none of the recent experimental studies have ever resolved the structure of the DBD G245S-mp53 in complex with DNA. Thus, to gain more information about this pivotal cell cycle protein, computational molecular modeling tools, such as protein dynamics analysis and/or thermodynamic properties at the atomic spatial resolution and microsecond temporal evolution, can be used. Demir and coworkers in 2011 and Koulgi *et al.* in 2013 computationally analyzed several hotspot mutants including the G245S-mp53 structural mutant [22,23]. In the former study, the overall protein flexibility of the apo wt-p53 DBD was compared to R175H, G245S, R248Q, R249S, R273H and R282W hotspot mutants through the clustering of molecular dynamics (MD) trajectories. The metric used to evaluate the protein flexibility was the number of clusters obtained by certain RMSD cutoff criteria. Among the several hotspot mutants considered, G245S-mp53 was also simulated. It showed a higher number of clusters with respect to the wt protein suggesting that the p53 hotspot mutations increase the flexibility of the p53 core domain, which indicates thermodynamic instability in agreement with experimental studies [18]. In the latter study by Koulgi and coworkers, the G245S-mp53 bound to DNA was analyzed using quantum and molecular mechanics simulations and was compared to the wt-p53-DNA complex. Furthermore, the free

energy of binding (EBE) between the p53 DBD and DNA, based on MD simulations, was calculated. The mutant showed a slightly higher EBE during a 30 ns trajectory. Hydrogen bonding also decreased and was estimated to occupy only 20% of the simulation time.

In our study, we carried out molecular dynamics simulations on both the wt-p53 and G245S-p53 mutant in complex with DNA and in their apo form (not bound to DNA) to understand the structural effects of the G245S mutation. We performed comparative conformational analysis between the wt and mutant proteins. Functional Mode Analysis (FMA) was also used to identify the collective atomic motions related to the fluctuations occurring in the mutated region. Clustering was used to identify representative conformations of the p53 dimer in complex with DNA. Furthermore, the binding free energy of the dimer with DNA was evaluated by means of the Molecular Mechanics Generalized Born Surface Area (MMGBSA) method. Our results have shown agreement with experimental data and demonstrated conformational change in the mutant p53 in both cases: DNA bound and apo forms.

3.2 Results

3.2.1 Conformational analysis: apo p53 proteins

The apo p53 proteins were simulated using MD for 1 μ s. The root mean square deviations (RMSD) of the proteins' backbones were calculated during the simulation, compared to their starting structures, in order to assess the proteins' equilibration. The RMSD plots of the apo p53 monomers (Figure 3.1) show that the RMSD values plateau after 550 ns for both proteins.

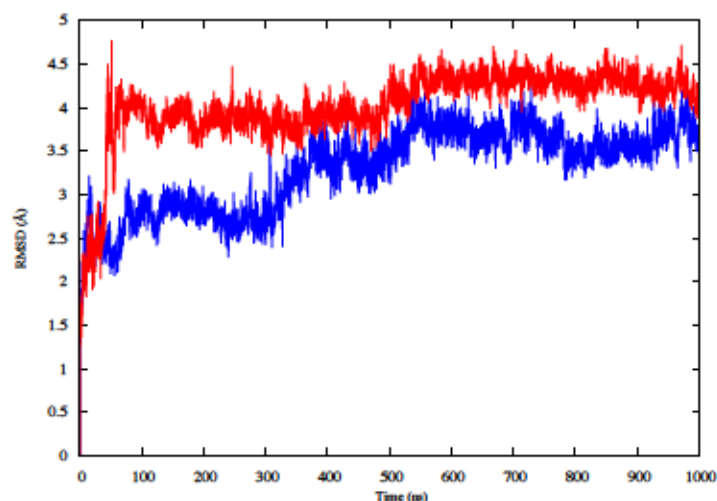


Figure 3.1. The RMSD plot of the backbone heavy atoms of both wt-p53 (blue) and G245S-p53 (red) apo monomers over 1 μ s of MD simulations.

The protein structures obtained in the last 450 ns of simulation were, therefore, used to assess the dynamic and structural differences between the wt and mutant proteins by means of calculating the root mean square fluctuation (RMSF) of the individual protein residues. For the apo protein structures, the proteins' backbones were aligned and the RMSF of the backbone atoms for all residues were evaluated and compared. In Figure 3.2, the wt (blue) and mutant (red) monomers show an overall difference in terms of dynamic behavior as reflected by the different patterns of the RMSF of the different protein residues. The differences in fluctuations are shown in the critical L1 loop of wt-p53 (RMSF of 5 Å) that interacts with the major groove of the DNA and in K120 that makes a sequence-specific contact with guanine and interacts with the phosphate backbone of the DNA through its amide (backbone) nitrogen [9]). On the other hand, loop L1 in the G245S mutant has lower RMSF values suggesting that this region becomes less flexible. The loss of the loop L1 flexibility may affect the binding of the mutant to DNA and thus reduce the tumor suppressor

activity of the protein. Further, loops L2 and L3 as well as helix H1 are other regions showing higher RMSF values in the wt-p53 compared to the mutant.

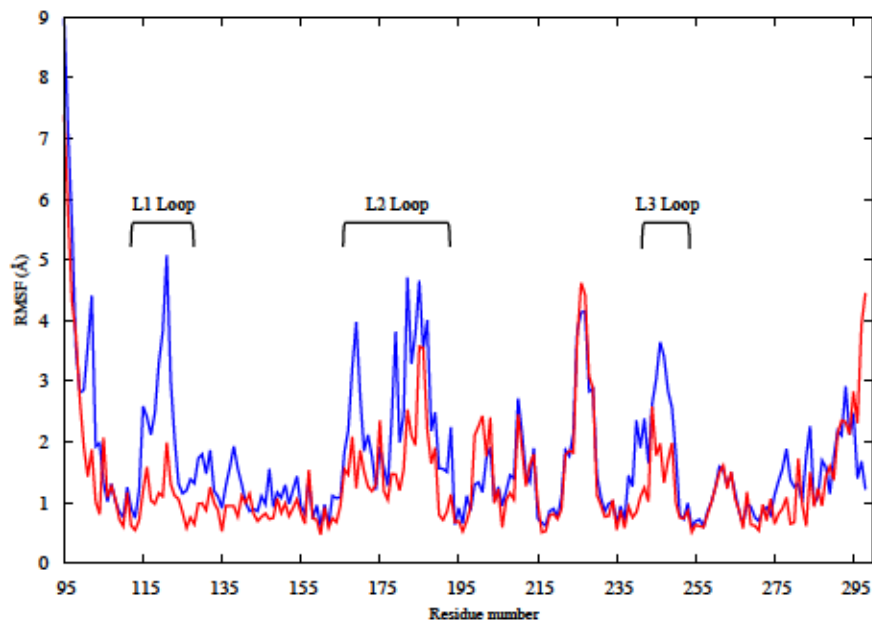


Figure 3.2. The RMSF plot of the backbone heavy atoms of the apo monomers of wt-p53 (blue) and G245S-mp53 (red). The loops L1, L2 and L3 are indicated

The higher fluctuation in the three above-mentioned regions could be explained by the fact that the residues pertaining to the DNA binding regions sample the space to find the DNA molecule, bind to it and finally stabilize it. In loop L3, a key role in DNA binding is played by R248 which, in wt-p53, anchors the protein's DBD to the minor groove of the DNA as shown in the minimized structure of the p53 dimer complexed with DNA (Figure 3.3).

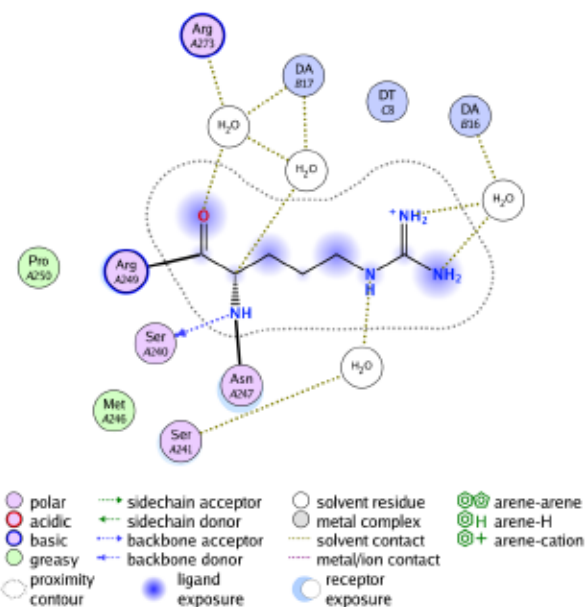


Figure 3.3. R248 in monomer B of wt-p53 makes direct or water mediated contacts with DNA backbone thus retaining its water crystal structures is important

Given that a mutation in L3 causes loss of flexibility in L1 and L2, it may be of interest to evaluate existing correlations among the above-mentioned protein areas. Functional Mode Analysis (FMA) was, therefore, employed, as explained in 3.4.4. In greater detail, FMA allowed the characterization of the contribution of individual PCA vectors to RMSD of loop L3, yielding a single vector, which drives the loop L3 fluctuation mode, referred to as the ensemble-weighted maximally correlated motion (ewMCM). The analysis of the MD trajectory filtered on the ewMCM, enabled the identification of the residues, which are maximally correlated with the fluctuation of L3 (Figure 3.4). The residue that contributes the most to the whole loop L3 (residues 239–251) fluctuation is G245 due to the inherent flexibility of the glycine amino acid. A high level of correlation was found between loops L2 and L3 as well as loop L3 and helix H1 (residues 163–178). A slightly lower, but significant correlation was also found between loops L3 and L1 (residues 112–124). These findings suggest collective atomic motions among key residues of p53 located at the DNA binding

interface. The high RMSF in loops L3, L2 and L1 of wt-p53 (Figure 3.2) and the FMA outcomes suggest a correlation between these crucial DNA binding loops. Cross-validation of the maximally correlated motion is shown in the Appendix Figure. i.

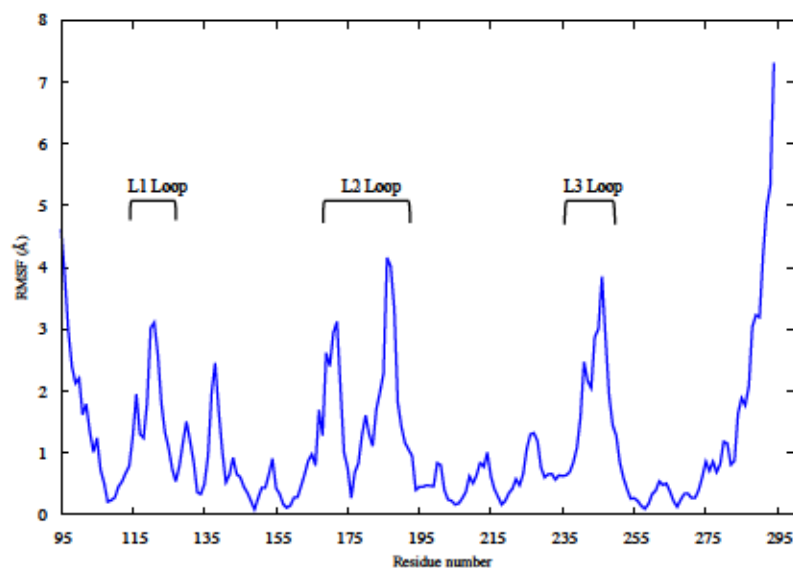


Figure 3.4. A plot of the RMSF of apo wt-p53 backbone calculated over all the MD trajectory filtered on the ewMCM. The loops L1, L2, L3 are labeled

3.2.2 Conformational analysis: p53 Dimers in Complex with the DNA

Figure 3.5 shows the RMSDs of the two monomers of the G245S-mp53 dimer, complexed with DNA, compared to the corresponding wt-p53 dimer-DNA complex. The RMSDs of the backbone atoms of all the p53 monomers were calculated compared to their positions at the start of the simulation; the RMSD is reasonably stable after about 500 ns. The analysis of the trajectories of the p53 dimer-DNA complexes demonstrated evidence of rotation of monomer B relative to DNA in the mutant protein models (Figure 3.6).

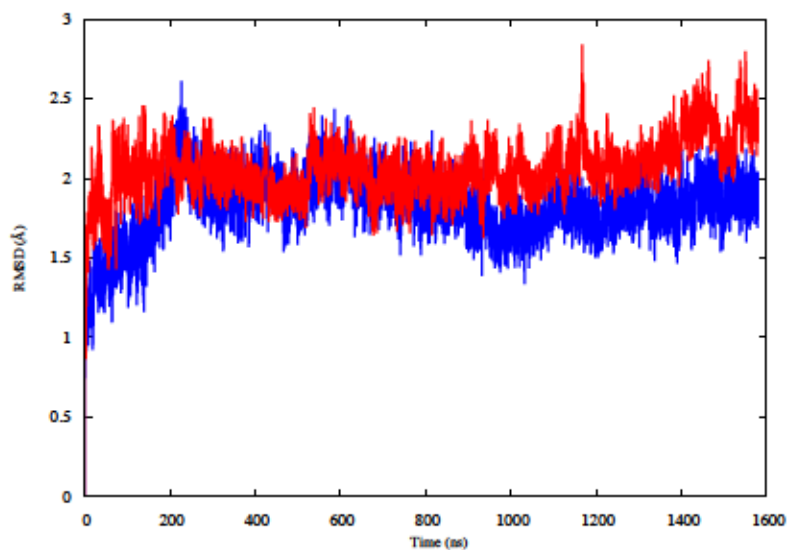


Figure 3.5. A plot of the RMSD of monomers B of the p53-dimer in complex with DNA; wt-p53 (blue), G245S-mp53 (red).

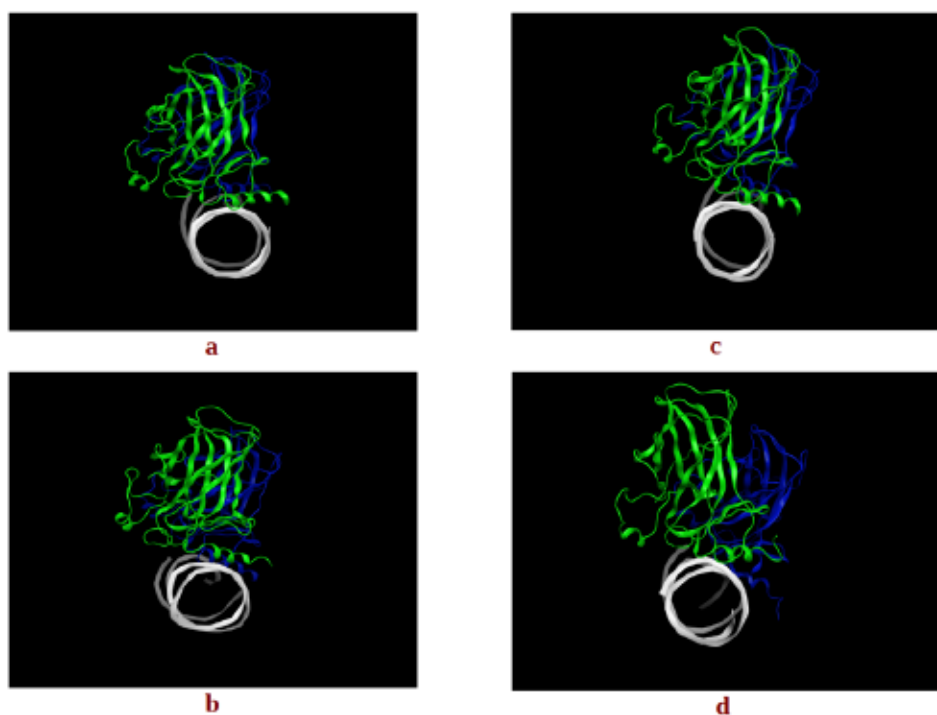


Figure 3.6. The centroids of the two most populated clusters, (a) wt-1 and (b) wt-2 of the wt-p53 dimer and (c) mt-1 and (d) mt-2 of the G245S-mp53 dimer. The rotation of monomer B in the mutant is evident in mt-2 in monomer B (blue) relative to monomer A (green).

To highlight the dynamic differences and thus potential structural differences between the wt and G245S-mp53, the RMSFs of the proteins were calculated for the equilibrated part of the trajectory. The RMSF plots of the backbone atoms for monomers B from both the wt/mp53-DNA complexes are shown in Figure 3.7. Residues E224, V225 and G226 have higher fluctuation in the mutated monomer B compared to the wt. These residues in the wt-p53 dimer are located in a turn that interfaces with the DBD of monomer A as shown in Figure 3.8.

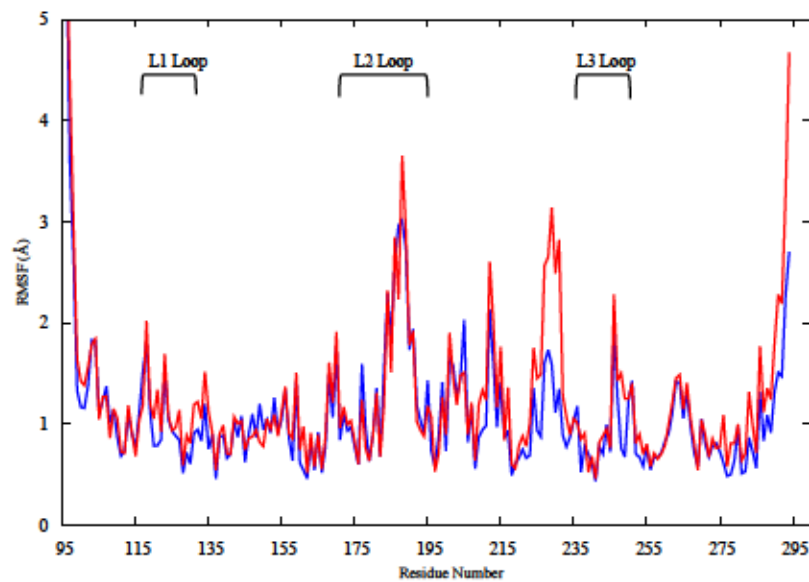


Figure 3.7. The RMSF plot for the backbone atoms of monomer B in the p53 dimer. Residues E224, V225 and G226 have higher fluctuations in G245S-mp53 compared to wt-p53.

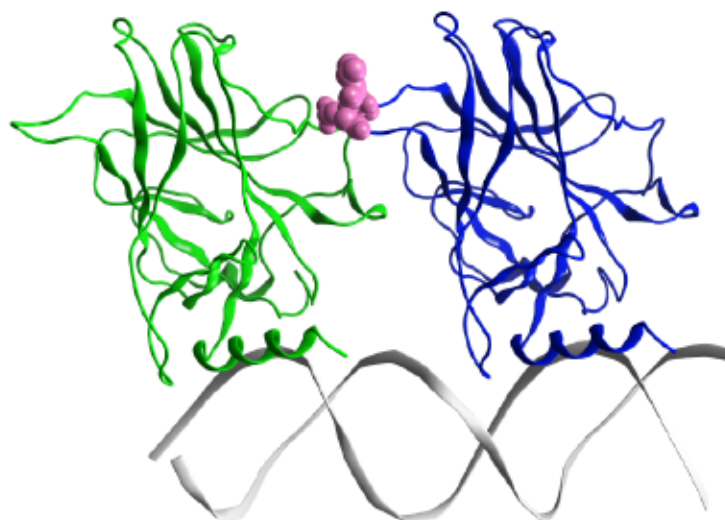


Figure 3.8. The minimized structure of the wt-p53 dimer in ribbon representation. Monomer A is in green, monomer B in blue and the DNA is grey. The magenta spheres are residues E224, V225 and G226, which are at the interface between the two p53 monomers. The loop L1 and helix-2 in monomer B interact with the major groove of DNA, while in monomer A they interact with the DNA terminus.

To assess the overall p53 dimer-DNA conformations sampled during the dynamic simulation, for both the wt and G245S-mp53, an RMSD-based clustering was performed on the equilibrated trajectory frames. The centroid-linkage, average-linkage and complete linkage algorithms were used to perform the RMSD-based structural analysis via clustering. The Davies-Bouldin index (DBI), pseudo F-statistic (pSF) and the ratio of the sum of squares regression to the total sum of squares (SSR/SST) clustering metrics were calculated for the last 525 ns of simulation (Figure 3.9). They were also used to assess the clustering quality of the average-linkage algorithm used and to guide the choice of the best cluster [22,24]. As the choice of the optimum number of clusters is usually made to correspond to a local minimum in the DBI value and a plateau in SSR/SST [24], a count of four clusters was chosen. The largest two of the four clusters contained 55% and 36% of all frames, respectively. The last two clusters contained a negligible number of frames as expected for MD simulations that

sample the conformational space according to the Boltzmann's distribution. The same procedure was followed for the protein residues of the G245S-mp53 dimer-DNA complex on the last 1.2 μ s (~1200 frames). The optimal number of clusters chosen was 3. Note that 59% and 40% of all frames were found in the two most populated clusters. In the case of the wt proteins, the p53 monomers had similar alignment to the DNA in the two representative structures of the most populated clusters (Figure 3.6). While the representative structure of the most populated cluster for the mutant proteins had a similar orientation to the DNA as the wt, the second most populated cluster showed misalignment between the two p53 mutant monomers.

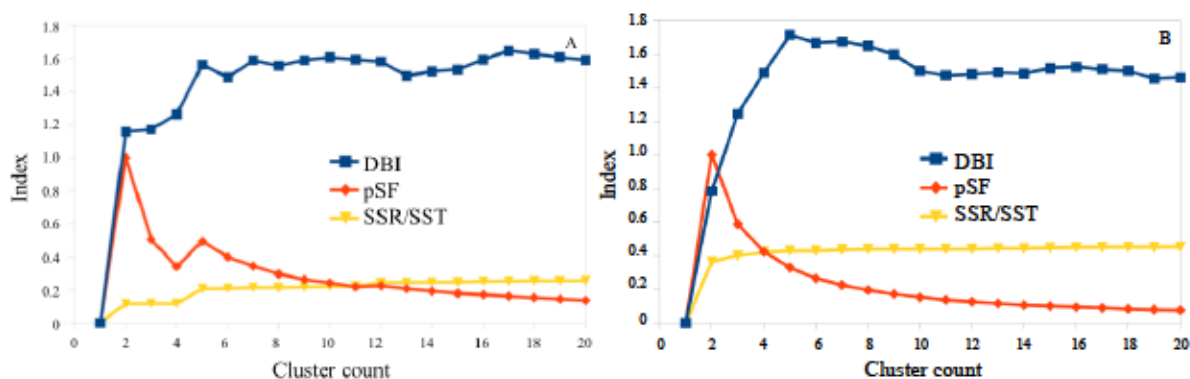


Figure 3.9. Plots of the DBI, pSF and SSR/SST clustering metrics for the equilibrated (A) apo and (B) DNA-bound G245S-mp53. The pSF values were normalized to fit on the graph.

3.2.3 EBE Analysis

For a more quantitative analysis of our results, the total and per-residue EBE between the p53 dimers and DNA during the equilibrated portion of the simulations were evaluated. Indeed, the EBE of the two monomers, A and B, to DNA can be evaluated independently. This is reasonable because the monomers can independently bind to the DNA [25].

The EBE ($\Delta\Delta G_0$) between p53 and DNA was evaluated using the molecular mechanics generalized Born surface area (MMGBSA) approach. For both the wt and mutant p53-DNA complexes, single equilibrated MD simulations were used to determine the energy values. The total binding energies between the protein dimers and the DNA for both the wt and mutant p53 are shown in Table 3.1. The calculated EBE between the wt-p53 dimers and DNA was $-100 \text{ kcal}\cdot\text{mol}^{-1}$ (with a standard deviation (SD) of $17 \text{ kcal}\cdot\text{mol}^{-1}$). The G245S-mp53 dimers were calculated to have a lower EBE with DNA of $-129 \text{ kcal}\cdot\text{mol}^{-1}$ (SD of $22 \text{ kcal}\cdot\text{mol}^{-1}$). The binding free energies between the individual monomers to DNA were also evaluated (Table 3.1). For the wt-p53, monomer A had a EBE to DNA of $-60 \text{ kcal}\cdot\text{mol}^{-1}$ (SD of $15 \text{ kcal}\cdot\text{mol}^{-1}$) while the G245S-mp53 had a comparable EBE to DNA of $-55 \text{ kcal}\cdot\text{mol}^{-1}$ (SD of $13 \text{ kcal}\cdot\text{mol}^{-1}$). For monomer B, however, the EBE of the wt-p53 to DNA was $-33 \text{ kcal}\cdot\text{mol}^{-1}$ (SD of $12 \text{ kcal}\cdot\text{mol}^{-1}$), while for G245S-mp53 the EBE was $-70 \text{ kcal}\cdot\text{mol}^{-1}$ (SD of $20 \text{ kcal}\cdot\text{mol}^{-1}$).

Table 3.1. A table of the EBE between the p53 dimer and the DNA, the BE between the p53 monomer A and B, the BE between monomer A and the DNA and the BE between monomer B and the DNA

EBE of the p53 Dimer to DNA			EBE of p53 Monomer A to B		
	EBE ($\text{kcal}\cdot\text{mol}^{-1}$)	SD ($\text{kcal}\cdot\text{mol}^{-1}$)		EBE ($\text{kcal}\cdot\text{mol}^{-1}$)	SD ($\text{kcal}\cdot\text{mol}^{-1}$)
Wt-p53	-100	17	Wt-p53	-4	7
G245S-mp53	-129	22	G245S-mp53	-2	7
EBE of p53 Monomer A to DNA			EBE of p53 Monomer B to DNA		
	EBE ($\text{kcal}\cdot\text{mol}^{-1}$)	SD ($\text{kcal}\cdot\text{mol}^{-1}$)		EBE ($\text{kcal}\cdot\text{mol}^{-1}$)	SD ($\text{kcal}\cdot\text{mol}^{-1}$)
Wt-p53	-60	15	Wt-p53	-33	12
G245S-mp53	-55	13	G245S-mp53	-70	20

We also calculated the EBE decomposition of the individual contributing residues. When comparing the per-residue decomposition, the residues of the wt monomers A had BE's very similar to those of the mutant. The plots in Figure 3.10 show EBE again in residues R280 (2 kcal·mol⁻¹) and R283 (4 kcal·mol⁻¹), which are both involved in the interaction with the DNA major groove. In the case of monomer B, an evident redistribution in the DNA binding residues can be seen clearly for the mutant (red bars) compared to the wt (gray bars). The residues located in the loop L3 (239–250), which are near the mutation, show an overall redistribution of binding energies: R248, which had the lowest EBE in the wt to DNA (-12 kcal·mol⁻¹), showed a EBE increase of about 6 kcal·mol⁻¹ in the mutant. Moreover, the mutant had a slight repulsion with residue C242. In addition, new interactions were formed between the DNA and residues C275, A276 and C277 of monomer B of the mutant but not wt-p53. The residues in loop L1 (114–124) of the mutant also had new DNA contacts with residues S121, V122.

In general, for monomer B of G245S-mp53, an increase in interactions is observed in the proximity of the major groove of the DNA, except for the key DNA interacting residue R280. Near the minor groove of DNA, R248, which is also an important DNA interacting residue, lost some of its affinity to DNA. This demonstrates destabilization of the DNA binding in the region near the mutation, but an increase in the affinity of loop L1 and other residues binding near the major groove of the DNA.

The BE's between the individual protein monomers were also calculated. Our results show that the wt monomers bind with a $\Delta\Delta G_0$ of -3.6 kcal·mol⁻¹ (SD of 7 kcal·mol⁻¹) while the mutant had a corresponding $\Delta\Delta G_0$ of only -2 kcal·mol⁻¹ (SD of 7 kcal·mol⁻¹).

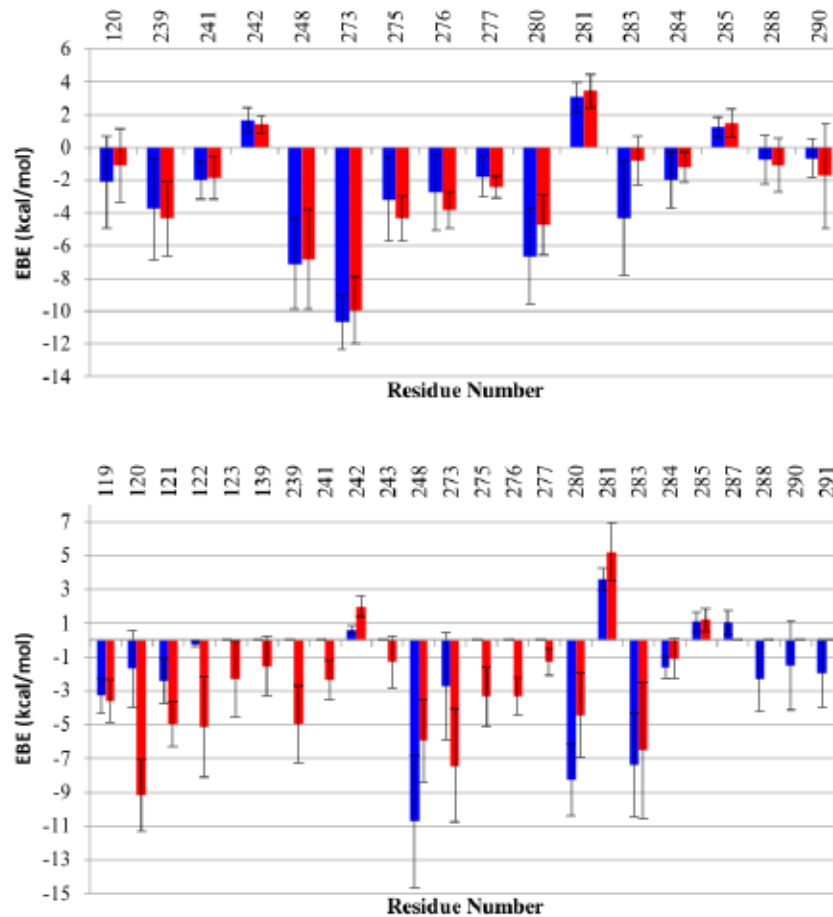


Figure 3.10. A histogram of the per-residue EBE decomposition for (A) monomers A and (B) monomers B, each in complex with DNA for both the wt-p53 (blue) and G245S-mp53 (red). Only the residues with EBE higher or lower than 1 kcal·mol⁻¹ are reported. The x-axis represents the residue numbers, the y-axis represents the EBE and the bars represent SD. A more pronounced redistribution of EBE is observed for monomer B.

3.3 Discussion

G245S-mp53 is a structural p53 mutant, in other words, a missense mutation produces structural perturbations within the DBD [26], and thus may indirectly affect the pivotal binding of p53 with the consensus site of the DNA, which is essential to maintaining the transcriptional activity of p53. Furthermore, p53 binds to DNA as a tetramer composed of

four identical subunits [27], consisting of a dimer of dimers located symmetrically on the consensus site [8,9]. A stabilized G245S variant (quadruple mutant) of the p53 core domain has been resolved by Joerger and his team [28]. It is a multi-site mutant of the p53 and not a single point mutation protein. Moreover, the dynamic behavior of the mutant cannot be observed using X-ray crystallography. In fact, crystal structures are not able to capture the wt protein's inherently unstable dynamic core domain that is known to have a melting temperature of about 42–44 °C [19]. This is even more true for oncogenic mutations that are thought to inactivate the native protein function by destabilizing or distorting the wt-p53 core domain [29]. Thus, computational simulations such as MD can be useful to complete the experimental results and explore new venues of this complex protein in both dynamic and thermodynamic terms.

The ultimate goal of our research is to generate, by means of *in silico* molecular modeling, a 3D structure of G245S-mp53 and develop detailed insights into its behavior when it is in the apo form or in complex with DNA. HSQC NMR spectroscopy can be used to experimentally detect the structural effect of a mutation on p53 [30]. In a study to compare the structures of the wt and G245S-mp53, Wong and coworkers used NMR spectroscopy [20]. They only found localized chemical shifts in the G245S-mp53, which indicates that the overall tertiary structure of the protein is similar to the wt-p53. Briefly, they found chemical shifts in the residues located in loops L2 and L3 as well as the terminal residues of the β -strands 4, 9 and 10. These differences are also reflected by the dynamic behavior shown in our study by the RMSF of the apo monomers backbone atoms (Figure 3.2); higher fluctuations in wt-p53 loops L1, L2, and L3 are evident.

FMA results identified a collective motion of loops L1, L2, helix H1 of wt-p53 that are maximally correlated to the fluctuation of loop L3, at which the G245S lies. FMA can identify motions of the protein that are not evident in other well-established methods such as Principal Component Analysis (PCA) and Normal Mode Analysis (NMA) [31,32]. PCA and NMA extract the collective motions with the largest contribution to the variance of the atomic fluctuation and the lowest frequency modes, respectively, whereas FMA accounts for collective modes distributed over a number of normal or PCA modes. As different motions of the protein could be related to the functional quantity (RMSD of loop L3 in our case), the generated frames of the protein are used to estimate the most probable collective motion that is responsible for the determined variation in the functional quantity. This is called ensemble-weighted maximal correlated motion (ewMCM). In the RMSF plot calculated over the MD trajectory filtered on the ewMCM (Figure 3.4), the high peak detected in G245 may be explained by the inherent ability of glycine to adopt unusual backbone dihedral angles that allows for a higher flexibility in the wt protein. However, when the residue is mutated to serine, there is a restriction on the allowed dihedral angles and thus the neighboring residues undergo dynamic stiffening (as observed in the RMSF plot of Figure 3.2). Moreover, residue C242 in the L3-loop, coordinates Zn^{2+} along with residues C176 and C179 in the L2-loop. Our results suggest that after the missense mutation of glycine to serine and its resultant dynamic stiffening on loop L3, a “domino effect” follows which causes a decrease in the L2-loop dynamics when compared to the wt-p53. Figure 3.2 also shows that the L1-loop of G245S-mp53 has lower fluctuations when compared with the wt protein. While it was difficult to find evidence of correlation between the L1 and L3 loops by visualizing the MD trajectory of the proteins, FMA data highlight a collective motion involving loops L1 and L3.

The dynamics of the central β -strands scaffold (res. 110–112; 141–146; 156–163; 195–198; 204–207; 214–219; 230–236; 251–258; 264–273) in the mutated apo protein are similar to that of the wt apo protein. However, reduced flexibility is observed in loops L1, L2 and L3 where the key residues K120 (L1), S241 (S8–L3) A248 (L3) are located and are known to interact directly with the DNA molecule [9]. This reduction of fluctuations in G245S-mp53 key regions may be the reason for defective binding with DNA and thus p53 inactivation. More specifically, R248 in wt-p53, which is close to the G245 mutation site and is the residue with the most gain in EBE with DNA upon mutation, is able to protrude into the minor groove of the DNA molecule resulting in favorable electrostatic interactions between the positively charged guanidinium group of R248 and the negatively charged DNA backbone. Furthermore, the minor groove adjacent to R248 is compressed and its bases are buckled so that the side chain of R248 makes three water mediated hydrogen bond contacts with the DNA molecule.

The evident differences in the dynamics of the key regions in p53, which are known to interact with DNA, have led us to also simulate the wt and G245S-mp53 proteins each in complex with DNA. To the best of our knowledge, there are no experimentally resolved structures of the G245S-mp53-DNA complex. To create this model, we used the crystal structure of wt-p53-DNA complex (PDB ID: 4HJE [8]), and virtually mutated residues G245 to serine in each monomer. We simulated the p53 dimer, both the wt and mutant proteins, in complex with DNA for more than 1.5 μ s using MD to reach a reasonable equilibrated complex structure.

For analysis, we assume monomer B is a better model for the p53-DNA interaction since loop L1 and helix-2 of monomer A interact with the terminus of the DNA rather than its major

groove. The RMSF plots of monomer B in the G245S and wt-p53 DNA complexes are shown in Figure 3.7. It is evident that the high residue fluctuations observed in the monomers in loops L1, L2 and L3 are not observed in the DNA complexed proteins. This is expected since the G245S-mp53 3D-model was created by a virtual single point mutation on the wt-p53-DNA complex. The wt protein, when in complex with the DNA, is expected to be more stable and hence the high fluctuations that were evident in the apo-monomers would decrease in the p53-DNA [33,34]. Furthermore, the overall [32,33] structure may assume a different conformation, even far from the DNA binding site, after DNA binding as confirmed by recent studies [35]. Nevertheless, our model shows that G245S-mp53 has higher fluctuations in the residues between β -strands 7 and 8 (residues 224, 225 and 226), which are normally located at the interface of the two protein monomers in the wt-p53. This relatively higher fluctuation in the mutant protein indicates a possible interruption in the monomer interaction and the exposure of these residues to the solvent. To further investigate this issue, the trajectory analysis showed a relative displacement between monomers A and B. This first qualitative result suggests that the mutant dimers undergo rearrangement upon DNA binding resulting in a dimer distortion without structural unfolding in agreement with experimental studies, which state that there is very little unfolding in G245S-mp53 that is not as structurally destabilized as other mutants [36]. To confirm the observation of monomer displacement, RMSD based clustering was performed to extract representative structures of all the conformational space sampled during the MD simulation. A comparison between the centroids of the most populated clusters has confirmed our observation. Indeed, Figure 3.6 shows symmetrical arrangement of the two protein monomers on the DNA in the wt-p53 for almost the whole

trajectory. However, there is distortion in the alignment of G245S-mp53 monomers in its second representative structure, which presents about 50% of the trajectory.

Interestingly, a previous study has shown evidence that mutations in the p53 tetramerization domain can inactivate the wt protein in a manner similar to that seen in the mutated DBD [37]. It is possible that the distortion in the dimer structure observed in G245S-mp53 might not allow the proper protein tetramerization and hence decreases or disables the tumor suppressor activity of the p53 [38].

To further understand the relationship between the G245S mutation and its evident consequence of monomer reorientation, a quantitative evaluation of the binding free energies between the individual monomers as well as between the dimers to the DNA was obtained by means of MMGBSA. This method combines the molecular mechanical energies with the continuum solvent approach where the electrostatic contribution to the solvent free energy is evaluated by the generalized Born method. Koulgi and his team previously employed a similar evaluation on a 30 ns trajectory [23]; the evaluated EBE of G245S-mp53 to DNA ranged from -65 to -40 kcal-mol⁻¹. In our work, longer equilibrated trajectories (the last 1 μ s) were used to identify the residues with lost or new interactions with DNA. However, we assume that the results for monomer B are more reliable as it is better centered on the DNA as explained earlier (Figure 3.8). Surprisingly, the binding energy of monomer B of G245S-mp53 to DNA was lower than that of the wt. This is not expected since G245S mp53 does not experimentally bind to p53 response elements [39]. Perhaps adding the entropic contributions to the EBE could give a more accurate binding energy. Also, the G245S-mp53 monomers could be stuck in a local minimum, especially that they were changing orientation with respect to DNA in our simulations.

The plots of the per-residue EBE decomposition of monomer B to DNA showed complete reorganization of the residues interacting with DNA. As shown in Figure 3.10, residues close to the G245S mutation such as R248 and C242 have a EBE increase of about 6 kcal·mol⁻¹ and 2.5 kcal·mol⁻¹, respectively, when compared to wt-p53. These results suggest a conformational rearrangement in the region close to G245S mutation. Consequently, the conformational rearrangement near the G245S mutation results in disorientation of the p53 monomers bound to DNA with a consequent increase in the EBE of the key DNA binding residue R280 of about 4.5 kcal·mol⁻¹ and gain of EBE of other residues such as R280 and R283 to the DNA along with the formation of non-canonical DNA interactions such as residues 122, 123 and 139.

The overall effect of EBE redistribution results in misalignment between the monomers that probably leads to destabilization of the dimer formation and hence an expected destabilization in the tetramer, which would lead to the decrease or loss of the transcriptional activity of p53. The binding energies between the protein monomers on the same site of the DNA are high. This is expected because the tetramerization domain has not been simulated, however a stronger interaction may be found between opposite DBD monomers bound on the same half site DNA [40].

Finally, from the outcome of our work emerges the suggestion that the L3-loop stiffening, which also affects the dynamics of L1 and L2, may be responsible for the reduction of p53 affinity to DNA in the mutated protein. Despite the fact that we simulated the protein for about 1.5 μ s, classical MD may still not be able to capture the whole protein dynamics due to the method's limited sampling capability. Nonetheless, our MD results clearly highlight the G245S mutation as responsible for a dimer reorganization and distortion not observed in the

wt-p53. Starting from our findings, enhanced sampling techniques, able to better sample the phase space in simulations of protein-protein and protein-nucleic acid molecular systems, together with dimensionality reduction [41-46] might provide further insights into the p53-DNA complex dynamics [47].

3.4 Materials and Methods

3.4.1 3D structure preparation

For the DNA bound proteins, the initial atomic coordinates of the wt-p53 DBD-DNA tetramer complex were obtained from the x-ray crystallographic structure with PDB ID: 4HJE [8]. In this structure, the DBD binds to DNA response elements composed of two decameric half-sites separated by 1bp (5'-TCACAAGTTAGAGDCAAGCCT-3') [48]. The crystal waters that mediated interactions between p53 and the DNA were retained. Only two of the four p53 monomers, which bind to DNA on the same side, as well as the bound DNA were included so our simulations could be carried out within a reasonable time. The starting structure of the G245S-mp53 dimer in complex with DNA was obtained from the wt p53 dimer-DNA complex by virtually mutating glycine 245 to serine using PyMol [49]. The protein structures were corrected using Molecular Operating Environment (MOE) software [50]. The protonation states of both the mutant and the wt were calculated using 3Dprotonate [51] in MOE at pH 7, with 0.1 M sodium chloride concentration at 310 K. Moreover, the Zn²⁺ coordinating residues (C176, H179, C238, C242) were deprotonated. Each system, comprised of a p53 dimer in complex with DNA and its co-crystallized water molecules, was solvated in

a TIP3P octahedral water box. The boundaries of the box were chosen to provide a water buffer of 12 Å around the complex along each dimension (a total of 26,178 explicit water molecules). Furthermore, chloride and sodium ions were added to simulate a physiological ionic concentration of 0.1 M. The ions were positioned to replace water molecules having the highest electrostatic energies on their oxygen atoms. For the apo p53 monomers, the initial atomic coordinates for the apo wt-p53 monomer were obtained from the NMR-resolved structure with PDB ID: 2FEJ [18]. The wt and G245S-mutant apo p53 monomers were both prepared in the same manner described for the dimers above. All the systems were solvated and prepared using AmberTools14 [52].

3.4.2 Molecular Dynamics Simulation

Similar to our previous study [53], the water molecules were minimized for 3000 steps of steepest descent followed by 2000 steps of conjugate gradient minimization; heavy restraints of 100 kcal/mol-Å² were placed on the proteins and DNA [52]. The restraints were then removed and a minimization of the whole system was performed through a series of 2500 steepest descent followed by 2500 conjugate gradient steps. Further, the system was gradually heated up to 310 K in 200 ps and maintained at 310 K for another 100 ps under constant volume conditions (NVT). The particle-mesh Ewald procedure was used to handle long-range electrostatic interactions with a 10 Å cut-off. The Langevin thermostat was used with a time collision frequency of 2 ps [54]. Hydrogen atoms were constrained by the SHAKE algorithm and the heavy atoms of the proteins backbone and DNA were heated using 2 kcal/mol-Å² restraints [55]. These restraints were then gradually reduced and the p53 dimers-DNA complexes were simulated for 1.5 μs while the p53 monomers were simulated for 1 μs. Before

running the production in the MD simulation, the systems were assessed by means of their potential, kinetic and total energies, the temperature, pressure and the density of the systems over the simulation times. All simulations were performed using the Amberff14SB force-field [56].

3.4.3 Conformational Change Analysis: RMSD and RMSF

The system's equilibrium and the dynamic fluctuation of p53 residues were analyzed by means of calculating mass-weighted root mean square deviation (RMSD) of the backbone atoms and the residues root mean square fluctuation (RMSF), respectively. These two metrics are measures of distance variation of the protein atoms during the simulation and were evaluated using AmberTools14 [52].

3.4.4 Conformational analysis: FMA

An ensemble of structures obtained from the MD simulations was used to underline the collective motions directly related to loop L3 fluctuation (functional quantity). We used a set of protein structures to find the collective protein motion that is maximally related to the "functional quantity" e.g., the RMSD of the L3 loop. In other words, we performed FMA on the whole simulated MD trajectory of the apo p53 monomers to highlight the collective motions directly correlated to the fluctuation of the region involved in DBD mutation as done in previous literature studies [44,45,57]. More specifically, considering the variable of interest as a linear function of principal components, the maximally correlated vector was obtained by maximizing the Pearson coefficient to quantify the contributions of the individual PCA vectors to the fluctuation of the variable of interest [57].

3.4.5 Clustering

RMSD-based clustering was used to extract protein structures to represent the overall protein flexibility and thus provide means of examining the sampled conformations during the MD simulation. RMSD based clustering was obtained with bottom up algorithms such as average-linkage, single linkage and centroid-linkage methods, all implemented in the utility of AMBER14. We used the equilibrated portions of the MD trajectories for RMSD based clustering using the average-linkage algorithm in AmberTools14 [52]). Several studies have discussed and validated the use of hierarchical algorithms in MD simulations [22,24]. Before clustering, a mass-weighted RMSD fit of the heavy atoms of the backbone to the protein starting structure was performed. To assess the clustering quality and find the optimum number of clusters, three clustering metrics: the Davies-Bouldin index (DBI) [58], the pseudo F-statistic [59], and the sum of square regression-sum of total sum of square ratio (SSR/SST), were plotted for each cluster count. The optimum number of clusters occurs at a local DBI value minimum, a local pSF value maximum and when the SSR/SST ratios plateau [24]. The centroid structures (the structures having the smallest RMSD relative to all the other members of the same cluster) of each cluster were extracted and used for comparative analyses.

3.4.6 Binding Energy Calculation

The binding free energies of p53 to DNA and the p53 dimers to each other, for both the wt and the G245S-mp53 mutant were calculated using the Molecular Mechanics Generalized Born Surface Area (MMGBSA) [60,61]. The free energy was thus calculated with the software AMBER14 [52]. The EBE's between p53 (receptor) and DNA (ligand) were calculated for the p53-DNA complexes for the equilibrated structures as:

Equation 3.1

$$\Delta G_{\text{bind}} = \Delta H - T\Delta S \approx \Delta E_{MM} + \Delta G_{\text{sol}} - T\Delta S$$

where ΔE_{MM} is the molecular mechanical energy in the gas phase and includes the bond, angle and dihedral energies as well as electrostatic and van der Waals energies:

Equation 3.2

$$\Delta E_{MM} = \Delta E_{\text{inter}} + \Delta E_{\text{elec}} + \Delta E_{vDW}$$

and ΔG_{sol} is the solvation free energy given by the sum of the electrostatic solvation energy or polar Energy and a non-electrostatic solvation component (non polar contribution). Here, the electrostatic solvation contribution is evaluated using the Generalized Born (GB) model, while the non-polar contribution is approximated by the solvent accessible area (SASA):

Equation 3.3

$$\Delta G_{\text{sol}} = \Delta G_{GB} + \Delta G_{SA}$$

The conformational entropy change $-T\Delta S$ can be computed by normal-mode analysis.

However, since we were interested in the relative rank of binding energies rather than the absolute values and since the calculation of the entropy term is computationally demanding, the entropy term was assumed to be constant. Therefore, we used the single trajectory approach to evaluate the EBE between the proteins and DNA and between the individual p53 monomers in the p53 dimer complexes by means of the thermodynamic cycle:

Equation 3.4

$$\Delta G_{\text{bind,solv}}^{\circ} = \Delta G_{p53-DNA,vacuum}^{\circ} + \Delta G_{p53-DNA,solv}^{\circ} - \Delta G_{\text{solv,DNA}}^{\circ} - \Delta G_{\text{solv,p53}}^{\circ}$$

3.5 References

1. Vogelstein B, Lane D, Levine AJ. Surfing the p53 network. *Nature* 2000 Nov 16;408(6810):307-310.
2. Goldstein I, Marcel V, Olivier M, Oren M, Rotter V, Hainaut P. Understanding wild-type and mutant p53 activities in human cancer: New landmarks on the way to targeted therapies. *Cancer gene therapy* 2011;18(1):2-11.
3. Wang Z, Sun Y. Targeting p53 for novel anticancer therapy. *Translational Oncology* 2010 - 2;3(1):1-12.
4. Bykov VJN, Wiman KG. Mutant p53 reactivation by small molecules makes its way to the clinic. *FEBS letters* 2014 Aug 19;588(16):2622-2627.
5. Kogan S, Carpizo D. Pharmacological targeting of mutant p53. *Translational Cancer Research* 2016 23/12;5(6):698-706.
6. Olivier M, Eeles R, Hollstein M, Khan MA, Harris CC, Hainaut P. The IARC TP53 database: New online mutation analysis and recommendations to users. *Human mutation* 2002;19(6):607-614.
7. McLure KG, Lee PW. How p53 binds DNA as a tetramer. *The EMBO Journal* 1998 -6-15;17(12):3342-3350.
8. Chen Y, Zhang X, Dantas Machado A, Carolina, Ding Y, Chen Z, Qin P,Z., Rohs R, Chen L. Structure of p53 binding to the BAX response element reveals DNA unwinding and compression to accommodate base-pair insertion. 2013;41(17):8368-8376.
9. Cho Y, Gorina S, Jeffrey PD, Pavletich NP. Crystal structure of a p53 tumor suppressor-DNA complex: Understanding tumorigenic mutations. *Science* 1994 July 15;265(5170):346-355.
10. Chen Y, Dey R, Chen L. Crystal structure of the p53 core domain bound to a full consensus site as a self-assembled tetramer. *Structure (London, England: 1993)* 2010 Feb 10;18(2):246-256.
11. Duan J, Nilsson L. Effect of Zn²⁺ on DNA recognition and stability of the p53 DNA-binding domain. *Biochemistry* 2006 Jun 20;45(24):7483-7492.

12. Hanel W, Marchenko N, Xu S, Yu SX, Weng W, Moll U. Two hot spot mutant p53 mouse models display differential gain of function in tumorigenesis. *Cell Death and Differentiation* 2013 Jul;20(7):898-909.
13. Xu J, Qian J, Hu Y, Wang J, Zhou X, Chen H, Fang J. Heterogeneity of li-fraumeni syndrome links to unequal gain-of-function effects of p53 mutations. *Scientific Reports* 2014 -02-27;4.
14. Samowitz WS, Curtin K, Ma K, Edwards S, Schaffer D, Leppert MF, Slattery ML. Prognostic significance of p53 mutations in colon cancer at the population level. *International Journal of Cancer* 2002 Jun 01;99(4):597-602.
15. Lehmann S, Bykov VJN, Ali D, Andren O, Cherif H, Tidefelt U, Uggla B, Yachnin J, Juliusson G, Moshfegh A, Paul C, Wiman KG, Andersson P. Targeting p53 in vivo: A first-in-human study with p53-targeting compound APR-246 in refractory hematologic malignancies and prostate cancer. *Journal of Clinical Oncology* 2012;30(29):3633-3639.
16. Wassman CD, Baronio R, Demir O, Wallentine BD, Chen C, Hall LV, Salehi F, Lin D, Chung BP, Hatfield GW, Chamberlin AR, Luecke H, Lathrop RH, Kaiser P, Amaro RE. Computational identification of a transiently open L1/S3 pocket for reactivation of mutant p53. *Nature Communications* 2013;4:1407.
17. Zhao K, Chai X, Johnston K, Clements A, Marmorstein R. Crystal structure of the mouse p53 core DNA-binding domain at 2.7 Å resolution. *The Journal of Biological Chemistry* 2001 Apr 13;276(15):12120-12127.
18. Cañadillas JMP, Tidow H, Freund SMV, Rutherford TJ, Ang HC, Fersht AR. Solution structure of p53 core domain: Structural basis for its instability. *Proceedings of the National Academy of Sciences* 2006 -02-14 00:00:00;103(7):2109-2114.
19. Bullock AN, Henckel J, DeDecker BS, Johnson CM, Nikolova PV, Proctor MR, Lane DP, Fersht AR. Thermodynamic stability of wild-type and mutant p53 core domain. *Proceedings of the National Academy of Sciences of the United States of America* 1997;94(26):14338-14342.
20. Wong K, DeDecker BS, Freund SMV, Proctor MR, Bycroft M, Fersht AR. Hot-spot mutants of p53 core domain evince characteristic local structural changes. *Proceedings of the National Academy of Sciences* 1999;96(15):8438-8442.
21. Joerger AC, Ang HC, Fersht AR. Structural basis for understanding oncogenic p53 mutations and designing rescue drugs. *Proceedings of the National Academy of Sciences of the United States of America* 2006 Oct 10;103(41):15056-15061.
22. Demir Ö, Baronio R, Salehi F, Wassman CD, Hall L, Hatfield GW, Chamberlin R, Kaiser P, Lathrop RH, Amaro RE. Ensemble-based computational approach discriminates functional

activity of p53 cancer and rescue mutants. *PLOS Computational Biology* 2011 Oct 20;;7(10):e1002238.

23. Koulgi S, Achalere A, Sharma N, Sonavane U, Joshi R. QM-MM simulations on p53-DNA complex: A study of hot spot and rescue mutants. *Journal of Molecular Modeling* 2013 Dec;19(12):5545-5559.

24. Shao J, Tanner SW, Thompson N, Cheatham TE,III. Clustering molecular dynamics trajectories: 1. characterizing the performance of different clustering algorithms. *Journal of Chemical Theory and Computation* 2007;3(6).

25. Wang Y, Schwedes JF, Parks D, Mann K, Tegtmeyer P. Interaction of p53 with its consensus DNA-binding site. *Molecular and Cellular Biology* 1995 Apr;15(4):2157-2165.

26. Soussi T, Lozano G. P53 mutation heterogeneity in cancer. *Biochemical and Biophysical Research Communications* 2005 Jun 10;;331(3):834-842.

27. Chan WM, Siu WY, Lau A, Poon RYC. How many mutant p53 molecules are needed to inactivate a tetramer? *Molecular and Cellular Biology* 2004 -4;24(8):3536-3551.

28. Joerger AC, Fersht AR. Structure–function–rescue: The diverse nature of common p53 cancer mutants. *Oncogene* 2007 -04;26(15):2226-2242.

29. Bullock AN, Fersht AR. Rescuing the function of mutant p53. *Nature Revisions Cancer* 2001 10/;1(1):68-76.

30. Friedler A, DeDecker BS, Freund SMV, Blair C, Rüdiger S, Fersht AR. Structural distortion of p53 by the mutation R249S and its rescue by a designed peptide: Implications for "mutant conformation". *Journal of Molecular Biology* 2004 Feb 06;;336(1):187-196.

31. David CC, Jacobs DJ. Principal component analysis: A method for determining the essential dynamics of proteins. *Methods in Molecular Biology (Clifton, N.J.)* 2014;1084:193-226.

32. Bahar I, Lezon TR, Yang L, Eyal E. Global dynamics of proteins: Bridging between structure and function. *Annual Review of Biophysics* 2010;39:23-42.

33. Lukman S, Lane DP, Verma CS. Mapping the structural and dynamical features of multiple p53 DNA binding domains: Insights into loop 1 intrinsic dynamics. *PLoS ONE* 2013;8(11).

34. Ishimaru D, Ano Bom, Ana Paula D., Lima, Luís Maurício T. R., Quesado PA, Oyama MFC, de Moura Gallo, Claudia V., Cordeiro Y, Silva JL. Cognate DNA stabilizes the tumor suppressor p53 and prevents misfolding and aggregation. *Biochemistry* 2009 July 7;;48(26):6126-6135.

35. Lambrugh M, De Gioia L, Gervasio FL, Lindorff-Larsen K, Nussinov R, Urani C, Bruschi M, Papaleo E. DNA-binding protects p53 from interactions with cofactors involved in transcription-independent functions. *Nucleic Acids Research* 2016 -11-02;44(19):9096-9109.
36. Selivanova G, Wiman KG. Reactivation of mutant p53: Molecular mechanisms and therapeutic potential. *Oncogene* 2007 Apr 02;;26(15):2243-2254.
37. Chène P. The role of tetramerization in p53 function. *Oncogene* 2001;20:2611.
38. Kamada R, Nomura T, Anderson CW, Sakaguchi K. Cancer-associated p53 tetramerization domain mutants: Quantitative analysis reveals a low threshold for tumor suppressor inactivation. *The Journal of Biological Chemistry* 2011 Jan 07;;286(1):252-258.
39. Menendez D, Inga A, Resnick MA. The biological impact of the human master regulator p53 can be altered by mutations that change the spectrum and expression of its target genes. *Molecular and Cellular Biology* 2006 Mar;26(6):2297-2308.
40. Ho WC, Fitzgerald MX, Marmorstein R. Structure of the p53 core domain dimer bound to DNA. *The Journal of Biological Chemistry* 2006 Jul 21;;281(29):20494-20502.
41. Paciello G, Acquaviva A, Ficarra E, Deriu MA, Macii E. A molecular dynamics study of a miRNA:mRNA interaction. *Journal of Molecular Modeling* 2011 Nov;17(11):2895-2906.
42. Grasso G, Tuszynski JA, Morbiducci U, Licandro G, Danani A, Deriu MA. Thermodynamic and kinetic stability of the josephin domain closed arrangement: Evidences from replica exchange molecular dynamics. *Biology Direct* 2017 Jan 19;;12(1):2.
43. Deriu MA, Grasso G, Tuszynski JA, Gallo D, Morbiducci U, Danani A. Josephin domain structural conformations explored by metadynamics in essential coordinates. *PLOS Computational Biology* 2016 Jan 8;;12(1):e1004699.
44. Deriu MA, Grasso G, Tuszynski JA, Massai D, Gallo D, Morbiducci U, Danani A. Characterization of the AXH domain of ataxin-1 using enhanced sampling and functional mode analysis. *Proteins* 2016 May;84(5):666-673.
45. Grasso G, Deriu MA, Tuszynski JA, Gallo D, Morbiducci U, Danani A. Conformational fluctuations of the AXH monomer of ataxin-1. *Proteins* 2016 Jan;84(1):52-59.
46. Grasso G, Deriu MA, Prat M, Rimondini L, Vernè E, Follenzi A, Danani A. Cell penetrating peptide adsorption on magnetite and silica surfaces: A computational investigation. *The Journal of Physical Chemistry B* 2015 July 2;;119(26):8239-8246.
47. Bernardi RC, Melo MCR, Schulten K. Enhanced sampling techniques in molecular dynamics simulations of biological systems. *Biochimica et Biophysica Acta (BBA) - General Subjects* 2015 May 1;;1850(5):872-877.

48. Wei C, Wu Q, Vega VB, Chiu KP, Ng P, Zhang T, Shahab A, Yong HC, Fu Y, Weng Z, Liu J, Zhao XD, Chew J, Lee YL, Kuznetsov VA, Sung W, Miller LD, Lim B, Liu ET, Yu Q, Ng H, Ruan Y. A global map of p53 transcription-factor binding sites in the human genome. *Cell* 2006 Jan 13,;124(1):207-219.
49. The PyMOL molecular graphics system, version 1.8 schrödinger, LLC.
50. Molecular operating environment (MOE), 2014.09; chemical computing group inc., 1010 sherbooke st. west, suite #910, montreal, QC, canada, H3A 2R7, 2014.
51. Labute P. The generalized born/volume integral implicit solvent model: Estimation of the free energy of hydration using london dispersion instead of atomic surface area. *Journal of Computational Chemistry* 2008 Jul 30,;29(10):1693-1698.
52. Case DA, Babin V, Berryman JT, Betz RM, Cai Q, Cerutti DS, Cheatham DSI, Darden TA, Duke RE, Gohlke H, Goetz AW, Gusarov S, Homeyer N, Janowski P, Kaus J, Kolossváry I, Kovalenko A, Lee TS, LeGrand S, Luchko T, Luo R, Madej B, Merz KM, Paesani F, Roe DR, Roitberg A, Sagui C, Salomon-Ferrer R, Seabra G, Simmerling CL, Smith W, Swails J, Walker RC, Wang J, Wolf RM, Wu X, Kollman PA. Amber 14. 2014.
53. Omar SI, Tuszynski J. Ranking the binding energies of p53 mutant activators and their ADMET properties. *Chemical Biology & Drug Design* 2014.
54. Loncharich RJ, Brooks BR, Pastor RW. Langevin dynamics of peptides: The frictional dependence of isomerization rates of N-acetylalanyl-N'-methylamide. *Biopolymers* 1992 May;32(5):523-535.
55. Ryckaert J, Ciccotti G, Berendsen HJC. Numerical integration of the cartesian equations of motion of a system with constraints: Molecular dynamics of n-alkanes. *Journal of Computational Physics* 1977 March 1,;23(3):327-341.
56. Maier JA, Martinez C, Kasavajhala K, Wickstrom L, Hauser KE, Simmerling C. ff14SB: Improving the accuracy of protein side chain and backbone parameters from ff99SB. *Journal of Chemical Theory and Computation* 2015 August 11,;11(8):3696-3713.
57. Hub JS, Groot BLd. Detection of functional modes in protein dynamics. *PLOS Computational Biology* 2009 Aug 28,;5(8):e1000480.
58. Davies DL, Bouldin DW. Cluster separation measure. *IEEE Transactions on Pattern Analysis and Machine Intelligence* 1979;1(2):224-227.
59. Caliński T, Harabasz J. A dendrite method for cluster analysis. *Communications in Statistics* 1974 January 1,;3(1):1-27.
60. Onufriev A, Bashford D, Case DA. Modification of the generalized born model suitable for macromolecules. *The Journal of Physical Chemistry B* 2000 April 1,;104(15):3712-3720.

61. Srinivasan J, Cheatham TE, Cieplak P, Kollman PA, Case DA. Continuum solvent studies of the stability of DNA, RNA, and Phosphoramidate–DNA helices. *Journal of the American Chemical Society* 1998 September 1,;120(37):9401-9409.

Chapter 4

Virtual screening using covalent docking to find activators for G245S mutant p53

Preface

This chapter has been accepted for publication in PLoS One:

Omar SI, Lepre MG, Morbiducci U, Deriu MA, Tuszynski JA. Virtual screening using covalent docking to find activators for G245S mutant p53

PLoS One is an open-access publisher that states: "PLOS applies the Creative Commons Attribution (CC BY) license to works we publish."

Contributions: SIO: conceived and designed the experiments, guided the student to do all *in silico* work, performed the modeling for the minimized ligand protein complex and ran ADMET predictions, analysed the data and wrote the paper. MGL: performed all the experiments, analyzed the data and wrote the paper.

Note: This chapter has been modified for consistency with the rest of the thesis; the methods section has been moved to the end of the chapter and some abbreviations have been changed. Additional information has been added to the introduction and discussion for clarification.

4.1 Introduction

The transcription factor, p53, binds to its response elements to activate the transcription of canonical p53 target genes [1]. It controls various processes in cells such as DNA repair, cell proliferation, metabolism, senescence and apoptosis [1-3]. Since p53 is a master tumor suppressor protein, it is not surprising that it is the most mutated protein in all cancer types [4]. Mutations in the *TP53* gene often result in a p53 mutant protein that loses its specific DNA binding ability, which consequently compromises or abolishes the protein's tumor suppression function [5, 6]. The great importance of p53 in the context of cancer has made it a logical target for anti-cancer treatment [2]. Indeed, the reconstitution of the wild type (wt) p53 activity in mice induced rapid tumor regression [7, 8] although in some cases it led to the emergence of p53-resistant tumors [8].

A synthetic nine amino acid peptide CDB3 (REDEDEIEW) has been found in a peptide screen to stabilize the p53 core domain [9]. Additionally, it was found to restore the sequence-specific binding of the I195T (isoleucine to threonine mutation in codon 195) mp53 to DNA [9]. CDB3 was derived from the p53 binding protein, apoptosis-stimulating of p53 protein 2 (ASPP2), which enhances the DNA binding and transactivation ability of p53 and consequently enhances the apoptotic function of the latter protein [10]. It has been hypothesized that CDB3 and its derivatives act as chaperones that bind to p53 and shift the equilibrium of the protein folding towards its native state [11]. CDB3 is then displaced by the specific DNA sequence [9, 11]. Such chaperone peptides have some obvious limitations due to their large size and poor bioavailability. In addition, they are unlikely to restore the DNA binding ability of contact mutants of p53.

Small molecule p53 activators, rather than peptides, have more advantages as therapeutic agents in terms of bioavailability, drug administration and compound synthesis. Attempts to develop small molecules aimed at restoring the wt activity to mutant p53 (mp53) have progressed in the past years. In 1999, Foster and colleagues [12] reported the discovery of CP-31398, obtained by a library screen based on an *in vitro* biochemical assay, in which antibodies were used to distinguish between the wt and mutant conformations of p53. CP-31398 was also shown to have a stabilizing effect on the p53 DNA binding domain (DBD) and enhance the transcriptional activity of wt-p53 in tumor xenografts expressing the mutant protein [12, 13]. However, determination of a detailed mechanism of action of CP-31398 still remains elusive [14]. A study has shown that the molecule binds tightly to the DNA [15] and another suggested that the molecule acts on other targets since CP-31398 altered gene expression in both p53 dependent and independent manners [15].

Other successful attempts at finding mp53 rescuers have identified PRIMA-1 ('p53 reactivation and induction of massive apoptosis') and MIRA-1 by means of an *in vitro* screen [17, 18]. The methylated derivative of PRIMA-1, called APR-246 [19], is the only small molecule mp53 activator that has reached clinical trials [20]. Both PRIMA-1 and APR-246 are prodrugs that decompose to methylene quinuclidinone (MQ) [19]. The active MQ, characterized by a reactive double bond, was found to react with the cysteine residues of p53 through a Michael addition reaction, which restores the wt conformation and transcriptional activity of the protein [19]. *In silico* analysis using molecular dynamics (MD) identified a transiently open pocket in the DBD of p53 formed between loop L1 and the S3 beta-sheet, which contains three cysteines at residues 124, 141 and 135 [21]. In that study, the wt, R175H, R273H and G245S mp53 proteins were simulated. The calculated solvent-accessible

surface area of the three different cysteines revealed that C124 was the most solvent exposed cysteine residue at that pocket. Hence, C124 was concluded to be the most likely residue at which MQ reacts with mp53 to restore its wt transcriptional activity [21]. This conclusion was further confirmed by the results from the site-directed mutagenesis of C124 to alanine [21]. MQ treatment could not inhibit the growth of Saos-2 cells in C124A-R175H-mp53 vs. R175H-mp53 transfected cells. Wassman *et al.* further performed virtual screening using non-covalent docking of the NCI diversity set II and identified stictic acid as a novel mp53 activator. Indeed, stictic acid was found to elicit the activation of p21, a p53 target gene product, in a dose-dependent manner in Saos-2 cells transfected with R175H-mp53. Additionally, stictic acid and MQ increased the thermal stability of R175H and G245S mp53. We have previously non-covalently docked small molecule activators of mp53 to R273H-mp53 [22]. The docked covalent p53 activators included MQ, NB, STIMA-1, MIRA-1 and CP-31398 [22]. While the five compounds were not predicted to interact directly with C124, they were within a short distance that would allow the reaction of the double bonds of the molecules with the thiol group of C124. On the other hand, our docking results of the non-covalent p53 activators suggest that the activator molecules interact directly with C124. In the same study, we also used ADMET Predictor to predict the pharmacokinetics and toxicity of the docked compounds. Although *in silico* toxicity predictions indicated that stictic acid is less toxic than MQ, the former compound was predicted to have poor pharmacokinetic properties.

The highest frequency, hotspot, mutations in p53 are categorized based on how the mutations alter the protein's binding to the DNA. p53 variants with a mutation in a residue that natively interacts with the DNA in the wt protein are classified as contact mutants. Other mutations in

the DNA binding domain of p53 are classified as structural mutants, since they alter the protein's structure and therefore affect its binding to the DNA [23]. G245S-mp53 is one of the p53 hotspot structural mutants, which carries a single-point mutation in codon 245 that changes the wild-type glycine residue to serine [23].

As explained above, previous efforts at finding p53 activators were mainly based on *in vitro* and *in vivo* studies [9, 14, 19]. *In silico* screening at C124 has been used to find stictic acid [21]. Docking at a cleft near loop L6 was also used to screen a library of two million compounds to find activators of Y220C-mp53, which successfully yielded PhiKan083 using non-covalent docking [24]. In this study, we used DOCKTITE [25], a covalent docking protocol, to screen a subset of the ZINC database at the C124 pocket to find potential activators of G245S-mp53. To refine our predictions, we also used a consensus scoring approach by combining two scoring functions to improve the pose and binding energy predictions. Here, we report potential G245S-mp53 activators and some of their predicted ADMET properties in this work.

4.2 Results and Discussion

4.2.1 G245S-mp53 protein models

We performed MD simulations of the apo G245S-mp53 as well as the DNA bound protein obtained from the virtual mutation of G245 of wt-p53 to serine in the experimentally determined structures with PDB ID: 2FEJ and 4HJE, respectively. This was to account for the different possible conformations of G245S-mp53. We also used the representative structures from the MD simulations to account for the protein's flexibility specifically at the binding

site. These representative structures were obtained by clustering the equilibrated protein [26] based on the RMSD of residues 113-124 and 141-146, which constitute the pocket around the reactive C124 residue. Clustering was performed based on the average-linkage algorithm [27] using the cpptraj utility in Ambertools [28]. The choice of the optimum number of clusters was guided by the calculated DBI, pSF and SSR/SST clustering metrics for each cluster count from 2 to 20.

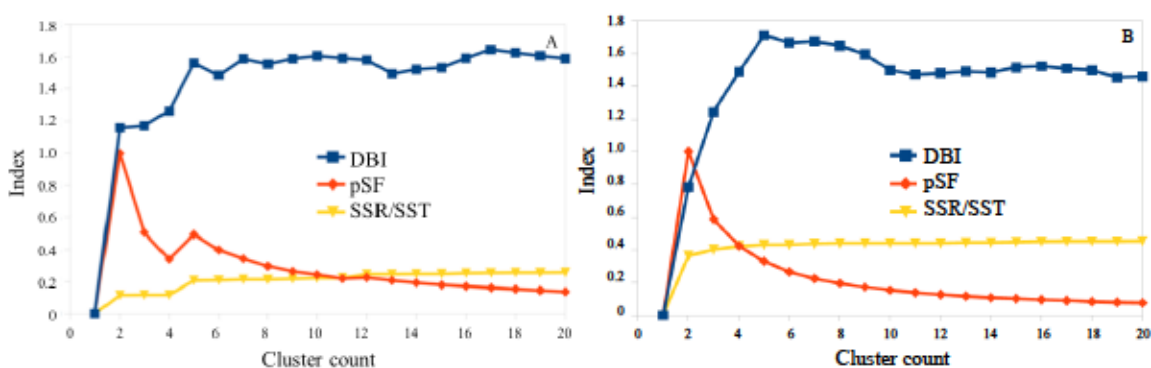


Figure 4.1: Plots of the DBI, pSF and SSR/SST clustering metrics for the equilibrated (A) apo and (B) DNA-bound G245S-mp53. The pSF values were normalized to fit on the graph.

The choice of the optimum cluster number is not trivial. Ideally, the best number of clusters falls at a local minimum DBI value, local maximum pSF value and where the SSR/SST ratio starts to plateau [27]. Our clustering metrics did not all fulfill these criteria at a particular cluster count, as shown in Figure 4.1. As partial fulfilment of these criteria, however, we chose cluster counts of 4 and 2 to represent the last 460 ns and 1 μ s of the equilibrated apo and DNA-bound G245S-mp53. The centroids of these clusters were used to represent the G245S-mp53 for covalent docking. We used monomer B in the DNA-bound G245S-mp53 models and removed the bound DNA for docking.

4.2.2 Covalent docking of the filtered ZINC library

While non-covalent docking is a vastly used virtual screening tool, covalent docking has been used less frequently in computational drug design. Nonetheless, covalent docking has been used successfully [29-31]. A previous study employing virtual screening using covalent docking on the vaccinia virus I7L ubiquitin-like proteinase homology model has reported a 21% successful hit rate [32].

In this study, we used a versatile covalent docking protocol in the Molecular Operating Environment (MOE) [33] called DOCKTITE [25]. We assigned the thiol of C124 as the reaction site for the screened library. We filtered the ZINC library to only include compounds that were in stock and had a molecular weight between 300 and 500 daltons, which falls within the weight range suggested by the Lipinski's rule of five [34]. We also filtered for compounds that had moderate to standard reactivity. This criterion was specified since we aimed to find covalent activators of p53 that could permanently restore the mutant protein's wild type activity. The final filtered library size was about 130,000 molecules.

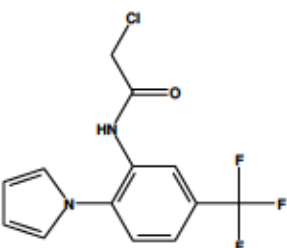
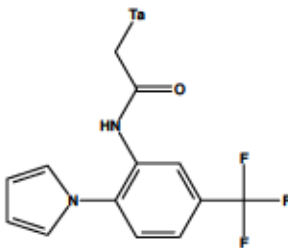
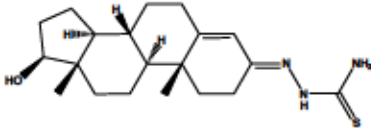
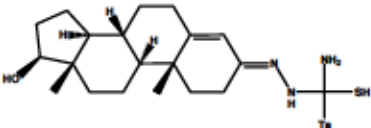
Each of the screened ligands was then tagged at its reaction site and additional stereoisomers were created for ligands with prochiral centers. A conformational search was performed in MOE until a maximum of 5,000 conformers were generated for each ligand and each isomer. A pharmacophore model was automatically generated by MOE to guide the placement of the generated conformers at the active site. The docked poses were then evaluated by the Affinity dG scoring function in MOE. The top 100 poses of each docked ligand were further refined. There are two possible refinement methods in MOE: energy and grid minimization. ROC curves of the two methods have demonstrated that the former is only marginally more accurate with an area under the curve of 0.81 vs. 0.79 [25]. This slight increase in accuracy

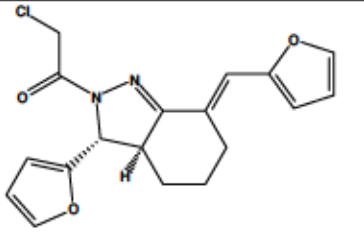
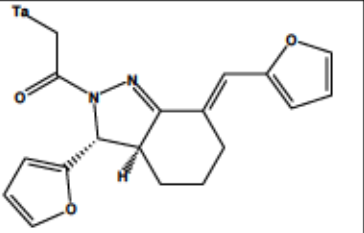
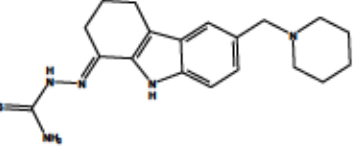
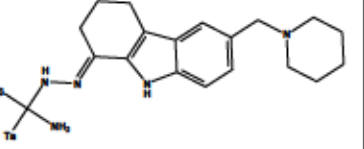
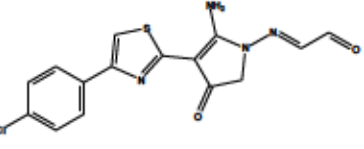
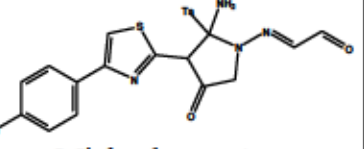
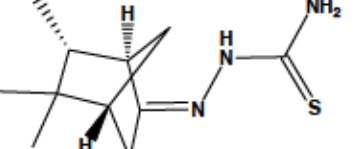
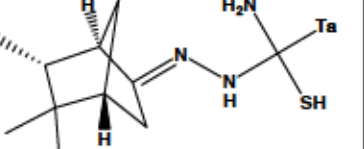
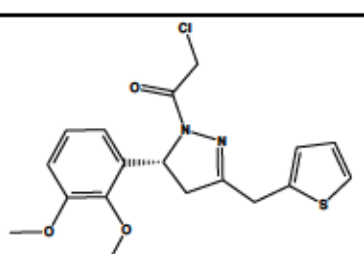
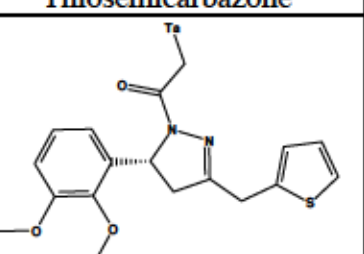
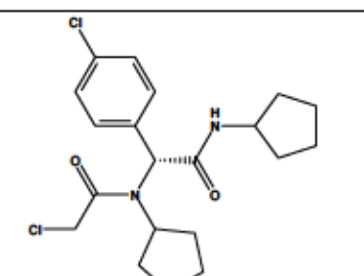
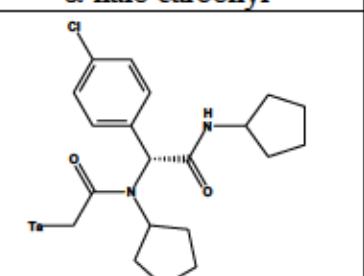
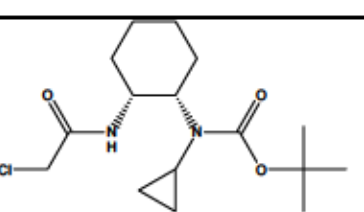
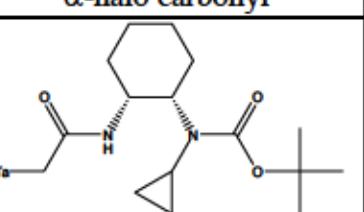
comes at the expense of forty times the computational cost [25]. For our virtual screening purposes we, therefore, used grid minimization for refinement and rescored the refined poses using the Affinity dG scoring function.

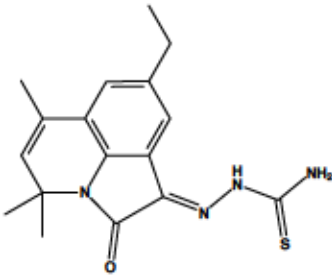
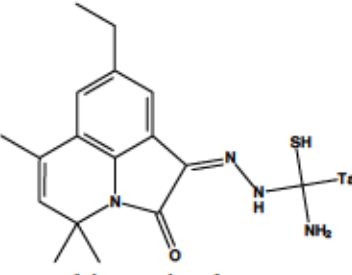
We used a consensus-based strategy to rank the top hits. To do this, the highest ranked pose for each compound was then detached and rescored by the DSX scoring function as a non-covalently bound ligand since it gives more accurate results [25]. While the Affinity dG scoring function predicts the binding energy of the ligand, the DSX is a knowledge-based function that scores ligands on how close they are to near-native poses i.e. experimentally resolved complex structures [25]. The screened compounds were ranked based on both scores. Table 4.1 shows a list of the top 10 potential activators based on their DSX scores and favorable predicted Affinity dG scores.

Table 4.1: The top ten hits from our covalent docking virtual screening.

The hits are ranked based on their DSX score. The reactive moiety of molecules is tagged by 'Ta', which marks the thiol group of C124 of G245S-mp53 in case of a true hit. Mwt= molecular weight of the compound.

No.	Molecule	Predicted reactive form And warhead type	DSX score	Affinity dG (kcal•mol ⁻¹)	Mwt
1		 α -halo carbonyl	-17.5	-2.5	303
2		 Thiosemicarbazone	-16.5	-3.8	362

3			-15.8	-2.8	345
		α-halo carbonyl			
4			-13	-2.9	356
		Thiosemicarbazone			
5			-10.5	-3.35	347
		Michael acceptor			
6			-9.8	-2.5	225
		Thiosemicarbazone			
7			-9.5	-2.4	379
		α-halo carbonyl			
8			-9.5	-2.3	397
		α-halo carbonyl			
9			-9.5	-2.2	331
		α-halo carbonyl			

10		 <p style="text-align: center;">Thiosemicarbazone</p>	-8	-2.66	328
----	---	--	----	-------	-----

Unlike all the previous covalent p53 activators such as MQ, STIMA-1 and MIRA-1, which are all Michael acceptors, five of our potential hits were thiosemicarbazones, four were halo-carbonyls and only one was a Michael acceptor molecule (Table 4.1). The DSX scores, which rank near-native binding modes, ranged from -17.5 to -8. The Affinity dG binding energies of the compounds ranged from -3.8 to -2.2 kcal·mol⁻¹.

In conventional non-covalent docking, especially when screening for competitive inhibitors, a higher binding affinity is an indication of better potential inhibition. This is due to the fact that a ligand that can bind strongly at the active-site will likely decrease the chance of the native substrate from binding. However, analysing the results of covalent molecules aimed at activating a protein, like our case, is less trivial. A good p53 mutant activator is a compound that not only interacts with C124, like MQ, but also alters the structure of the protein to restore its wild type activity. Nonetheless, a higher DSX score, being an indication of the pose being near-native, is an indication that the conformation is likely to exist. Indeed, a 21% hit rate was achieved in a previous study where virtual screening using covalent docking was used.

4.2.3 ADMET property predictions

The toxicities of the top 10 compounds were predicted using ADMET Predictor™ and were compared to those of APR-246's active metabolite called MQ. The prodrug APR-246 is the only mp53 activator that is currently in clinical trials [20]. Some of the predicted properties are listed in Table 4.2.

Table 4.2: The predicted ADMET properties of MQ and the top 10 potential hits from our covalent docking screen.

Values between brackets indicate confidence levels.

Compound	ADMET risk score	BBB filter	hERG filter	Pgp Inh	Pgp substr	Ser ALT	Ser AST
1	3.8	High	Yes (85%)	No (94%)	No (95%)	Elevated (98%)	Elevated (94%)
2	1.0	High	No (95%)	No (63%)	No (59%)	Normal (78%)	Normal (62%)
3	2.9	High	No (95%)	Yes (83%)	No (95%)	Normal (73%)	Elevated (94%)
4	3.7	High	No (95%)	Yes (69%)	Yes (97%)	Normal (52%)	Normal (70%)
5	6.0	High	No (59%)	No (65%)	No (58%)	Elevated (84%)	Elevated (94%)
6	2.8	High	No (95%)	No (94%)	No (85%)	Normal (95%)	Normal (65%)
7	0.4	High	No (95%)	No (65%)	No (95%)	Normal (60%)	Elevated (69%)
8	4.4	High	No (82%)	Yes (70%)	No (95%)	Elevated (66%)	Elevated (94%)
9	1.0	High	No (76%)	No (62%)	No (79%)	Normal (99%)	Normal (89%)

10	4.2	Low	No (95%)	No (94%)	No (59%)	Elevated (70%)	Elevated (59%)
MQ	3.0	High	No (95%)	No (94%)	No (75%)	Elevated (79%)	Elevated (94%)

ADMET Predictor™ assigns an ADMET risk score to each compound based on its calculated pharmacokinetic (PK) and pharmacodynamics (PD) properties; higher scores are assigned to less favorable properties. This parameter has been developed using drugs from the World Drug Index as a training set. Only 10% of the focused subset of the World Drug Index have an ADMET risk score of more than 6.5. MQ had a predicted risk score of 3. Only compounds 2, 6, 7 and 9 had lower risk scores than MQ (Table 4.2). Interestingly, all the top hits as well as MQ, are predicted to cross the blood brain barrier, except compound 10. While compound 1 was predicted to be cardiotoxic, the remaining compounds, including MQ, were not predicted to inhibit the hERG channel. Additionally, most compounds were predicted to be non-inhibitory to p-glycoproteins, nor were substrates to these protein pumps that export drugs out of cells. The only exceptions to this were compounds 3 and 8, which were predicted to inhibit p-glycoproteins. Compound 4 was predicted to be both a p-glycoprotein substrate and inhibitor. Like MQ, compounds 1, 5, 8 and 10 were predicted to be hepatotoxic and likely to cause an elevation in serum levels of both ALT and AST. None of the other compounds are expected to elevate serum levels of the two enzymes, except compounds 3 and 7, which were predicted to elevate serum AST levels. It is worth noting that none of our potential hits violates Lipinski's rule of five [34].

4.2.4 Compound 2: The best potential hit

From the results above, compound 1 had a DSX score of -17.5, an Affinity dG score of -2.5 kcal·mol⁻¹ and an ADMET risk score of 3.8. Compound 2, which had the second highest DSX score of -16.5, had the highest Affinity dG score of -3.5 kcal·mol⁻¹ and the second best ADMET score of 1. The compound with the best ADMET risk score of 0.4, had DSX and Affinity dG scores of -9.5 and -2.4 kcal·mol⁻¹, respectively. Collectively, these predictions indicate that compound 2 has the best potential as a G245S-mp53 activator.

Figure 4.2 shows the minimized G245S-mp53 bound to compound 2 at C124. Our model shows that compound 2 becomes buried in the core of the protein (Figure 4.2A). This is especially true for the fused ring system of compound 2, which becomes surrounded by F109, L111, F113, V143, L145, A159, I195, Y234, Y236, I255 and F270 (Figure 4.2B). Additionally, the amine group of compound 2 is predicted to be protonated while the neighboring C141 thiol of G245S-mp53 becomes deprotonated. These moieties are predicted to form a salt bridge. The amine group of compound 2 also forms a hydrogen bond with the backbone of C141 of the protein. Also, R110 backbone forms a hydrogen bond with the hydroxyl of compound 2. These interactions could likely confer a conformational change in G245S-mp53 that could lead to better binding of the protein to its response elements and hence restore the wild activity to this mutant.

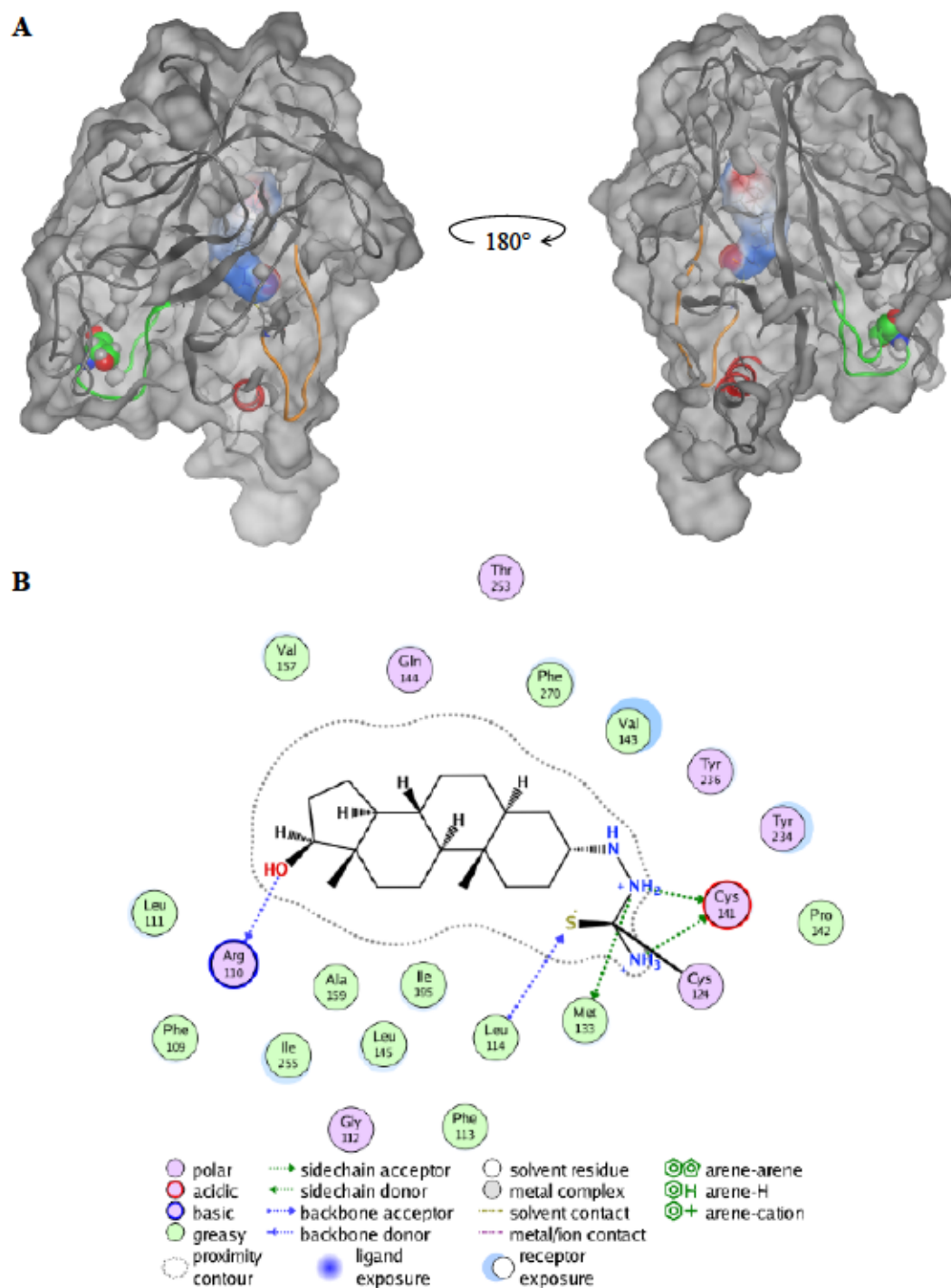


Figure 4.2: Compound 2 covalently bound to G245S-mp53.

(A) The protein's molecular surface is shown in grey. Loop L1, where compound 2 is covalently bound, is colored as an orange ribbon. Helix H2 and loop L3, which interact with the DNA are colored red and green, respectively. The mutated S245 in loop L3 is shown as green spheres. Compound 2 is represented by its molecular surface and is colored based on its electrostatic potential. (B) The ligand interaction scheme of compound 2 with the minimized G245S-mp53.

4.3 Conclusions

Restoring the wt activity to mp53 is a promising strategy to treat cancer. APR-246 is the only mp53 activator that is currently in clinical trials. Our aim was to find potential G245S-mp53 activators. We created atomistic *in silico* models of the mutant protein and virtually screened the ZINC database library using DOCKTITE's covalent docking protocol. The filtered library was assigned to bind at C124 of G245S-mp53. The ligands were ranked based on consensus scoring. We used both the knowledge-based DSX and Affinity dG empirical scoring functions. We also used ADMET Predictor™ to predict possible toxicities of the compounds. Our results show that compound 2 has the best potential as a G245S-mp53 activator. The minimized structure of the complex composed of Compound 2 and G245S-mp53 protein shows that the compound becomes buried in the protein and its hydrophobic portion forms van der Waals interactions with the hydrophobic core of the protein. *In vitro* testing will be required to validate our predictions and, provided this is successful, further select a subset of the predicted hits for preclinical development. It is hoped that the work reported here opens new avenues for targeting this important cancer biomarker.

4.4 Methods and Models

4.4.1 Ligand library preparation

We screened the ZINC15 database, which originally contains about 13 million compounds [35]. We applied three criteria to filter the compounds and reduce the size of the docked database. Our filtered sub-library contained compounds with molecular weights between 300

and 500 Daltons and had an octanol-water partition coefficient (logP) between -1 and 5. We also limited our search to compounds that were in stock and were categorized as mild to reactive. Our final library size was about 130,000 drug-like compounds. We downloaded the 3D representations of the ligands including their different protomer and tautomers.

4.4.2 G245S-mp53 preparation

We created the G245S-mp53 models as described in our previous work [26]. Briefly, we used the NMR resolved apo wt-p53 with PDB ID: 2FEJ [36] as well as the X-ray resolved wt p53-DNA complex (PDB ID: 4HJE [37]) as the starting structures for our models. We used PyMol to virtually mutate residue 245 from glycine to serine [38]. We MD-simulated the mutated models for 1 and 1.5 μ s, respectively as described in [26].

4.4.3 RMSD-based Clustering

To account for the flexibility of the protein's binding site using a manageable number of representative protein models, the structure of the last 460 ns of the equilibrated apo G245S-mp53 monomer (from 2FEJ) and the last 1 μ s of the G245S-mp53 monomer B (from 4HJE) were clustered using the cptraj utility in Ambergtools [28]. Clustering using the average-linkage bottom-up algorithm was based on the root-mean-squared deviation of residues 113-124 and 141-146, constituting the pocket around the C124 site. We used the Davies-Bouldin index (DBI), the pseudo F-statistic (pSF) and the sum of square regression-sum of total sum of square ratio (SSR/SST) clustering metrics to determine the clustering quality and the optimum number of representative clusters [27]. Generally, lower DBI and higher pSF values signal better clustering. The SSR/SST ratio was used following the "elbow criterion" for the

choice of the number of clusters [27]. The centroid structures, which have the lowest RMSD to all the other conformations in the cluster, were used to represent the flexibility of the active site during docking.

4.4.4 Covalent docking using DOCKTITE

We employed the DOCKTITE protocol to virtually screen the filtered sub-library using covalent docking [25]. The first step of the protocol is to screen the molecules for reactive electrophilic warheads. For each compound in the filtered sub-library, the ligands are each attached to the nucleophilic thiol of C124. Additionally, stereoisomers were also created for prochiral compounds. A pharmacophore model of the active site is also automatically generated. The active site was defined by residues 113-124 and 141-146 as well as all atoms within 9 Å from the center of the selected residues. As part of the DOCKTITE protocol, stochastic sampling was used to generate 5,000 possible conformations of the ligands. Docking of the 5,000 conformers was then performed and was guided by the previously generated pharmacophore model. The docked conformers were first evaluated by the empirical Affinity dG scoring function. Based on their scores, the top 100 poses are further refined using the grid minimization method then rescored using the Affinity dG scoring function. For better estimation of the results, the ligands were then cleaved from the nucleophilic side-chains and rescored. Identification of the top hits at this stage was based on consensus scoring. The external knowledge-based scoring function, DSX [39], was used to rank the different poses of a compound based on their similarities to near-native poses. The binding energy of the pose that ranked first with the DSX function was then recalculated with MOE's Affinity dG empirical scoring function.

4.4.5 ADMET Predictor™

We used ADMET Predictor™ of SimulationsPlus [40] to predict compound toxicities. ADMET predictor is a machine learning algorithm that calculates various properties and toxicities of compounds and assigns an ADMET risk score to them called ‘ADMET risk’; higher scores indicate less favorable pharmacokinetic and pharmacodynamic properties. We calculated the ligands’ blood brain barrier penetration ‘BBB filter’, their inhibition of the hERG potassium channel of the heart ‘hERG filter’, the likelihood of the compounds to inhibit or be substrates of p-glycoproteins ‘Pgp Inh’ and ‘Pgp substr’, respectively. We also calculated the hepatotoxic potential of the compounds by predicting their effect on serum alanine transaminase ‘Ser ALT’ and aspartate transaminase ‘Ser AST’ liver enzymes.

4.5 References

1. Levine AJ, Oren M. The first 30 years of p53: growing ever more complex. *Nature Reviews Cancer*. 2009; 9: 749-758.
2. Sabapathy K, Lane DP. Therapeutic targeting of p53: all mutants are equal, but some mutants are more equal than others. *Nature Reviews Clinical Oncology*. 2018; 15: 13.
3. Kruiswijk F, Labuschagne CF, Vousden KH. p53 in survival, death and metabolic health: a lifeguard with a licence to kill. *Nature Reviews Molecular Cell Biology*. 2015; 16: 393.
4. Duffy MJ, Synnott NC, Crown J. Mutant p53 as a target for cancer treatment. *European Journal of Cancer*. 2017; 83: 258-265.
5. Brosh R, Rotter V. When mutants gain new powers: news from the mutant p53 field. *Nature Reviews Cancer*. 2009; 9: 701.
6. Petitjean A, Mathe E, Kato S, Ishioka C, Tavtigian SV, Hainaut P, Olivier M. Impact of mutant p53 functional properties on TP53 mutation patterns and tumor phenotype: lessons from recent developments in the IARC TP53 database. *Human Mutation*. 2007; 28: 622-629.
7. Ventura A, Kirsch DG, McLaughlin ME, Tuveson DA, Grimm J, Lintault L, Newman J, Reczek EE, Weissleder R, Jacks T. Restoration of p53 function leads to tumour regression in vivo. *Nature*. 2007; 445: 661-665.
8. Martins CP, Brown-Swigart L, Evan GI. Modeling the Therapeutic Efficacy of p53 Restoration in Tumors. *Cell*. 2006; 127: 1323-1334.
9. Friedler A, Hansson LO, Veprintsev DB, Freund SMV, Rippin TM, Nikolova PV, Proctor MR, Rüdiger S, Fersht AR. A peptide that binds and stabilizes p53 core domain: chaperone strategy for rescue of oncogenic mutants. *Proceedings of the National Academy of Sciences of the United States of America*. 2002; 99: 937-942.
10. Gorina S, Pavletich NP. Structure of the p53 tumor suppressor bound to the ankyrin and SH3 domains of 53BP2. *Science (New York, N.Y.)*. 1996; 274: 1001-1005.
11. Friedler A, Veprintsev DB, Hansson LO, Fersht AR. Kinetic Instability of p53 Core Domain Mutants IMPLICATIONS FOR RESCUE BY SMALL MOLECULES. *Journal of Biological Chemistry*. 2003; 278: 24108-24112.
12. Foster BA, Coffey HA, Morin MJ, Rastinejad F. Pharmacological rescue of mutant p53 conformation and function. *Science (New York, N.Y.)*. 1999; 286: 2507-2510.

13. Demma MJ, Wong S, Maxwell E, Dasmahapatra B. CP-31398 restores DNA-binding activity to mutant p53 in vitro but does not affect p53 homologs p63 and p73. *The Journal of Biological Chemistry*. 2004; 279: 45887-45896.
14. Stefan Tanner, Alcide Barberis. CP-31398, a putative p53-stabilizing molecule tested in mammalian cells and in yeast for its effects on p53 transcriptional activity. *Journal of negative results in biomedicine*. 2004; 3: 5.
15. Rippin TM, Bykov VJN, Freund SMV, Selivanova G, Wiman KG, Fersht AR. Characterization of the p53-rescue drug CP-31398 in vitro and in living cells. *Oncogene*. 2002; 21: 2119-2129.
16. Selivanova G, Wiman KG. Reactivation of mutant p53: molecular mechanisms and therapeutic potential. *Oncogene*. 2007; 26: 2243-2254.
17. Bykov VJN, Issaeva N, Shilov A, Hultcrantz M, Pugacheva E, Chumakov P, Bergman J, Wiman KG, Selivanova G. Restoration of the tumor suppressor function to mutant p53 by a low-molecular-weight compound. *Nature medicine*. 2002; 8: 282-288.
18. Bykov VJN, Issaeva N, Zache N, Shilov A, Hultcrantz M, Bergman J, Selivanova G, Wiman KG. Reactivation of mutant p53 and induction of apoptosis in human tumor cells by maleimide analogs. *The Journal of Biological Chemistry*. 2005; 280: 30384-30391.
19. Lambert JMR, Gorzov P, Veprintsev DB, Soderqvist M, Segerback D, Bergman J, Fersht AR, Hainaut P, Wiman KG, Bykov VJN. PRIMA-1 Reactivates Mutant p53 by Covalent Binding to the Core Domain. *Cancer Cell*. 2009; 15: 376-388.
20. Lehmann S, Bykov VJN, Ali D, Andren O, Cherif H, Tidefelt U, Uggla B, Yachnin J, Juliusson G, Moshfegh A, Paul C, Wiman KG, Andersson P. Targeting p53 in Vivo: A First-in-Human Study With p53-Targeting Compound APR-246 in Refractory Hematologic Malignancies and Prostate Cancer. *Journal of Clinical Oncology*. 2012; 30: 3633-3639.
21. Wassman CD, Baronio R, Demir O, Wallentine BD, Chen C, Hall LV, Salehi F, Lin D, Chung BP, Hatfield GW, Chamberlin AR, Luecke H, Lathrop RH, et al. Computational identification of a transiently open L1/S3 pocket for reactivation of mutant p53. *Nature Communications*. 2013; 4: 1407.
22. Omar SI, Tuszynski J. Ranking the Binding Energies of p53 Mutant Activators and Their ADMET Properties. *Chemical Biology & Drug Design*. 2014.
23. Bullock AN, Fersht AR. Rescuing the function of mutant p53. *Nature Revisions Cancer*. 2001; 1: 68-76.
24. Boeckler FM, Joerger AC, Jaggi G, Rutherford TJ, Veprintsev DB, Fersht AR. Targeted rescue of a destabilized mutant of p53 by an in silico screened drug. *Proceedings of the National Academy of Sciences of the United States of America*. 2008; 105: 10360-10365.

25. Scholz C, Knorr S, Hamacher K, Schmidt B. DOCKTITE-a highly versatile step-by-step workflow for covalent docking and virtual screening in the molecular operating environment. *Journal of Chemical Information and Modeling*. 2015; 55: 398-406.
26. Lepre MG, Omar SI, Grasso G, Morbiducci U, Deriu MA, Tuszynski JA. Insights into the Effect of the G245S Single Point Mutation on the Structure of p53 and the Binding of the Protein to DNA. *Molecules (Basel, Switzerland)*. 2017; 22.
27. Shao J, Tanner SW, Thompson N, Cheatham TE,III. Clustering molecular dynamics trajectories: 1. Characterizing the performance of different clustering algorithms. *Journal of Chemical Theory and Computation*. 2007; 3.
28. Case DA, Babin V, Berryman JT, Betz RM, Cai Q, Cerutti DS, Cheatham DSI, Darden TA, Duke RE, Gohlke H, Goetz AW, Gusarov S, Homeyer N, et al. *Amber 14*. 2014.
29. Zhang S, Shi Y, Jin H, Liu Z, Zhang L, Zhang L. Covalent complexes of proteasome model with peptide aldehyde inhibitors MG132 and MG101: docking and molecular dynamics study. *Journal of Molecular Modeling*. 2009; 15: 1481.
30. Lawandi J, Toumieux S, Seyer V, Campbell P, Thielges S, Juillerat-Jeanneret L, Moitessier N. Constrained Peptidomimetics Reveal Detailed Geometric Requirements of Covalent Prolyl Oligopeptidase Inhibitors. *Journal of Medicinal Chemistry*. 2009; 52: 6672-6684.
31. Kumalo HM, Bhakat S, Soliman MES. Theory and applications of covalent docking in drug discovery: merits and pitfalls. *Molecules (Basel, Switzerland)*. 2015; 20: 1984-2000.
32. Katritch V, Byrd C, Tseitin V, Dai D, Raush E, Totrov M, Abagyan R, Jordan R, Hruby D. Discovery of small molecule inhibitors of ubiquitin-like poxvirus proteinase I7L using homology modeling and covalent docking approaches. *Journal of Computer-Aided Molecular Design*. 2007; 21: 549-558.
33. Molecular Operating Environment (MOE), 2014.09; Chemical Computing Group Inc., 1010 Sherbooke St. West, Suite #910, Montreal, QC, Canada, H3A 2R7, 2014.
34. Lipinski CA, Lombardo F, Dominy BW, Feeney PJ. Experimental and computational approaches to estimate solubility and permeability in drug discovery and development settings. *Advanced Drug Delivery Reviews*. 1997; 23: 3-25.
35. Teague Sterling, John J Irwin. ZINC 15 - Ligand Discovery for Everyone. *Journal of Chemical Information and Modeling*. 2015; 55: 2324.
36. Cañadillas JMP, Tidow H, Freund SMV, Rutherford TJ, Ang HC, Fersht AR. Solution structure of p53 core domain: Structural basis for its instability. *Proceedings of the National Academy of Sciences*. 2006; 103: 2109-2114.

37. Chen Y, Zhang X, Dantas Machado A, Carolina, Ding Y, Chen Z, Qin P,Z., Rohs R, Chen L. Structure of p53 binding to the BAX response element reveals DNA unwinding and compression to accommodate base-pair insertion. *Nucleic Acids Research*. 2013; 41: 8368-8376.
38. The PyMOL Molecular Graphics System, Version 1.8 Schrödinger, LLC.
39. Neudert G, Klebe G. DSX: a knowledge-based scoring function for the assessment of protein-ligand complexes. *Journal of Chemical Information and Modeling*. 2011; 51: 2731-2745.
40. ADMET Predictor(TM) is distributed by Simulations Plus, Inc., Lancaster CA 93534 (<http://simulations-plus.com>); 8.0.4.6.

Chapter 5

The molecular mechanism of action of methylene quinuclidinone and its effects on the structure of p53 mutants

Preface

This Chapter has been published in Oncotarget as:

Omar SI, Tuszynski JA. The molecular mechanism of action of methylene quinuclidinone and its effects on the structure of p53 mutants. Oncotarget 2018; 9 (98).

Oncotarget is an open access scientific journal that states: “Oncotarget applies the Creative Commons Attribution 3.0 License (CC BY 3.0) to all works we publish (read the human-readable summary or the full license legal code). Under the CC BY, authors retain ownership of the copyright for their article, but authors allow anyone to download, reuse, reprint, modify, distribute, and/or copy articles in Oncotarget, so long as the original authors and source are cited.”

Note: This chapter has been modified for consistency with the rest of the thesis. Some abbreviations have been changed and supplementary material in the original publication has been moved to the body of the chapter. Additional information has been added to the discussion for clarification.

5.1 Introduction

p53 is the master tumor suppressor protein [1-3]. It regulates diverse cellular processes including cell proliferation, apoptosis, senescence, metabolism and DNA repair [1-3]. While p53 is involved in several transcription-independent protein-protein interactions [4], it primarily mediates its activities by acting as a transcription factor that binds to p53 response elements to activate the transcription of canonical p53 target genes [3]. Given the vital importance of p53 in eukaryotic cells, especially its unequivocal tumor suppressor activity, it is not surprising that the p53 pathways are almost always disrupted in all types of cancers [5]. With a mutation rate of more than 50%, *TP53* is the most mutated gene in cancer [6]. These mutations often result in the loss of the tumor suppressor activity of p53 [7, 8]. The great importance of p53 in the context of cancer has made it an obvious but elusive target for anti-cancer treatment. Many strategies have been undertaken to reactivate the p53 pathways; one of these strategies is the restoration of the wild-type (wt) activity to mutant p53 (mp53) [1]. A few compounds have been identified to restore the wt activity to mp53 including PRIMA-1 (short for ‘p53 reactivation and induction of massive apoptosis’) [9], mutant p53-dependent induction of rapid apoptosis-1 (MIRA-1) [10], CP-31398 [11], 3-Methylene-2-norbornanone (NB) [12], SH group Targeting and Induction of Massive Apoptosis (STIMA-1) [13] and stictic acid [14].

APR-246, the methylated derivative of PRIMA-1, is the only mp53 activator that is currently in clinical trials [1, 15, 16]. A study by Lambert *et al.* [9] showed that PRIMA-1 and APR-246 are both prodrugs whose active product is methylene quinuclidinone (MQ). While it has been well-established that MQ restores the wt activity to mp53, additional mechanisms of

MQ action, reviewed in [17], have been proposed. Nevertheless, MQ was primarily found to restore the transcriptional activity of mp53. This is supported by the fact that PRIMA-1-treated-mp53, transferred to p53 null cells using the Chariot protein transfer reagent., led to the activation of p53 target genes transcription and the induction of apoptosis [9]. Moreover, PRIMA-1 restores the correct folding of mp53 as evidenced by the binding of mp53 to wild-type p53 (wt-p53) conformation-specific PAb 1620 antibodies [9, 17, 18]. Also, differential scanning fluorimetry assays demonstrate that MQ increases the thermal stabilization of both G245S and R175H [14].

As mentioned above, MQ is the active product that reactivates mp53. MQ is a Michael acceptor, an α,β -unsaturated carbonyl compound, that reacts with and binds covalently to thiol groups in p53 increasing the mass of the protein and decreasing the percentage of its free thiols [9]. *In silico* modeling has shown that C124 is the most solvent accessible cysteine in p53 [14]. Furthermore, a pocket formed by loop L1 (residues 113-123) and beta-sheet S3 (residues 141-146), near C124, was found to transiently open during molecular dynamics (MD) simulations of the protein. Site-directed mutagenesis of C124 to alanine further confirmed the importance of this cysteine for the reactivation of mp53 by MQ [14]. The same study has also identified stictic acid as a p53 reactivator by virtually screening the NCI library at the C124 pocket [14].

We have previously docked MQ, NB, MIRA-1, STIMA-1, CP-31398, ellipticine, 9-hydroxy-ellipticine, WR-1065 and WR-2721 at the L1/S3 site near C124 [19]. As a result of this research, we have found that the reactive double bonds of the alkylating molecules MQ, NB, MIRA-1, STIMA-1 and CP-31398, are all directed towards the C124 thiol group in their best

binding poses. However, ellipticine, 9-hydroxy-ellipticine, WR-1065 and WR-2721, which are non-alkylating p53 activators, were predicted to interact directly with C124.

Two of the highest frequency p53 mutant proteins, are R175H and R273H mp53, which differ from the wt protein sequence by a single missense mutation of the DNA binding domain arginine residues at positions 175 and 273 to histidine, respectively [7, 8]. The former p53 variant belongs to a class called structural mutants [20]. These proteins have a mutation in the DNA binding domain (DBD) residues, which do not directly interact with DNA yet cause structural unfolding, which prevents p53 from binding to its response elements [20]. The latter protein is classified under contact mutants, in which the mutation is in one of the residues that directly interact with DNA [20]. Although R175H and R273H mp53 are different types of mutants, which are structurally distinct [20], these two p53 variants are reactivated by MQ [9, 14].

Considering the unquestionable importance of p53 in maintaining and protecting the integrity of cells, it is disappointing that only one mp53 reactivator is currently in clinical trials. This fact has been attributed to the general perception that p53 is undruggable [1]. In this study, in order to challenge this perception we aim to understand the structural effect of the covalent binding of MQ to C124 of the two mp53 proteins. Moreover, we aim to understand if MQ alters structural (R175H-mp53) and contact (R273H-mp53) mutants differently. To this end, we have created equilibrated *in silico* atomistic models of the wt protein, the two mutants, as well as their 'drugged' forms in which MQ is covalently bound to residue C124 in the two mutants. The protein-DNA complexes were simulated for 750 ns to help achieve these goals. We analyzed the structures of these p53-DNA complex variants and compared them to the wt-p53-DNA complex. Important consequences emerged, which are discussed below.

5.2 Results

5.2.1 p53-DNA complex structures

Mutant proteins: We used chain B of the p53-DNA complex 1TSR [21] PDB structure to create our models. R175H and R273H mp53 proteins were created by virtually mutating the arginine residues, at positions 175 and 273, to histidine using Pymol [22], respectively.

Drugged mutant proteins: We extracted the representative structures of R175H and R273H mp53 for the MD simulation times from 60 to 80 ns. We covalently docked MQ to C124 of the representative structures of the most populated clusters of each mutant. The covalent docking results for both R175H-mp53 and R273H-mp53 are described in Table 5.1. The fact that MQ binds better to the less-populated clusters of mp53 can be attributed to the fact that the L1/S3 pocket (around C124) opens transiently [14]. The reaction of MQ's methylene with the sulphide of cysteine renders the reactive carbon of MQ chiral. Therefore, there are two possible modified-C124 epimers from this reaction, which we refer to as 'CmQA' and 'CmQB' in this chapter. The chosen poses from covalent docking were the drugged protein starting structures for our MD simulations.

Following this, the wt-p53, R175H-mp53, R175H-CmQA-p53, R175H-CmQB-p53, R273H-mp53, R273H-CmQA-p53 and R273H-CmQB-p53 each complexed with DNA were simulated in explicit solvent using MD for 750 ns. These simulations are referred to as the original simulations in this chapter. We calculated the root-mean-square deviation (RMSD) of all the p53 variants' non-hydrogen atoms over the course of the simulations to assess the proteins' equilibration. Figure 5.1 shows that all the p53 variants have equilibrated after 300

ns of the simulation. This is evident by the plateauing in the RMSD values after 300 ns. All further analysis and comparisons reported in this chapter were performed on the last 450 ns of the MD simulations (from 300 to 750 ns).

Additionally, we ran 500 ns simulations of R175H-CmQB-p53 and R273H-CmQB-p53 DNA complexes as controls to assess the reproducibility of our results.

Table 5.1. Covalent docking results of MQ to C124 of the representative structures of the two p53 mutants.

CovalentDock webserver runs the docking calculation ten times. We chose the best binding pose to start our MD simulations based on the predicted binding energy and number of poses in the cluster. The docking results of the third representative structure of R175H-mp53 had the best-predicted binding energies for both epimers A and B and all the predicted poses belonged to the same docking bin. For R273H-mp53, the second representative structure from MD simulations had better docking cluster sizes than the first and their predicted binding energies were almost the same.

Epimer	Lowest binding energy (kcal·mol ⁻¹)	Cluster size to which the best pose belongs	Number of clusters from docking
R175H-mp53 representative structure 1			
A	-7.22	6	5
B	-7.76	5	3
R175H-mp53 representative structure 2			
A	-7.48	10	1
B	-8.12	2	3
R175H-mp53 representative structure 3			
A	-9.74	10	1
B	-10.03	10	1
R273H-mp53 representative structure 1			
A	-9.73	8	2
B	-9.99	10	1
R273H-mp53 representative structure 2			
A	-9.18	10	1
B	-9.50	10	1

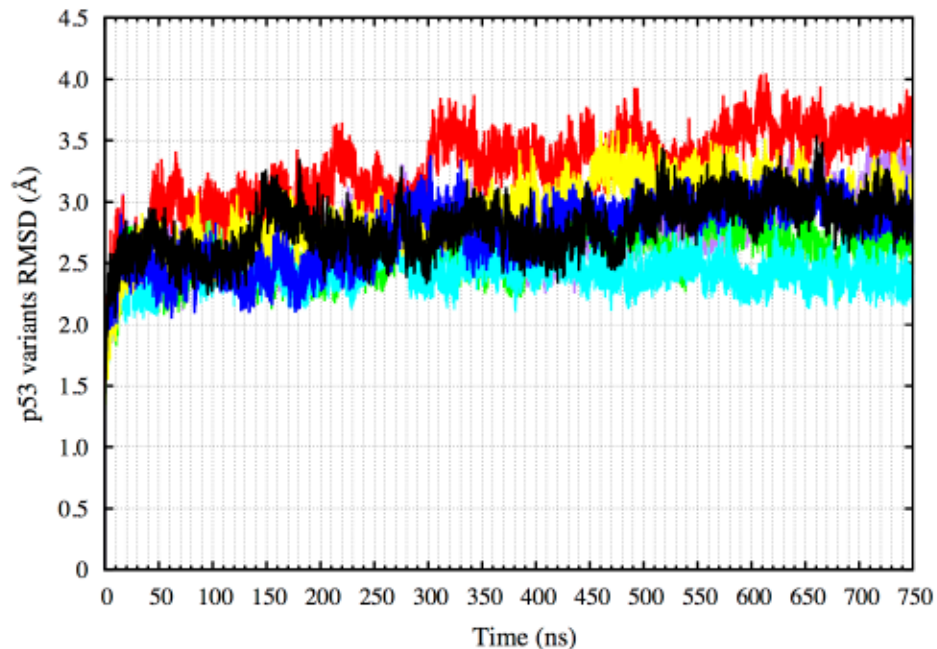


Figure 5.1. RMSD of the p53 variants non-hydrogen atoms over 750 ns. The plot shows that all the p53 variants have equilibrated after 300 ns. Color scheme: wt-p53 (black), R175H-mp53 (red), R175H-CmQA-p53 (yellow), R175H-CmQB-p53 (blue), R273H-mp53 (cyan), R273H-CmQA-p53 (purple) and R273H-CmQB-p53 (green).

5.2.2 Binding energy of p53 to DNA

Total binding energy

We used MMPBSA.py [23] in Ambertools to evaluate the binding energies of the p53 variants to DNA over the last 450 ns of the MD simulations (Figure 5.2). The calculated binding energies constituted the enthalpic and solvation energy contributions due to binding. Similar to our previous study [24], the change in conformational entropy due to binding was not included in our calculations; we refer to this calculated binding energy as the estimated binding energy (EBE). For the wt-p53, the EBE of the protein to DNA was $-58 \text{ kcal}\cdot\text{mol}^{-1}$ with a standard deviation (SD) of $17 \text{ kcal}\cdot\text{mol}^{-1}$. The structural mutant R175H-mp53 had an EBE of $-39 \text{ kcal}\cdot\text{mol}^{-1}$ (SD= $11 \text{ kcal}\cdot\text{mol}^{-1}$), which is almost $20 \text{ kcal}\cdot\text{mol}^{-1}$ more than the wt.

For R175H-CmQA-p53 and R175H-CmQB-p53, however, the EBE was -95 (SD=14 kcal·mol⁻¹) and -110 kcal·mol⁻¹ (SD=19 kcal·mol⁻¹), respectively. This shows that there was a marked increase in the affinity of the drugged *versus* undrugged structural mutants to the DNA.

The contact mutant, R273H-mp53, on the other hand, had an EBE of -49 kcal·mol⁻¹ (SD=15 kcal·mol⁻¹) and its drugged variants, with the CmQA124 and CmQB124 residues, had EBEs of -49 kcal·mol⁻¹ (SD=15 kcal·mol⁻¹) and -36 kcal·mol⁻¹ (SD=12 kcal·mol⁻¹), respectively. It is expected that R273H-mp53 would have a lower affinity to DNA than wt-p53 since the native R273, which normally forms an electrostatic interaction with the DNA backbone, is mutated to the uncharged histidine residue. The EBEs of R273H-CmQA-p53 and R273H-CmQB-p53 indicate that the binding of MQ to R273H-mp53 does not increase the binding affinity of the modified protein to the p53 response elements. This is an indication that the gain in binding energy due to the mutation of arginine is not restored by the reaction of MQ with R273H-mp53. In fact, the mutant with epimer B has an even lower affinity to the DNA, -36 kcal·mol⁻¹ (SD=12 kcal·mol⁻¹) compared to -49 kcal·mol⁻¹ (SD=15 kcal·mol⁻¹) even when taking the standard deviation of the EBE into account.

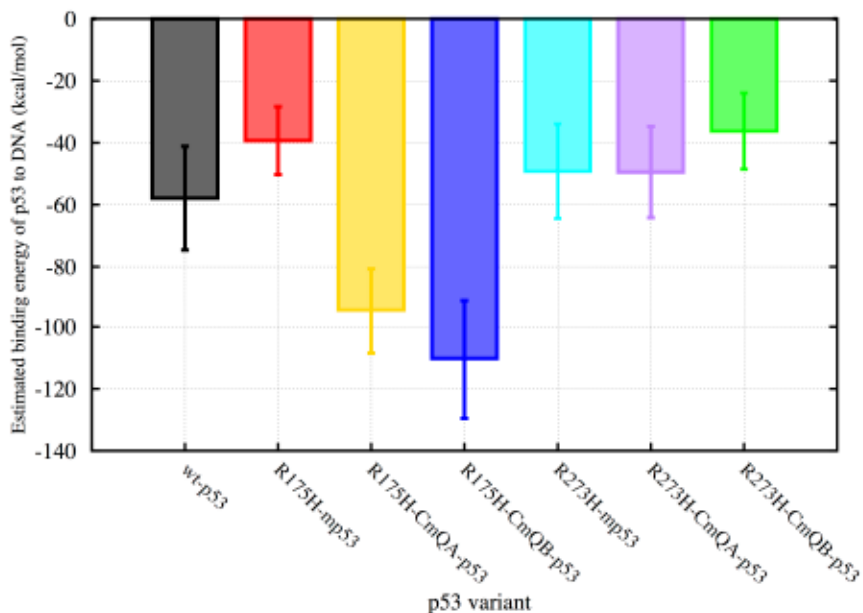


Figure 5.2. A bar graph of the EBEs of the p53 variants to DNA.

The binding energies of wt-p53, R175H-mp53, R175H-CmQA-p53, R175H-CmQB-p53, R273H-mp53, R273H-CmQA-p53 and R273H-CmQB-p53 to DNA were estimated using MMGBSA calculations from time 300 to 750 ns of the MD simulations. The error bars represent the standard deviation of the estimated binding energies during the simulation. Color scheme: wt-p53 (black), R175H-mp53 (red), R175H-CmQA-p53 (yellow), R175H-CmQB-p53 (blue), R273H-mp53 (cyan), R273H-CmQA-p53 (purple) and R273H-CmQB-p53 (green).

Per-residue EBE

We further calculated the decomposition of the EBE per each residue of the complex to better understand the change in the interaction between the different p53 models and DNA. Figure 5.3 shows the contributions of the residues that had a lower EBE than $-1 \text{ kcal}\cdot\text{mol}^{-1}$ or higher than $1 \text{ kcal}\cdot\text{mol}^{-1}$, for any of the p53 variants. Additionally, we also calculated the differences of these contributions between each residue of the p53 variants ($\Delta G_{\text{p53 variant res}}$) and the residues of wt-p53 ($\Delta G_{\text{wt-p53 res}}$) (Equation 5.1). These differences ($\Delta\Delta G_{\text{res diff}}$) were depicted on the p53 variants-DNA complex structures; the residues were colored as heat maps, ranging from blue (largest gain in EBE) to red (largest loss in EBE).

Equation 5.1

$$\Delta\Delta G_{\text{res diff}} = \Delta G_{\text{p53 variant res}} - \Delta G_{\text{wt-p53 res}}$$

Mutants vs. wt-p53: For the wt protein, Figure 5.3A shows that there were interactions between the DNA and R273, R283, R280, R248, K120, R249, N239, Zn²⁺, S241, N247, S121, S240, C277, A119, V122, C242, D281 and E285, in the order of increasing EBE. The structural mutant, R175H-mp53, which had a higher EBE to the DNA compared to the wt-p53 (-39 kcal·mol⁻¹ vs. -58 kcal·mol⁻¹), had fewer residues interacting with the DNA, namely: R273, R248, N239, C275, A276, S241, R280, C277, D281 and E285. Interestingly, some interactions with the DNA away from the mutated H175 residue were conserved in R175H-mp53, especially R273, R248 and N239. However, the interactions natively formed by M243 (albeit very weak) and N247, which are within 10 Å of the mutated H175, were completely lost (Figure 5.3A). Residues A119, K120, S121 and V122, which are in the L1 loop, also lost their interactions with the DNA in the structural mutant. Also, residues R249 and R283, which has the second highest affinity to DNA in wt-p53, completely lost their interactions with the DNA in R175H-mp53. Interestingly, A276 interacted with the DNA in R175H-mp53 but not in wt-p53. All other interactions between wt-p53 and the DNA were also present in R175H-mp53 and are within their standard deviation ranges with the exception of C275 of R175H-mp53, which was stronger in the structural mutant compared to the wt protein. A heat map of these interactions is shown in Figure 5.4A.

Although R273H-mp53 had a comparable EBE to DNA as the wt-p53, the contact mutant had more interactions with DNA. In the order of decreasing favorability, the residues contributing to the EBE for R273H-mp53 were: Zn²⁺, R283, Q136, R280, R248, C275, N239, A276,

K139, H178, L137, H115, R181, V274, M243, E287, D281, C176 and C242. R273 had the highest affinity to DNA in the wt and R175H-mp53 models, with an EBE of about -10 kcal·mol⁻¹ (Figure 5.3A). However, this interaction was completely lost in R273H-mp53 since the positively charged arginine residue is mutated to the neutral histidine, which also has a shorter side-chain. Figure 5.3A shows that the interactions with K120, S121 and V122 of loop L1 as well as N247 and R249 were diminished in R273H-mp53 compared to the wt protein. On the contrary, there were new interactions formed between the DNA and H115, Q136, L137, K139, H178, R181 and A276 of R273H-mp53 (Figure 5.3A). Like R175H-mp53, almost all the other interactions in wt-p53 were also present in R273H-mp53, within their standard deviation ranges, with the exception of C275, which is much stronger in R273H-mp53.

The interaction profiles of R175H-mp53 and R273H-mp53 with DNA suggest that these mutants have different binding poses to DNA compared to the wt-p53.

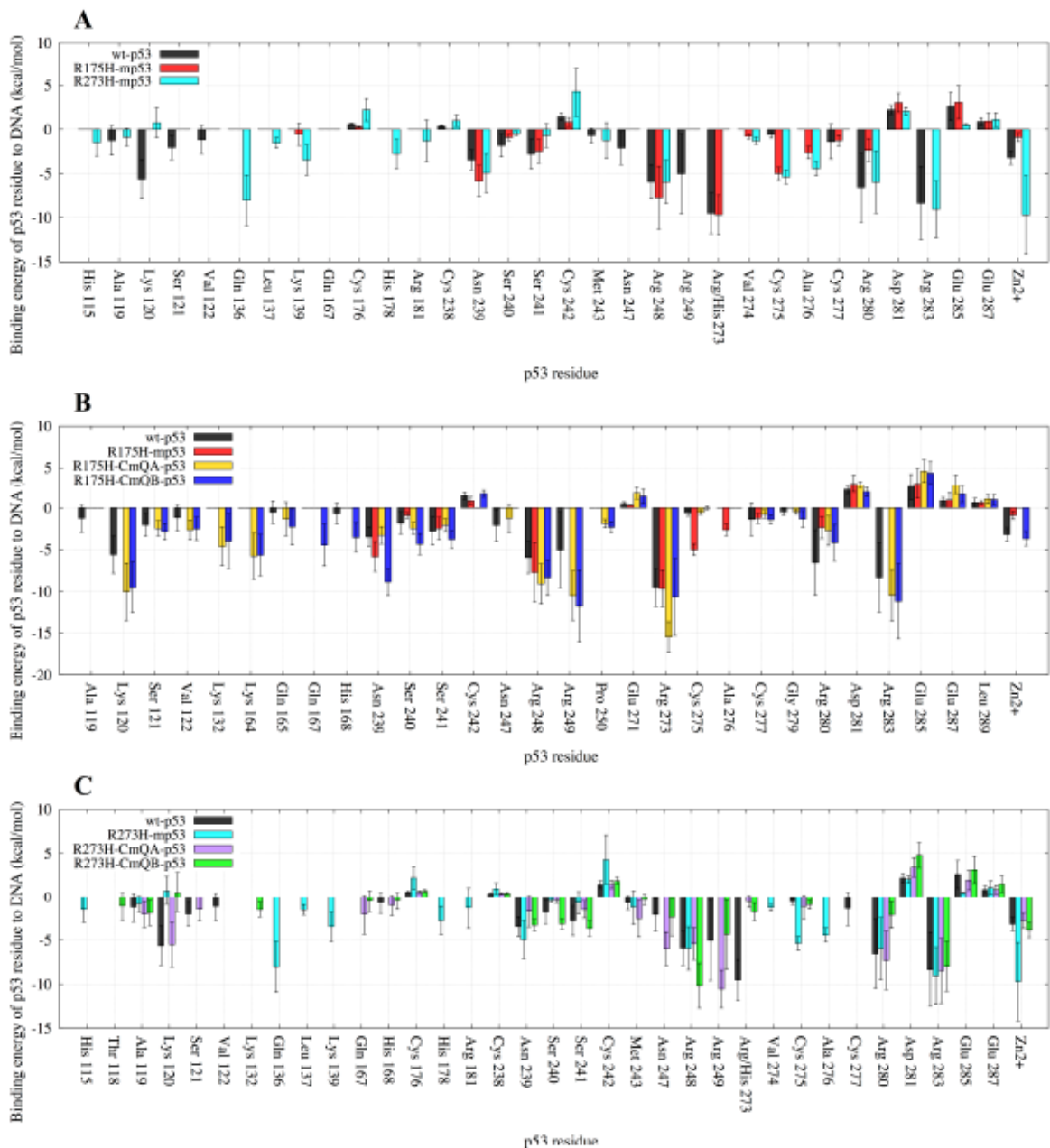


Figure 5.3. A bar graph of the decomposition of the EBE per-residue of p53 to the DNA. Only the residues contributing more or less than 1 kcal·mol⁻¹ to the EBE are shown. (A) Comparison between wt-p53 and the mutants: R175H-mp53 and R273H-mp53. (B) Comparison between wt-p53, R175H-mp53 and its drugged variants R175H-CmQA-p53 and R175H-CmQB-p53. (C) Comparison between wt-p53, R273H-mp53 and its drugged variants R273H-CmQA-p53 and R273H-CmQB-p53. The error bars represent the standard deviation of the EBE for each residue. Color scheme: wt-p53 (black), R175H-mp53 (red), R175H-CmQA-p53 (yellow), R175H-CmQB-p53 (blue), R273H-mp53 (cyan), R273H-CmQA-p53 (purple) and R273H-CmQB-p53 (green).

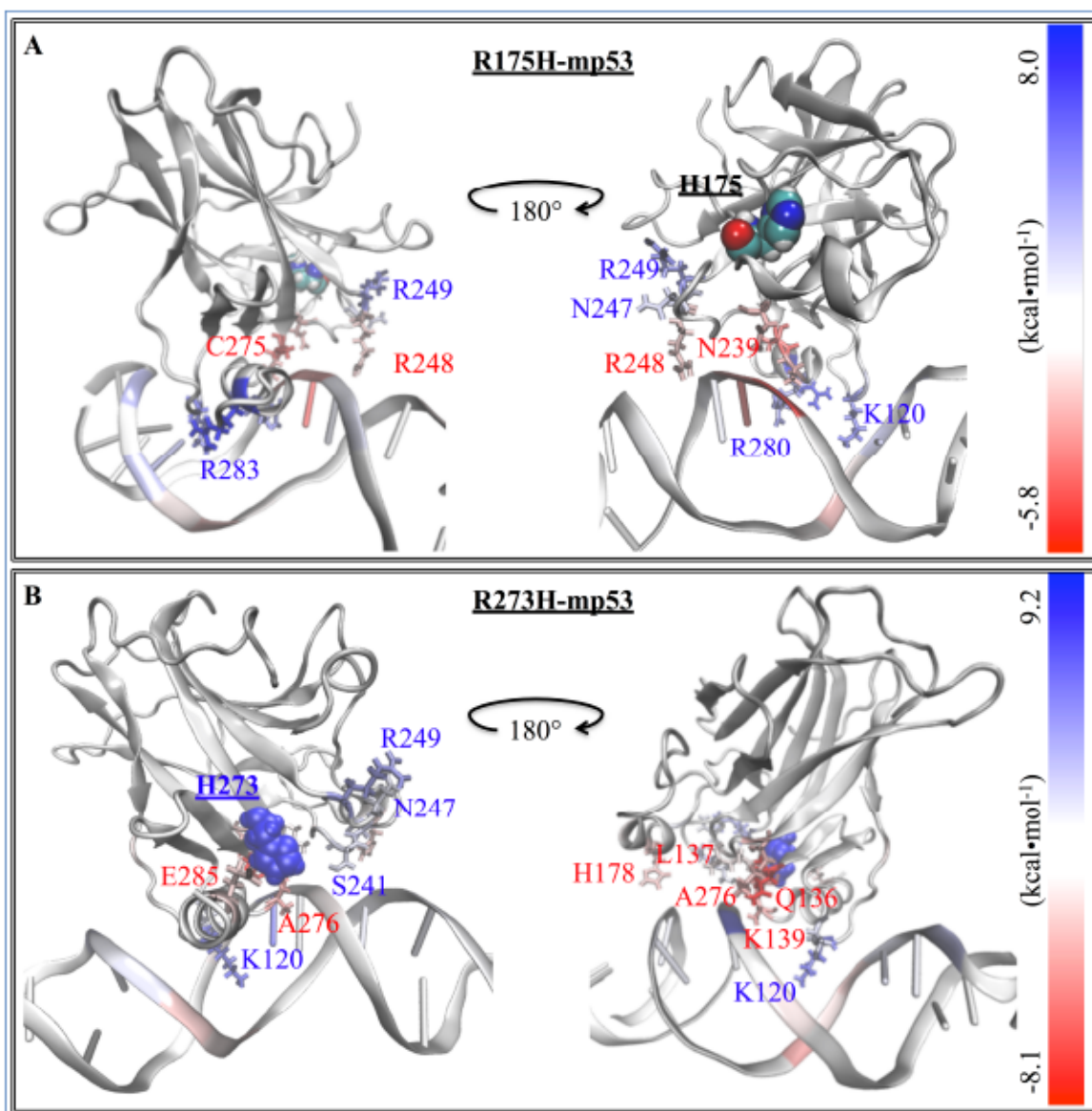


Figure 5.4. The difference in the EBE contribution of the mutant protein residues vs. wt-p53.

A heat map representation of the difference between the EBE contributions of the residues ($\Delta\Delta G_{\text{res diff}}$) in the (A) R175H-mp53 and (B) R273H-mp53 vs. wt-p53 residues. The mutation sites are shown by their vdW representation. DNA interacting residues are shown by their line representation and color-coded according to their $\Delta\Delta G_{\text{res diff}}$, shown on the scale.

Drugged R175H-mp53 versus wt-p53: R175H-CmQA-p53 and R175H-CmQB-p53 had an EBE of -95 and -110 $\text{kcal}\cdot\text{mol}^{-1}$, respectively, which was lower than the EBE of the wt-p53 to DNA (-58 $\text{kcal}\cdot\text{mol}^{-1}$). On further analysis of the interactions between the individual p53

residues and the DNA, Figure 5.3B and Figure 5.5 revealed that both drugged mutant epimers, not only restored most of the lost interactions due to mutation, but also formed new interactions with the DNA.

Compared to R175H-mp53, the interactions of K120, S121 and V122 in loop L1, where the C124 MQ reaction site is also located, were restored in both drugged variants (Figure 5.3B). In addition, the strong interactions of R249 and R283, which had the second highest affinity to DNA in the wt-p53, were also restored. The interaction of Q165 in loop L2 was only present in wt-p53 and both drugged forms of the mutant protein. The relatively weaker N247 interaction present in the wt protein was also recovered in R175H-CmQA-p53. Also, the weak interaction of H168 with the DNA and wt-p53 was also present in R175H-CmQB-p53. It is most intriguing that both R175H-CmQA-p53 and R175H-CmQB-p53 also formed new interactions with DNA via K132, P250 as well as K164 in loop L2. Moreover, R175H-CmQB-p53 formed an additional new interaction through Q167.

However, the only residue whose interaction was not restored by either drugged form was a weak interaction of $-1 \text{ kcal}\cdot\text{mol}^{-1}$ formed by A119 in the wt-p53-DNA complex. Interestingly, the interactions with DNA *via* residues C275 and A276, which were formed in R175H-mp53, were almost absent in the drugged structural mutants, like the wt protein.

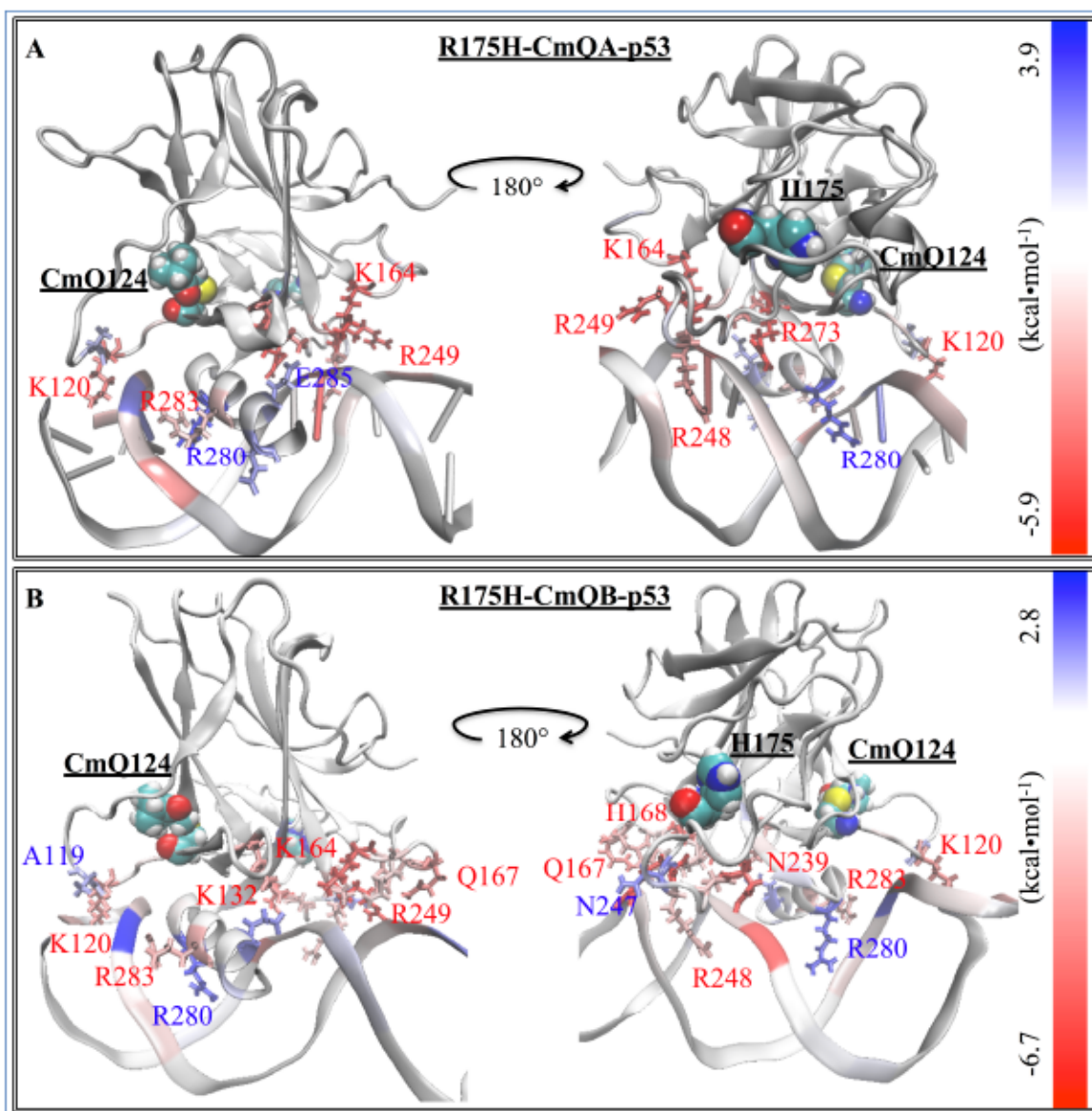


Figure 5.5. The difference in the EBE contribution of R175H-CmQA-p53 and R175H-CmQB-p53 vs. wt-p53.

A heat map representation of the difference between the EBE residue contributions ($\Delta\Delta G_{\text{res}}^{\text{diff}}$) of the (A) R175H-CmQA-p53 and (B) R175H-CmQB-p53 vs. wt-p53. The H175 and CmQ124 are shown by their vdW representation. DNA interacting residues are shown by their line representation and color-coded according to the EBE difference from wt-p53, shown on the scale.

Drugged R273H-mp53 vs. wt-p53: The decomposition of the EBE for these variants are shown in Figure 5.3C and the heat maps of the complexes in Figure 5.6. Our models show that in both R273H-CmQA-p53 and R273H-CmQB-p53, the favorable interactions of R283,

R280, R248, N239, A119 and M243 with the DNA were maintained, like the wt and the non-drugged contact mutant form. Figure 5.3C suggests that MQ binding restored the interaction of R249 and N247, like wt-p53, but not R273H-mp53, with the DNA. Also, R273H-CmQA-p53, like the wt, formed interactions with the DNA via K120 and S121 in loop L1. R273H-CmQB-p53, on the other hand, formed weak interactions with the DNA via residues T118. It is worth mentioning that R273H-CmQB-p53 also formed an interaction with K132, like the R175H-mp53 drugged forms, although it was stronger in the latter models. R273H-CmQA-p53, like R175H-CmQB-p53, also interacted with the DNA via Q167.

While our R273H-mp53 model interacted with the DNA via residues H115, Q136, L137, K139, H178, R181 and V274, none of these interactions existed in the drugged form of the mutant nor wt-p53. The drugged protein variants, however, unlike the wt protein, did not interact with the DNA via V122, C277 nor with the mutated H273 residue.

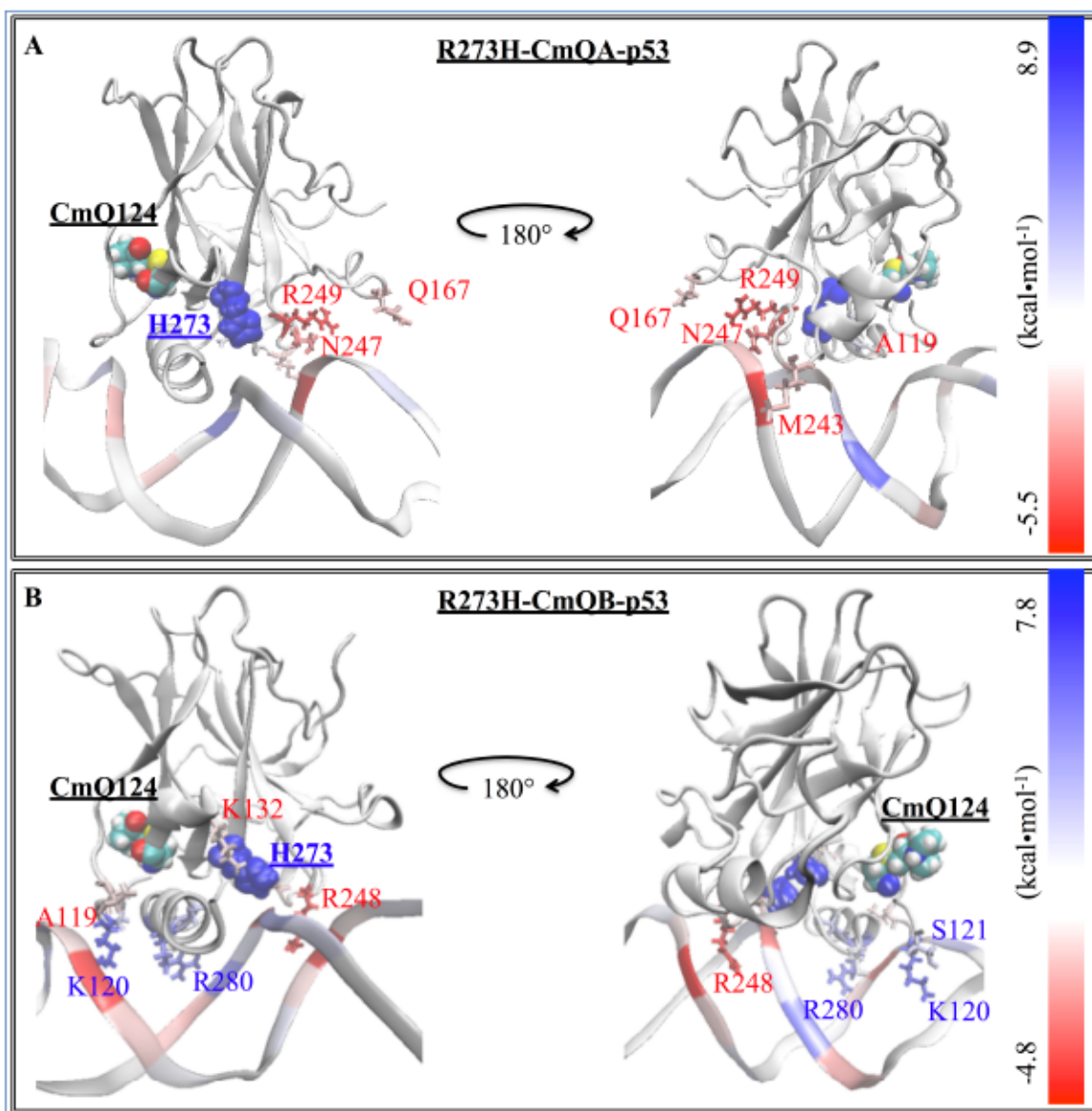


Figure 5.6. The difference in the EBE contribution of R273H-CmQA-p53 and R273H-CmQB-p53 vs. wt-p53.

A heat map representation of the difference between the EBE contributions of the (A) R273H-CmQA-p53 and (B) R273H-CmQB-p53 residues vs. wt-p53. The H273 and CmQ124 are shown by their van der Waals (vdW) representation. DNA interacting residues are shown by their line representation and color-coded according to the EBE difference from wt-p53, shown on the scale.

5.2.3 Placement of the DNA

Alignment of the DNA to p53: We used Ambertools [25] to create the average structure of each p53-variant-DNA complex over the equilibrated part of the MD simulations (from 300 to 750 ns). We fitted the p53 variants' backbone to the wt-p53 to compare the relative DNA positions of the different complexes. In Figure 5.7, the DNA of wt-p53 was horizontally on the plane, marked by its DA5' end. However, the DA5' ends of the DNA of R175H-mp53 and R273H-mp53 were projected in and out of the plane, respectively (Figure 5.7A). However, the superimposition of the drugged p53 variants average structures on the wt protein revealed that their complexed DNA stayed in the plane in a manner similar to that of the wt-p53-DNA (Figure 5.7B).

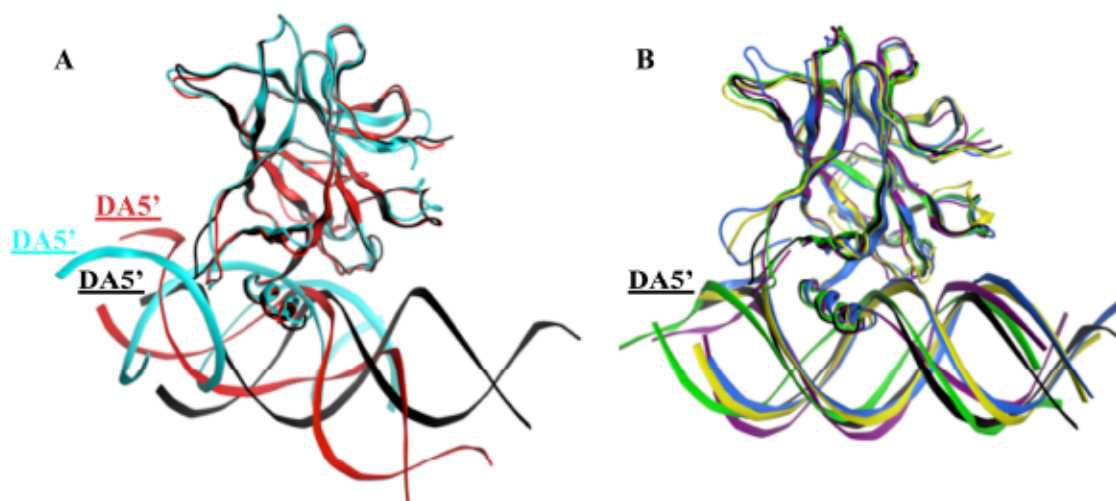


Figure 5.7. Superimposition of the p53 variants shows the displacement of the DNA in the mutants' complexes.

(A) The DNA in the R175H-mp53-DNA and R273H-mp53-DNA complexes are displaced compared to the wt-p53-DNA complex. (B) The DNA molecules of the drugged mutants complexes were better overlaid with the DNA of the wt-p53. Color scheme: wt-p53 (black), R175H-mp53 (red), R175H-CmQA-p53 (yellow), R175H-CmQB-p53 (blue), R273H-mp53 (cyan), R273H-CmQA-p53 (purple) and R273H-CmQB-p53 (green).

RMSD of the DNA: We also calculated the RMSD of the DNA in the different complexes relative to the DNA in the average wt-p53 complex structure to assess the DNA alignment in a more quantitative manner. Figure 5.8 shows that the RMSD of the wt-p53 DNA had an average value of about 3.6 Å and reaches 9.6 Å during the simulation, relative to the wt-p53 average structure. The DNA of the structural mutant had average and maximum RMSD values of 12.8 and 21.9 Å, respectively, compared to the average wt-p53 DNA. Its drugged forms, on the other hand, had much lower RMSD compared to the mutants with average values of 7.2 Å and 5.5 Å for the ‘A’ and ‘B’ forms, respectively.

The DNA of R273H-mp53 had the highest RMSD from that of the wt with average and maximum RMSD values reaching 22.3 Å and 28.5 Å, respectively. Although both R273H-CmQA-p53 and R273H-CmQB-p53 had lower average RMSD of 9.7 and 12.4 Å, respectively, only the former lied within the RMSD ranges of the wt.

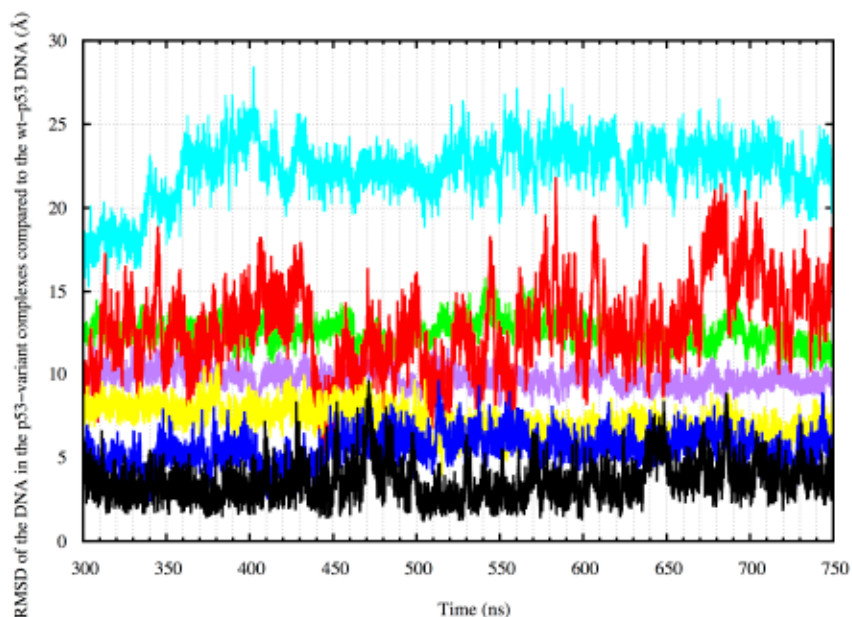


Figure 5.8. DNA RMSD in the p53 variant complexes compared to the wt-p53 DNA from 300 to 750 ns.

Wt-p53 has an RMSD of about 3 Å compared to its average structure. The drugged mutants have average RMSD values ranging from 9-15 Å. R175H-mp53 and R273H-mp53 on the other hand have average RMSD values of 18 and 20 Å, respectively. Color scheme: wt-p53 (black), R175H-mp53 (red), R175H-CmQA-p53 (yellow), R175H-CmQB-p53 (blue), R273H-mp53 (cyan), R273H-CmQA-p53 (purple) and R273H-CmQB-p53 (green).

5.2.4 RMSF of p53 residues

We calculated the root-mean-squared-fluctuation (RMSF) of the protein residues in all the p53 variants over the equilibrated part of the MD simulations, from 300 to 750 ns (Figure 5.9). The coordinated zinc ions were assigned residue number 290 in each model.

Wt-p53: Most residues in the wt protein complex had low RMSF values reaching about 2 Å. The N-terminus residues had the highest RMSF, reaching more than 5.5 Å. However, the L1 loop, of which residues A119, K120, S121 and V122 are involved in DNA binding, had RMSF values reaching about 4 Å. On visually assessing this loop, our MD simulations showed that the L1 loop of wt-p53 visited two states known as the extended and recessed states. These states have previously been experimentally observed [26, 27]. In the former state, K120 side chain is buried in the DNA major groove, while in the latter, the residue is out of the groove and interacts with the backbone phosphate of the DNA [28]. Another region with high fluctuations was loop L6, reaching more than 4.5 Å. This region is usually involved in the interface contact between the monomers of DNA-bound p53 dimers.

R175H-mp53 and its drugged variants: The R175H-mp53 structural mutant generally had the highest RMSF (see Figure 5.9A). This was specially observed for the L2 loop, where the R175H mutation lies. In addition, helix H2 had an RMSF that reaches about 5.5 Å compared to the wt, which had a maximum RMSF of about 3 Å for this region. Figure 5.9B shows that

there were two distinct patterns for the fluctuations in R175H-CmQA-p53 vs. R175H-CmQB-p53. The latter was generally less fluctuating than its undrugged mutant, epimer A variant and the wt protein, especially near loop L2 close to the R175H mutation.

R273H-mp53 and its drugged variants: The p53 contact mutant had an RMSF pattern very similar to that of wt-p53 with only slightly lower RMSF, especially for the L1 loop residues (Figure 5.9A). Interestingly, there were also two distinct fluctuation patterns for the two drugged R273H-mp53 variants (Figure 5.9C). The RMSF pattern of R273H-CmQB-p53 was the same as that of R273H-mp53. However, the RMSF of R273H-CmQA-p53 closely resembled that of the wt-p53 except in residues 208 to 212.

A closer look at the fluctuations of epimers A *versus* B of both mutants revealed that p53 variants with the same epimers had similar RMSF patterns. This was shown in Figure 5.10A; the L1 loop of the drugged R175H-mp53 and R273H-mp53 with epimer A both had RMSF values reaching 4 Å as the wt-p53. However, R175H-CmQA-p53 had a higher RMSF than both the wt-p53 and R273H-CmQA-p53 in loop L2, where the R175H mutation lies. The resemblance between the RMSF patterns of R175H-CmQB-p53 and R273H-CmQB-p53 was more evident (see Figure 5.10), especially in loops L1 and L2, which had lower RMSF values than the wt protein.

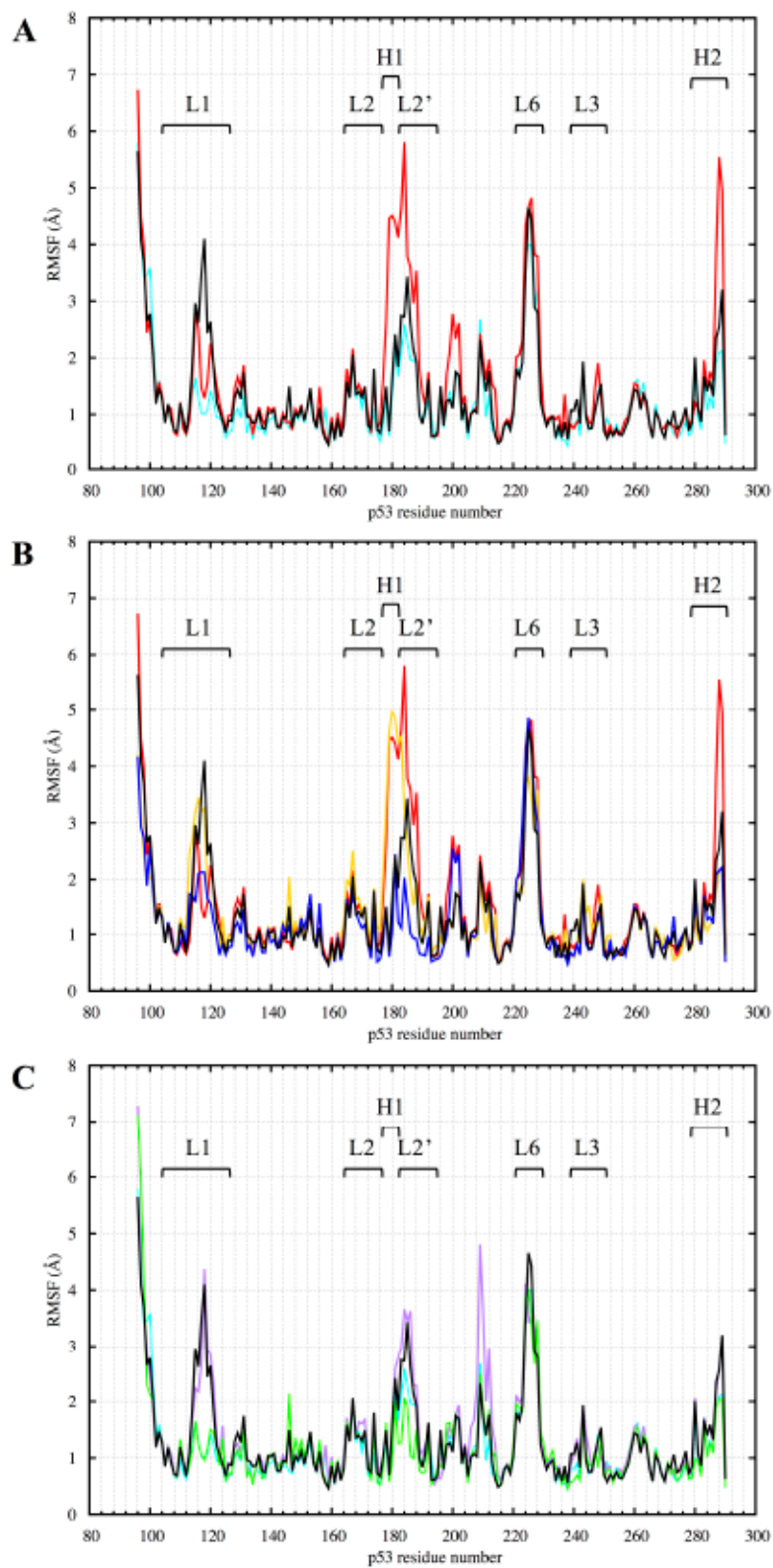


Figure 5.9. RMSF of the p53 variants DBD from 300 to 750 ns of the MD simulation.

(A) Comparison between R175H-mp53 and R273H-mp53 vs. wt-p53. (B) Comparison between R175H-mp53 and its drugged variants vs. wt-p53. (C) Comparison between R273H-mp53 and its drugged variants vs. wt-p53. Residue 290 is the Zn^{2+} ion. Marked are loops L1 (114-123), L2 (164-176, 182-194), L3 (237-250) and L6 (220-229) as well as helices H1 (177-181) and H2 (278-287). Color scheme: wt-p53 (black), R175H-mp53 (red), R175H-CmQA-p53 (yellow), R175H-CmQB-p53 (blue), R273H-mp53 (cyan), R273H-CmQA-p53 (purple) and R273H-CmQB-p53 (green).

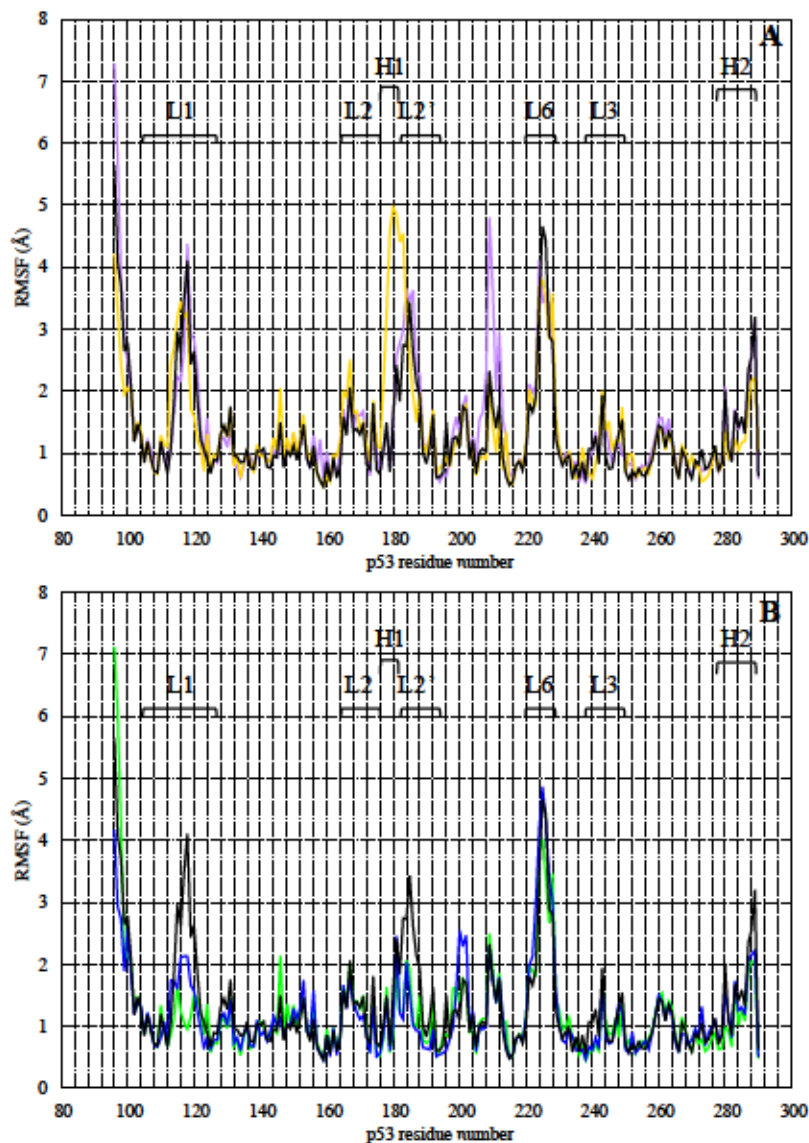


Figure 5.10. RMSF of the p53 drugged mutants' DBD from 300 to 750 ns of the MD simulation.

(A) Comparison between the RMSF of the DBD residues of R175H-CmQA-p53 and R273H-CmQA-p53 vs. wt-p53. (B) Comparison between the RMSF of the DBD residues of R175H-CmQB-p53 and R273H-CmQB-p53 vs. wt-p53. Residue 290 is Zn^{2+} . Marked are loops L1

(114-123), L2 (164-176, 182-194), L3 (237-250) and L6 (220-229) as well as helices H1 (177-181) and H2 (278-287). Color scheme: wt-p53 (black), R175H-mp53 (red), R175H-CmQA-p53 (yellow), R175H-CmQB-p53 (blue), R273H-mp53 (cyan), R273H-CmQA-p53 (purple) and R273H-CmQB-p53 (green).

5.2.5 Control R175H-CmQB-p53 and R273H-CmQB-p53 simulations

We also ran shorter 500 ns simulations of epimers B of the drugged variants. For these control simulations, analysis was performed on the last 100 ns. The EBE of R175H-CmQB-p53 and R273H-CmQB-p53 to DNA were -106 and -57 kcal·mol⁻¹, respectively. The EBE decomposition per each residue of the control complexes versus the wt, mutants and epimers B of the drugged p53 variants from the longer simulations are shown in Figure 5.11.

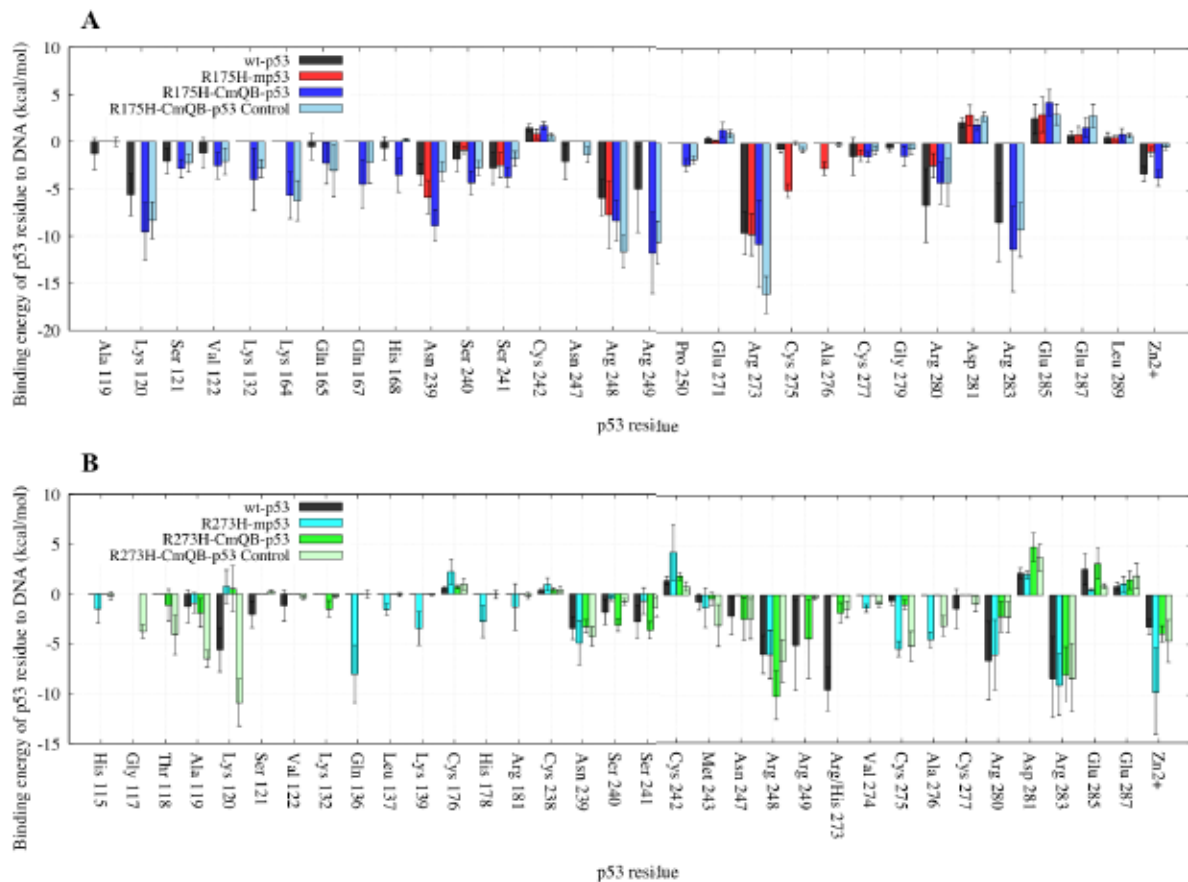


Figure 5.11. A bar graph of the EBE per-residue decomposition of p53 to DNA in the control simulations.

Only the residues contributing more or less than 1 kcal·mol⁻¹ to the EBE are shown. (A) Comparison between wt-p53, R175H-mp53, R175H-CmQB-p53 (average structure from the last 450 ns of the 750 ns simulation) and R175H-CmQB-p53 (average structure from the last 100 ns of the 500 ns control simulation). (B) Comparison between wt-p53, R273H-mp53, R273H-CmQB-p53 (average structure from the last 450 ns of the 750 ns simulation) and R273H-CmQB-p53 (average structure from the last 100 ns of the 500 ns control simulation). The error bars represent the standard deviation of the EBE for each residue. Color scheme: wt-p53 (black), R175H-mp53 (red), R175H-CmQB-p53 (blue), R175H-CmQB-p53 from control simulations (light blue), R273H-mp53 (cyan), R273H-CmQB-p53 (green) and R273H-CmQB-p53 from control simulations (light green).

The R175H-CmQB-p53 control variant had a very similar DNA interaction pattern as the same variant from the original simulations. The only exception was residue H168, which formed a stronger interaction in the original drugged variant, but not wt-p53. Also, N247

interacted with DNA in the control variant, like wt-p53, but not in the original R175H-CmQB-p53 complex (Figure 5.11A).

On the other hand, there were discrepancies between R273H-CmQB-p53 original and control variants. More specifically, residues G117, T118, A119, K120, C275 and A276 interacted with the DNA in the control but not the original variants. Also, interactions between K132, S240, S241 and R249 of the original drugged variant were not reproduced in the control variant.

Visual assessment of the DNA alignment in the control complexes average structures revealed that the DNA in the original and control R175H-CmQB-p53 complexes aligns well with the DNA in wt-p53. For the contact mutant drugged variants, however, the DNA in the control R273H-CmQB-p53 complex was less aligned with the DNA in wt-p53 than the DNA in R273H-CmQB-p53 from the original simulations (Figure 5.12).

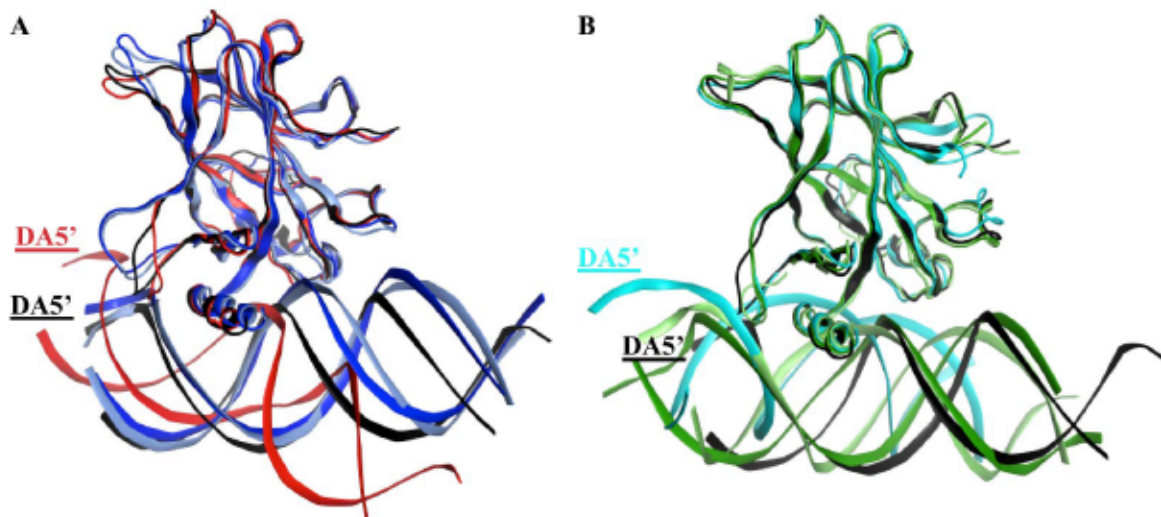


Figure 5.12. Superimposition of the p53 variants shows the displacement of the DNA in the mutants' complexes and R273H-CmQB-p53 from the control simulations.

(A) The DNA in the R175H-CmQB-p53 complexes in both the original and control simulations are well overlaid with the DNA of the wt-p53 but not R175H-mp53. (B) The DNA molecule of R273H-CmQB-p53 control simulation is slightly displaced compared to the

wt-p53-DNA complex. Color scheme: wt-p53 (black), R175H-mp53 (red), R175H-CmQB-p53 (blue), R175H-CmQB-p53 from control simulations (light blue), R273H-mp53 (cyan), R273H-CmQB-p53 (green) and R273H-CmQB-p53 from control simulations (light green).

5.3 Discussion

5.3.1 Binding and alignment of p53 to DNA

We calculated the EBE of the p53 variants to DNA for the equilibrated portion of the MD simulation from 300 to 750 ns using the Molecular Mechanics Generalized Born Surface Area (MMGBSA) approach. Wt-p53 had an EBE of $-58 \text{ kcal}\cdot\text{mol}^{-1}$ to DNA. Our calculations showed that both mutants, R175H-mp53 and R273H-mp53, had lower affinities to DNA with EBE of -39 and $-49 \text{ kcal}\cdot\text{mol}^{-1}$, respectively. The R175H mutation is known to cause unfolding of the protein and a loss in its tumor suppressor ability [20] and hence the increase in EBE of this structural mutant is expected. Similarly, the increase in the EBE of the contact mutant is also expected but for a different reason: the native positively charged R273, which interacts with the backbone phosphate groups of the DNA in the wt protein, is mutated to the neutral histidine.

Our results showed that the reaction of MQ with C124 of the mutant proteins had different effects on their binding energies (Figure 5.2). The EBE of the drugged structural mutants to DNA were -95 and $-110 \text{ kcal}\cdot\text{mol}^{-1}$ while those of the contact mutant were -49 and $-36 \text{ kcal}\cdot\text{mol}^{-1}$. Collectively, these results indicate that the binding of MQ to the mutants induced a conformational change in the protein, especially that C124, the reaction site of MQ with p53, is not one of the DNA binding residues of p53. While the results for the drugged structural mutant indicate that MQ could be restoring the inactivity of mutated proteins by

increasing their affinity, the drugged R273H-mp53 results showed that this was not always the case. In fact, the R273H-CmQB-p53 had an even lower affinity to DNA, namely 36 kcal·mol⁻¹ (15 kcal·mol⁻¹ SD) compared to the undrugged mutant, 50 kcal·mol⁻¹ (12 kcal·mol⁻¹ SD), even when taking the standard deviation of the EBE into account. It has previously been shown that the binding affinity of the wt-p53 was less than ten times stronger to its specific *versus* non-specific sequences [26, 29]. This small difference in affinities has shed light on the fact that the protein's affinity is not the only driving force for the recognition of p53 to its specific DNA sequences but rather its binding kinetics [26]. In fact, in a previous study, a designed S121F-V122G p53 double mutant-DNA complex had a half-life that was five-fold shorter than the wt-p53-DNA complex despite the fact that the designed double mutant had a binding affinity four times higher than that of wt-p53 [26]. This had lead us to examine other effects of MQ binding on the mutant p53 structure including assessing the individual residues that contribute to the binding energy.

Wt-p53: Our wt-p53 model showed that the protein interacted with the DNA through loops L1, helix H2 (see Figure 5.3). A visual illustration of these p53 regions is shown in Figure 5.13. Residue R273, loops L1 and L3 as well as helix H2 can be seen as a 'base', by which the p53 sits on the DNA. Loop L1 can be considered the left side of this base. During our simulation, L1 loop of wt-p53 was mostly in its recessed form but also visited the extended state (Figure 5.13). This flexibility was reflected in the relatively higher RMSF of the L1 loop residues (Figure 5.9). Loop L3 can be considered the right side of the base, which interacts with the minor groove of the DNA (Figure 5.13). R273 and helix H2 form the center of the base (Figure 5.13); the latter interacted with the major groove of the DNA. It is through these

interactions that the wt-p53 maintained its alignment with the DNA (Figure 5.7). Our models only constitute the DBD of the p53 variants. However, the fully functional p53-DNA complex is composed of a p53 tetramer. This tetramer is formed by both the interactions of the p53 tetramerization domains (not included in our models) as well as the interactions of the individual DBD with each other through residues in loop L6. It has been shown that p53 with a deleted tetramerization domain can both bind to DNA and possesses transcriptional activity [30-32]. Nevertheless, wt-p53 has a 100 times higher affinity to DNA as a tetramer than as a monomer [31, 33]. When binding to DNA, the symmetric alignment of p53 with the DNA is important to enable both the tetramerization of the protein and the cooperative binding of the DBD [34, 35].

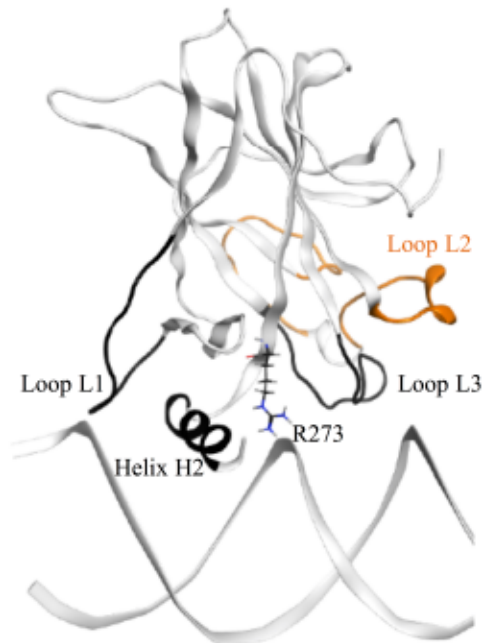


Figure 5.13. The wt-p53-DNA complex structure. The L1 and L3 loops, helix H2 and R273, which form the main interactions with the DNA, are colored in black. They form a 'base', which sits on the DNA. Loop L2 is shown in orange.

R175H-mp53: This structural mutant is known to have a distorted conformational stability. The relatively higher RMSF values of the individual residues of R175H-mp53 agree with this property (Figure 5.9). This was especially more pronounced in residue D184 in the L2 loop where the mutation site lies. On examination of the pairwise binding energy decomposition of R175 in wt-p53 vs. H175 in R175H-mp53, our results show that R175 formed electrostatic interactions with E180 and D184 during the simulation in wt-p53. In addition, R175 also formed electrostatic interactions with the Zn^{2+} coordinating H179. All these interactions were completely lost in R175H-mp53. Additionally, the mutation induced flexibility also caused the loss of coordination of Zn^{2+} by H179. Together, these local effects destabilized the mutant protein, especially at loop L2 as reflected in its high RMSF (Figure 5.9A). Visual inspection of the H2 helix during the simulation also revealed that the helix was partially unfolded towards its C-terminus and hence its high residue fluctuation.

Figure 5.3A shows that the increase in the EBE of R175H-mp53 was due to the decrease in the number of residues that would normally interact with the DNA in the wt protein. Overall, it is evident that R175H-mp53 lost all its L1 loop interactions (the left side of the base) and three of eight loop L3 interactions (right side of the base) with the minor groove of the DNA (Figure 5.4A). We have previously used functional mode analysis to identify residues that correlate with the fluctuations in loop L3 [24]. Indeed, a correlation was found between the fluctuations in loops L2 and L3 as well as loops L3 and L1. This correlation can explain how a mutation in H175 (loop L2) can affect residues in loop L3, which subsequently affects residues in the L1 loop. Further, Figure 5.7 illustrates that R175H-mp53 did not maintain the same alignment pattern with DNA as the wt-p53. A more qualitative assessment of the DNA alignment is shown in Figure 5.8. The DNA of the mutant had an RMSD that exceeds 21 Å

from the wt-p53. Additionally, the relative RMSD of the DNA in the structural mutant complex had the highest variation range from about 12.8 to over 21 Å.

Together, these results suggest that the R175H mutation caused a conformational change that altered the specific binding of p53 to the DNA response element. This could consequently contribute to the loss of the wt transcriptional activity of the mutant as well as its dominant negative effect since the mutant would not be able to form the symmetric tetramers around DNA.

R175H-CmQA-p53 and R175H-CmQB-p53: Both R175H-CmQA-p53 and R175H-CmQB-p53, not only restored most of the wt interactions with DNA lost due to mutation, but also formed new interactions with it. These interactions were reproduced in our control simulations for R175H-CmQB-p53 (Figure 5.11). As mentioned before, the wt protein interacted with DNA primarily through residues in loops L1 and L3 as well as through helix H2. Similarly, its drugged variants also maintained the same interactions except for A119. R175H-CmQB-p53 also lost the N247 interaction with the DNA.

Our models suggest that MQ binding to R175H-mp53 restored the L1 loop interactions (left side of the base) that were completely lost in the mutant protein. During our MD simulations, the L1 loops of both variants were in the recessed conformation but did not visit the extended conformation. This can explain the slightly lower RMSF of the L1 loop in both variants. Further on, the RMSF of the drugged variants, H175 of R175H-CmQA-p53 formed electrostatic interactions with D184 but not E180. There was, therefore, a slightly different RMSF pattern for that variant with E180 having the highest fluctuation in that region. Zn²⁺ was also not coordinated by H179 in R175H-CmQA-p53 probably due to the high fluctuation

of its neighboring E180 residue. For R175H-CmQB-p53, on the other hand, H175 formed electrostatic interactions with E180, but not D184, which allowed the coordination of Zn^{2+} by H179. Hence the L2 loop in R175H-CmQB-p53 had a lower RMSF. Although the binding of MQ to R175H-mp53 seemed to at least partially restore the conformational stability of loop L2, the shorter mutated histidine residue side chain was still too short to interact with both E180 and D184.

The drugged structural mutants also formed additional interactions with DNA through their loop L2 residues, which do not usually do so in the native protein. These interactions seemed to have strengthened the right side of the base (Figure 5.5). Moreover, interactions in the L3 loop and H2 helix, which represent the right and center of the base, respectively, were also restored by MQ binding. It is worth mentioning that the unfolding of the H2 helix was not observed in the drugged variants, unlike R175H-mp53, as reflected in their RMSF. Overall, Figure 5.5 illustrates that both R175H-CmQA-p53 and R175H-CmQB-p53 lost some of the interactions in the wt-p53 with the DNA, yet maintained the base interactions with the DNA (red and white residues) that allowed it to align with the DNA in a manner similar to the wt (Figure 5.7B).

The RMSD of the DNA in both the R175H-CmQA-p53 and R175H-CmQB-p53 was higher than that of the wt protein's DNA to its average structure (Figure 5.8), yet still mostly lied below its maximum range. Nonetheless, the drugged variants had a much lower RMSD than their mutant form. Collectively, our findings indicate that MQ binding to R175H-mp53 did not restore the drugged mutant complex to become exactly like the wt-p53, yet the drugged complexes are structurally more similar to the wt protein than the mutant. The alignment of the proteins with the DNA also indicates that they would be more likely to form tetramers.

The same alignment pattern was also observed in the R175H-CmQB-p53 control simulation (Figure 5.12)

R273H-mp53: In R273H-mp53, there was an expected loss in the interaction between H273 and DNA – the center of base. Further analysis indicated that this mutant had a different binding pattern to the DNA (Figure 5.3A). R273H-mp53 did not interact with DNA via loop L1 – left side of the base (Figure 5.3 and Figure 5.4A). In fact, the L1 loop remained buried in the major groove of the DNA albeit at a different angle than the wt-p53. This had not allowed the same extended flexibility range for the loop and hence its lower RMSF (Figure 5.9A). Actually, R273H-mp53 generally had a similar or lower RMSF pattern to wt-p53 consistent with the fact that the R273H mutation is a contact one, which does not cause the unfolding of the protein. R273H-mp53 also formed weaker interactions with the DNA via its loop L3 representing the right side of the base, especially through residues N247 and R249 (Figure 5.4B).

Figure 5.7A shows that the loss in the base interactions of R273H-mp53 with DNA led to the loss of the protein's alignment with DNA, which was confirmed by the RMSD of the R273H-mp53 DNA relative to the wt-p53 DNA average structure (Figure 5.8). These findings can explain why this mutant loses its transcription ability in cells, since the misalignment of the protein with the DNA can hinder cooperative binding and tetramerization of the mutant.

R273H-CmQA-p53 and R273H-CmQB-p53: The reaction of MQ with R273H-mp53 did not improve the binding affinity of the protein. However, it changed the binding profile of the protein to the DNA. R273H-CmQA-p53 formed very similar interactions with the DNA like

the wt-p53 especially in loops L1 and L3 as well as helix H2. This is evident in Figure 5.6A representing a heat map: the protein was mostly white ($\Delta\Delta G_{diff}=0$). The L1 loop interactions, which make the left side of the base were all restored except V122, which greatly deviated in the wt. Interactions via Q167 and H168 in the loop L2 were introduced, which made the right side of the base stronger. Additionally, the R249 interaction with the DNA minor groove, also making the right side of the base, was restored and even became stronger. It is evident from Figure 5.7B that R273H-CmQA-p53 had a similar alignment to the DNA like wt-p53 despite the fact that the interaction with residue 273 was not restored. This indicates that the right and left components of the base were enough to maintain the protein in the correct position relative to DNA. The RMSD of the DNA in this complex was closer to the wt than the mutant, although it was still higher than the latter. In addition, it was also similar to the R175H-mp53 drugged mutants, which have a higher affinity to DNA.

For R273H-CmQB-p53, several important interactions remained diminished, especially at the left of the base. However, this drugged p53 variant still formed interactions through A119 and a new interaction through T118 in the L1 loop. In addition, our models showed that MQ binding to R273H-mp53 also restored the S240, S241, N247 and R249 interaction, which were lost in the mutant and constitute the center of the base. Although the binding pattern of R273H-CmQB-p53 did not show a strong binding profile like the other drugged variants, especially in the loop L1, it still seemed to form enough interactions for R273H-CmQB-p53 to maintain its alignment with DNA (Figure 5.7B). As mentioned above, R273H-mp53 did not align with DNA like the wt protein. It, therefore, formed unexpected interactions of beta-sheet sandwich residues with the DNA via Q136, L137 and K139. This was not the case in the drugged mutant variants. The qualitative assessment of the DNA RMSD in R273H-

CmQB-p53 vs. wt-p53 showed that the RMSD of the former was closer to the DNA of the wt than R273H-mp53. Nonetheless, the deviation of the R273H-CmQB-p53 complex from the typical ‘base’ interactions was reflected in its DNA RMSD, which was the highest among all the drugged mutants (Figure 5.8).

Control simulations of R273H-CmQB-p53 further revealed a discrepancy in the interactions formed between R273H-CmQB-p53 in the control versus original simulations indicating that at least this drugged variant might not be activated by MQ, especially that the DNA in the control simulations did not well align with the DNA in the wt-p53.

As mentioned above, MQ has been previously shown to have other anti-cancer effects in cells [17]. It is possible that other mechanisms of MQ on other cellular targets cause the anti-cancer effect of MQ in treated cells carrying R273H-CmQB-p53.

On a general note, loop L6 of all the p53 variants was another region with high RMSF (Figure 5.9). Normally, the L6 loop residues are involved in p53 monomer-monomer interactions. Since our models represent a single p53 monomer bound to the DNA, it is expected that loop L6 would be more flexible and hence its high RMSF values in all the p53 variants. We have previously modeled wt-p53 apo monomers as well as a p53 dimer bound to the DNA. Evidently, the RMSF of loop L6 was indeed high in the apo monomers, however, it decreased in the p53 dimer bound to the DNA for the wt protein [24].

5.4 Additional commentary

DNA Structures: To assess any distortions in the DNA structures bound to the p53 variants, we measured the distance between the sixth thymidine of one strand and the twelfth

thymidine in the other DNA strand as a representation for the DNA major groove length. The measured distances in the wt, R175H-mp53 and R273H-mp53 DNA average complex structures were 18.98 Å, 24.89 Å and 22.10 Å, respectively. The distances in DNA for R175H-CmQA-p53 and R175H-CmQB-p53 were 20.00 Å and 20.88 Å, respectively. For R273H-CmQA-p53 and R273H-CmQB-p53, the measured distances were 17.56 Å and 24.90 Å, respectively. The DNA distances for the R175H-CmQA-p53, R175H-CmQB-p53 and R273H-CmQA-p53 complexes were all within the 2 Å range to the wt DNA. On the other hand, the distances in R175H-mp53, R273H-mp53 and R273H-CmQB-p53 were the longest, indicating a distortion in the DNA structure. Combined with the DNA RMSD patterns in Figure 5.8, these findings suggest that the p53 variants altered the structure of their bound DNA, especially the mutants. Alterations in the bound DNA structures have been experimentally observed in previous studies on different rescued p53 mutants, including the R273H-T284R rescued double mutant [36].

Comparison to reported thermostability: It has previously been reported that the R175H structural mutation globally denatures p53 and destabilizes the apo protein structure by 3.0 kcal·mol⁻¹ [37, 38]. On the other hand, R273H-mp53 maintains the native protein fold and is stabilized by 0.4 kcal·mol⁻¹ relative to the wt protein [37, 38]. The higher calculated RMSF values for the p53 residues in R175H-mp53 *versus* wt-p53 in our models (Figure 5.9) qualitatively reflect this destabilization. Similarly, the relatively low calculated RMSF values of R273H-mp53 residues agree with these experimental findings. It should be noted, however, that our models are of the DNA bound protein structures rather than the apo proteins.

Relevant experimentally-resolved p53 mutants: There are no experimentally resolved structures of neither R175H-mp53 nor R273H-mp53 bound to DNA. However, X-ray resolved crystal structures of stabilized R273H mutants have been reported [36, 39]. In a structural study, the R273H mutant was found to be rescued by a T284R second site mutation [36]. X-ray resolved structures showed that the R273H-T284R double-mutant formed a new interaction with DNA through the mutated R284 residue, which made up for the lost interaction due to the R273H mutation [36]. This rescue mechanism is different from the potential activation due to MQ binding since our models suggest that MQ is not involved in a direct interaction with DNA but rather alters the conformation of the protein.

5.5 Conclusions

p53 is an architecturally fascinating molecule. Our models have shown that single point mutations at different sites of the protein can have profoundly different effects on the structure of the protein. Interestingly, the reaction of MQ at C124 with R175H-mp53 and R273H-mp53, which are essentially two different proteins especially in the way they interact with DNA, have one specific effect: they introduce interactions with DNA *via* loop L1. Since CmQ124 is not involved in direct interactions with DNA, this indicates that MQ could restore the transcriptional activity of the two mutants by inducing a conformational change in the protein. This conformational change seems to have led to the anchoring of p53 on the DNA, *via* loop L1, in a way that maintains the base interactions in the complex. This L1 anchoring was less pronounced in the original R273H-CmQB-p53 simulations, which indicates that that protein variant could be less active, especially that it had a much lower binding energy to DNA. However, control simulations of the same variant indicate that non-specific L1 loop

interactions are also non-favorable since control R273H-CmQB-p53 interacted via G117, T118 with the DNA, yet did not well align with it like wt-p53.

The p53 mutants have been shown to have a lower binding energy to DNA, to form fewer interactions with it, especially the key base interactions and consequently are not aligned with DNA like the wt protein. The latter property is very important for the proper formation of p53 tetramers – the most transcriptionally active form of the complex. Site-directed mutagenesis studies have provided evidence that MQ covalently binds to p53 mutants at C124 [14]. However, a very recent study suggested that C277 was also key for reactivation of the mutants [40]. Our models provided evidence that MQ binding to C124 does indeed alter the binding of the drugged p53 mutants to the DNA. This is reflected in the restoration of key interactions with the DNA as well as the alignment of the proteins with the DNA in a manner more similar to wt-p53 than their mutants, from which the *in silico* models were built. Our results provide an understanding of the mechanism of action of MQ in the restoration of wt activity to mutant p53. This approach also provides a method of screening for potential p53 mutant activators that alter the protein structure, which is a very challenging task compared to screening for agonists or antagonists of a protein.

Since we do not observe a direct interaction pattern of MQ with p53, it is difficult to suggest specific recommendations for drug development of mp53 activators based on our models. Nonetheless, the work protocol used in this chapter could be used to assess the effect of potential activators on the interaction and alignment of p53 with DNA. Our study suggests that a successful mp53 activator would form the base interactions with DNA and align with DNA in a manner similar to wt-p53.

5.6 Methods and Models

5.6.1 Creating the p53-DNA complex models

Wild type p53-DNA complex: We used chain B of the 1TSR [21] X-ray determined structure of the wt-p53-DNA. We simulated this complex for 750 ns, using MD simulations (outlined below), to study the wt complex structure and compare it as a control to the mutant and drugged-mutant variants of the protein.

Mutant p53-DNA complexes: We virtually mutated the arginine residues at positions 175 and 273, in the chain B of the 1TSR wt-p53 structure, to histidines using Pymol [22] to create the starting complex structures of R175H mp53-DNA and R273H mp53-DNA, respectively. The chosen histidine rotamers were those that had the best fit to the structure, as scored by Pymol. Using the MD simulation protocol outlined below, the mutant complexes were simulated for 750 ns.

Drugged mutant p53-DNA complexes: We used CovalentDock [41] webserver to covalently dock MQ to C124 of both R175H-mp53 and R273H-mp53 (further explained below). Since the non-standard cysteine bound to MQ residue (CmQ) formed is a central peptide fragment, we created a dimethyl dipeptide of the non-standard cysteine fragment (Figure 5.14) for parameterization. We used Gaussian [42] to optimize the geometry of the molecule and to derive its restrained electrostatic potential (RESP) charges with the HF 6-31G* basis set. We then used the PyRED webserver [43-46] to build the force-field libraries and parameters based on Amberff10, which is compatible with the more recent Amberff14SB. The parameterized drugged-mp53-DNA complexes were also simulated for 750 ns.

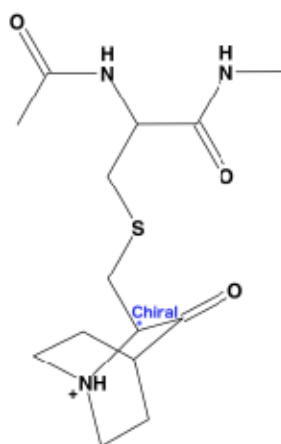


Figure 5.14. Structure of the capped CmQ residue.

CmQ is a modified C124 residue after the Michael addition reaction with MQ. The N-terminal cap is an acetyl group and the C-terminal cap is methylamine. The asterisk marks the chiral carbon, which leads to the formation of the A and B epimers of the molecule.

5.6.2 MD simulations of p53

We used MOE [47] to protonate the p53-DNA complexes at pH 7, temperature of 310 K and 0.15 M salinity. The zinc ion coordinating C176, C238 and C242 were deprotonated. The parameters used for zinc ions were obtained from [48]. The protein-DNA complexes were all solvated in 12 Å TIP3P water boxes. Sodium ions were first added to neutralize the systems. Further, sodium chloride ions were then added randomly to reach a concentration of 0.15 M to simulate physiological conditions. We used AMBER [49] to run the MD simulations. The systems were minimized then gradually heated from 0 to 310 K with heavy restraints placed on the DNA and the protein backbone atoms. Before production, the restraints were gradually decreased until they were completely removed. The non-restrained systems were then simulated for 750 ns each at constant pressure and temperature of 310 K (body temperature). The SHAKE algorithm was also used to constrain the bond lengths to hydrogen atoms and enable the use of a 2 femtosecond timestep.

5.6.3 Covalent docking

We used the CovalentDock [41] webserver to perform Michael addition covalent docking. To obtain the receptor structures, we clustered R175H and R273H mp53 from 60 to 80 ns in a manner similar to our previous work [19, 24]. We fit and clustered the p53 variants based on residues 114-117, 121-126, 133, 140-144, which surround C124. We used the representative structures of the most populated clusters for covalent docking. The DNA was removed from these structures and the mutant proteins were protonated in MOE [47]. C124 was set as the Michael addition site.

5.6.4 Root-mean-square deviation and residue fluctuations

We calculated the root-mean-square-deviation (RMSD) of each complex during the simulation relative to its starting structure to assess the equilibration of the system using Ambertools' cpptraj. We also calculated the RMSD values of the DNA in each complex relative to the wt-p53 DNA average structure by fitting the p53 variant structures to the backbone of wt-p53 average structure (from 300 to 750 ns). Since the N-terminal residues of the p53 DBD are flexible loops, we excluded the first 4 residues from the RMSD selection masks. We also calculated the root-mean-square-fluctuations (RMSF) of the p53 variants during the MD simulations.

5.6.5 Binding energy calculations

The binding free energies of the equilibrated p53 variants to DNA were calculated using the Molecular Mechanics-Generalized Born Surface Area (MM-GBSA) in Ambertools [25]:

Equation 5.2

$$\Delta G_{bind} = \Delta H - T\Delta S \approx \Delta E_{MM} + \Delta G_{sol} - T\Delta S$$

In Equation 6.1, ΔE_{MM} is the molecular mechanic energy in gas phase, defined by the sum of the bond, angle, dihedral angles, electrostatic and van der Waals energies. ΔG_{sol} is the solvation free energy defined by the sum of the electrostatic and non-electrostatic components. The binding energies of the p53 variants to the DNA were calculated by Equation 5.3 as:

Equation 5.3

$$\Delta G_{bind,solv}^{\circ} = \Delta G_{p53-DNA,vacuum}^{\circ} + \Delta G_{p53-DNA,solv}^{\circ} - \Delta G_{DNA,solv}^{\circ} - \Delta G_{p53-p53,solv}^{\circ}$$

5.7 References

1. Sabapathy K, Lane DP. Therapeutic targeting of p53: all mutants are equal, but some mutants are more equal than others. *Nature Reviews Clinical Oncology*. 2018; 15: 13.
2. Kruiswijk F, Labuschagne CF, Vousden KH. p53 in survival, death and metabolic health: a lifeguard with a licence to kill. *Nature Reviews Molecular Cell Biology*. 2015; 16: 393.
3. Levine AJ, Oren M. The first 30 years of p53: growing ever more complex. *Nature Reviews Cancer*. 2009; 9: 749-758.
4. Comel A, Sorrentino G, Capaci V, Del Sal G. The cytoplasmic side of p53's oncosuppressive activities. *FEBS Letters*. 2014; 588: 2600-2609.
5. Vogelstein B, Lane D, Levine AJ. Surfing the p53 network. *Nature*. 2000; 408: 307-310.
6. Duffy MJ, Synnott NC, Crown J. Mutant p53 as a target for cancer treatment. *European Journal of Cancer*. 2017; 83: 258-265.
7. Brosh R, Rotter V. When mutants gain new powers: news from the mutant p53 field. *Nature reviews.Cancer*. 2009; 9: 701-713.
8. Petitjean A, Mathe E, Kato S, Ishioka C, Tavtigian SV, Hainaut P, Olivier M. Impact of mutant p53 functional properties on TP53 mutation patterns and tumor phenotype: lessons from recent developments in the IARC TP53 database. *Human mutation*. 2007; 28: 622-629.
9. Lambert JMR, Gorzov P, Veprintsev DB, Soderqvist M, Segerback D, Bergman J, Fersht AR, Hainaut P, Wiman KG, Bykov VJN. PRIMA-1 Reactivates Mutant p53 by Covalent Binding to the Core Domain. *Cancer Cell*. 2009; 15: 376-388.
10. Bykov VJN, Issaeva N, Zache N, Shilov A, Hultcrantz M, Bergman J, Selivanova G, Wiman KG. Reactivation of mutant p53 and induction of apoptosis in human tumor cells by maleimide analogs. *The Journal of Biological Chemistry*. 2005; 280: 30384-30391.
11. Demma MJ, Wong S, Maxwell E, Dasmahapatra B. CP-31398 restores DNA-binding activity to mutant p53 in vitro but does not affect p53 homologs p63 and p73. *The Journal of Biological Chemistry*. 2004; 279: 45887-45896.
12. Reddy NL, Hill J, Ye L, Fernandes PB, Stout DM. Identification and structure-activity relationship studies of 3-methylene-2-norbornanone as potent anti-proliferative agents presumably working through p53 mediated apoptosis. *Bioorganic & medicinal chemistry letters*. 2004; 14: 5645-5649.

13. Zache N, Lambert JMR, Rokaesus N, Shen J, Hainaut P, Bergman J, Wiman KG, Bykov VN. Mutant p53 targeting by the low molecular weight compound STIMA-1. *Molecular Oncology*. 2008; 2: 70-80.
14. Wassman CD, Baronio R, Demir O, Wallentine BD, Chen C, Hall LV, Salehi F, Lin D, Chung BP, Hatfield GW, Chamberlin AR, Luecke H, Lathrop RH, et al. Computational identification of a transiently open L1/S3 pocket for reactivation of mutant p53. *Nature Communications*. 2013; 4: 1407.
15. APR-246 Clinical Trials (<https://www.clinicaltrials.gov/ct2/results?cond=&term=APR-246&cntry=&state=&city=&dist=>). 2018.
16. Lehmann S, Bykov VJN, Ali D, Andren O, Cherif H, Tidefelt U, Uggla B, Yachnin J, Juliusson G, Moshfegh A, Paul C, Wiman KG, Andersson P. Targeting p53 in Vivo: A First-in-Human Study With p53-Targeting Compound APR-246 in Refractory Hematologic Malignancies and Prostate Cancer. *Journal of Clinical Oncology*. 2012; 30: 3633-3639.
17. Anne Perdrix, Ahmad Najem, Sven Saussez, Ahmad Awada, Fabrice Journe, Ghanem Ghanem, Mohammad Krayem. PRIMA-1 and PRIMA-1Met (APR-246): From Mutant/Wild Type p53 Reactivation to Unexpected Mechanisms Underlying Their Potent Anti-Tumor Effect in Combinatorial Therapies. *Cancers*. 2017; 9: 172.
18. Bykov VJN, Issaeva N, Shilov A, Hultcrantz M, Pugacheva E, Chumakov P, Bergman J, Wiman KG, Selivanova G. Restoration of the tumor suppressor function to mutant p53 by a low-molecular-weight compound. *Nature medicine*. 2002; 8: 282-288.
19. Omar SI, Tuszynski J. Ranking the Binding Energies of p53 Mutant Activators and Their ADMET Properties. *Chemical Biology & Drug Design*. 2014.
20. Bullock AN, Fersht AR. Rescuing the function of mutant p53. *Nature Reviews Cancer*. 2001; 1: 68-76.
21. Cho Y, Gorina S, Jeffrey PD, Pavletich NP. Crystal structure of a p53 tumor suppressor-DNA complex: understanding tumorigenic mutations. *Science*. 1994; 265: 346-355.
22. The PyMOL Molecular Graphics System, Version 1.8 Schrödinger, LLC.
23. Miller BR, McGee TD, Swails JM, Homeyer N, Gohlke H, Roitberg AE. MMPBSA.py: An Efficient Program for End-State Free Energy Calculations. *Journal of Chemical Theory and Computation*. 2012; 8: 3314-3321.
24. Lepre MG, Omar SI, Grasso G, Morbiducci U, Deriu MA, Tuszynski JA. Insights into the Effect of the G245S Single Point Mutation on the Structure of p53 and the Binding of the Protein to DNA. *Molecules (Basel, Switzerland)*. 2017; 22.

25. Case DA, Babin V, Berryman JT, Betz RM, Cai Q, Cerutti DS, Cheatham DSI, Darden TA, Duke RE, Gohlke H, Goetz AW, Gusarov S, Homeyer N, et al. Amber 14. 2014.
26. Petty TJ, Emamzadah S, Costantino L, Petkova I, Stavridi ES, Saven JG, Vauthey E, Halazonetis TD. An induced fit mechanism regulates p53 DNA binding kinetics to confer sequence specificity. *The EMBO journal*. 2011; 30: 2167-2176.
27. Emamzadah S, Tropia L, Halazonetis TD. Crystal Structure of a Multidomain Human p53 Tetramer Bound to the Natural CDKN1A (p21) p53-Response Element. *Molecular Cancer Research*. 2011; 9: 1493-1499.
28. Lukman S, Lane DP, Verma CS. Mapping the Structural and Dynamical Features of Multiple p53 DNA Binding Domains: Insights into Loop 1 Intrinsic Dynamics. *PLoS ONE*. 2013; 8.
29. Weinberg RL, Veprintsev DB, Fersht AR. Cooperative Binding of Tetrameric p53 to DNA. *Journal of Molecular Biology*. 2004; 341: 1145-1159.
30. Balagurumoorthy P, Sakamoto H, Lewis MS, Zambrano N, Clore GM, Gronenborn AM, Appella E, Harrington RE. Four p53 DNA-binding domain peptides bind natural p53-response elements and bend the DNA. *Proceedings of the National Academy of Sciences*. 1995; 92: 8591-8595.
31. Chène P. The role of tetramerization in p53 function. *Oncogene*. 2001; 20: 2611.
32. Shaulian E, Zauberman A, Milner J, Davies EA, Oren M. Tight DNA binding and oligomerization are dispensable for the ability of p53 to transactivate target genes and suppress transformation. *The EMBO journal*. 1993; 12: 2789-2797.
33. Kamada R, Toguchi Y, Nomura T, Imagawa T, Sakaguchi K. Tetramer formation of tumor suppressor protein p53: Structure, function, and applications. *Peptide Science*. 2016; 106: 598-612.
34. Chen Y, Zhang X, Dantas Machado A, Carolina, Ding Y, Chen Z, Qin P,Z., Rohs R, Chen L. Structure of p53 binding to the BAX response element reveals DNA unwinding and compression to accommodate base-pair insertion. *Nucleic Acids Research*. 2013; 41: 8368-8376.
35. Demir Ö, Jeong PU, Amaro RE. Full-length p53 tetramer bound to DNA and its quaternary dynamics. *Oncogene*. 2016; 36: 1451.
36. Eldar A, Rozenberg H, Diskin-Posner Y, Rohs R, Shakked Z. Structural studies of p53 inactivation by DNA-contact mutations and its rescue by suppressor mutations via alternative protein-DNA interactions. *Nucleic acids research*. 2013; 41: 8748-8759.

37. Bullock AN, Henckel J, DeDecker BS, Johnson CM, Nikolova PV, Proctor MR, Lane DP, Fersht AR. Thermodynamic stability of wild-type and mutant p53 core domain. *Proceedings of the National Academy of Sciences of the United States of America*. 1997; 94: 14338-14342.
38. Bullock AN, Henckel J, Fersht AR. Quantitative analysis of residual folding and DNA binding in mutant p53 core domain: definition of mutant states for rescue in cancer therapy. *Oncogene*. 2000; 19: 1245-1256.
39. Joerger AC, Ang HC, Veprintsev DB, Blair CM, Fersht AR. Structures of p53 cancer mutants and mechanism of rescue by second-site suppressor mutations. *The Journal of Biological Chemistry*. 2005; 280: 16030-16037.
40. Zhang Q, Bykov VJN, Wiman KG, Zawacka-Pankau J. APR-246 reactivates mutant p53 by targeting cysteines 124 and 277. *Cell Death & Disease*. 2018; 9: 439.
41. Ouyang X, Zhou S, Su CTT, Ge Z, Li R, Kwoh CK. CovalentDock: automated covalent docking with parameterized covalent linkage energy estimation and molecular geometry constraints. *Journal of Computational Chemistry*. 2013; 34: 326-336.
42. Frisch MJ, Trucks GW, Schlegel HB, Scuseria GE, Robb MA, Cheeseman JR, Scalmani G, Barone V, Mennucci B, Petersson GA, Nakatsuji H, Caricato M, Li X, et al. *Gaussian 09, Revision E.01*. 2009.
43. Wang F, Becker J, Cieplak P, Dupradeau F. RED Python: Object oriented programming for Amber force fields. *Abstracts of Papers of the American Chemical Society*. 2014; 247.
44. Dupradeau F, Pigache A, Zaffran T, Savineau C, Lelong R, Grivel N, Lelong D, Rosanski W, Cieplak P. The R.E.D. tools: advances in RESP and ESP charge derivation and force field library building. *Physical chemistry chemical physics: PCCP*. 2010; 12: 7821-7839.
45. Vanquelf E, Simon S, Marquant G, Garcia E, Klimerak G, Delepine JC, Cieplak P, Dupradeau F. R.E.D. Server: a web service for deriving RESP and ESP charges and building force field libraries for new molecules and molecular fragments. *Nucleic Acids Research*. 2011; 39: 511.
46. Bayly CI, Cieplak P, Cornell W, Kollman PA. A well-behaved electrostatic potential based method using charge restraints for deriving atomic charges: the RESP model. *The Journal of Physical Chemistry*. 1993; 97: 10269-10280.
47. *Molecular Operating Environment (MOE)*, 2016.08; Chemical Computing Group Inc., 1010 Sherbrooke St. West, Suite #910, Montreal, QC, Canada, H3A 2R7, 2016.
48. Hoops SC, Anderson KW, Merz KM. Force field design for metalloproteins. *Journal of the American Chemical Society*. 1991; 113: 8262-8270.

49. Case DA, Darden TA, Cheatham I,T.E., Simmerling CL, Wang J, Duke RE, Luo R, Walker RC, Zhang W, Merz KM, Roberts B, Hayik S, Roitberg A, et al. AMBER 12. 2012.

Chapter 6

Finding novel PNKP inhibitors using multiple-technique
virtual screening

Preface

Contributions:

All *in silico* modeling in this chapter was performed by Sara Ibrahim Omar.

In vitro experiments for measuring the dissociation constants of the predicted top hits were performed by Rajam S. Mani (Weinfeld lab). The IC₅₀ values were obtained by *in vitro* experiments performed by Zahra Shire and Xiaoyan Yang (Weinfeld lab). The electrophoretic mobility shift assay was performed by Cameron Murray (Glover lab).

6.1 Introduction

The second protein target discussed in this thesis is a DNA repair enzyme called polynucleotide phosphatase kinase (PNKP). Our aim was to virtually screen for molecules that could potentially inhibit the phosphatase activity of the protein. These inhibitors are designed for use in combination cancer therapy. There are no experimentally-resolved structures of PNKP inhibitors bound to the protein. Moreover, the human PNKP (hPNKP) structure has not been experimentally-resolved. In this chapter, we describe our work of creating the hPNKP homology model and screening the Commercial Compound Collection (CoCoCo) database [1] against the phosphatase active-site of the DNA repair inhibitor. The ligand interaction patterns, dissociation constants and the half maximal inhibitory concentrations of six of the predicted top hits are reported.

6.2 Results

6.2.1 hPNKP homology model

There are no experimentally-resolved structures of hPNKP. The Molecular Operating Environment (MOE) software [2] was used to create the homology model of hPNKP using the X-ray determined crystal structure of mouse PNKP, PDB ID: 3U7G [3] as a template. The 3U7G model constitutes residues 144 to 522 of mouse PNKP.

The generated hPNKP homology model was simulated for 250 ns using AMBER molecular dynamics (MD) software [4]. We calculated the root-mean-square-deviation (RMSD) of the backbone of the entire protein, except for the first three residues at both termini. The RMSD

of the non-hydrogen atoms of residues constituting the phosphatase active-site: residues 171, 173, 184, 185, 218, 220, 221, 224, 226, 289, 290, 306, 307 and 310 were also calculated. The RMSD was calculated to assess the equilibration of the protein. Figure 6.1 shows that the RMSD of the PNKP backbone and active-site residues plateau after about 20 ns. We extracted the PNKP-DNA complex structures every 0.5 ns for the simulation time from 20 to 250 ns for a total of 460 representative structures. These structures were used as a representative ensemble of the conformations visited during the simulation.

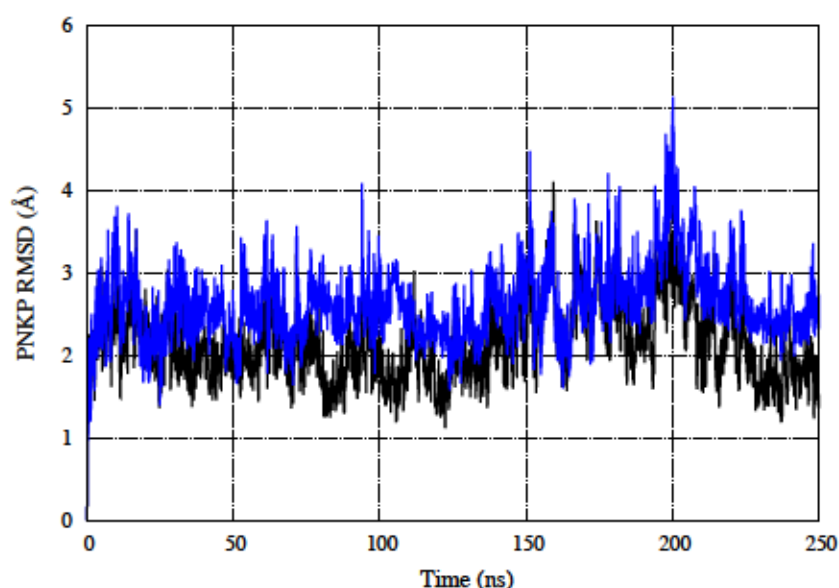


Figure 6.1. The RMSD of PNKP during 250 ns of MD simulations. The RMSD of PNKP backbone is in black and that of the phosphatase active site is in blue.

6.2.2 Stage I: Pharmacophore screening

The Commercial Compound Collection (CoCoCo) database [1] constitutes over 3.7 million unique compounds and we used the multiconformer version of the database, which included tautomers, stereoisomers as well as multiple low energy conformations of each compound.

The multiconformer database consisted of more than 144 million conformers. A schematic of the workflow is shown in Figure 6.2.

LigandScout [5] was utilized to automatically generate pharmacophore models for the 460 representative structures. The multiconformer database was screened against each of the 460 pharmacophore models. A total of 460 filtered databases were obtained after this step of screening. Filtered databases with more than 200,000 unique compounds were excluded. Based on this criterion, 144 filtered databases were carried forward to stage II of screening.

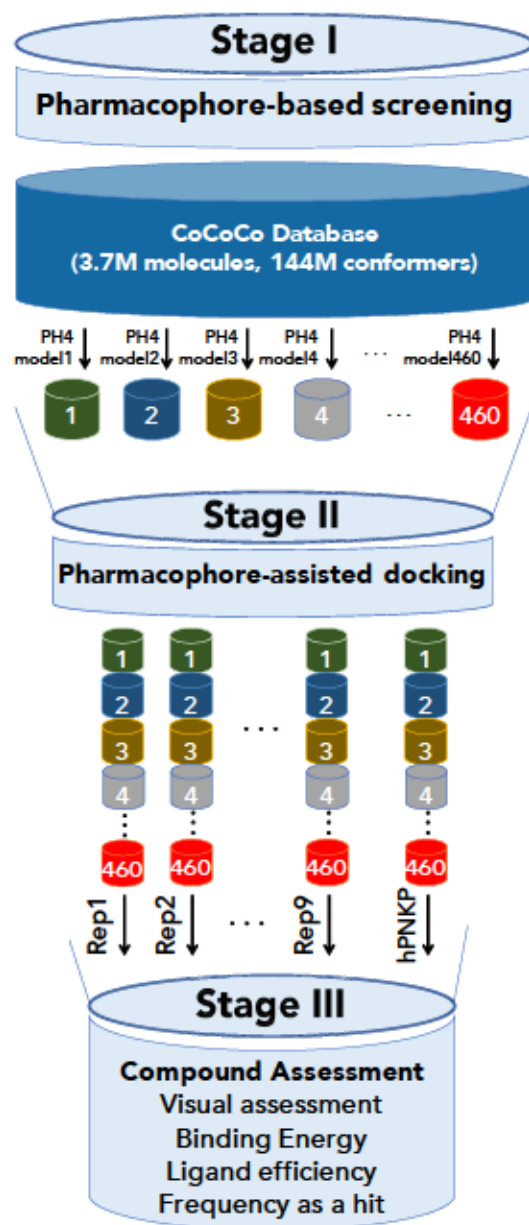


Figure 6.2. A schematic of the screening workflow to find potential PNKP phosphatase inhibitors.

Pharmacophore based screening was used in stage I. This was followed by stage II pharmacophore-based docking using ten different PNKP structures. Potential hits from stage II were further filtered based on the binding energy of the compounds in docking, the number of times they scored as a hit, their ligand efficiency and by visually assessing the compounds in the binding pocket.

6.2.3 Stage II: Pharmacophore-assisted docking

Pharmacophore-assisted docking of the 144 filtered databases at the phosphatase domain of ten PNKP conformers was performed using MOE. We also used MOE to create a pharmacophore model for each PNKP structure at this step, instead of the automatically created pharmacophore models from the previous stage. The choice of the pharmacophore features was based on the atoms in the DNA that had the lowest binding energy to PNKP in the complex. In most cases, the anionic oxygens of the 3' phosphate had the lowest energy to the DNA followed by the anionic oxygen of the 5' phosphate of the same nucleotide. Also, the aromatic rings of the two nucleotides had low binding energies to PNKP. The pharmacophore models were set such that they would contain 3 to 7 features and that the feature representing the anionic oxygen at the 3' phosphate end was always essential. An example of a pharmacophore model is shown in Figure 6.3 below. In that model, a ligand would have to have an anion/hydrogen bond acceptor at position F1 and an aromatic ring at position F4 shown in Figure 6.3. Also, a ligand would need to have at least an anion/hydrogen bond acceptor at positions F2, F3, F5 or F6 or an aromatic ring at position F7.

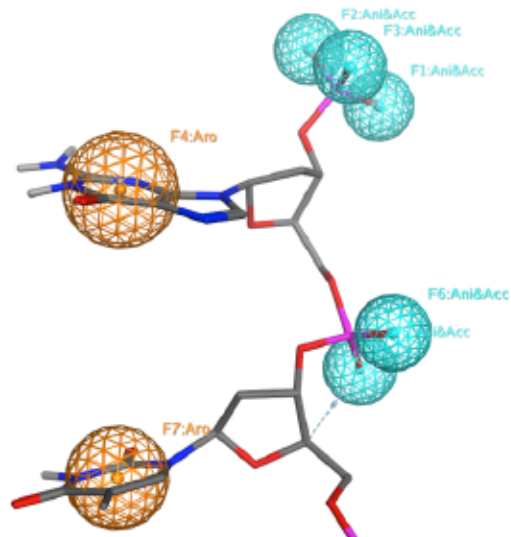


Figure 6.3. An example of a pharmacophore model for the PNKP complex structure. In this model, seven pharmacophore features have been set, of which at least three features have to be met by a potential ligand. Features F1:Ani&Acc and F4:Aro were also set as essential features. Ani&Acc = anion or H-bond acceptor, Aro = aromatic.

To account for the flexibility of the protein, we used ten PNKP structures for pharmacophore-assisted docking: 9 structures obtained from the MD simulation and the hPNKP homology model structure. The choice of the nine structures was based on three criteria: (a) the binding energy of the bound DNA to PNKP was at a local minimum in the complex structure, (b) the structures were spread-out over the 230 ns of the equilibrated simulation time and (c) the pharmacophore-assisted docking of DNA could replicate the DNA-PNKP complex structure from the MD simulation. The nine PNKP structures used in docking are marked by asterisks in Figure 6.4. The docked DNA in hPNKP had the least binding energy to the homology model out of the ten structures. The interactions of the docked DNA in this protein model are shown in Figure 6.5. The least binding energy of the DNA from docking was $-38 \text{ kcal}\cdot\text{mol}^{-1}$ and its ligand efficiency (LE) was $-0.81 \text{ kcal}\cdot\text{mol}^{-1}/\text{heavy atom}$.

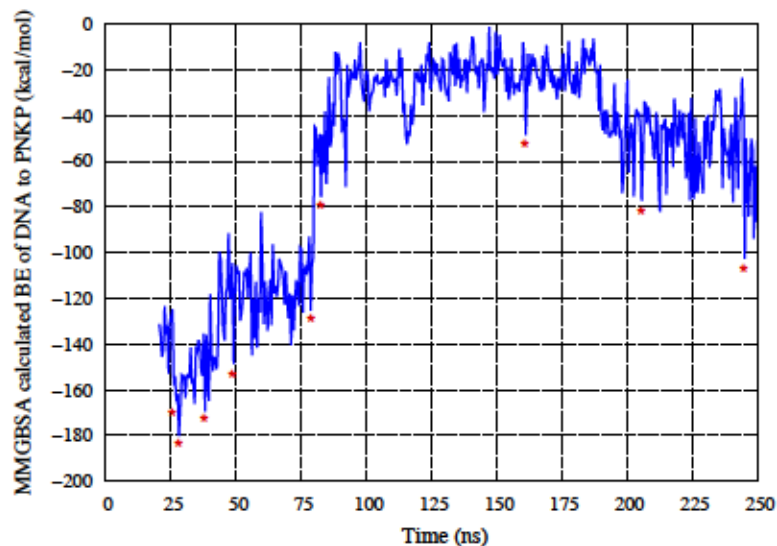


Figure 6.4. The MMGBSA calculated binding energy ($\text{kcal}\cdot\text{mol}^{-1}$) of the DNA to PNKP from 20 to 250 ns.

Structures at local minima were considered for use in pharmacophore-assisted docking. The final nine structures marked by asterisks, along with the hPNKP homology model created, were used for stage II of screening.

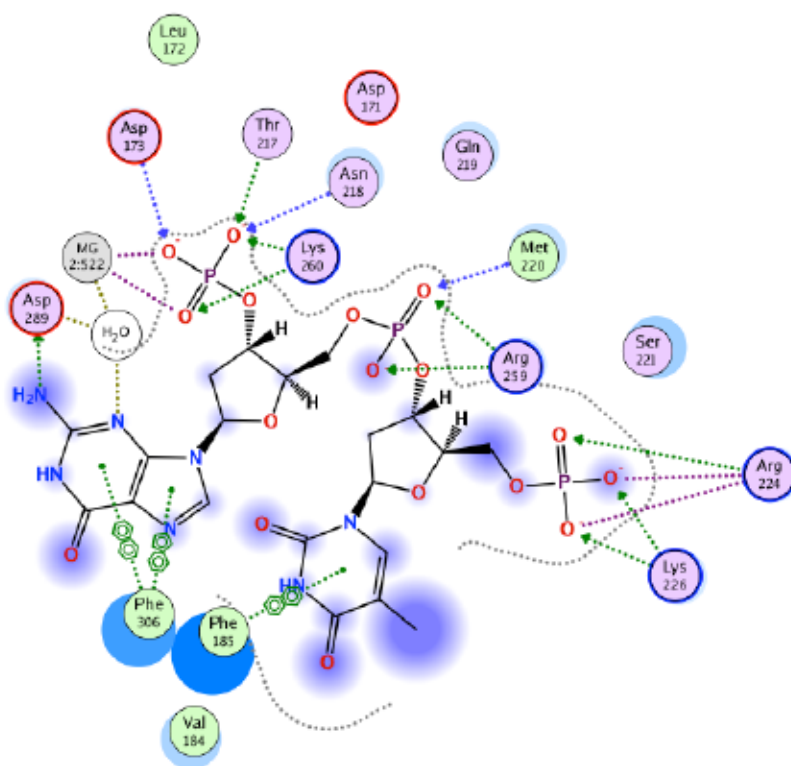




Figure 6.5. The interaction scheme of the docked DNA with PNKP in its lowest binding energy conformation.

The ligand interactions legend describing the interaction annotations are shown at the bottom.

6.2.4 Stage III: Compound assessment

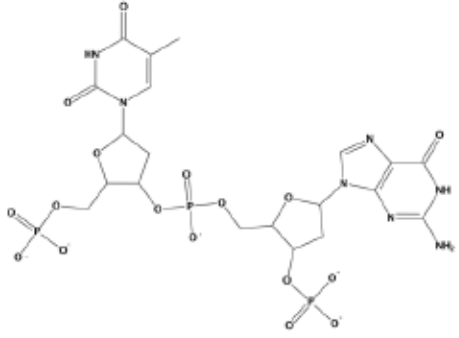
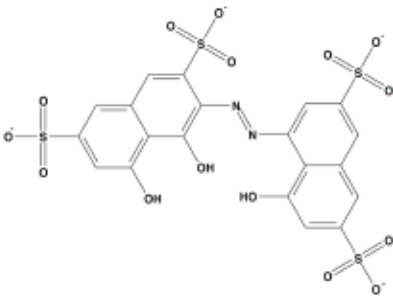
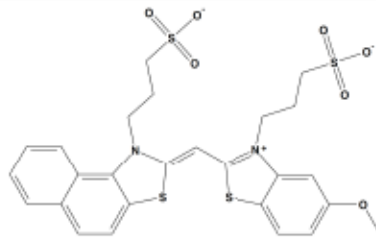
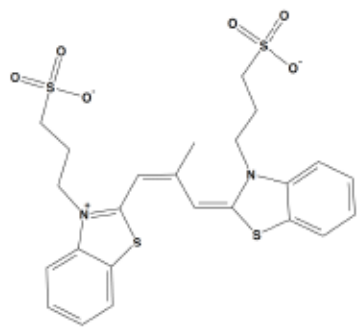
The pharmacophore-assisted docking results were further analyzed. At this stage we only included compounds with a maximum binding energy of $-30 \text{ kcal}\cdot\text{mol}^{-1}$. Only compounds that scored as a hit (also referred to as ‘frequency as hit’) more than 300 times were included. This narrowed down our hits to 67 potential PNKP phosphatase inhibitors. Several of those compounds had terminal phosphate groups; these molecules were also excluded since they could be substrates of the protein and thus would be dephosphorylated, which could make them weaker inhibitors. We also visually assessed the molecules and excluded the ones that did not occupy the binding pocket in a manner similar to DNA. Tautomers and stereoisomers of the compounds top hits were also excluded so that only unique molecules would remain. Following these elimination criteria, 20 compounds remained (Appendix II). Since all these hits had an LE of less than $-0.3 \text{ kcal}\cdot\text{mol}^{-1}/\text{heavy atom}$, none of them was excluded based on this criterion. Appendix II shows the structures of the top hits, their binding energies and LE as well as their frequencies as hits.

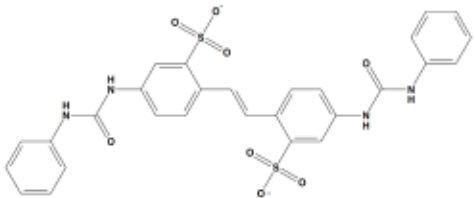
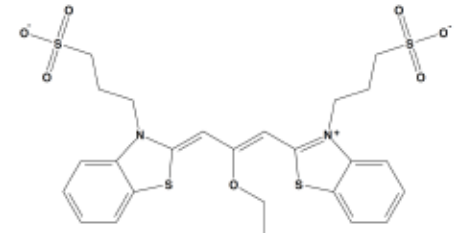
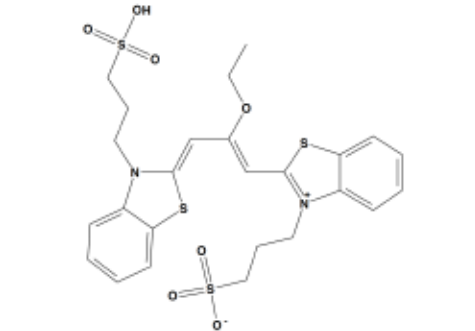
We chose seven of these compounds for experimental testing based on their binding energy, the number of times they scored as hits, LE, structural diversity and price. One of the seven purchased compounds was insoluble and was, therefore, not tested experimentally. The dissociation constants (K_d) of the six remaining compounds were calculated as a function of

the intrinsic fluorescence quenching of PNKP [6]. The compounds concentrations that cause half maximal inhibition (IC_{50}) were also determined *in vitro* using two different fluorescence-based assays (Appendix III). These results are shown in Table 6.1 along with the compound structures, binding energies and LE. Figure 6.6 shows the interactions of each of the six compounds with PNKP in its lowest binding energy pose. Interestingly, the protein structure to which the DNA and the six compounds had the least binding energies was the hPNKP homology model. Figure 6.5 and Figure 6.6 show that the DNA and the six compounds formed similar interactions with PNKP; they all had the following interactions: T217 side-chain H-bond donor, N218 backbone H-bond donor, M220 backbone H-bond donor, R259 side-chain H-bond donor and K260 side-chain H-bond donor. However, compounds B and D also formed R259 ionic interactions with the sulphonic groups of the molecules. Compounds B, D and F also formed additional K260 ionic interactions with the second sulphonic groups of the compounds. D173 was also a backbone H-bond donor to the DNA and all the compounds except C. On visual inspection of the latter compound in complex with PNKP, however, we found the H-bond acceptor in compound C is less than 0.3 Å away from forming that interaction, which indicates that this interaction was also formed by compound C.

Table 6.1. Results of the six compounds that were purchased for experimental validation.

LE = ligand efficiency, NA = not applicable, NT = not tested, Freq = Number of times scored as a hit

#	Structure	Binding energy (kcal·mol ⁻¹)	LE (kcal·mol ⁻¹ /heavy atom)	Freq	K _d ^{††} (nM)	IC ₅₀ (μM)
DNA		-38	-0.81	NA	NA	NA
A		-34	-0.82	339	120±10	3.7*
B		-32	-0.81	373	450±20	12.5†
C		-31	-0.86	471	170±10	23.5*

D		-31	-0.74	309	165±10	88.6*
E		-30	-0.80	533	110±10	NT
F		-30	-0.80	328	55±5	Too high†

††K_d values were determined using a tryptophan fluorescence quenching assay performed by Rajam S. Mani (Weinfeld lab)

* IC₅₀ values were determined using a Universal Molecular Beacon (U-MB) assay performed by Xiaoyan Yang (Weinfeld lab) (Appendix III). Control experiments using 3' hydroxyl DNA instead of 3' phosphate are still pending.

† IC₅₀ values were determined using a 2-aminopurine assay performed by Zahra Shire (Weinfeld lab) (Appendix III).

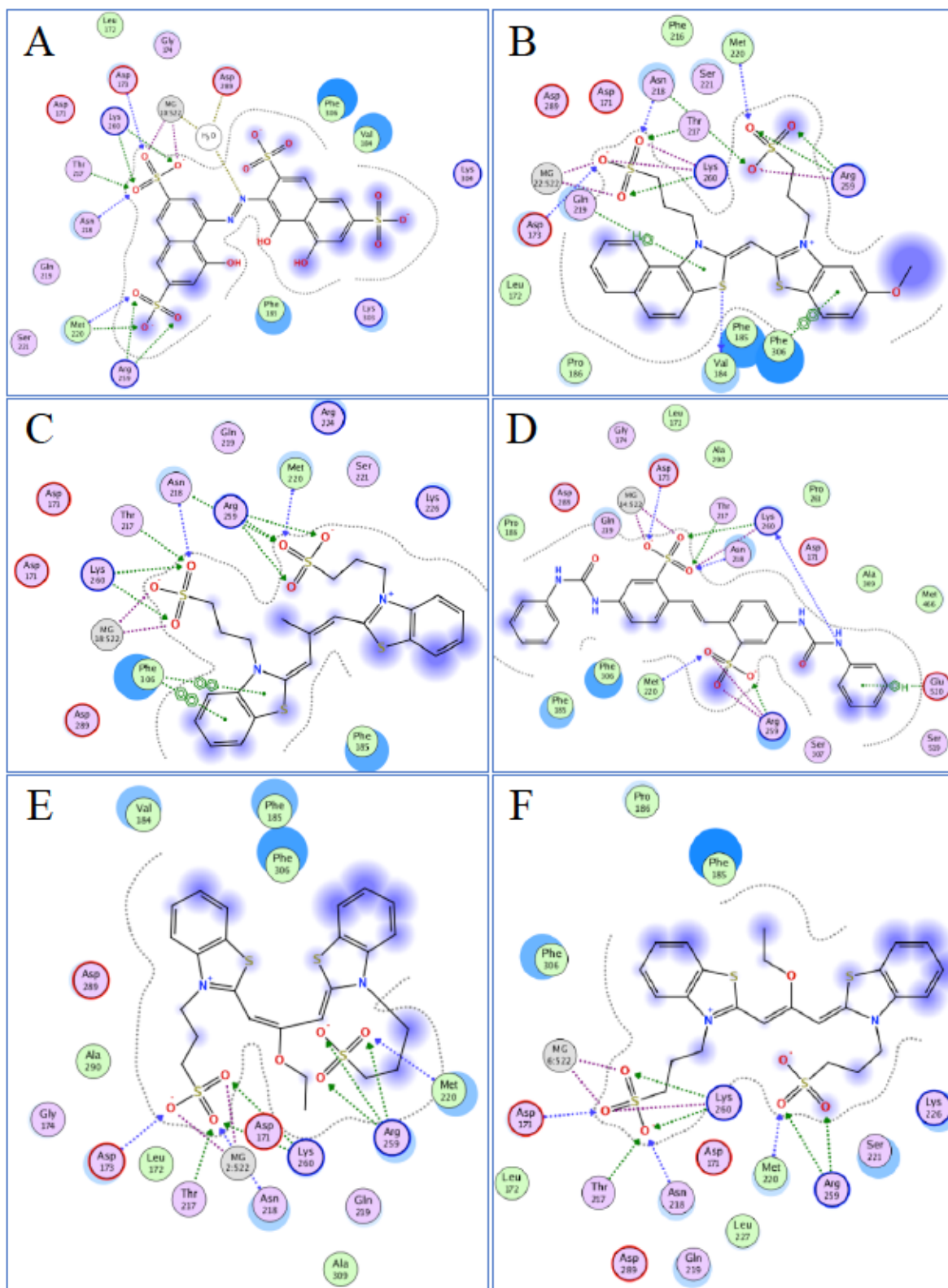


Figure 6.6. The ligand interactions between the six tested compounds (A-F) and hPNKP homology model.

The interaction annotations are the same as in Figure 6.5.

Our collaborators also performed electrophoretic mobility shift assay (EMSA) [7] using the purified D170A mouse protein (Figure 6.7). The results from this assay showed that compounds A and D displaced the bound DNA, which indicated that they inhibit PNKP competitively. Compounds E and F were too fluorescent and interfered with the assay measurements. Although no conclusions could be made for those two compounds, they were visually seen to localize with the protein, which indicates that they bind to the protein. Compounds B and C, on the other hand, localized with both PNKP and DNA in the same band, which indicated that they both bind to PNKP but do not inhibit DNA binding to the protein.

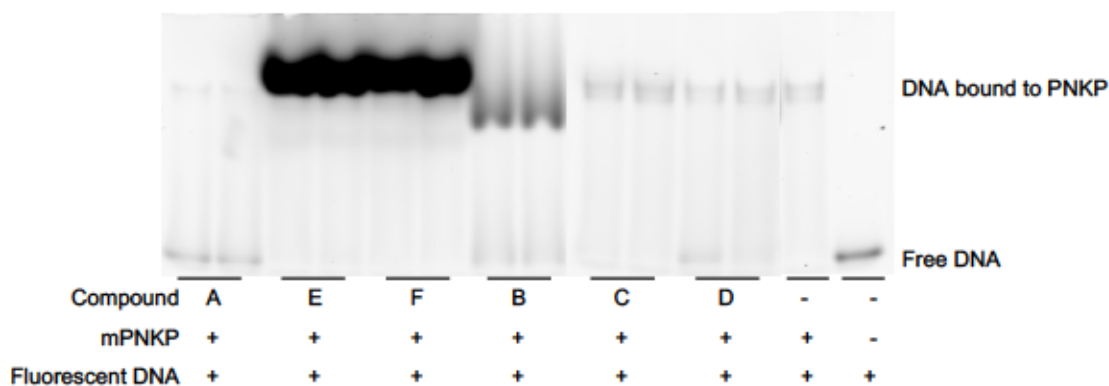


Figure 6.7. The EMSA results for compounds A-F obtained from Cameron Murray (Glover lab) who performed the experiments and interpreted the results. Lanes A-F contained the indicated compound, mouse (mPNKP) and DNA. Each compound was tested twice. The last two panels were the negative (mouse PNKP + DNA only) and positive (DNA only) controls, respectively. Compounds E and F were too fluorescent and maxed out the detector, hence the other bands look weak. The EMSA results for molecules A and D indicate that the compounds could be competitively inhibiting the protein as demonstrated by the separate DNA band at the bottom on the gel. The EMSA was performed in a similar manner to [7].

6.3 Discussion

6.3.1 hPNKP protein model

The DNA repair enzyme, PNKP, is composed of a forkhead associated domain joined by a flexible linker to a fused phosphatase-kinase domain [8]. Since the latter domain is active independently, we only simulated the fused phosphatase-kinase domain of the protein. The 3U7G structure used as a template for homology modeling is a D170A mutant mouse PNKP model composed of the phosphatase and kinase domains of the protein. The 3U7G sequence is 90% similar and 83% identical to that of hPNKP. This gives high confidence in the homology model generated.

Although the crystallized protein was bound to a single-stranded DNA pentanucleotide, only the positions of the first two nucleotides have been resolved experimentally. We included this dinucleotide, the bound magnesium ion at the phosphatase active-site and its neighbouring crystal water molecule in our model. We simulated the complex for 250 ns of MD simulations to obtain different conformations of the protein and thus account for its flexibility during screening. The fluctuation pattern of the PNKP backbone as well as its phosphatase active-site non-hydrogen atoms indicated that the protein structure equilibrated after about 20 ns of MD simulations, as reflected in the plateauing of its RMSD (Figure 6.1). The three residues at each terminus, which form loops, were excluded from the protein backbone RMSD calculation since they were expected to be flexible. We also calculated the binding free energy of the DNA to PNKP using MMGBSA in Ambertools [4]. Figure 6.4 shows that the binding energy of DNA to PNKP increases during the simulation. On visual examination of the bound dinucleotide in our model, it was observed that the terminal 5' phosphate was

fluctuating during the simulation and was not always interacting with the protein, which led to the increase in binding energy. While the crystal structure used as a template for homology modelling was of a pentapeptide bound to PNKP, only the first two 3' nucleotides were actually resolved. Since our model was of PNKP bound to a dinucleotide, it is likely that the absence of the third nucleotide led to the loss of stabilizing interactions of the 5' phosphate, which could explain the observed increase binding energy in our simulations. This is not unexpected especially that it has been experimentally shown that trinucleotides have a higher affinity to the protein than dinucleotides [9].

6.3.2 Virtual screening of the CoCoCo database

In the screen for PNKP phosphatase inhibitors, a consensus-based approach was used to enrich the results and therefore the results were filtered using multiple techniques. We followed the Common Hits Approach (CHA) [10] in stage I of screening. CHA is based on virtual screening using multiple pharmacophore models obtained from hundreds of complex structures. This approach has been found to enrich screening results up to more than five-fold compared to screening based on the experimentally-determined complex structure alone [10]. In the screen, 460 complex structures obtained every 0.5 ns from 20 ns to 250 ns of MD simulations were used. It is worth mentioning that the pharmacophore models were based on the bound DNA, the native PNKP substrate, rather than a PNKP inhibitor as there are no experimentally-determined structures of PNKP bound to a phosphatase inhibitor.

LigandScout was used to automatically generate an ensemble of steric and electronic features that define the interaction features of DNA with PNKP. MOE was used to search for ligands in the CoCoCo database that fulfill these pharmacophore models i.e. have the required

features at the same relative positions. It is for this reason that the multiconformer database was used so that different features of the ligands would be represented in the different orientations that they could likely take. Pharmacophore screening using MOE resulted in 460 different filtered libraries, each based on a pharmacophore model at a certain simulation time point. We excluded filtered libraries that included zero or more than 200,000 unique ligands to make the docking step more feasible. This decreased the filtered libraries to 144 instead of 460. The biggest and smallest filtered databases of these 144 contained 193566 and 3 compounds, respectively.

In stage II of screening, pharmacophore-assisted docking was utilized to further narrow down the screening results. While docking alone is a powerful screening tool, yet the high flexibility of the DNA limits the power of this technique due to the molecule's consequent large conformational space search. Using pharmacophore modeling to assist docking helps overcome this limitation. We manually created pharmacophore models based on the DNA atoms that had the lowest binding energy to PNKP, with the expectation that those would be the most important interactions for binding. The pharmacophore models constituted 3 to 7 features, which is generally optimum so the model would not be too general nor too specific [11]. Besides being the highest affinity interaction with the DNA, at least one of the anionic oxygens of the 3' phosphate was always set as an essential pharmacophore feature in our models since it plays an important role in catalysis [3].

To account for the backbone flexibility of the protein during docking, ten representative structures of the protein were used: the hPNKP homology model as well as the nine structures from the MD simulation. We selected all the complex structures with local DNA binding

energy minima to PNKP over the simulation time then ranked them based on their DNA affinity. For each structure, we tweaked the manually created pharmacophore models and redocked the DNA in PNKP as control for assessment of the created pharmacophore features. The PNKP structures in which the docked DNA had an RMSD $< 2 \text{ \AA}$ compared to the original structure from MD were used for pharmacophore-assisted docking. Also, the structures were chosen so they would be spread-out over the equilibrated simulation time so they would be better representative of the protein flexibility. The final nine hPNKP structures, marked in Figure 6.4, along with the protein's homology model were all used for pharmacophore-assisted docking.

Since we docked 144 databases to ten protein structures, then a compound that would successfully pass the criteria in both screening stages would rank as a hit 1440 times. Analysis of our results show that 87 of our compounds had more than 20% success rate i.e. scored as a hit more than 300 times, only 67 of those had binding energies lower than $-30 \text{ kcal}\cdot\text{mol}^{-1}$. Several molecules from the top hits had terminal phosphate groups. This is expected since such compounds would greatly fit the screening criteria due to their high similarity to the native DNA structure. However, we excluded those compounds since they could be substrates rather than inhibitors of PNKP. It is worth mentioning that all our top hits had an LE of less than $-0.3 \text{ kcal}\cdot\text{mol}^{-1}/\text{heavy atom}$, which is generally the ideal range for high throughput screening and drug optimization [12].

Figure 6.5 and Figure 6.6 show the interacting residues of hPNKP with DNA and six of the top hits, respectively. Most interactions between the DNA and PNKP were also present in the six compounds. R224 and K226, which interact with DNA, are not predicted to interact with

any of the six compounds. This is expected since these residues interact with the terminal 5' phosphate of DNA, the equivalent of which is absent in our compounds.

As explained above, the binding energy values, LE and frequencies of the compounds were used to choose the top hits since these are all factors that can contribute to the success of a compound as a binder. We primarily ranked compounds based on their binding energies then their LE. It is important to understand that the calculated binding energy values should be used to rank the compounds rather than provide exact binding energy values. Although K_d values are a better indication of ligand binding than IC_{50} values, there was no correlation between the measured K_d and calculated binding energies (Table 6.1). This could be attributed to the fact that the fluorescence quenching assay used is an indirect way of measuring the dissociation constants especially that the intrinsic fluorescence of PNPK is attributed to W402 in the kinase domain of the protein. Also, the calculated binding energies were calculated for PNKP structures based on the DNA-protein complex. It could be that the compounds have higher affinities to other conformations of the protein and hence their ranking would be different. Another explanation for the lack of correlation between the calculated binding energies and the measured K_d values could be the difficulty in estimating the entropic contribution to binding especially that the potential hits have flexible alkyl chains.

A closer look at the compounds' measured IC_{50} values, however, shows that their calculated rank is identical to their ranking based on their IC_{50} values. It could be that the IC_{50} values are a better measure of the compounds' activity. In that case, our compounds show good inhibition for first generation compounds especially inhibitor A, which had an IC_{50} value of 3.7 μ M. However, it should be mentioned that compounds A, C and D still need to be tested

for activity against the polymerase enzyme, which was used in the U-MB assay. While the intrinsic fluorescence assays and EMSA indicate that our compounds do bind to PNKP, nonetheless, the control experiments for the U-MB need to be performed. It is noteworthy to explain that the fluorescence of our compounds interfered with the IC_{50} assays. Therefore, two different assays with different excitation and emission frequencies were used.

6.4 Conclusions

Inhibition of PNKP for combination cancer therapy can provide synergistic effects to enhance some of the current cancer treatment regimens. Rational drug design based on the understanding the ligand interaction with the biological target is one of the best and effective ways for drug discovery and development. Our aim in this chapter was to find potential PNKP inhibitors.

We used pharmacophore modeling, a fast screening technique, as well as pharmacophore-assisted docking to screen a library of 3.7 million compounds. The idea of using multiple technique screening was to enrich the screening results by combining the strengths of different methodologies. Our collaborators measured the K_d and IC_{50} values of six of the top hits. Compound A showed the highest potential as a competitive PNKP inhibitor as confirmed by the fluorescent based assays as well as the EMSA. Knowing the inhibitor-PNKP structure allows for insightful optimization of the lead compounds to develop more potent hits that can reach clinical trials.

6.5 Methods and Models

6.5.1 Creating the hPNKP models

We used the mouse PNKP model with PDB ID 3U7G as a template to create the hPNKP homology model in MOE [2]. The co-crystallized DNA fragment and the magnesium ion at the phosphatase active-site along with its neighbouring water molecule were also incorporated in the model. The hPNKP homology model created was then solvated in a 12 Å TIP3P water box using Ambertools [4]. Sodium ions were added to neutralize the system. Sodium chloride ions were then added randomly to adjust the salinity of the solvated system to 0.15 M to simulate physiological conditions. The system was then MD simulated using Amber [4]; the system was first minimized then gradually heated from 0 to 310 K with heavy restraints placed on the DNA and hPNKP atoms. The restraints were then gradually removed and the non-restrained system was simulated for 250 ns at 310 K (body temperature). We calculated the RMSD of the protein backbone atoms, using Ambertools [4], for residues 147 to 528 to evaluate the equilibration of the protein and for residues 171, 173, 184, 185, 218, 220, 221, 224, 226, 289, 290, 306, 307 and 310, which constitute the PNKP phosphatase active-site.

6.5.2 DNA binding energy calculations

We used Ambertools' Molecular Mechanics-Generalized Born Surface Area (MMGBSA) (described in Chapter 3) to calculate the binding free energy of the DNA dinucleotide to the equilibrated hPNKP.

6.5.3 Virtual screening using pharmacophore modeling and docking

In stage I, we utilized LigandScout to automatically generate the 460 structure-based pharmacophore models using the default feature definitions. These features are defined in the LigandScout manual [13]. The multiconformer CoCoCo database [1] was screened using MOE against these generated pharmacophore models. In stage II, MOE was used to generate the pharmacophore features as well as to dock the filtered databases from stage I. We used two different scoring functions in MOE called the Affinity dG and London dG scoring functions. The former is a linear function that estimates the enthalpic contribution of the free energy of binding (Equation 6.1).

Equation 6.1

$$\Delta G = C_{hb}f_{hb} + C_{ion}f_{ion} + C_{mlig}f_{mlig} + C_{hh}f_{hh} + C_{hp}f_{hp} + C_{aa}f_{aa}$$

From the MOE manual [2], “the ‘*f*’ terms in the equation above fractionally count atomic contacts of specific types and the ‘*C*’ terms represent weight coefficients for each term. Also, ‘*hb*’ are the hydrogen bond acceptor-donor pairs, ‘*ion*’ is a Coulomb-like term for ionic interactions, ‘*mlig*’ are metal ligation interactions, ‘*hh*’ are hydrophobic interactions, ‘*hp*’ are interactions between hydrophobic and polar atoms, ‘*aa*’ are interactions between any two atoms.”

The London dG scoring function, which estimates the free energy of binding, is calculated by Equation 6.2 as:

Equation 6.2

$$\Delta G = c + E_{flex} + \sum_{h-bonds} c_{HB} f_{HB} + \sum_{m-lig} c_M f_M + \sum_{atoms\ i} \Delta D_i$$

From the MOE manual [14], “where ‘*c*’ is the loss/gain of rotational and translational entropy, ‘*E_{flex}*’ is the energy due to the loss of flexibility of the ligand, ‘*f_{HB}*’ is a value between 0 to 1 that measures the hydrogen bonds geometric imperfections, ‘*c_{HB}*’ is the energy of an ideal hydrogen bond, ‘*f_M*’ is a value between 0 to 1 and measures geometric imperfections of metal ligations, ‘*c_M*’ is the energy of an ideal metal ligation and ‘*D_i*’ is the desolvation energy of atom ‘*i*’”.

We also calculated the ligand efficiencies for the predicted top hits using Equation 6.3:

Equation 6.3

$$LE = \frac{\text{MOE calculated binding energy}}{\text{number of heavy atoms}}$$

6.6 References

1. Rio AD, Barbosa AJM, Caporuscio F, Mangiatordi GF. CoCoCo: A free suite of multiconformational chemical databases for high-throughput virtual screening purposes. *Molecular BioSystems* 2010 -11-01;6(11):2122-2128.
2. Molecular operating environment (MOE), 2016.08; chemical computing group inc., 1010 sherbrooke st. west, suite #910, montreal, QC, canada, H3A 2R7, 2016.
3. Coquelle N, Havali-Shahriari Z, Bernstein N, Green R, Glover JNM. Structural basis for the phosphatase activity of polynucleotide kinase/phosphatase on single- and double-stranded DNA substrates. *Proceedings of the National Academy of Sciences of the United States of America* 2011;108(52):21022-21027.
4. Case DA, Babin V, Berryman JT, Betz RM, Cai Q, Cerutti DS, Cheatham DSI, Darden TA, Duke RE, Gohlke H, Goetz AW, Gusarov S, Homeyer N, Janowski P, Kaus J, Kolossváry I, Kovalenko A, Lee TS, LeGrand S, Luchko T, Luo R, Madej B, Merz KM, Paesani F, Roe DR, Roitberg A, Sagui C, Salomon-Ferrer R, Seabra G, Simmerling CL, Smith W, Swails J, Walker RC, Wang J, Wolf RM, Wu X, Kollman PA. *Amber 14*. 2014.
5. Wolber G, Langer T. LigandScout: 3-D pharmacophores derived from protein-bound ligands and their use as virtual screening filters. *Journal of Chemical Information and Modeling* 2005 January 1;45(1):160-169.
6. Freschauf GK, Mani RS, Mereniuk TR, Fanta M, Virgen CA, Dianov GL, Grassot J, Hall DG, Weinfeld M. Mechanism of action of an imidopiperidine inhibitor of human polynucleotide kinase/phosphatase. *Journal of Biological Chemistry* 2010;285(4):2351-2360.
7. Havali-Shahriari Z, Weinfeld M, Glover JNM. Characterization of DNA substrate binding to the phosphatase domain of the DNA repair enzyme polynucleotide kinase/phosphatase. *Biochemistry* 2017 03 28;56(12):1737-1745.
8. Weinfeld M, Mani RS, Abdou I, Aceytuno RD, Glover JNM. Tidying up loose ends: The role of polynucleotide kinase/phosphatase in DNA strand break repair. *Trends in biochemical sciences* 2011;36(5):262-271.
9. Bernstein NK, Williams RS, Rakovszky ML, Cui D, Green R, Karimi-Busheri F, Mani RS, Galicia S, Koch CA, Cass CE, Durocher D, Weinfeld M, Glover JNM. The molecular architecture of the mammalian DNA repair enzyme, polynucleotide kinase. *Molecular Cell* 2005 -03-04;17(5):657-670.

10. Marcus Wieder, Arthur Garon, Ugo Perricone, Stefan Boresch, Thomas Seidel, Anna Maria Almerico, Thierry Langer. Common hits approach: Combining pharmacophore modeling and molecular dynamics simulations. *Journal of Chemical Information and Modeling* 2017 Feb 27;;57(2):365-385.
11. Yang S. Pharmacophore modeling and applications in drug discovery: Challenges and recent advances. *Drug Discovery Today* 2010 June 1;;15(11):444-450.
12. Cavalluzzi MM, Mangiatordi GF, Nicolotti O, Lentini G. Ligand efficiency metrics in drug discovery: The pros and cons from a practical perspective. *Expert Opinion on Drug Discovery* 2017 11;12(11):1087-1104.
13. LigandScout Manual. Available from: <http://www.inteligand.com/ligandscout/manual/>.
14. Molecular operating environment (MOE), 2016.08; chemical computing group inc., 1010 sherbrooke st. west, suite #910, montreal, QC, canada, H3A 2R7, 2016.

Chapter 7

Conclusions and Future Directions

7.1 Mutant p53

7.1.1 Summary

Our choice of mutant p53 (mp53) as a target was motivated by its high mutational frequency, confirming the high importance of the protein as a master tumor suppressor. In addition, p53 mutations are common in various types of cancer, which increases the applicability of potential drugs to a wide population of cancer patients [1]. Also, mp53 accumulates in cancer cells [2]. Therefore, the reactivation of mp53 should induce a strong apoptotic response as demonstrated by PRIMA-1 (p53-reactivation and induction of massive apoptosis) [2, 3]. Moreover, the choice of mp53 is highly specific to abnormal cells, which increases the potential of mp53 reactivators to have minimal side effects. Four main goals on p53 were discussed in this thesis:

- The first was to understand the interaction of known mutant protein activators from the literature with p53 at the C124 site.
- The second was to understand the effect of the G245S single point mutation on the protein structure both in its apo and DNA-bound forms.
- The third aim was to screen for potential G245S-mp53 activators using covalent docking.
- The last aim was to compare the R175H-mp53 and R273H-mp53 DNA complex structures both in their methylene quinuclidinone (MQ) drugged and undrugged forms with respect to the wild-type (wt) p53 complex.

In Chapter 2, our aim was to evaluate the binding and ADMET properties of known mp53 activators. This chapter was published in [4]. A study by Wassman *et al.* proposed that C124 is the site at which alkylating mp53 activators bind to restore the wt activity to the mutant protein [5]. An equilibrated atomistic model of the hotspot R273H-mp53 was created. We docked the alkylating mp53 activators MQ, NB, STIMA-1, CP-31398, MIRA-1 and stictic acid, which all have a reactive double-bond (DB), at the C124 pocket. We also docked the non-alkylating activators WR-1065, ellipticine and 9-hydroxy ellipticine at the same site. Docking results showed that the DB of all alkylating ligands were positioned towards the thiol of C124. While alkylating ligands were not predicted to directly interact with C124, our molecular dynamics (MD) simulations suggested that the compounds could come within a close distance for reaction, owing to the flexibility of the protein. The only exception for this observation was stictic acid which was predicted to interact with C124. However, this molecule was the only mp53 reactivator discovered by *in silico* screening using non-covalent docking specifically at the C124 site [5].

On the other hand, non-alkylating mp53 reactivators were predicted to directly interact with C124. These results suggested that alkylating ligands formed transient interactions with mp53 before reacting with C124 while non-alkylating directly interacted with the site. This is logical given that non-alkylating molecules were not expected to react with the protein – the predicted pose could be the final reactivation destination.

There was also a qualitative correlation between the relative ranking of STIMA-1, NB and MQ from our docking calculations and the reported experimental half maximal inhibition concentrations (IC_{50}) of the compounds on Saos cells carrying R273H-mp53 [3, 6, 7]. MQ, the active metabolite of APR-246, which is currently in clinical trials has been reported to

have dose-limiting toxicities resulting from increased liver enzymes, confusion, fatigue and impaired speech [8]. We, therefore, used ADMET Predictor™ [9] to compare the predicted toxicities and solubilities of the compounds. While stictic acid was the only compound with a better predicted toxicity profile, especially in terms of its low blood-brain-barrier permeability, it had low predicted solubility, which would likely result in low bioavailability of the molecule as a drug. We, therefore, performed a virtual screen using covalent docking to find new potential mp53 activators (discussed in Chapter 4).

In Chapter 3, we modelled G245S-mp53 both as a dimer bound to DNA and in its apo form and compared the models to the wt protein. This chapter was published in [10]. A decrease in residue fluctuations of loop L3, where the G245S mutation lies, was expected since the possible dihedral angles that can be adopted by serine are more restricted than the wt's native glycine. However, a decrease in residue fluctuations of loops L1 and L2 was also observed. Functional mode analysis revealed a correlation between loops L3 and loops L1 and L2, which explains the observed fluctuation pattern.

Moreover, high residue fluctuations were calculated for residues 224, 225 and 226 of G245S-mp53, which are at the interaction interface between the two monomers in the DNA bound complex in the wt complex. This suggested a possible interruption of the monomer-monomer interaction. This was further confirmed by the distortion of the dimer arrangement on the DNA compared to the wt dimer when bound to DNA. These results are in agreement with experimental findings, which demonstrated that G245S structural mutant does not undergo structural destabilization as the other structural mutants [11]. Indeed, a redistribution of binding energy of G245S-mp53 residues to DNA was also observed, especially in residues

close to the mutation site. It has been reported that wt-p53 had a hundred times its affinity to DNA as a tetramer than as a monomer [12, 13]. It is likely that the dimer distortion observed in our models leads to loss of the tumor suppressor activity of this structural mutant.

In Chapter 4, a virtual screen to find potential G245S-mp53 activators using covalent docking was performed. This chapter has been accepted for publication in PLoS One. Six representative structures obtained from clustering G245S-mp53 structures from MD simulations (in Chapter 3) were used to represent the mutant protein conformations. We set screening criteria to filter the ZINC library (13 million compounds) to about 130,000 molecules. DOCKTITE, a docking protocol in the Molecular Operating Environment (MOE) software was used to covalently dock different low energy conformations of the molecules at C124 of G245S-mp53. To enrich our results, a consensus-based scoring approach was used based on both Affinity dG and DSX scoring functions. MQ, NB, STIMA-1 and MIRA-1 alkylating mp53 activators are all Michael acceptors. For the top hits from our covalent docking screening, however, new classes of covalent binders were found including: five thiosemicarbazones, four halo-carbonyls and only one Michael acceptor molecule. Based solely on *in silico* results, compound 2 seems to be the best mp53 activator in terms of binding energy to G245S-mp53 and predicted toxicity. However, since covalent docking does not give enough insight into the effect of the covalently bound molecule on the protein structure, further validation is required to confirm the covalent docking results.

In Chapter 5, our aim was to understand the effect of MQ binding on R175H-mp53 and R273H-mp53 structures when the modified proteins were bound to DNA. This chapter has

been submitted to Oncotarget. *In silico* atomistic models of R175H-mp53 and R273H-mp53 each in complex with DNA were created by virtual mutation of the wt-p53 DNA complex structure obtained from PDB: 1TSR. To generate the drugged variants of the mutant proteins, covalent docking was used to find the best fit starting structure of MQ bound to each of the mutants. PyRED [14-16] was used to parameterize CmQ, the MQ bound C124 residue. These proteins each in complex with the DNA were simulated using MD for 750 ns to obtain the equilibrated complex structures as assessed by the root-mean-square deviation (RMSD) of the proteins backbones. Analysis was performed on the last 450 ns of the simulations.

The p53-DNA complex models suggested that the binding of MQ at C124 induced a conformational change in the drugged protein variants, which resulted in the introduction of new interactions between loop L1 of the drugged protein variants and DNA. Visual assessment of the superposed p53 variants revealed a misalignment of the mutant proteins with DNA compared to wt-p53. This finding was further supported by the high DNA RMSD values of the undrugged mutants from the average DNA structure in the wt-p53 complex. Contrary to the mutants, the drugged protein variants had a similar alignment with the DNA like wt-p53. Also, their DNA RMSD values from the wt-p53 DNA average structure were lower than their respective mutants. It has previously been found that MQ can restore the wt activity to mp53 including the restoration of p53 target genes transcription [3]. Collectively, our results indicated that the conformational change induced in the mutants allowed loop L1 to anchor p53 to DNA. It is possible that this anchoring allows for the drugged mutants to bind in a manner that enables the transcription of p53 target genes, especially that the proper alignment of p53 with the DNA would likely allow for the tetramerization of p53, which is essential for proper and efficient transcriptional activity [12, 13].

Additionally, it was found that the binding energy (EBE) of the mutants to the DNA, calculated using Molecular Mechanics Generalized Born Surface Area (MMGBSA) in Ambertools, increased compared to wt-p53, with this increase being slightly more pronounced for the R175H structural mutant. The binding of MQ to R175H-mp53 increased the affinity of the drugged mutant protein to DNA. In the case of the contact mutant, however, MQ could not restore the binding affinity lost due to the R273H mutation. However, it changed the binding profile of the modified proteins with DNA as reflected in the contributions of the p53 residues to the EBE to DNA.

In general, it was observed that the interacting residues of wt-p53 in loops L1, L3 and helix H2 as well as R273 formed a base, with which the protein 'sat' on DNA. R175H-mp53, which was misaligned with the DNA compared to wt-p53, lost the right and left sides of the base interactions, while R273H-mp53 lost the right, center and some of the interactions with the left side of the base as well. On the contrary, R175H-CmQA-p53, R175H-CmQB-p53 and R273H-CmQA-p53 all maintained their base interactions with the DNA. The only exception was R273H-CmQB-p53, which formed weaker interactions on the left side of the base, suggesting that this epimer could be less active.

7.1.2 Future directions

Putting the main objective of finding novel mp53 activators in perspective, future work should focus on experimentally validating the drugged mutant variants-DNA complex models created using methods such as X-ray crystallography, NMR or even electron microscopy in a manner similar to [17]. Alternatively, site-directed mutagenesis of the new key residues that were predicted to anchor drugged p53 proteins to DNA could be performed. Disruption of

these interactions would be expected to negatively impact the reactivation effect of MQ. *In silico* alanine scanning could be used to choose the residues for the site-directed mutagenesis experiments.

A recent study has shown that C277 was also important for mp53 reactivation by MQ. It would be worth studying the effect of MQ binding on the structure of mp53 when bound to C277 and when bound to both C124 and C277. This comparison would provide the required detailed insight to identify the exact requirements for mp53 reactivation with respect to its DNA binding behaviour. While it is still possible that in cells the reactive MQ would still sometimes bind to C124, C277 or both, it is possible that not all these modified variants would be active. Knowing the exact required protein modifications would help design better mp53 activators that would bind specifically as required. Consequently, the optimized mp53 activators would enhance the protein's transcriptional activity and have improved efficacy and potency.

The next step for the potential hits identified in Chapter 4 would be to test the compounds both *in silico* and *in vitro*. Similar to our protocol in Chapter 5, the effect of these potential hits on the mutant protein structures and binding profile with DNA would be examined. An alternative to classical MD simulations used in Chapter 5 would be using enhanced sampling methods such as accelerated MD to ensure that the conformational change, induced by the binding of the candidate molecule, is complete. The equilibrated model would be examined in terms of the modified protein's alignment and base interactions with DNA. To validate the effect of a hit *in vitro*, cell viability and functional assays would also be performed on p53 null cells transfected with constructs carrying wt-p53 or the respective mp53. Additionally,

differential scanning fluorimetry can be used to confirm the thermal stabilization of the mp53 structures by the potential hits [5].

The top compounds would then be tested *in vivo* on xenograft animal models. Cycles of drug optimizations would follow to enhance the pharmacodynamic and pharmacokinetic profiles of the lead drugs. ADMET Predictor™ [9] can also be utilized as a useful tool to prioritize compounds with the best predicted properties.

It is important to keep in mind that the architecture of p53 makes it sensitive to structural alterations as demonstrated by the effects of single-point mutations or alkylation of the mutant proteins. Therefore, the most successful drug would restore all wt-p53 interactions in cells without introducing new malicious ones. However, it is possible that a lead compound would restore only some of these interactions. Moreover, it is even possible that a compound would restore some of the wt-p53 functions, such as the transcription of apoptotic p53 target genes, but also acquire gain-of-function (GOF) activities. Such compounds would be addressed on a case-by-case basis; theoretically, as an example, a compound that leads to the expression of apoptotic genes but also a few oncogenic genes might still be successful if the net result was the death of cancer cells without adverse effects on normal surviving cells.

7.2 Polynucleotide kinase phosphatase (PNKP)

7.2.1 Summary

PNKP is a novel anti-cancer target that can sensitize cells to traditional cancer regimens including ionizing radiation (IR) and the DNA-damaging irinotecan [18-20]. PNKP inhibitors will likely decrease cancer cell resistance caused by the overexpression of PNKP in cells. The

idea behind inhibiting PNKP is to exploit resistance mechanisms on which cancer cells rely for survival. The combination use of PNKP inhibitors can also decrease the required IR or DNA-damaging agents' dose required and hence decrease their side-effects.

In Chapter 6, the aim was to find potential PNKP inhibitors by virtually screening the Commercial Compound Collection (CoCoCo) over two stages in a consensus-based approach. The Common Hits Approach (CHA) pharmacophore screening was utilized in the first stage. More specifically, the database was filtered against 460 automatically generated pharmacophore models based on structures obtained from the equilibrated MD simulations of the human PNKP (hPNKP) homology model. 144 sub-libraries were obtained after this step. Ten representative hPNKP structures were then chosen and used for pharmacophore-assisted docking. Several of the predicted top hits were compounds with terminal phosphate groups. These were excluded from our results. Six of the potential hits were purchased and their dissociation constants were measured using a tryptophan fluorescence quenching assay. Also, the half maximal inhibition concentrations (IC_{50}) were also measured by fluorescence quenching assays. There was a qualitative correlation between the *in silico* calculated binding energies and the measured IC_{50} values. However, some control experiments for the two enzyme Universal Molecular Beacon assay are still to be carried out.

7.2.2 Future directions

To further validate the top hits, the Lineweaver-Burk plot of the Michaelis-Menten enzyme kinetics could be used to confirm that the potential hits are indeed competitive inhibitors [21]. Also, a more thorough electrophoretic mobility shift assay could be performed [22]. The potential hits would also be tested on cells treated with ionizing radiation or irinotecan to test

the sensitizing effect of the compounds. Additionally, the compounds would also be tested on PTEN or SHP-1 deficient cells to test their synthetic lethality. The best PNKP inhibitors would then be tested *in vivo* on xenograft mouse models. Again, iterations of modifications to optimize the structures of the lead compounds would likely follow till a suitable potent compound is produced.

7.3 References

1. Bouaoun L, Sonkin D, Ardin M, Hollstein M, Byrnes G, Zavadil J, Olivier M. TP53 Variations in Human Cancers: New Lessons from the IARC TP53 Database and Genomics Data. *Human Mutation*. 2016; 37: 865-876.
2. Bykov VJN, Issaeva N, Shilov A, Hultcrantz M, Pugacheva E, Chumakov P, Bergman J, Wiman KG, Selivanova G. Restoration of the tumor suppressor function to mutant p53 by a low-molecular-weight compound. *Nature medicine*. 2002; 8: 282-288.
3. Lambert JMR, Gorzov P, Veprintsev DB, Soderqvist M, Segerback D, Bergman J, Fersht AR, Hainaut P, Wiman KG, Bykov VJN. PRIMA-1 Reactivates Mutant p53 by Covalent Binding to the Core Domain. *Cancer Cell*. 2009; 15: 376-388.
4. Omar SI, Tuszynski J. Ranking the Binding Energies of p53 Mutant Activators and Their ADMET Properties. *Chemical Biology & Drug Design*. 2014.
5. Wassman CD, Baronio R, Demir O, Wallentine BD, Chen C, Hall LV, Salehi F, Lin D, Chung BP, Hatfield GW, Chamberlin AR, Luecke H, Lathrop RH, et al. Computational identification of a transiently open L1/S3 pocket for reactivation of mutant p53. *Nature Communications*. 2013; 4: 1407.
6. Zache N, Lambert JMR, Rokaeus N, Shen J, Hainaut P, Bergman J, Wiman KG, Bykov VN. Mutant p53 targeting by the low molecular weight compound STIMA-1. *Molecular Oncology*. 2008; 2: 70-80.
7. Bykov VJN, Issaeva N, Zache N, Shilov A, Hultcrantz M, Bergman J, Selivanova G, Wiman KG. Reactivation of mutant p53 and induction of apoptosis in human tumor cells by maleimide analogs. *The Journal of Biological Chemistry*. 2005; 280: 30384-30391.
8. Lehmann S, Bykov VJN, Ali D, Andren O, Cherif H, Tidefelt U, Ugglä B, Yachnin J, Juliusson G, Moshfegh A, Paul C, Wiman KG, Andersson P. Targeting p53 in Vivo: A First-in-Human Study With p53-Targeting Compound APR-246 in Refractory Hematologic Malignancies and Prostate Cancer. *Journal of Clinical Oncology*. 2012; 30: 3633-3639.
9. ADMET Predictor(TM) is distributed by Simulations Plus, Inc., Lancaster CA 93534 (<http://simulations-plus.com>); 8.0.4.6.
10. Lepre MG, Omar SI, Grasso G, Morbiducci U, Deriu MA, Tuszynski JA. Insights into the Effect of the G245S Single Point Mutation on the Structure of p53 and the Binding of the Protein to DNA. *Molecules (Basel, Switzerland)*. 2017; 22.

11. Selivanova G, Wiman KG. Reactivation of mutant p53: molecular mechanisms and therapeutic potential. *Oncogene*. 2007; 26: 2243-2254.
12. Chène P. The role of tetramerization in p53 function. *Oncogene*. 2001; 20: 2611.
13. Kamada R, Toguchi Y, Nomura T, Imagawa T, Sakaguchi K. Tetramer formation of tumor suppressor protein p53: Structure, function, and applications. *Peptide Science*. 2016; 106: 598-612.
14. Wang F, Becker J, Cieplak P, Dupradeau F. RED Python: Object oriented programming for Amber force fields. *Abstracts of Papers of the American Chemical Society*. 2014; 247.
15. Dupradeau F, Pigache A, Zaffran T, Savineau C, Lelong R, Grivel N, Lelong D, Rosanski W, Cieplak P. The R.E.D. tools: advances in RESP and ESP charge derivation and force field library building. *Physical chemistry chemical physics: PCCP*. 2010; 12: 7821-7839.
16. Vanquenef E, Simon S, Marquant G, Garcia E, Klimerak G, Delepine JC, Cieplak P, Dupradeau F. R.E.D. Server: a web service for deriving RESP and ESP charges and building force field libraries for new molecules and molecular fragments. *Nucleic Acids Research*. 2011; 39: 511.
17. Demir Ö, Jeong PU, Amaro RE. Full-length p53 tetramer bound to DNA and its quaternary dynamics. *Oncogene*. 2016; 36: 1451.
18. Pearl LH, Schierz AC, Ward SE, Al-Lazikani B, Pearl FMG. Therapeutic opportunities within the DNA damage response. *Nature Reviews. Cancer*. 2015; 15: 166-180.
19. Rasouli-Nia A, Karimi-Busheri F, Weinfeld M. Stable down-regulation of human polynucleotide kinase enhances spontaneous mutation frequency and sensitizes cells to genotoxic agents. *Proceedings of the National Academy of Sciences of the United States of America*. 2004; 101: 6905-6910.
20. Freschauf GK, Karimi-Busheri F, Ulaczyk-Lesanko A, Mereniuk TR, Ahrens A, Koshy JM, Rasouli-Nia A, Pasarj P, Holmes CFB, Rininsland F, Hall DG, Weinfeld M. Identification of a Small Molecule Inhibitor of the Human DNA Repair Enzyme Polynucleotide Kinase/Phosphatase. *Cancer research*. 2009; 69: 7739-7746.
21. Freschauf GK, Mani RS, Mereniuk TR, Fanta M, Virgen CA, Dianov GL, Grassot J, Hall DG, Weinfeld M. Mechanism of Action of an Imidopiperidine Inhibitor of Human Polynucleotide Kinase/Phosphatase. *Journal of Biological Chemistry*. 2010; 285: 2351-2360.
22. Havalı-Shahriari Z, Weinfeld M, Glover JNM. Characterization of DNA Substrate Binding to the Phosphatase Domain of the DNA Repair Enzyme Polynucleotide Kinase/Phosphatase. *Biochemistry*. 2017; 56: 1737-1745.

Bibliography

10.2210/Pdb1tsr/Pdb a.

10.2210/Pdb2vuk/Pdb b.

Abbotts, Rachel and David M. Wilson. 2017. "Coordination of DNA Single Strand Break Repair." *Free Radical Biology and Medicine* 107: 228-244.

Abegglen, Lisa M., Aleah F. Caulin, Ashley Chan, Kristy Lee, Rosann Robinson, Michael S. Campbell, Wendy K. Kiso, et al. 2015. "Potential Mechanisms for Cancer Resistance in Elephants and Comparative Cellular Response to DNA Damage in Humans." *Jama* 314 (17): 1850-1860.

Aceytuno, R. Daniel, Cortt G. Pielt, Zahra Havali-Shahriari, Ross A. Edwards, Martial Rey, Ruiqiong Ye, Fatima Javed, et al. 2017. "Structural and Functional Characterization of the PNKP-XRCC4-LigIV DNA Repair Complex." *Nucleic Acids Research* 45 (10): 6238-6251.

ADMET Predictor(TM) is Distributed by Simulations Plus, Inc., Lancaster CA 93534 ([Http://Simulations-Plus.Com](http://Simulations-Plus.Com)) a. Vol. 8.0.4.6.

ADMET Predictor(TM) is Distributed by Simulations Plus, Inc., Lancaster CA 93534 ([Http://Simulations-Plus.Com](http://Simulations-Plus.Com)). c.

Alexandrova, Evguenia M., Safia A. Mirza, Sulan Xu, Ramona Schulz-Heddergott, Natalia D. Marchenko, and Ute M. Moll. 2017. "P53 Loss-of-Heterozygosity is a Necessary Prerequisite for Mutant P53 Stabilization and Gain-of-Function in Vivo." *Cell Death & Disease* 8 (3): e2661.

- Allinson, Sarah L. 2010. "DNA End-Processing Enzyme Polynucleotide Kinase as a Potential Target in the Treatment of Cancer." *Future Oncology* (London, England) 6 (6): 1031-1042.
- Anne Perdrix, Ahmad Najem, Sven Saussez, Ahmad Awada, Fabrice Journe, Ghanem Ghanem, and Mohammad Krayem. 2017. "PRIMA-1 and PRIMA-1Met (APR-246): From Mutant/Wild Type p53 Reactivation to Unexpected Mechanisms Underlying their Potent Anti-Tumor Effect in Combinatorial Therapies." *Cancers* 9 (12): 172.
- APR-246 Clinical Trials
 (<https://www.clinicaltrials.gov/ct2/Results?Cond=&term=APR-246&Cntry=&State=&City=&Dist=>), last modified July 2nd,
 (<https://www.clinicaltrials.gov/ct2/results?cond=&term=APR-246&cntry=&state=&city=&dist=>).
- Arlt, Christian, Christian H. Ihling, and Andrea Sinz. "Structure of Full-Length p53 Tumor Suppressor Probed by Chemical Cross-Linking and Mass Spectrometry." *Proteomics* 15 (16): 2746-2755.
- Bahar, Ivet, Timothy R. Lezon, Lee-Wei Yang, and Eran Eyal. 2010. "Global Dynamics of Proteins: Bridging between Structure and Function." *Annual Review of Biophysics* 39: 23-42.
- Balagurumoorthy, Pichumani, Hiroshi Sakamoto, Marc S. Lewis, Nicola Zambrano, G. Marius Clore, Angela M. Gronenborn, Ettore Appella, and Rodney E. Harrington. 1995. "Four p53 DNA-Binding Domain Peptides Bind Natural p53-Response Elements and Bend the DNA." *Proceedings of the National Academy of Sciences* 92 (19): 8591-8595.
- Barakat, Khaled, Bilkiss B. Issack, Maria Stepanova, and Jack Tuszynski. 2011. "Effects of Temperature on the p53-DNA Binding Interactions and their Dynamical Behavior: Comparing the Wild Type to the R248Q Mutant." *PloS One* 6 (11).
- Barakat, Khaled, Jonathan Mane, Douglas Friesen, and Jack Tuszynski. 2010. "Ensemble-Based Virtual Screening Reveals Dual-Inhibitors for the p53-MDM2/MDMX Interactions." *Journal of Molecular Graphics & Modelling* 28 (6): 555-568.
- Bassett, Emily A., Wenge Wang, Farzan Rastinejad, and Wafik S. El-Deiry. 2008. "Structural and Functional Basis for Therapeutic Modulation of p53 Signaling." *Clinical Cancer Research: An Official Journal of the American Association for Cancer Research* 14 (20): 6376-6386.
- Baugh, Evan H., Hua Ke, Arnold J. Levine, Richard A. Bonneau, and Chang S. Chan. 2018. "Why are there Hotspot Mutations in the TP53 Gene in Human Cancers?" *Cell Death and Differentiation* 25 (1): 154-160.

- Bayly, Christopher I., Piotr Cieplak, Wendy Cornell, and Peter A. Kollman. 1993. "A Well-Behaved Electrostatic Potential Based Method using Charge Restraints for Deriving Atomic Charges: The RESP Model." *The Journal of Physical Chemistry* 97 (40): 10269-10280.
- Beckerman, Rachel and Carol Prives. 2010. "Transcriptional Regulation by p53." *Cold Spring Harbor Perspectives in Biology* 2 (8): a000935.
- Berger, Michael, Ronit Vogt Sionov, Arnold J. Levine, and Ygal Haupt. 2001. "A Role for the Polyproline Domain of p53 in its Regulation by Mdm2." *Journal of Biological Chemistry* 276 (6): 3785-3790.
- Bernardi, Rafael C., Marcelo C. R. Melo, and Klaus Schulten. 2015. "Enhanced Sampling Techniques in Molecular Dynamics Simulations of Biological Systems." *Biochimica Et Biophysica Acta (BBA) - General Subjects* 1850 (5): 872-877.
- Bernstein, N. K., F. Karimi-Busheri, A. Rasouli-Nia, R. Mani, G. Dianov, J. N. M. Glover, and M. Weinfeld. 2008. "Polynucleotide Kinase as a Potential Target for Enhancing Cytotoxicity by Ionizing Radiation and Topoisomerase I Inhibitors." *Anti-Cancer Agents in Medicinal Chemistry* 8 (4): 358-367.
- Bernstein, Nina K., R. Scott Williams, Melissa L. Rakovszky, Diana Cui, Ruth Green, Feridoun Karimi-Busheri, Rajam S. Mani, et al. 2005. "The Molecular Architecture of the Mammalian DNA Repair Enzyme, Polynucleotide Kinase." *Molecular Cell* 17 (5): 657-670.
- Bieging, Kathryn T. and Laura D. Attardi. 2012. "Deconstructing p53 Transcriptional Networks in Tumor Suppression." *Trends in Cell Biology* 22 (2): 97-106.
- Bissantz, Caterina, Bernd Kuhn, and Martin Stahl. 2010. "A Medicinal Chemist's Guide to Molecular Interactions." *Journal of Medicinal Chemistry* 53 (14): 5061-5084.
- Blagosklonny, Mikhail V. 2000. "P53 from Complexity to Simplicity: Mutant P53 Stabilization, Gain-of-Function, and Dominant-Negative Effect." *The FASEB Journal* 14 (13): 1901-1907.
- Blandino, Giovanni and Silvia Di Agostino. 2018. "New Therapeutic Strategies to Treat Human Cancers Expressing Mutant p53 Proteins." *Journal of Experimental & Clinical Cancer Research: CR* 37 (1): 30.
- Boeckler, Frank M., Andreas C. Joerger, Gaurav Jaggi, Trevor J. Rutherford, Dmitry B. Vepintsev, and Alan R. Fersht. 2008. "Targeted Rescue of a Destabilized Mutant of p53 by an *in Silico* Screened Drug." *Proceedings of the National Academy of Sciences of the United States of America* 105 (30): 10360-10365.

- Boehme, Karen A. and Christine Blattner. 2009. "Regulation of p53—Insights into a Complex Process." *Critical Reviews in Biochemistry and Molecular Biology* 44 (6): 367-392.
- Bouaoun, Liacine, Dmitriy Sonkin, Maude Ardin, Monica Hollstein, Graham Byrnes, Jiri Zavadil, and Magali Olivier. 2016. "TP53 Variations in Human Cancers: New Lessons from the IARC TP53 Database and Genomics Data." *Human Mutation* 37 (9): 865-876.
- Brooks, Christopher and Wei Gu. 2011. "The Impact of Acetylation and Deacetylation on the p53 Pathway." *Protein & Cell* 2 (6): 456-462.
- Brosh, Ran and Varda Rotter. 2009. "When Mutants Gain New Powers: News from the Mutant p53 Field." *Nature Reviews.Cancer* 9 (10): 701-713.
- Brown, Christopher J., Sonia Lain, Chandra S. Verma, Alan R. Fersht, and David P. Lane. 2009. "Awakening Guardian Angels: Drugging the p53 Pathway." *Nature Reviews Cancer* 9 (12): 862-873.
- Bullock, Alex N. and Alan R. Fersht. 2001. "Rescuing the Function of Mutant p53." *Nature Revisions Cancer* 1 (1): 68-76.
- Bullock, Alex N., Julia Henckel, Brian S. DeDecker, Christopher M. Johnson, Penka V. Nikolova, Mark R. Proctor, David P. Lane, and Alan R. Fersht. 1997. "Thermodynamic Stability of Wild-Type and Mutant p53 Core Domain." *Proceedings of the National Academy of Sciences of the United States of America* 94 (26): 14338-14342.
- Bullock, Alex N., Julia Henckel, and Alan R. Fersht. 2000. "Quantitative Analysis of Residual Folding and DNA Binding in Mutant p53 Core Domain: Definition of Mutant States for Rescue in Cancer Therapy." *Oncogene* 19 (10): 1245-1256.
- Buolamwini, John K., James Addo, Shantaram Kamath, Shivaputra Patil, Mason Mason, and Marian Ores. 2005. "Small Molecule Antagonists of the MDM2 Oncoprotein as Anticancer Agents." *Current Cancer Drug Targets* 5 (1): 57-68.
- Bykov, Vladimir J. N. and Klas G. Wiman. 2014. "Mutant p53 Reactivation by Small Molecules Makes its Way to the Clinic." *FEBS Letters* 588 (16): 2622-2627.
- Bykov, Vladimir J. N., Natalia Issaeva, Alexandre Shilov, Monica Hultcrantz, Elena Pugacheva, Peter Chumakov, Jan Bergman, Klas G. Wiman, and Galina Selivanova. 2002. "Restoration of the Tumor Suppressor Function to Mutant p53 by a Low-Molecular-Weight Compound." *Nature Medicine* 8 (3): 282-288.
- Bykov, Vladimir J. N., Natalia Issaeva, Nicole Zache, Alexandre Shilov, Monica Hultcrantz, Jan Bergman, Galina Selivanova, and Klas G. Wiman. 2005. "Reactivation of Mutant p53 and Induction of Apoptosis in Human Tumor Cells by Maleimide Analogs." *The Journal of Biological Chemistry* 280 (34): 30384-30391.

- Bykov, Vladimir J. N., Sofi E. Eriksson, Julie Bianchi, and Klas G. Wiman. 2018. "Targeting Mutant p53 for Efficient Cancer Therapy." *Nature Reviews Cancer* 18 (2): 89-102.
- Caldecott, Keith W. 2014. "DNA Single-Strand Break Repair." *Experimental Cell Research* 329 (1): 2-8.
- Caliński, Tadeusz and Jerzy Harabasz. 1974. "A Dendrite Method for Cluster Analysis." *Communications in Statistics* 3 (1): 1-27.
- Cañadillas, José Manuel Pérez, Henning Tidow, Stefan M. V. Freund, Trevor J. Rutherford, Hwee Ching Ang, and Alan R. Fersht. 2006. "Solution Structure of p53 Core Domain: Structural Basis for its Instability." *Proceedings of the National Academy of Sciences* 103 (7): 2109-2114.
- Cancer Statistics at a Glance - Canadian Cancer Society. [www.cancer.ca](http://www.cancer.ca/en/cancer-information/cancer-101/cancer-statistics-at-a-glance/?region=on), accessed Jul 8, 2018, <http://www.cancer.ca/en/cancer-information/cancer-101/cancer-statistics-at-a-glance/?region=on>.
- Case, D. A., T. A. Darden, III Cheatham T.E., C. L. Simmerling, J. Wang, R. E. Duke, R. Luo, R. C. Walker, W. Zhang, K. M. Merz, B. Roberts, S. Hayik, A. Roitberg, G. Seabra, J. Swails, A. W. Goetz, I. Kolossváry, K. F. Wong, F. Paesani, J. Vanicek, R. M. Wolf, J. Liu, X. Wu, S. R. Brozell, T. Steinbrecher, H. Gohlke, Q. Cai, X. Ye, J. Wang, M. -J Hsieh, G. Cui, D. R. Roe, D. H. Mathews, M. G. Seetin, R. Salomon-Ferrer, C. Sagui, V. Babin, T. Luchko, S. Gusarov, A. Kovalenko, and P. A. Kollman. 2012. Amber 12. University of California, San Francisco.
- Case, D. A., V. Babin, J. T. Berryman, R. M. Betz, Q. Cai, D. S. Cerutti, D. S. III Cheatham, T. A. Darden, R. E. Duke, H. Gohlke, A. W. Goetz, S. Gusarov, N. Homeyer, P. Janowski, J. Kaus, I. Kolossváry, A. Kovalenko, T. S. Lee, S. LeGrand, T. Luchko, R. Luo, B. Madej, K. M. Merz, F. Paesani, D. R. Roe, A. Roitberg, C. Sagui, R. Salomon-Ferrer, G. Seabra, C. L. Simmerling, W. Smith, J. Swails, R. C. Walker, J. Wang, R. M. Wolf, X. Wu, and P. A. Kollman. 2014. Amber 14. University of California, San Francisco.
- Cavalluzzi, Maria Maddalena, Giuseppe Felice Mangiatordi, Orazio Nicolotti, and Giovanni Lentini. 2017. "Ligand Efficiency Metrics in Drug Discovery: The Pros and Cons from a Practical Perspective." *Expert Opinion on Drug Discovery* 12 (11): 1087-1104.
- Ceccaldi, Raphael, Beatrice Rondinelli, and Alan D. D'Andrea. 2016. "Repair Pathway Choices and Consequences at the Double-Strand Break." *Trends in Cell Biology* 26 (1): 52-64.
- Chalasani, Sri Lakshmi, Ajinkya S. Kawale, Konstantin Akopiants, Yaping Yu, Mesfin Fanta, Michael Weinfeld, and Lawrence F. Povirk. 2018. "Persistent 3'-Phosphate Termini and Increased Cytotoxicity of Radiomimetic DNA Double-Strand Breaks in Cells Lacking

- Polynucleotide Kinase/Phosphatase Despite Presence of an Alternative 3'-Phosphatase." *Dna Repair* 68: 12-24.
- Chan, Wan Mui, Wai Yi Siu, Anita Lau, and Randy Y. C. Poon. 2004. "How Many Mutant p53 Molecules are Needed to Inactivate a Tetramer?" *Molecular and Cellular Biology* 24 (8): 3536-3551.
- Chang, Yong S., Bradford Graves, Vincent Guerlavais, Christian Tovar, Kathryn Packman, Kwong-Him To, Karen A. Olson, et al. 2013. "Stapled A-helical Peptide Drug Development: A Potent Dual Inhibitor of MDM2 and MDMX for p53-Dependent Cancer Therapy." *Proceedings of the National Academy of Sciences of the United States of America* 110 (36): E3454.
- Chen, Jiandong. 2016. "Intra Molecular Interactions in the Regulation of p53 Pathway." *Translational Cancer Research* 5 (6): 639-649.
- Chen, Yongheng, Raja Dey, and Lin Chen. 2010. "Crystal Structure of the p53 Core Domain Bound to a Full Consensus Site as a Self-Assembled Tetramer." *Structure (London, England: 1993)* 18 (2): 246-256.
- Chen, Yongheng, Xiaojun Zhang, Ana Dantas Machado Carolina, Yuan Ding, Zhuchu Chen, Peter Qin Z., Remo Rohs, and Lin Chen. 2013. "Structure of p53 Binding to the BAX Response Element Reveals DNA Unwinding and Compression to Accommodate Base-Pair Insertion." *Nucleic Acids Research* 41 (17): 8368-8376.
- Chène, Patrick. 2001. "The Role of Tetramerization in p53 Function." *Oncogene* 20: 2611.
- Chi, Seung-Wook, Si-Hyung Lee, Do-Hyoung Kim, Min-Jung Ahn, Jae-Sung Kim, Jin-Young Woo, Takuya Torizawa, Masatsune Kainosho, and Kyou-Hoon Han. 2005. "Structural Details on Mdm2-p53 Interaction." *The Journal of Biological Chemistry* 280 (46): 38795-38802.
- Cho, Yunje, Svetlana Gorina, Philip D. Jeffrey, and Nikola P. Pavletich. 1994. "Crystal Structure of a p53 Tumor Suppressor-DNA Complex: Understanding Tumorigenic Mutations." *Science* 265 (5170): 346-355.
- Comel, Anna, Giovanni Sorrentino, Valeria Capaci, and Giannino Del Sal. 2014. "The Cytoplasmic Side of p53's Oncosuppressive Activities." *FEBS Letters* 588 (16): 2600-2609.
- Connolly, I. D., J. D. Hixson, and S. Nagpal. 2016. "An Overview of DNA Topoisomerase I Inhibitors Under Development." *Drugs of the Future* 41: 731.
- Coquelle, Nicolas, Zahra Haveli-Shahriari, Nina Bernstein, Ruth Green, and J. N. Mark Glover. 2011. "Structural Basis for the Phosphatase Activity of Polynucleotide Kinase/Phosphatase on Single- and Double-Stranded DNA Substrates." *Proceedings of*

- the National Academy of Sciences of the United States of America 108 (52): 21022-21027.
- David, Charles C. and Donald J. Jacobs. 2014. "Principal Component Analysis: A Method for Determining the Essential Dynamics of Proteins." *Methods in Molecular Biology* (Clifton, N.J.) 1084: 193-226.
- Davies, David L. and Donald W. Bouldin. 1979. "Cluster Separation Measure." *IEEE Transactions on Pattern Analysis and Machine Intelligence* 1 (2): 224-227.
- Davis, Anthony J. and David J. Chen. 2013. "DNA Double Strand Break Repair Via Non-Homologous End-Joining." *Translational Cancer Research* 2 (3): 130-143.
- Demir, Özlem, Pek U. Leong, and Rommie E. Amaro. 2016. "Full-Length p53 Tetramer Bound to DNA and its Quaternary Dynamics." *Oncogene* 36: 1451
- Demir, Özlem, Roberta Baronio, Faezeh Salehi, Christopher D. Wassman, Linda Hall, G. Wesley Hatfield, Richard Chamberlin, Peter Kaiser, Richard H. Lathrop, and Rommie E. Amaro. 2011. "Ensemble-Based Computational Approach Discriminates Functional Activity of p53 Cancer and Rescue Mutants." *PLOS Computational Biology* 7 (10): e1002238.
- Demma, Mark J., Serena Wong, Eugene Maxwell, and Bimalendu Dasmahapatra. 2004. "CP-31398 Restores DNA-Binding Activity to Mutant p53 in Vitro but does Not Affect p53 Homologs p63 and p73." *The Journal of Biological Chemistry* 279 (44): 45887-45896.
- Deriu, Marco A., Gianvito Grasso, Jack A. Tuszynski, Diana Massai, Diego Gallo, Umberto Morbiducci, and Andrea Danani. 2016. "Characterization of the AXH Domain of Ataxin-1 using Enhanced Sampling and Functional Mode Analysis." *Proteins* 84 (5): 666-673.
- Deriu, Marco A., Gianvito Grasso, Jack A. Tuszynski, Diego Gallo, Umberto Morbiducci, and Andrea Danani. 2016. "Josephin Domain Structural Conformations Explored by Metadynamics in Essential Coordinates." *PLOS Computational Biology* 12 (1): e1004699.
- Dobson, Caroline J. and Sarah L. Allinson. 2006. "The Phosphatase Activity of Mammalian Polynucleotide Kinase Takes Precedence Over its Kinase Activity in Repair of Single Strand Breaks." *Nucleic Acids Research* 34 (8): 2230-2237.
- Dolinsky, Todd J., Paul Czodrowski, Hui Li, Jens E. Nielsen, Jan H. Jensen, Gerhard Klebe, and Nathan A. Baker. 2007. "PDB2PQR: Expanding and Upgrading Automated Preparation of Biomolecular Structures for Molecular Simulations." *Nucleic Acids Research* 35: 522.
- Duan, Jianxin and Lennart Nilsson. 2006. "Effect of Zn²⁺ on DNA Recognition and Stability of the p53 DNA-Binding Domain." *Biochemistry* 45 (24): 7483-7492.

- Duffy, Michael J., Naoise C. Synnott, and John Crown. 2017. "Mutant p53 as a Target for Cancer Treatment." *European Journal of Cancer* 83: 258-265.
- Dupradeau, François-Yves, Adrien Pigache, Thomas Zaffran, Corentin Savineau, Rodolphe Lelong, Nicolas Grivel, Dimitri Lelong, Wilfried Rosanski, and Piotr Cieplak. 2010. "The R.E.D. Tools: Advances in RESP and ESP Charge Derivation and Force Field Library Building." *Physical Chemistry Chemical Physics: PCCP* 12 (28): 7821-7839.
- Eldar, Amir, Haim Rozenberg, Yael Diskin-Posner, Remo Rohs, and Zippora Shakked. 2013. "Structural Studies of p53 Inactivation by DNA-Contact Mutations and its Rescue by Suppressor Mutations Via Alternative Protein-DNA Interactions." *Nucleic Acids Research* 41 (18): 8748-8759.
- Emamzadah, Soheila, Laurence Tropa, and Thanos D. Halazonetis. 2011. "Crystal Structure of a Multidomain Human p53 Tetramer Bound to the Natural CDKN1A (p21) p53-Response Element." *Molecular Cancer Research* 9 (11): 1493-1499.
- Feki, Anis and Irmgard Irminger-Finger. 2004. "Mutational Spectrum of p53 Mutations in Primary Breast and Ovarian Tumors." *Critical Reviews in Oncology/Hematology* 52 (2): 103-116.
- Follis, Arielle Viacava, Fabien Llambi, Li Ou, Katherine Baran, Douglas R. Green, and Richard W. Kriwacki. 2014. "The DNA-Binding Domain Mediates both Nuclear and Cytosolic Functions of p53." *Nature Structural & Molecular Biology* 21 (6): 535-543.
- Foster, Barbara A., Heather A. Coffey, Michael J. Morin, and Farzan Rastinejad. 1999. "Pharmacological Rescue of Mutant p53 Conformation and Function." *Science (New York, N.Y.)* 286 (5449): 2507-2510.
- Freed-Pastor, William and Carol Prives. 2012. "Mutant p53: One Name, Many Proteins." *Genes & Development* 26 (12): 1268-1286.
- Freschauf, Gary K., Feridoun Karimi-Busheri, Agnieszka Ulaczyk-Lesanko, Todd R. Mereniuk, Ashley Ahrens, Jonathan M. Koshy, Aghdass Rasouli-Nia, et al. 2009. "Identification of a Small Molecule Inhibitor of the Human DNA Repair Enzyme Polynucleotide Kinase/Phosphatase." *Cancer Research* 69 (19): 7739-7746.
- Freschauf, Gary K., Rajam S. Mani, Todd R. Mereniuk, Mesfin Fanta, Caesar A. Virgen, Grigory L. Dianov, Jean-Marie Grassot, Dennis G. Hall, and Michael Weinfeld. 2010. "Mechanism of Action of an Imidopiperidine Inhibitor of Human Polynucleotide Kinase/Phosphatase." *Journal of Biological Chemistry* 285 (4): 2351-2360.
- Friedler, Assaf, Brian S. DeDecker, Stefan M. V. Freund, Caroline Blair, Stefan Rüdiger, and Alan R. Fersht. 2004. "Structural Distortion of p53 by the Mutation R249S and its Rescue by a Designed Peptide: Implications for "Mutant Conformation"." *Journal of Molecular Biology* 336 (1): 187-196.

- Friedler, Assaf, Dmitry B. Veprintsev, Lars O. Hansson, and Alan R. Fersht. 2003. "Kinetic Instability of p53 Core Domain Mutants IMPLICATIONS FOR RESCUE BY SMALL MOLECULES." *Journal of Biological Chemistry* 278 (26): 24108-24112.
- Friedler, Assaf, Lars O. Hansson, Dmitry B. Veprintsev, Stefan M. V. Freund, Thomas M. Rippin, Penka V. Nikolova, Mark R. Proctor, Stefan Rüdiger, and Alan R. Fersht. 2002. "A Peptide that Binds and Stabilizes p53 Core Domain: Chaperone Strategy for Rescue of Oncogenic Mutants." *Proceedings of the National Academy of Sciences of the United States of America* 99 (2): 937-942.
- Frisch, M. J., G. W. Trucks, H. B. Schlegel, G. E. Scuseria, M. A. Robb, J. R. Cheeseman, G. Scalmani, V. Barone, B. Mennucci, G. A. Petersson, H. Nakatsuji, M. Caricato, X. Li, H. P. Hratchian, A. F. Izmaylov, J. Bloino, G. Zheng, J. L. Sonnenberg, M. Hada, M. Ehara, K. Toyota, R. Fukuda, J. Hasegawa, M. Ishida, T. Nakajima, Y. Honda, O. Kitao, H. Nakai, T. Vreven, J. A. Montgomery Jr., J. E. Peralta, F. Ogliaro, M. Bearpark, J. J. Heyd, E. Brothers, K. N. Kudin, V. N. Staroverov, R. Kobayashi, J. Normand, K. Raghavachari, A. Rendell, J. C. Burant, S. S. Iyengar, J. Tomasi, M. Cossi, N. Rega, J. M. Millam, M. Klene, J. E. Knox, J. B. Cross, V. Bakken, C. Adamo, J. Jaramillo, R. Gomperts, R. E. Stratmann, O. Yazyev, A. J. Austin, R. Cammi, C. Pomelli, J. W. Ochterski, R. L. Martin, K. Morokuma, V. G. Zakrzewski, G. A. Voth, P. Salvador, J. J. Dannenberg, S. Dapprich, A. D. Daniels, Ö Farkas, J. B. Foresman, J. V. Ortiz, J. Cioslowski, and D. J. Fox. 2009. Gaussian 09, Revision E.01 . Gaussian, Inc., Wallingford CT.
- Gaglia, Giorgio, Yinghua Guan, Jagesh V. Shah, and Galit Lahav. 2013. "Activation and Control of p53 Tetramerization in Individual Living Cells." *Proceedings of the National Academy of Sciences* 110 (38): 15497-15501.
- Garces, Fernando, Laurence H. Pearl, and Antony W. Oliver. 2011. "The Structural Basis for Substrate Recognition by Mammalian Polynucleotide Kinase 3 ' Phosphatase." *Molecular Cell* 44 (3): 385-396.
- Gasteiger, Johann and Mario Marsili. 1980. "Iterative Partial Equalization of Orbital Electronegativity- a Rapid Access to Atomic Charges." *Tetrahedron* 36 (22): 3219-3228.
- Gatti, Laura. and Franco. Zunino. 2005. "Overview of Tumor Cell Chemoresistance Mechanisms." *Chemosensitivity Vol 2: In Vivo Models, Imaging, and Molecular Regulators* 111: 127-148.
- Gavande, Navnath S., Pamela S. VanderVere-Carozza, Hilary D. Hinshaw, Shadia I. Jalal, Catherine R. Sears, Katherine S. Pawelczak, and John J. Turchi. 2016. "DNA Repair Targeted Therapy: The Past Or Future of Cancer Treatment?" *Pharmacology & Therapeutics* 160: 65-83.

- Goldstein, I., V. Marcel, M. Olivier, M. Oren, V. Rotter, and P. Hainaut. 2011. "Understanding Wild-Type and Mutant p53 Activities in Human Cancer: New Landmarks on the Way to Targeted Therapies." *Cancer Gene Therapy* 18 (1): 2-11.
- Gorina, Svetlana and Nikola P. Pavletich. 1996. "Structure of the p53 Tumor Suppressor Bound to the Ankyrin and SH3 Domains of 53BP2." *Science (New York, N.Y.)* 274 (5289): 1001-1005.
- Grasso, Gianvito, Jack A. Tuszynski, Umberto Morbiducci, Ginevra Licandro, Andrea Danani, and Marco A. Deriu. 2017. "Thermodynamic and Kinetic Stability of the Josephin Domain Closed Arrangement: Evidences from Replica Exchange Molecular Dynamics." *Biology Direct* 12 (1): 2.
- Grasso, Gianvito, Marco A. Deriu, Jack A. Tuszynski, Diego Gallo, Umberto Morbiducci, and Andrea Danani. 2016. "Conformational Fluctuations of the AXH Monomer of Ataxin-1." *Proteins* 84 (1): 52-59.
- Grasso, Gianvito, Marco A. Deriu, Maria Prat, Lia Rimondini, Enrica Vernè, Antonia Follenzi, and Andrea Danani. 2015. "Cell Penetrating Peptide Adsorption on Magnetite and Silica Surfaces: A Computational Investigation." *The Journal of Physical Chemistry B* 119 (26): 8239-8246.
- Green, Douglas R. and Guido Kroemer. 2009. "Cytoplasmic Functions of the Tumour Suppressor p53." *Nature* 458 (7242): 1127-1130.
- Gu, Bo and Wei-Guo Zhu. 2012. "Surf the Post-Translational Modification Network of p53 Regulation." *International Journal of Biological Sciences* 8 (5): 672.
- Guex, Nicolas and Manuel C. Peitsch. 1997. "SWISS-MODEL and the Swiss-PdbViewer: An Environment for Comparative Protein Modeling." *Electrophoresis* 18 (15): 2714-2723.
- Hainaut, P., T. Hernandez, A. Robinson, P. Rodriguez-Tome, T. Flores, M. Hollstein, C. C. Harris, and R. Montesano. 1998. "IARC Database of p53 Gene Mutations in Human Tumors and Cell Lines: Updated Compilation, Revised Formats and New Visualisation Tools." *Nucleic Acids Research* 26 (1): 205-213.
- Hanahan, Douglas and Robert A. Weinberg. 2011. "Hallmarks of Cancer: The Next Generation." *Cell* 144 (5): 646-674.
- Hanel, W., N. Marchenko, S. Xu, S. Xiaofeng Yu, W. Weng, and U. Moll. 2013. "Two Hot Spot Mutant p53 Mouse Models Display Differential Gain of Function in Tumorigenesis." *Cell Death and Differentiation* 20 (7): 898-909.
- Havali-Shahriari, Zahra, Michael Weinfeld, and J. N. Mark Glover. 2017. "Characterization of DNA Substrate Binding to the Phosphatase Domain of the DNA Repair Enzyme Polynucleotide Kinase/Phosphatase." *Biochemistry* 56 (12): 1737-1745.

- Henner, W. D., S. M. Grunberg, and W. A. Haseltine. 1983. "Enzyme Action at 3'-Termini of Ionizing Radiation-Induced Dna Strand Breaks." *Journal of Biological Chemistry* 258 (24): 5198-5205.
- Ho, William C., Mary X. Fitzgerald, and Ronen Marmorstein. 2006. "Structure of the p53 Core Domain Dimer Bound to DNA." *The Journal of Biological Chemistry* 281 (29): 20494-20502.
- Hoops, Stephen C., Kenneth W. Anderson, and Kenneth M. Merz. 1991. "Force Field Design for Metalloproteins." *Journal of the American Chemical Society* 113 (22): 8262-8270.
- Hornak, Viktor, Robert Abel, Asim Okur, Bentley Strockbine, Adrian Roitberg, and Carlos Simmerling. 2006. "Comparison of Multiple Amber Force Fields and Development of Improved Protein Backbone Parameters." *Proteins* 65 (3): 712-725.
- Hosoya, Noriko and Kiyoshi Miyagawa. 2014. "Targeting DNA Damage Response in Cancer Therapy." *Cancer Science* 105 (4): 370-388.
- Hub, Jochen S. and Bert L. de Groot. 2009. "Detection of Functional Modes in Protein Dynamics." *PLOS Computational Biology* 5 (8): e1000480.
- Ishimaru, Daniella, Ano Bom, Ana Paula D., Lima, Luís Maurício T. R., Pablo A. Quesado, Marcos F. C. Oyama, de Moura Gallo, Claudia V., Yraima Cordeiro, and Jerson L. Silva. 2009. "Cognate DNA Stabilizes the Tumor Suppressor p53 and Prevents Misfolding and Aggregation." *Biochemistry* 48 (26): 6126-6135.
- Jilani, Arshad, Dindial Ramotar, Carolyn Slack, Colin Ong, Xiao Ming Yang, Stephen W. Scherer, and Dana D. Lasko. 1999. "Molecular Cloning of the Human Gene, PNKP, Encoding a Polynucleotide Kinase 3'-Phosphatase and Evidence for its Role in Repair of DNA Strand Breaks Caused by Oxidative Damage." *The Journal of Biological Chemistry* 274 (34): 24176-24186.
- Joerger, Andreas C. and Alan R. Fersht. 2007. "Structure–function–rescue: The Diverse Nature of Common p53 Cancer Mutants." *Oncogene* 26 (15): 2226-2242.
- Joerger, Andreas C. and Alan R. Fersht. 2010. "The Tumor Suppressor p53: From Structures to Drug Discovery." *Cold Spring Harbor Perspectives in Biology* 2 (6).
- Joerger, Andreas C., Hwee Ching Ang, and Alan R. Fersht. 2006. "Structural Basis for Understanding Oncogenic p53 Mutations and Designing Rescue Drugs." *Proceedings of the National Academy of Sciences of the United States of America* 103 (41): 15056-15061.
- Joerger, Andreas C., Hwee Ching Ang, Dmitry B. Veprintsev, Caroline M. Blair, and Alan R. Fersht. 2005. "Structures of p53 Cancer Mutants and Mechanism of Rescue by Second-

- Site Suppressor Mutations." *The Journal of Biological Chemistry* 280 (16): 16030-16037.
- Jordan, Jennifer J., Daniel Menendez, Alberto Inga, Maher Nourredine, Douglas Bell, and Michael A. Resnick. 2008. "Noncanonical DNA Motifs as Transactivation Targets by Wild Type and Mutant p53." *PLoS Genetics* 4 (6).
- Kachalaki, Saeed, Mina Ebrahimi, Leila Mohamed Khosroshahi, Sina Mohammadinejad, and Behzad Baradaran. 2016. "Cancer Chemoresistance; Biochemical and Molecular Aspects: A Brief Overview." *European Journal of Pharmaceutical Sciences* 89: 20-30.
- Kamada, Rui, Takao Nomura, Carl W. Anderson, and Kazuyasu Sakaguchi. 2011. "Cancer-Associated p53 Tetramerization Domain Mutants: Quantitative Analysis Reveals a Low Threshold for Tumor Suppressor Inactivation." *The Journal of Biological Chemistry* 286 (1): 252-258.
- Kamada, Rui, Yu Toguchi, Takao Nomura, Toshiaki Imagawa, and Kazuyasu Sakaguchi. 2016. "Tetramer Formation of Tumor Suppressor Protein p53: Structure, Function, and Applications." *Peptide Science* 106 (4): 598-612.
- Kastenhuber, Edward R. and Scott W. Lowe. 2017. "Putting p53 in Context." *Cell* 170 (6): 1062-1078.
- Katritch, Vsevolod, Chelsea Byrd, Vladimir Tseitin, Dongcheng Dai, Eugene Raush, Maxim Totrov, Ruben Abagyan, Robert Jordan, and Dennis Hruby. 2007. "Discovery of Small Molecule Inhibitors of Ubiquitin-Like Poxvirus Proteinase I7L using Homology Modeling and Covalent Docking Approaches." *Journal of Computer-Aided Molecular Design* 21 (10): 549-558.
- Khoo, Kian Hoe, Khoo Kian Hoe, Chandra S. Verma, and David P. Lane. 2014. "Drugging the p53 Pathway: Understanding the Route to Clinical Efficacy." *Nature Reviews. Drug Discovery* 13 (3): 217-236.
- Koblish, Holly K., Shuyuan Y. Zhao, Carol F. Franks, Robert R. Donatelli, Rose M. Tominovich, Louis V. LaFrance, Kristi A. Leonard, et al. 2006. "Benzodiazepinedione Inhibitors of the Hdm2 : p53 Complex Suppress Human Tumor Cell Proliferation in Vitro and Sensitize Tumors to Doxorubicin in Vivo." *Molecular Cancer Therapeutics* 5 (1): 160-169.
- Kogan, Samuel and Darren Carpizo. 2016. "Pharmacological Targeting of Mutant p53." *Translational Cancer Research* 5 (6): 698-706.
- Koulgi, Shruti, Archana Achalere, Neeru Sharma, Uddhavesb Sonavane, and Rajendra Joshi. 2013. "QM-MM Simulations on p53-DNA Complex: A Study of Hot Spot and Rescue Mutants." *Journal of Molecular Modeling* 19 (12): 5545-5559.

- Kroemer, G., J. M. Bravo-San Pedro, and L. Galluzzi. 2015. "Novel Function of Cytoplasmic p53 at the Interface between Mitochondria and the Endoplasmic Reticulum." *Cell Death & Disease* 6 (3): e1698.
- Krokan, Hans E. and Magnar Bjørås. 2013. "Base Excision Repair." Chap. 4, In *DNA Repair, Mutagenesis, and Other Responses to DNA Damage*. Vol. 5, 45-66. Cold Spring Harbor Perspectives in Biology: Cold Spring Harbor Lab.
- Kruiswijk, Flore, Christiaan F. Labuschagne, and Karen H. Vousden. 2015. "P53 in Survival, Death and Metabolic Health: A Lifeguard with a Licence to Kill." *Nature Reviews Molecular Cell Biology* 16 (7): 393.
- Kruse, Jan-Philipp and Wei Gu. 2008. "SnapShot: p53 Posttranslational Modifications." *Cell* 133 (5): 930.e1.
- Kruse, Jan-Philipp and Wei Gu. 2008. "Modes of p53 regulation." *Cell* 137 (4): 609-622.
- Kubbutat, Michael H. G., Stephen N. Jones, and Karen H. Vousden. 1997. "Regulation of p53 Stability by Mdm2." *Nature* 387 (6630): 299-303.
- Kumalo, Hezekiel Mathambo, Soumendranath Bhakat, and Mahmoud E. S. Soliman. 2015. "Theory and Applications of Covalent Docking in Drug Discovery: Merits and Pitfalls." *Molecules (Basel, Switzerland)* 20 (2): 1984-2000.
- Kussie, Paul H., Svetlana Gorina, Vincent Marechal, Brian Elenbaas, Jacque Moreau, Arnold J. Levine, and Nikola P. Pavletich. 1996. "Structure of the MDM2 Oncoprotein Bound to the p53 Tumor Suppressor Transactivation Domain." *Science (New York, N.Y.)* 274 (5289): 948-953.
- Labute, Paul. 2008. "The Generalized Born/Volume Integral Implicit Solvent Model: Estimation of the Free Energy of Hydration using London Dispersion Instead of Atomic Surface Area." *Journal of Computational Chemistry* 29 (10): 1693-1698.
- Lambert, Jeremy M. R., Petr Gorzov, Dimitry B. Veprintsev, Maja Soderqvist, Dan Segerback, Jan Bergman, Alan R. Fersht, Pierre Hainaut, Klas G. Wiman, and Vladimir J. N. Bykov. 2009. "PRIMA-1 Reactivates Mutant p53 by Covalent Binding to the Core Domain." *Cancer Cell* 15 (5): 376-388.
- Lambrugh, Matteo, Luca De Gioia, Francesco Luigi Gervasio, Kresten Lindorff-Larsen, Ruth Nussinov, Chiara Urani, Maurizio Bruschi, and Elena Papaleo. 2016. "DNA-Binding Protects p53 from Interactions with Cofactors Involved in Transcription-Independent Functions." *Nucleic Acids Research* 44 (19): 9096-9109.
- Laptenko, Oleg, David R. Tong, James Manfredi, and Carol Prives. 2016. "The Tail that Wags the Dog: How the Disordered C-Terminal Domain Controls the Transcriptional

- Activities of the p53 Tumor-Suppressor Protein." *Trends in Biochemical Sciences* 41 (12): 1022-1034.
- Laptenko, Oleg, Idit Shiff, Will Freed-Pastor, Andrew Zupnick, Melissa Mattia, Ella Freulich, Inbal Shamir, et al. 2015. "The p53 C Terminus Controls Site-Specific DNA Binding and Promotes Structural Changes within the Central DNA Binding Domain." *Molecular Cell* 57 (6): 1034-1046.
- Lawandi, Janice, Sylvestre Toumieux, Valentine Seyer, Philip Campbell, Sabine Thielges, Lucienne Juillerat-Jeanneret, and Nicolas Moitessier. 2009. "Constrained Peptidomimetics Reveal Detailed Geometric Requirements of Covalent Prolyl Oligopeptidase Inhibitors." *Journal of Medicinal Chemistry* 52 (21): 6672-6684.
- Lee, Chul Won, Maria A. Martinez-Yamout, H. Jane Dyson, and Peter E. Wright. 2010. "Structure of the p53 Transactivation Domain in Complex with the Nuclear Receptor Coactivator Binding Domain of CREB Binding Protein." *Biochemistry* 49 (46): 9964.
- Lee, Chul Won, Munehito Arai, Maria A. Martinez-Yamout, H. Jane Dyson, and Peter E. Wright. 2009. "Mapping the Interactions of the p53 Transactivation Domain with the KIX Domain of CBP." *Biochemistry* 48 (10): 2115-2124.
- Lehmann, Soren, Vladimir J. N. Bykov, Dina Ali, Ove Andren, Honar Cherif, Ulf Tidefelt, Bertil Uggla, et al. 2012. "Targeting p53 in Vivo: A First-in-Human Study with p53-Targeting Compound APR-246 in Refractory Hematologic Malignancies and Prostate Cancer." *Journal of Clinical Oncology* 30 (29): 3633-3639.
- Lepre, Marco Gaetano, Sara Ibrahim Omar, Gianvito Grasso, Umberto Morbiducci, Marco Agostino Deriu, and Jack A. Tuszynski. 2017. "Insights into the Effect of the G245S Single Point Mutation on the Structure of p53 and the Binding of the Protein to DNA." *Molecules (Basel, Switzerland)* 22 (8).
- Leroy, Bernard, Martha Anderson, and Thierry Soussi. 2014. "TP53 Mutations in Human Cancer: Database Reassessment and Prospects for the Next Decade." *Human Mutation* 35 (6): 672-688.
- Levine, Arnold J. and Moshe Oren. 2009. "The First 30 Years of p53: Growing Ever More Complex." *Nature Reviews Cancer* 9 (10): 749-758.
- Li, Fengzhi, Tao Jiang, Qingyong Li, and Xiang Ling. 2017. "Camptothecin (CPT) and its Derivatives are Known to Target Topoisomerase I (Top1) as their Mechanism of Action: Did we Miss Something in CPT Analogue Molecular Targets for Treating Human Disease such as Cancer?" *American Journal of Cancer Research* 7 (12): 2350-2394.
- LigandScout Manual. <http://www.inteligand.com/ligandscout/manual/>.

- Lipinski, Christopher A., Franco Lombardo, Beryl W. Dominy, and Paul J. Feeney. 1997. "Experimental and Computational Approaches to Estimate Solubility and Permeability in Drug Discovery and Development Settings." *Advanced Drug Delivery Reviews* 23 (1-3): 3-25.
- Liu, Min, Chong Li, Marzena Pazgier, Changqing Li, Yubin Mao, Yifan Lv, Bing Gu, et al. 2010. "D-Peptide Inhibitors of the p53–MDM2 Interaction for Targeted Molecular Therapy of Malignant Neoplasms." *Proceedings of the National Academy of Sciences* 107 (32): 14321-14326.
- Loncharich, Richard J., Bernard R. Brooks, and Richard W. Pastor. 1992. "Langevin Dynamics of Peptides: The Frictional Dependence of Isomerization Rates of N-Acetylalanyl-N'-Methylamide." *Biopolymers* 32 (5): 523-535.
- Lu, Meiling, Rajam S. Mani, Feridoun Karimi-Busheri, Mesfin Fanta, Hailin Wang, David W. Litchfield, and Michael Weinfeld. 2010. "Independent Mechanisms of Stimulation of Polynucleotide Kinase/Phosphatase by Phosphorylated and Non-Phosphorylated XRCC1." *Nucleic Acids Research* 38 (2): 510-521.
- Lukman, Suryani, David P. Lane, and Chandra S. Verma. 2013. "Mapping the Structural and Dynamical Features of Multiple p53 DNA Binding Domains: Insights into Loop 1 Intrinsic Dynamics." *PLoS ONE* 8 (11).
- Ma, Jianhong, John D. Martin, Hong Zhang, Kurt R. Auger, Thau F. Ho, Robert B. Kirkpatrick, Michael H. Grooms, et al. 2006. "A Second p53 Binding Site in the Central Domain of Mdm2 is Essential for p53 Ubiquitination." *Biochemistry* 45 (30): 9238-9245.
- Maddocks, Oliver D. K. and Karen H. Vousden. 2011. "Metabolic Regulation by p53." *Journal of Molecular Medicine (Berlin, Germany)* 89 (3): 237-245.
- Madhusudan, Srinivasan and Mark R. Middleton. 2005. "The Emerging Role of DNA Repair Proteins as Predictive, Prognostic and Therapeutic Targets in Cancer." *Cancer Treatment Reviews* 31 (8): 603-617.
- Maier, James A., Carmenza Martinez, Koushik Kasavajhala, Lauren Wickstrom, Kevin E. Hauser, and Carlos Simmerling. 2015. "ff14SB: Improving the Accuracy of Protein Side Chain and Backbone Parameters from ff99SB." *Journal of Chemical Theory and Computation* 11 (8): 3696-3713.
- Malkin, David. 2011. "Li-Fraumeni Syndrome." *Genes & Cancer* 2 (4): 475-484.
- Mandinova, Anna and Sam W. Lee. 2011. "The p53 Pathway as a Target in Cancer Therapeutics: Obstacles and Promise." *Science Translational Medicine* 3 (64).
- Mani, Rajam S., Feridoun Karimi-Busheri, Mesfin Fanta, Carol E. Cass, and Michael Weinfeld. 2003. "Spectroscopic Studies of DNA and ATP Binding to Human

- Polynucleotide Kinase: Evidence for a Ternary Complex." *Biochemistry* 42 (41): 12077-12084.
- Mantovani, Fiamma, Dawid Walerych, and Giannino Del Sal. 2017. "Targeting Mutant p53 in Cancer: A Long Road to Precision Therapy." *The FEBS Journal* 284 (6): 837-850.
- Marcel, Virginie, Flora Nguyen Van Long, and Jean-Jacques Diaz. 2018. "40 Years of Research Put p53 in Translation." *Cancers* 10 (5): 152.
- Marcus Wieder, Arthur Garon, Ugo Perricone, Stefan Boresch, Thomas Seidel, Anna Maria Almerico, and Thierry Langer. 2017. "Common Hits Approach: Combining Pharmacophore Modeling and Molecular Dynamics Simulations." *Journal of Chemical Information and Modeling* 57 (2): 365-385.
- Marine, Jean-Christophe and Aart G. Jochemsen. 2004. "Mdmx and Mdm2: Brothers in Arms?" *Cell Cycle (Georgetown, Tex.)* 3 (7): 900-904.
- Martins, Carla P., Lamorna Brown-Swigart, and Gerard I. Evan. 2006. "Modeling the Therapeutic Efficacy of p53 Restoration in Tumors." *Cell* 127 (7): 1323-1334.
- McKinney, Kristine, Melissa Mattia, Vanesa Gottifredi, and Carol Prives. 2004. "p53 Linear Diffusion Along DNA Requires its C Terminus." *Molecular Cell* 16 (3): 413-424.
- McLure, Kevin G. and Patrick W. Lee. 1998. "How p53 Binds DNA as a Tetramer." *The EMBO Journal* 17 (12): 3342-3350.
- Meek, David W. 2015. "Regulation of the p53 Response and its Relationship to Cancer." *The Biochemical Journal* 469 (3): 325-346.
- Meek, David W. and Carl W. Anderson. 2009. "Posttranslational Modification of p53: Cooperative Integrators of Function." *Cold Spring Harbor Perspectives in Biology* 1 (6): a000950.
- Menendez, Daniel, Alberto Inga, and Michael A. Resnick. 2006. "The Biological Impact of the Human Master Regulator p53 can be Altered by Mutations that Change the Spectrum and Expression of its Target Genes." *Molecular and Cellular Biology* 26 (6): 2297-2308.
- Menendez, Daniel, Alberto Inga, and Michael A. Resnick. 2009. "The Expanding Universe of p53 Targets." *Nature Reviews.Cancer* 9 (10): 724-737.
- Mereniuk, Todd R., Mohamed A. El Gendy, Ana M. Mendes-Pereira, Christopher J. Lord, Sunita Ghosh, Edan Foley, Alan Ashworth, and Michael Weinfield. 2013. "Synthetic Lethal Targeting of PTEN-Deficient Cancer Cells using Selective Disruption of Polynucleotide Kinase/Phosphatase." *Molecular Cancer Therapeutics* 12 (10): 2135-2144.

- Mereniuk, Todd R., Robert A. Maranchuk, Anja Schindler, Jonathan Penner-Chea, Gary K. Freschauf, Samar Hegazy, Raymond Lai, Edan Foley, and Michael Weinfeld. 2012. "Genetic Screening for Synthetic Lethal Partners of Polynucleotide Kinase/Phosphatase: Potential for Targeting SHP-1-Depleted Cancers." *Cancer Research* 72 (22): 5934-5944.
- Merkel, Olaf, Ninon Taylor, Nicole Prutsch, Philipp B. Staber, Richard Moriggl, Suzanne D. Turner, and Lukas Kenner. 2017. "When the Guardian Sleeps: Reactivation of the p53 Pathway in Cancer." *Mutation Research/Reviews in Mutation Research* 773: 1-13.
- Miller, Bill R., T. Dwight McGee, Jason M. Swails, Nadine Homeyer, Holger Gohlke, and Adrian E. Roitberg. 2012. "MMPBSA.Py: An Efficient Program for End-State Free Energy Calculations." *Journal of Chemical Theory and Computation* 8 (9): 3314-3321.
- Miller, Madison, Nitin Shirole, Ruxiao Tian, Debjani Pal, and Raffaella Sordella. 2016. "The Evolution of TP53 Mutations: From Loss-of-Function to Separation-of-Function Mutants." *Journal of Cancer Biology & Research* 4 (4).
- Molecular Operating Environment (MOE), 2012.10; Chemical Computing Group Inc., 1010 Sherbrooke St. West, Suite #910, Montreal, QC, Canada, H3A 2R7, 2016. d.
- Molecular Operating Environment (MOE), 2014.09; Chemical Computing Group Inc., 1010 Sherbooke St. West, Suite #910, Montreal, QC, Canada, H3A 2R7, 2014. b.
- Moll, Ute M. and Oleksi Petrenko. 2003. "The MDM2-p53 Interaction." *Molecular Cancer Research* 1 (14): 1001-1008.
- Momand, Jamil, David Jung, Sharon Wilczynski, and Joyce Niland. 1998. "The MDM2 Gene Amplification Database." *Nucleic Acids Research* 26 (15): 3453-3459.
- Monti, Paola, Chiara Perfumo, Alessandra Bisio, Yari Ciribilli, Paola Menichini, Debora Russo, David M. Umbach, Michael A. Resnick, Alberto Inga, and Gilberto Fronza. 2011. "Dominant-Negative Features of Mutant p53 in Germline Carriers have Limited Impact on Cancer Outcomes." *Molecular Cancer Research : MCR* 9 (3): 271-279.
- Moor, N. A. and O. I. Lavrik. 2018. "Protein-Protein Interactions in DNA Base Excision Repair." *Biochemistry (Moscow)* 83 (4): 411-422.
- Morris, Garrett M., David S. Goodsell, M. E. Pique, William Lindstrom, Ruth Huey, S. Forli, W. E. Hart, Scott Halliday, Richard Belew, and Arthur J. Olson. 2010. "AutoDock Version 4.2: Automated Docking of Flexible Ligands to Flexible Receptors." The Scripps Research Institute: California.
- Morris, Garrett M., David S. Goodsell, R. Scott Halliday, Ruth Huey, W. E. Hart, Richard K. Belew, and Arthur J. Olson. 1998. "Automated Docking using a Lamarckian Genetic Algorithm and an Empirical Binding Free Energy Function." *Journal of Computational Chemistry* 19 (14).

- Morris, Garrett M., Ruth Huey, William Lindstrom, Michel F. Sanner, Richard K. Belew, David S. Goodsell, and Arthur J. Olson. 2009. "AutoDock4 and AutoDockTools4: Automated Docking with Selective Receptor Flexibility." *Journal of Computational Chemistry* 30 (16).
- Moschos, Stergios J., Shahneen Kaur Sandhu, Karl D. Lewis, Ryan J. Sullivan, Douglas Buckner Johnson, Yilong Zhang, Erik Rasmussen, Haby A. Henary, and Georgina V. Long. 2017. "Phase 1 Study of the p53-MDM2 Inhibitor AMG 232 Combined with Trametinib Plus Dabrafenib Or Trametinib in Patients (Pts) with TP53 Wild Type (TP53WT) Metastatic Cutaneous Melanoma (MCM)." *Journal of Clinical Oncology* 35 (15_suppl): 2575-2575.
- Muller, Patricia A J. and Karen H Vousden. 2014. "Mutant p53 in Cancer: New Functions and Therapeutic Opportunities." *Cancer Cell* 25 (3): 304-317.
- Muller, Patricia A. J. and Karen H. Vousden. 2013. "P53 Mutations in Cancer." *Nature Cell Biology* 15 (1): 2-8.
- Nag, S., X. Zhang, K. S. Srivenugopal, M. -H Wang, W. Wang, and R. Zhang. 2014. "Targeting MDM2-p53 Interaction for Cancer Therapy: Are we there Yet?" *Current Medicinal Chemistry* 21 (5): 553-574.
- Neudert, Gerd and Gerhard Klebe. 2011. "DSX: A Knowledge-Based Scoring Function for the Assessment of Protein-Ligand Complexes." *Journal of Chemical Information and Modeling* 51 (10): 2731-2745.
- Nguyen, Daniel, Wenjuan Liao, Shelya X. Zeng, and Hua Lu. 2017. "Reviving the Guardian of the Genome: Small Molecule Activators of p53." *Pharmacology & Therapeutics* 178: 92-108.
- Nijman, Sebastian M. B. 2011. "Synthetic Lethality: General Principles, Utility and Detection using Genetic Screens in Human Cells." *Febs Letters* 585 (1): 1-6.
- North, S., F. El-Ghissassi, O. Pluquet, G. Verhaegh, and P. Hainaut. 2000. "The Cytoprotective Aminothiol WR1065 Activates p21(Waf-1) and Down Regulates Cell Cycle Progression through a p53-Dependent Pathway." *Oncogene* 19 (9): 1206-1214.
- North, Sophie, Olivier Pluquet, Daniela Maurici, Fatiha El-Ghissassi, and Pierre Hainaut. 2002. "Restoration of Wild-Type Conformation and Activity of a Temperature-Sensitive Mutant of p53 (p53(V272M)) by the Cytoprotective Aminothiol WR1065 in the Esophageal Cancer Cell Line TE-1." *Molecular Carcinogenesis* 33 (3): 181-188.
- Ohashi, Motoaki and Toshikazu Oki. 1996. "Ellipticine and Related Anticancer Agents." *Expert Opinion on Therapeutic Patents* 6 (12): 1285-1294.

- Ohashi, Motoaki, Emiko Sugikawa, and Noriyuki Nakanishi. 1995. "Inhibition of P53 Protein-Phosphorylation by 9-Hydroxyellipticine - a Possible Anticancer Mechanism." *Japanese Journal of Cancer Research* 86 (9): 819-827.
- Olivier, Magali, Monica Hollstein, and Pierre Hainaut. 2010. "TP53 Mutations in Human Cancers: Origins, Consequences, and Clinical Use." Chap. 1, In *Cold Spring Harbor Perspectives in Biology Collection*. Vol. 2, 123-139. United States.
- Olivier, Magali, Ros Eeles, Monica Hollstein, Mohammed A. Khan, Curtis C. Harris, and Pierre Hainaut. 2002. "The IARC TP53 Database: New Online Mutation Analysis and Recommendations to Users." *Human Mutation* 19 (6): 607-614.
- Olotu, Fisayo A. and Mahmoud E. S. Soliman. "From Mutational Inactivation to Aberrant Gain-of-Function: Unraveling the Structural Basis of Mutant p53 Oncogenic Transition." *Journal of Cellular Biochemistry* 119 (3): 2646-2652.
- Omar, Sara Ibrahim and Jack Tuszynski. 2014. "Ranking the Binding Energies of p53 Mutant Activators and their ADMET Properties." *Chemical Biology & Drug Design*.
- Onufriev, Alexey, Donald Bashford, and David A. Case. 2000. "Modification of the Generalized Born Model Suitable for Macromolecules." *The Journal of Physical Chemistry B* 104 (15): 3712-3720.
- Oren, Moshe 1999. "Regulation of the p53 Tumor Suppressor Protein." *The Journal of Biological Chemistry* 274 (51): 36031-36034.
- Ouyang, Xuchang, Shuo Zhou, Chinh Tran To Su, Zemei Ge, Runtao Li, and Chee Keong Kwok. 2013. "CovalentDock: Automated Covalent Docking with Parameterized Covalent Linkage Energy Estimation and Molecular Geometry Constraints." *Journal of Computational Chemistry* 34 (4): 326-336.
- Ozaki, Toshinori and Akira Nakagawara. 2011. "Role of p53 in Cell Death and Human Cancers." *Cancers* 3 (1): 994-1013.
- Paciello, Giulia, Andrea Acquaviva, Elisa Ficarra, Marco Agostino Deriu, and Enrico Macii. 2011. "A Molecular Dynamics Study of a miRNA:mRNA Interaction." *Journal of Molecular Modeling* 17 (11): 2895-2906.
- Panganiban, Ronald-Allan M., Andrew L. Snow, and Regina M. Day. 2013. "Mechanisms of Radiation Toxicity in Transformed and Non-Transformed Cells." *International Journal of Molecular Sciences* 14 (8): 15931-15958.
- Patel, Sharmila and Mark R. Player. 2008. "Small-Molecule Inhibitors of the p53-HDM2 Interaction for the Treatment of Cancer." *Expert Opinion on Investigational Drugs* 17 (12): 1865-1882.

- Pearl, Laurence H., Amanda C. Schierz, Simon E. Ward, Bissan Al-Lazikani, and Frances M. G. Pearl. 2015. "Therapeutic Opportunities within the DNA Damage Response." *Nature Reviews. Cancer* 15 (3): 166-180.
- Peng, Yanhua H., Changgong G. Li, Lihong H. Chen, Said Sebti, and Jiandong D. Chen. 2003. "Rescue of Mutant p53 Transcription Function by Ellipticine." *Oncogene* 22 (29): 4478-4487.
- Petitjean, Audrey, Maria I.W. Achatz, Anne-Lise Borresen-Dale, Pierre Hainaut, and Magali Olivier. 2007. "TP53 Mutations in Human Cancers: Functional Selection and Impact on Cancer Prognosis and Outcomes." *Oncogene* 26 (15): 2157-2165.
- Petitjean, Audrey, Ewy Mathe, Shunsuke Kato, Chikashi Ishioka, Sean V. Tavtigian, Pierre Hainaut, and Magali Olivier. 2007. "Impact of Mutant p53 Functional Properties on TP53 Mutation Patterns and Tumor Phenotype: Lessons from Recent Developments in the IARC TP53 Database." *Human Mutation* 28 (6): 622-629.
- Petty, Tom J., Soheila Emamzadah, Lorenzo Costantino, Irina Petkova, Elena S. Stavridi, Jeffery G. Saven, Eric Vauthey, and Thanos D. Halazonetis. 2011. "An Induced Fit Mechanism Regulates p53 DNA Binding Kinetics to Confer Sequence Specificity." *The EMBO Journal* 30 (11): 2167-2176.
- Pham, Nam, Armando Lucumi, Nikki Cheung, and Hector Viadiu. 2012. "The Tetramer of p53 in the Absence of DNA Forms a Relaxed Quaternary State." *Biochemistry (Washington)* 51 (41): 8055.
- Phan, Jason, Zhenyu Li, Agnieszka Kasprzak, Baozong Li, Said Sebti, Wayne Guida, Ernst Schönbrunn, and Jiandong Chen. 2010. "Structure-Based Design of High Affinity Peptides Inhibiting the Interaction of p53 with MDM2 and MDMX." *Journal of Biological Chemistry* 285 (3): 2174-2183.
- Phillips, James C., Rosemary Braun, Wei Wang, James Gumbart, Emad Tajkhorshid, Elizabeth Villa, Christophe Chipot, Robert D. Skeel, Laxmikant Kale, and Klaus Schulten. 2005. "Scalable Molecular Dynamics with NAMD." *Journal of Computational Chemistry* 26: 1781-1802.
- Pommier, Yves, Elisabetta Leo, HongLiang Zhang, and Christophe Marchand. 2010. "DNA Topoisomerases and their Poisoning by Anticancer and Antibacterial Drugs." *Chemistry & Biology* 17 (5): 421-433.
- Povirk, Lawrence F. 2012. "Processing of Damaged DNA Ends for Double-Strand Break Repair in Mammalian Cells." *ISRN Molecular Biology* 2012.
- Raj, Nitin and Laura D. Attardi. 2017. "The Transactivation Domains of the p53 Protein." *Cold Spring Harbor Perspectives in Medicine* 7 (1).

- Ranjha, Lepakshi, Sean M. Howard, and Petr Cejka. 2018. "Main Steps in DNA Double-Strand Break Repair: An Introduction to Homologous Recombination and Related Processes." *Chromosoma* 127 (2): 187-214.
- Rasouli-Nia, Aghdass, Feridoun Karimi-Busheri, and Michael Weinfeld. 2004. "Stable Down-Regulation of Human Polynucleotide Kinase Enhances Spontaneous Mutation Frequency and Sensitizes Cells to Genotoxic Agents." *Proceedings of the National Academy of Sciences of the United States of America* 101 (18): 6905-6910.
- Reddy, N. Laxma, Jeanette Hill, Long Ye, Prabhavathi B. Fernandes, and David M. Stout. 2004. "Identification and Structure-Activity Relationship Studies of 3-Methylene-2-Norbornanone as Potent Anti-Proliferative Agents Presumably Working through p53 Mediated Apoptosis." *Bioorganic & Medicinal Chemistry Letters* 14 (22): 5645-5649.
- Retzlaff, Marco, Julia Rohrberg, Natascha Jennifer Küpper, Stephan Lagleder, Alexander Bepperling, Florian Manzenrieder, Jirka Peschek, Horst Kessler, and Johannes Buchner. 2013. "The Regulatory Domain Stabilizes the p53 Tetramer by Intersubunit Contacts with the DNA Binding Domain." *Journal of Molecular Biology* 425 (1): 144-155.
- Riedinger, Christiane and James M. McDonnell. 2009. "Inhibitors of MDM2 and MDMX: A Structural Perspective." *Future Medicinal Chemistry* 1 (6): 1075-1094.
- Rio, Alberto Del, Arménio Jorge Moura Barbosa, Fabiana Caporuscio, and Giuseppe Felice Mangiatordi. 2010. "CoCoCo: A Free Suite of Multiconformational Chemical Databases for High-Throughput Virtual Screening Purposes." *Molecular BioSystems* 6 (11): 2122-2128.
- Rippin, Thomas M., Vladimir J. N. Bykov, Stefan M. V. Freund, Galina Selivanova, Klas G. Wiman, and Alan R. Fersht. 2002. "Characterization of the p53-Rescue Drug CP-31398 in Vitro and in Living Cells." *Oncogene* 21 (14): 2119-2129.
- Roh, Jong-Lyel, Sung Koo Kang, Il Minn, Joseph A. Califano, David Sidransky, and Wayne M. Koch. 2011. "p53-Reactivating Small Molecules Induce Apoptosis and Enhance Chemotherapeutic Cytotoxicity in Head and Neck Squamous Cell Carcinoma." *Oral Oncology* 47 (1): 8-15.
- Ryckaert, Jean-Paul, Giovanni Ciccotti, and Herman J. C. Berendsen. 1977. "Numerical Integration of the Cartesian Equations of Motion of a System with Constraints: Molecular Dynamics of N-Alkanes." *Journal of Computational Physics* 23 (3): 327-341.
- Sabapathy, Kanaga and David P. Lane. 2018. "Therapeutic Targeting of p53: All Mutants are Equal, but some Mutants are More Equal than Others." *Nature Reviews Clinical Oncology* 15 (1): 13.

- Samowitz, Wade S., Karen Curtin, Khe-ni Ma, Sandra Edwards, Donna Schaffer, Mark F. Leppert, and Martha L. Slattery. 2002. "Prognostic Significance of p53 Mutations in Colon Cancer at the Population Level." *International Journal of Cancer* 99 (4): 597-602.
- Schneider, Katherine, Kristin Zelle, Kim E. Nichols, and Judy Garber. 1993. "Li-Fraumeni Syndrome." In *GeneReviews®*, edited by Margaret P. Adam, Holly H. Ardinger, Roberta A. Pagon, Stephanie E. Wallace, Lora JH Bean, Karen Stephens and Anne Amemiya. Seattle (WA): University of Washington, Seattle.
- Scholz, Christoph, Sabine Knorr, Kay Hamacher, and Boris Schmidt. 2015. "DOCKTITE-a Highly Versatile Step-by-Step Workflow for Covalent Docking and Virtual Screening in the Molecular Operating Environment." *Journal of Chemical Information and Modeling* 55 (2): 398-406.
- Seemann, Séverine, Daniela Maurici, Magali Olivier, de Claude Caron Fromentel, and Pierre Hainaut. 2004. "The Tumor Suppressor Gene TP53: Implications for Cancer Management and Therapy." *Critical Reviews in Clinical Laboratory Sciences* 41 (5-6): 551-583.
- Selivanova, Galina and Klas G. Wiman. 2007. "Reactivation of Mutant p53: Molecular Mechanisms and Therapeutic Potential." *Oncogene* 26 (15): 2243-2254.
- Shadfan, Miriam, Vanessa Lopez-Pajares, and Zhi-Min Yuan. 2012. "MDM2 and MDMX: Alone and Together in Regulation of p53." *Translational Cancer Research* 1 (2): 88-89.
- Shan, Bing, Da-Wei Li, Lei Brüscheiler-Li, and Rafael Brüscheiler. 2012. "Competitive Binding between Dynamic p53 Transactivation Subdomains to Human MDM2 Protein IMPLICATIONS FOR REGULATING THE p53-MDM2/MDMX INTERACTION." *Journal of Biological Chemistry* 287 (36): 30376-30384.
- Shangary, Sanjeev and Shaomeng Wang. 2009. "Small-Molecule Inhibitors of the MDM2-p53 Protein-Protein Interaction to Reactivate p53 Function: A Novel Approach for Cancer Therapy." *Annual Review of Pharmacology and Toxicology* 49: 223-241.
- Shao, Jianyin, Stephen W. Tanner, Nephi Thompson, and Thomas E. Cheatham III. 2007. "Clustering Molecular Dynamics Trajectories: 1. Characterizing the Performance of Different Clustering Algorithms." *Journal of Chemical Theory and Computation* 3 (6).
- Shaulian, Eitan, Arie Zauberman, Jo Milner, E. A. Davies, and M. Oren. 1993. "Tight DNA Binding and Oligomerization are Dispensable for the Ability of p53 to Transactivate Target Genes and Suppress Transformation." *The EMBO Journal* 12 (7): 2789-2797.
- Shvarts, Avi, Wilma T. Steegenga, Nicole Riteco, Theo van Laar, Patrick Dekker, Merlijn Bazuine, Reinier C. van Ham, et al. 1996. "MDMX: A Novel p53-Binding Protein with some Functional Properties of MDM2." *The EMBO Journal* 15 (19): 5349-5357.

- Sigal, Alex and Varda Rotter. 2000. "Oncogenic Mutations of the p53 Tumor Suppressor: The Demons of the Guardian of the Genome." *Cancer Research* 60 (24): 6788-6793.
- Sionov, Ronit Vogt, Igal Louria Hayon, and Ygal Haupt. 2013. *The Regulation of p53 Growth Suppression* Landes Bioscience.
- Sjöblom, Tobias, Siân Jones, Laura D. Wood, D. W. Parsons, Jimmy Lin, Thomas D. Barber, Diana Mandelker, et al. 2006. "The Consensus Coding Sequences of Human Breast and Colorectal Cancers." *Science (New York, N.Y.)* 314 (5797): 268-274.
- Soussi, Thierry 2007. "P53 Alterations in Human Cancer: More Questions than Answers." *Oncogene* 26 (15): 2145-2156.
- Soussi, Thierry and Guillermina Lozano. 2005. "P53 Mutation Heterogeneity in Cancer." *Biochemical and Biophysical Research Communications* 331 (3): 834-842.
- Soussi, Thierry and Klas G. Wiman. 2015. "TP53: An Oncogene in Disguise." *Cell Death and Differentiation* 22 (8): 1239-1249.
- Srinivasan, Jayashree, Thomas E. Cheatham, Piotr Cieplak, Peter A. Kollman, and David A. Case. 1998. "Continuum Solvent Studies of the Stability of DNA, RNA, and Phosphoramidate–DNA Helices." *Journal of the American Chemical Society* 120 (37): 9401-9409.
- Srivastava, Pallavi, Asitikantha Sarma, and Chandra Mohini Chaturvedi. 2018. "Targeting DNA Repair with PNKP Inhibition Sensitizes Radioresistant Prostate Cancer Cells to High LET Radiation." *Plos One* 13 (1): e0190516.
- Stefan Tanner and Alcide Barberis. 2004. "CP-31398, a Putative p53-Stabilizing Molecule Tested in Mammalian Cells and in Yeast for its Effects on p53 Transcriptional Activity." *Journal of Negative Results in Biomedicine* 3 (1): 5.
- Sugikawa, E., T. Hosoi, N. Yazaki, M. Gamanuma, N. Nakanishi, and M. Ohashi. 1999. "Mutant p53 Mediated Induction of Cell Cycle Arrest and Apoptosis at G1 Phase by 9-Hydroxyellipticine." *Anticancer Research* 19 (4): 3099-3108.
- Sun, Daqing, Zhihong Li, Yosup Rew, Michael Gribble, Michael D. Bartberger, Hilary P. Beck, Jude Canon, et al. 2014. "Discovery of AMG 232, a Potent, Selective, and Orally Bioavailable MDM2–p53 Inhibitor in Clinical Development." *Journal of Medicinal Chemistry* 57 (4): 1454-1472.
- Sutton, Leslie E., ed. 1965. *Tables of Interatomic Distances and Configuration in Molecules & Ions*. Special Publication No. 18 ed. Burlington House, London: The Chemical Society.

- Tahbaz, Nasser, Sudip Subedi, and Michael Weinfeld. 2012. "Role of Polynucleotide Kinase/Phosphatase in Mitochondrial DNA Repair." *Nucleic Acids Research* 40 (8): 3484-3495.
- Teague Sterling and John J Irwin. 2015. "ZINC 15 - Ligand Discovery for Everyone." *Journal of Chemical Information and Modeling* 55 (11): 2324.
- Teodoro, Jose G., Sara K. Evans, and Michael R. Green. 2007. "Inhibition of Tumor Angiogenesis by p53: A New Role for the Guardian of the Genome." *Journal of Molecular Medicine* 85 (11): 1175-1186.
- The PyMOL Molecular Graphics System, Version 1.8 Schrödinger, LLC. c.
- The PyMOL Molecular Graphics System, Version 1.8 Schrödinger, LLC. e.
- The PyMOL Molecular Graphics System, Version 1.8 Schrödinger, LLC. f.
- Tidow, Henning, Roberto Melero, Efstratios Mylonas, Stefan M. V. Freund, J. Guenter Grossmann, José María Carazo, Dmitri I. Svergun, Mikel Valle, and Alan R. Fersht. 2007. "Quaternary Structures of Tumor Suppressor p53 and a Specific p53–DNA Complex." *Proceedings of the National Academy of Sciences* 104 (30): 12324-12329.
- Tollis, Marc, Amy M. Boddy, and Carlo C. Maley. 2017. "Peto's Paradox: How has Evolution Solved the Problem of Cancer Prevention?" *BMC Biology* 15 (1): 60.
- Vanquelef, Enguerran, Sabrina Simon, Gaele Marquant, Elodie Garcia, Geoffroy Klimerak, Jean Charles Delepine, Piotr Cieplak, and François-Yves Dupradeau. 2011. "R.E.D. Server: A Web Service for Deriving RESP and ESP Charges and Building Force Field Libraries for New Molecules and Molecular Fragments." *Nucleic Acids Research* 39 (Web Server issue): 511.
- Vens, Conchita and Adrian C. Begg. 2010. "Targeting Base Excision Repair as a Sensitization Strategy in Radiotherapy." *Seminars in Radiation Oncology* 20 (4): 241-249.
- Ventura, Andrea, David G. Kirsch, Margaret E. McLaughlin, David A. Tuveson, Jan Grimm, Laura Lintault, Jamie Newman, Elizabeth E. Reczek, Ralph Weissleder, and Tyler Jacks. 2007. "Restoration of p53 Function Leads to Tumour Regression in Vivo." *Nature* 445 (7128): 661-665.
- Vogelstein, Bert, David Lane, and Arnold J. Levine. 2000. "Surfing the p53 Network." *Nature* 408 (6810): 307-310.
- Vousden, Karen H. and Xin Lu. 2002. "Live Or Let Die: The Cell's Response to p53." *Nature Reviews.Cancer* 2 (8): 594-604.

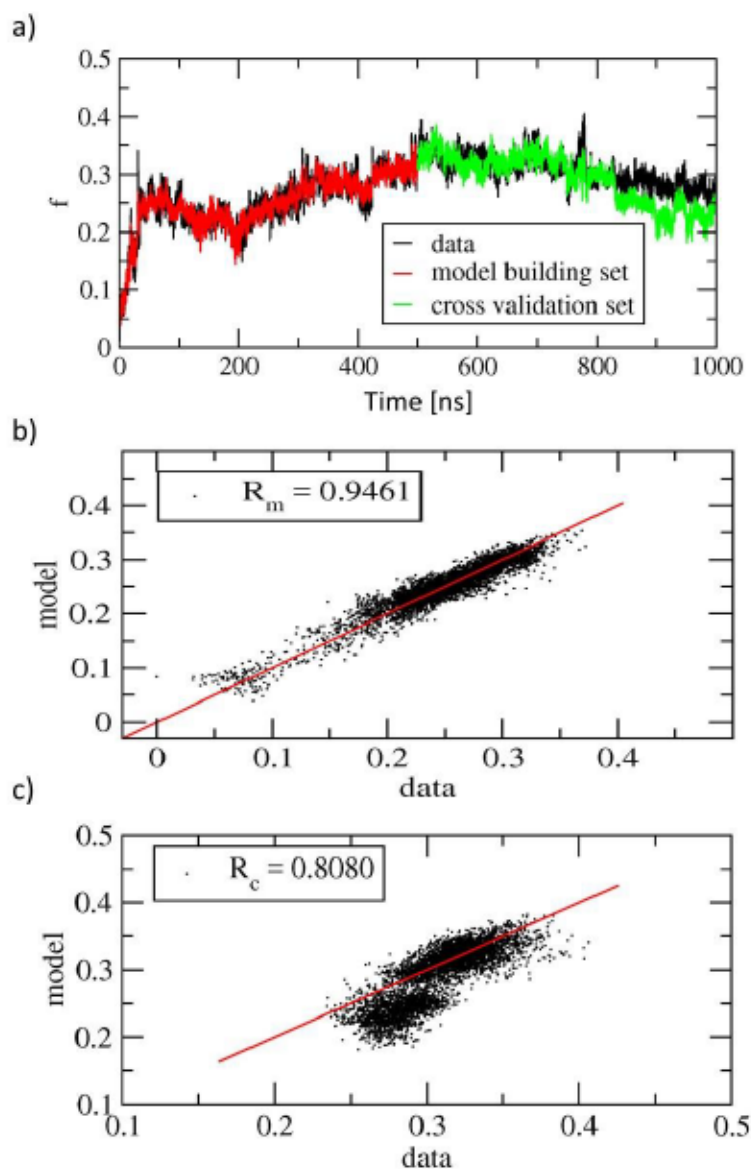
- Vyas, Pratik, Itai Benoit, Zhiqun Xi, Yan Stein, Dmitriy Golovenko, Naama Kessler, Varda Rotter, Zippora Shakked, and Tali E. Haran. 2017. "Diverse p53/DNA Binding Modes Expand the Repertoire of p53 Response Elements." *Proceedings of the National Academy of Sciences* 114 (40): 10624-10629.
- Wade, Mark, Yao-Cheng Li, and Geoffrey M. Wahl. 2013. "MDM2, MDMX and p53 in Oncogenesis and Cancer Therapy." *Nature Reviews Cancer* 13 (2): 83-96.
- Wade, Mark, Yunyuan V. Wang, and Geoffrey M. Wahl. 2010. "The p53 Orchestra: Mdm2 and Mdmx Set the Tone." *Trends in Cell Biology* 20 (5): 299-309.
- Walker, Kristen K. and Arnold J. Levine. 1996. "Identification of a Novel p53 Functional Domain that is Necessary for Efficient growth suppression." *Proceedings of the National Academy of Sciences* 93 (26): 15335-15340.
- Wang, Bei, Ziwei Xiao, and Ee Chee Ren. 2009. "Redefining the p53 Response Element." *Proceedings of the National Academy of Sciences* 106 (34): 14373-14378.
- Wang, Bei, Ziwei Xiao, Hui Ling Ko, and Ee-Chee Ren. 2010. "The p53 Response Element and Transcriptional Repression." *Cell Cycle* 9 (5): 870-879.
- Wang, Fan, Jean-Paul Becker, Piotr Cieplak, and Francois-Yves Dupradeau. 2014. "RED Python: Object Oriented Programming for Amber Force Fields." *Abstracts of Papers of the American Chemical Society* 247.
- Wang, Y., John F. Schwedes, Dorothy Parks, Kristine Mann, and Peter Tegtmeier. 1995. "Interaction of p53 with its Consensus DNA-Binding Site." *Molecular and Cellular Biology* 15 (4): 2157-2165.
- Wang, Zhen and Yi Sun. 2010. "Targeting p53 for Novel Anticancer Therapy." *Translational Oncology* 3 (1): 1-12.
- Warner, Wayne A., Ricardo Sanchez, Alex Dawoodian, Esther Li, and Jamil Momand. 2012. "Identification of FDA-Approved Drugs that Computationally Bind to MDM2." *Chemical Biology & Drug Design* 80 (4): 631-637.
- Wassman, Christopher D., Roberta Baronio, Oezlem Demir, Brad D. Wallentine, Chiung-Kuang Chen, Linda V. Hall, Faezeh Salehi, et al. 2013. "Computational Identification of a Transiently Open L1/S3 Pocket for Reactivation of Mutant p53." *Nature Communications* 4: 1407.
- Wei, Chia-Lin, Qiang Wu, Vinsensius B. Vega, Kuo Ping Chiu, Patrick Ng, Tao Zhang, Atif Shahab, et al. 2006. "A Global Map of p53 Transcription-Factor Binding Sites in the Human Genome." *Cell* 124 (1): 207-219.

- Weinberg, Richard L., Dmitry B. Veprintsev, and Alan R. Fersht. 2004. Cooperative Binding of Tetrameric p53 to DNA. Vol. 341.
- Weinfeld, Michael, Rajam S. Mani, Ismail Abdou, R. Daniel Aceytuno, and J. N. Mark Glover. 2011. "Tidying Up Loose Ends: The Role of Polynucleotide Kinase/Phosphatase in DNA Strand Break Repair." *Trends in Biochemical Sciences* 36 (5): 262-271.
- Wiederhold, Lee, John B. Leppard, Padmini Kedar, Feridoun Karimi-Busheri, Aghdass Rasouli-Nia, Michael Weinfeld, Alan E. Tomkinson, Tadahide Izumi, Rajendra Prasad, and Samuel H. Wilson. 2004. "AP Endonuclease-Independent DNA Base Excision Repair in Human Cells." *Molecular Cell* 15 (2): 209-220.
- Willis, Amy, Eun Joo Jung, Therese Wakefield, and Xinbin Chen. 2004. "Mutant p53 Exerts a Dominant Negative Effect by Preventing Wild-Type p53 from Binding to the Promoter of its Target Genes." *Oncogene* 23 (13): 2330-2338.
- Wolber, Gerhard and Thierry Langer. 2005. "LigandScout: 3-D Pharmacophores Derived from Protein-Bound Ligands and their use as Virtual Screening Filters." *Journal of Chemical Information and Modeling* 45 (1): 160-169.
- Wolkowicz, R. and Varda Rotter. 1997. "The DNA Binding Regulatory Domain of p53: See the C." *Pathologie Biologie* 45 (10): 785-796.
- Wong, Kam-Bo, Brian S. DeDecker, Stefan M. V. Freund, Mark R. Proctor, Mark Bycroft, and Alan R. Fersht. 1999. "Hot-Spot Mutants of p53 Core Domain Evince Characteristic Local Structural Changes." *Proceedings of the National Academy of Sciences* 96 (15): 8438-8442.
- Xu, Jie, Jin Qian, Ye Hu, Jilin Wang, Xiaolin Zhou, Haoyan Chen, and Jing-Yuan Fang. 2014. "Heterogeneity of Li-Fraumeni Syndrome Links to Unequal Gain-of-Function Effects of p53 Mutations." *Scientific Reports* 4.
- Yang, Sheng-Yong. 2010. "Pharmacophore Modeling and Applications in Drug Discovery: Challenges and Recent Advances." *Drug Discovery Today* 15 (11): 444-450.
- Zache, Nicole, Jeremy M. R. Lambert, Nina Rokaeus, Jinfeng Shen, Pierre Hainaut, Jan Bergman, Klas G. Wiman, and Vladimir J. N. Bykov. 2008. "Mutant p53 Targeting by the Low Molecular Weight Compound STIMA-1." *Molecular Oncology* 2 (1): 70-80.
- Zhang, Bian, Bernard T. Golding, and Ian R. Hardcastle. 2015. "Small-Molecule MDM2-p53 Inhibitors: Recent Advances." *Future Medicinal Chemistry* 7 (5): 631-645.
- Zhang, Qiang, Vladimir J. N. Bykov, Klas G. Wiman, and Joanna Zawacka-Pankau. 2018. "APR-246 Reactivates Mutant p53 by Targeting Cysteines 124 and 277." *Cell Death & Disease* 9 (5): 439.

- Zhang, Siwei, Yawei Shi, Hongwei Jin, Zhenming Liu, Liangren Zhang, and Lihe Zhang. 2009. "Covalent Complexes of Proteasome Model with Peptide Aldehyde Inhibitors MG132 and MG101: Docking and Molecular Dynamics Study." *Journal of Molecular Modeling* 15 (12): 1481.
- Zhang, Zhuming, Xin-Jie Chu, Jin-Jun Liu, Qingjie Ding, Jing Zhang, David Bartkovitz, Nan Jiang, et al. 2014. "Discovery of Potent and Orally Active p53-MDM2 Inhibitors RO5353 and RO2468 for Potential Clinical Development." *Acs Medicinal Chemistry Letters* 5 (2): 124-127.
- Zhao, Kehao, Xiaomei Chai, Karen Johnston, Adrienne Clements, and Ronen Marmorstein. 2001. "Crystal Structure of the Mouse p53 Core DNA-Binding Domain at 2.7 Å Resolution." *The Journal of Biological Chemistry* 276 (15): 12120-12127.
- Zou, Peng, Nan Zheng, Yanke Yu, Shanghai Yu, Wei Sun, Donna McEachern, Yongsheng Yang, Lawrence X. Yu, Shaomeng Wang, and Duxin Sun. 2012. "Preclinical Pharmacokinetics of MI-219, a Novel Human Double Minute 2 (HDM2) Inhibitor and Prediction of Human Pharmacokinetics." *Journal of Pharmacy and Pharmaceutical Sciences* 15 (2): 265-280.

Appendices

Appendix I.



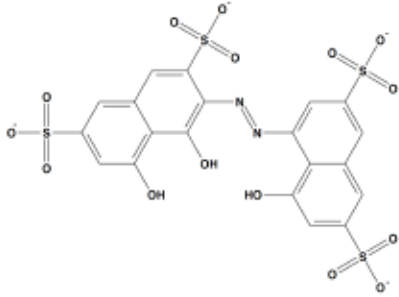
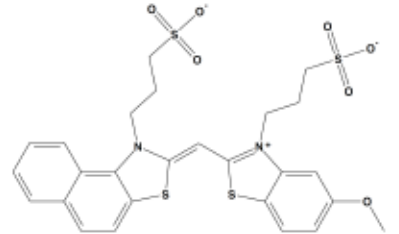
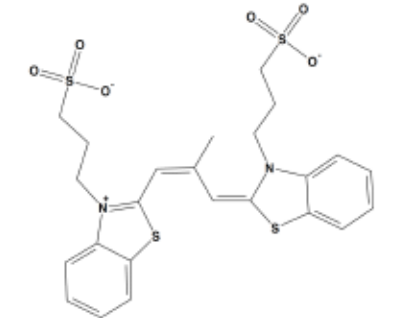
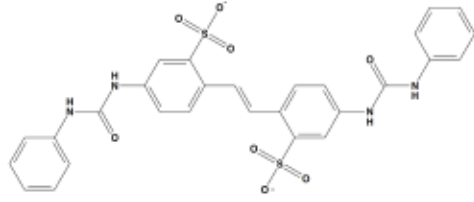
Appendix Figure. i. Cross-validation of the maximally correlated motion by FMA employing as functional quantity the RMSD of loop L3 throughout the whole MD simulation.

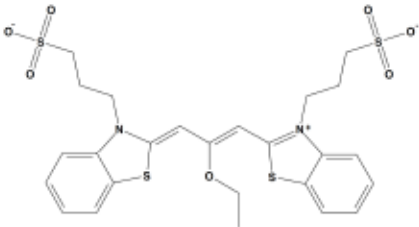
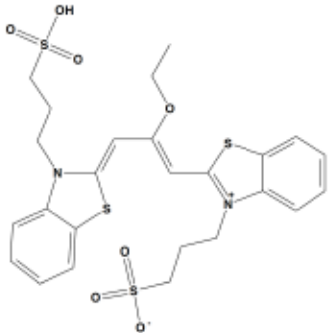
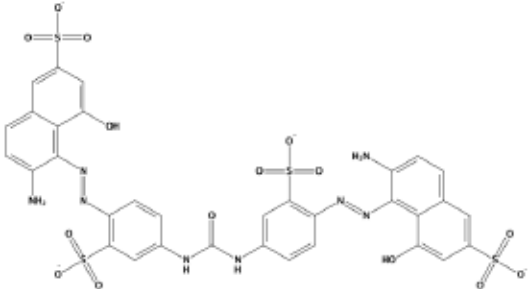
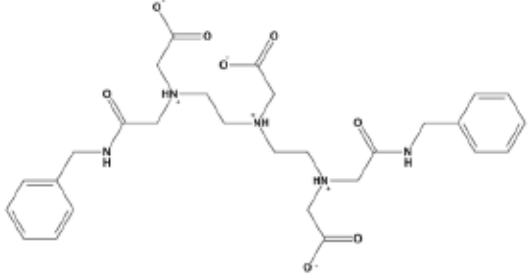
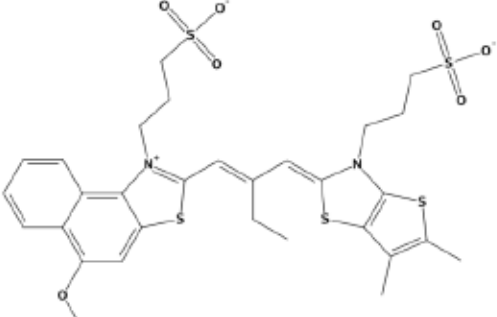
a) Loop L3 RMSD along the MD simulation (black); model in the model building set (red); model in the validation set (green). b) scatter plot (data-model) of the model building with its R_m value, that is the correlation between data and model in the model building set. c) Scatter plot (data-model) of the cross-validation set along with the correlation R_c .

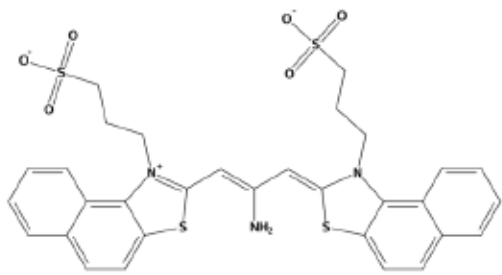
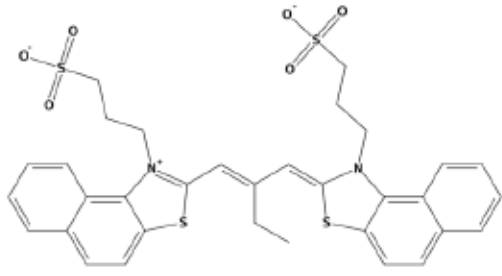
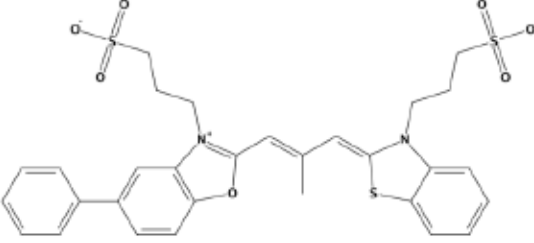
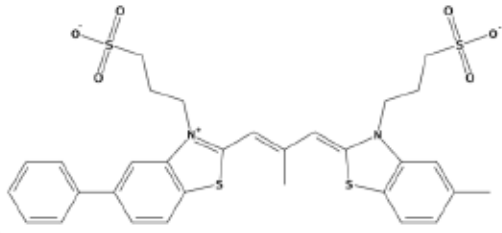
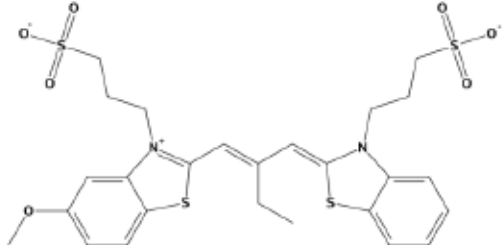
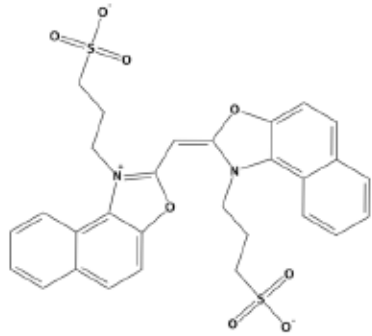
Appendix II.

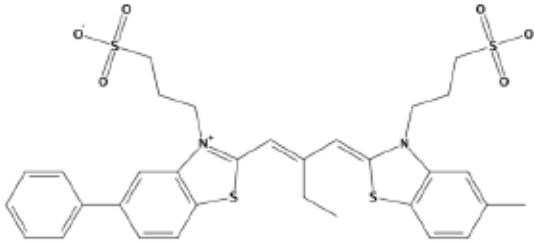
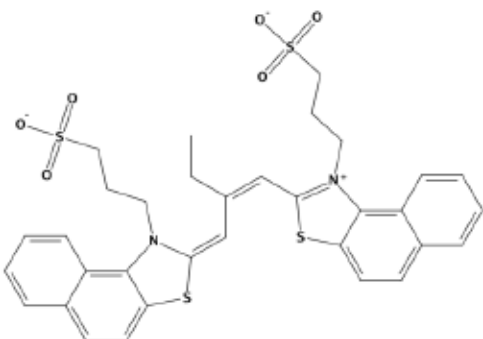
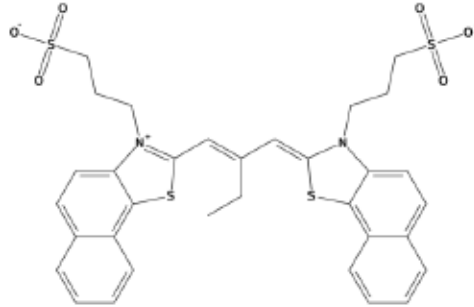
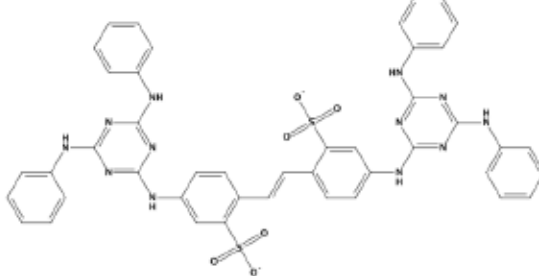
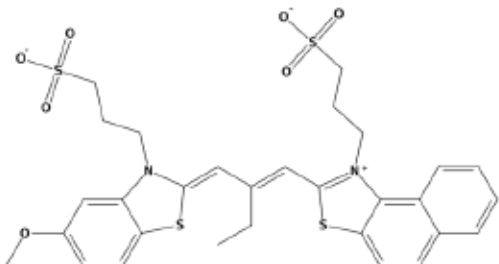
Appendix Table i. The predicted top twenty potential PNKP phosphatase inhibitors from our *in silico* screen.

LE = ligand efficiency, Freq = Number of times scored as a hit

#	Structure	Binding energy (kcal·mol ⁻¹)	LE (kcal·mol ⁻¹ /heavy atom)	Freq
A		-34	-0.82	339
B		-32	-0.81	373
C		-31	-0.86	471
D		-31	-0.74	309

E		-30	-0.80	533
F		-30	-0.80	328
		-37	-0.62	338
		-34	-0.83	556
		-34	-0.76	541

		-33	-0.75	507
		-33	-0.73	523
		-32	-0.76	513
		-32	-0.74	412
		-31	-0.79	348
		-31	-0.77	333

		-31	-0.70	520
		-31	-0.70	515
		-31	-0.70	463
		-31	-0.49	342
		-30	-0.70	533

Appendix III.

Below is a brief explanation of concepts of the two fluorescence-based assays used for the determination of the potential PNKP inhibitors IC_{50} values:

Universal Molecular Beacon (U-MB) assay**:

In this assay, an oligonucleotide (U-MB) with a 5' fluorescent fluorescein and a 3' dabcyl quencher is used along with a complementary nucleotide template. These are annealed together at 95°C. Consequently, the template binds to the complementary loop portion of the U-MB, which is unfolded by the high temperature causing the generated oligonucleotide to be fluorescent. Addition of deoxynucleotides, polymerase and hPNKP allow for the dephosphorylation of the 3' phosphate by hPNKP and the elongation of the template by the polymerase enzyme until the template is complete. This causes the release of the U-MB, which folds forming a stable hairpin structure in which the fluorescein signal is quenched by the dabcyl group. The phosphatase activity of hPNKP can, therefore, be monitored by measuring the fluorescence over time. The same procedure is repeated with the inactivated hPNKP and U-MB only as positive and negative controls. To ensure that the compound activity is of hPNKP inhibition rather than polymerase enzyme inhibition, the experiment is also repeated using a 3' hydroxyl template.

(** Adapted from the Protocol of hPNKP inhibitor IC_{50} assay, Weinfeld lab)

2-Aminopurine (2-AP) fluorescence assay:

This is a rapid fluorescence-based assay developed by the Weinfeld lab to assess the inhibition of the phosphatase activity of hPNKP. It is conceptually similar to the assay used to measure the inhibition of the kinase activity of T4-PNKP [1], the prokaryotic homologue of PNKP. In this assay, the adenine analogue, 2-AP, is incorporated in a hairpin probe that has a 3'-phosphate terminus. While intrinsically fluorescent in its free form, the fluorescence of 2-AP is quenched when it is incorporated in the probe due to the stacking interactions of its neighboring nucleotides [1]. Addition of hPNKP and T4 DNA polymerase (3' to 5' exonuclease enzyme) leads to the dephosphorylation of the 3' phosphate by PNKP and the digestion of the hairpin by T4 DNA polymerase. The fluorescence of the free 2-AP is detected and the activity of hPNKP is determined as a function of this fluorescence. A hairpin probe with a 3'-hydroxyl end is used as a positive control to exclude the possibility of ligand off-target interactions with T4 DNA polymerase.

References

1. Ma C, Liu H, Du J, Chen H, He H, Jin S, Wang K, Wang J. Quencher-free hairpin probes for real-time detection of T4 polynucleotide kinase activity. *Analytical Biochemistry*. 2016; 494: 1-3.